NASA/TM—2009-213641

Impact Testing on Reinforced Carbon-Carbon Flat Panels With Ice Projectiles for the Space Shuttle Return to Flight Program

Matthew E. Melis, Duane M. Revilock, and Michael J. Pereira
Glenn Research Center, Cleveland, Ohio

Karen H. Lyle
Langley Research Center, Hampton, Virginia

November 2009

NASA STI Program . . . in Profile

Since its founding, NASA has been dedicated to the advancement of aeronautics and space science. The NASA Scientific and Technical Information (STI) program plays a key part in helping NASA maintain this important role.

The NASA STI Program operates under the auspices of the Agency Chief Information Officer. It collects, organizes, provides for archiving, and disseminates NASA's STI. The NASA STI program provides access to the NASA Aeronautics and Space Database and its public interface, the NASA Technical Reports Server, thus providing one of the largest collections of aeronautical and space science STI in the world. Results are published in both non-NASA channels and by NASA in the NASA STI Report Series, which includes the following report types:

- TECHNICAL PUBLICATION. Reports of completed research or a major significant phase of research that present the results of NASA programs and include extensive data or theoretical analysis. Includes compilations of significant scientific and technical data and information deemed to be of continuing reference value. NASA counterpart of peer-reviewed formal professional papers but has less stringent limitations on manuscript length and extent of graphic presentations.

- TECHNICAL MEMORANDUM. Scientific and technical findings that are preliminary or of specialized interest, e.g., quick release reports, working papers, and bibliographies that contain minimal annotation. Does not contain extensive analysis.

- CONTRACTOR REPORT. Scientific and technical findings by NASA-sponsored contractors and grantees.

- CONFERENCE PUBLICATION. Collected papers from scientific and technical conferences, symposia, seminars, or other meetings sponsored or cosponsored by NASA.

- SPECIAL PUBLICATION. Scientific, technical, or historical information from NASA programs, projects, and missions, often concerned with subjects having substantial public interest.

- TECHNICAL TRANSLATION. English-language translations of foreign scientific and technical material pertinent to NASA's mission.

Specialized services also include creating custom thesauri, building customized databases, organizing and publishing research results.

For more information about the NASA STI program, see the following:

- Access the NASA STI program home page at *http://www.sti.nasa.gov*

- E-mail your question via the Internet to *help@sti.nasa.gov*

- Fax your question to the NASA STI Help Desk at 443–757–5803

- Telephone the NASA STI Help Desk at 443–757–5802

- Write to:
  NASA Center for AeroSpace Information (CASI)
  7115 Standard Drive
  Hanover, MD 21076–1320

NASA/TM—2009-213641

Impact Testing on Reinforced Carbon-Carbon Flat Panels With Ice Projectiles for the Space Shuttle Return to Flight Program

Matthew E. Melis, Duane M. Revilock, and Michael J. Pereira
Glenn Research Center, Cleveland, Ohio

Karen H. Lyle
Langley Research Center, Hampton, Virginia

National Aeronautics and
Space Administration

Glenn Research Center
Cleveland, Ohio 44135

November 2009

Level of Review: This material has been technically reviewed by technical management.

Available from

NASA Center for Aerospace Information
7115 Standard Drive
Hanover, MD 21076–1320

National Technical Information Service
5285 Port Royal Road
Springfield, VA 22161

Available electronically at http://gltrs.grc.nasa.gov

Impact Testing on Reinforced Carbon-Carbon Flat Panels With Ice Projectiles for the Space Shuttle Return to Flight Program

Matthew E. Melis, Duane M. Revilock, and Michael J. Pereira
National Aeronautics and Space Administration
Glenn Research Center
Cleveland, Ohio 44135

Karen H. Lyle
National Aeronautics and Space Administration
Langley Research Center
Hampton, Virginia 23681

Summary

Following the tragedy of the Orbiter *Columbia* (STS–107) on February 1, 2003, a major effort commenced to develop a better understanding of debris impacts and their effect on the space shuttle subsystems. An initiative to develop and validate physics-based computer models to predict damage from such impacts was a fundamental component of this effort. To develop the models it was necessary to physically characterize reinforced carbon-carbon (RCC) along with ice and foam debris materials, which could shed on ascent and impact the orbiter RCC leading edges. The validated models enabled the launch system community to use the impact analysis software LS–DYNA (Livermore Software Technology Corp.) to predict damage by potential and actual impact events on the orbiter leading edge and nose cap thermal protection systems.

Validation of the material models was done through a three-level approach: Level 1—fundamental tests to obtain independent static and dynamic constitutive model properties of materials of interest, Level 2—subcomponent impact tests to provide highly controlled impact test data for the correlation and validation of the models, and Level 3—full-scale orbiter leading-edge impact tests to establish the final level of confidence for the analysis methodology.

This report discusses the Level 2 test program conducted in the NASA Glenn Research Center (GRC) Ballistic Impact Laboratory with ice projectile impact tests on flat RCC panels, and presents the data observed. The Level 2 testing consisted of 54 impact tests in the NASA GRC Ballistic Impact Laboratory on 6- by 6-in. and 6- by 12-in. flat plates of RCC and evaluated three types of debris projectiles: single-crystal, polycrystal, and "soft" ice. These impact tests helped determine the level of damage generated in the RCC flat plates by each projectile and validated the use of the ice and RCC models for use in LS–DYNA.

Introduction

On February 1, 2003, the Orbiter *Columbia* broke apart during reentry resulting in the loss of seven crewmembers. For the next several months an extensive investigation of the accident ensued, involving a nationwide team of experts spanning dozens of technical disciplines from NASA, industry, and academia.

The Columbia Accident Investigation Board (CAIB), a group of experts assembled to conduct an investigation independent of NASA, concluded in August 2003 that the cause of the loss of *Columbia* and its crew was a breach in the left-wing leading-edge reinforced carbon-carbon (RCC) thermal protection system initiated by the impact of thermal insulating foam that had separated from the orbiter's external fuel tank 81 seconds into that mission's launch. During reentry, this breach allowed superheated air to penetrate behind the leading edge and erode the aluminum structure of the left wing, which ultimately led to the breakup of the orbiter.

The CAIB report (ref. 1) made over two dozen recommendations to increase the overall safety of the shuttle for future launches. Prior to the *Columbia* accident, there were no sophisticated analysis tools in

existence to reliably quantify the debris impact damage threat to the shuttle system. As a consequence, CAIB recommendation R3.8–2 directed NASA to "Develop, validate, and maintain physics-based computer models to evaluate thermal protection system damage from debris impacts. These tools should provide realistic and timely estimates of any impact damage from possible debris from any source that may ultimately impact the orbiter. Establish impact damage thresholds that trigger responsive corrective action, such as on-orbit inspection and repair, when indicated." In response to R3.8–2, an Agency debris assessment team, often informally referred to as the DYNA team, consisting of members from Glenn Research Center (GRC), Langley Research Center (LaRC), Johnson Space Center (JSC), and Boeing, was assembled to develop such a tool using LS–DYNA (ref. 2). LS–DYNA is a commercial finite element code that utilizes an explicit formulation (as opposed to the more common implicit formulation) to predict a wide range of transient dynamic phenomena.

As a critical path element of NASA's Return to Flight Program for the STS–114 mission, the primary objectives set for the DYNA team were to develop analysis models for potential debris and RCC materials. RCC is used as the thermal protection system on the orbiter leading edge and nose cap. To address these objectives, the team established a three-level approach: (1) fundamental tests to obtain independent static and dynamic constitutive model properties of materials of interest, (2) subcomponent impact tests to provide highly controlled impact test data for the correlation and validation of the models, and (3) full-scale impact tests to establish the final level of confidence for the analysis methodology. The debris materials under primary consideration were external tank thermal protection foams BX–265 and PDL, and ice, which also might shed off of the external tank.

All of the Level 2 impact testing for this program was conducted at the NASA GRC Ballistic Impact Laboratory in Cleveland, Ohio. The objective of this report is to provide details of the Level 2 ice impact test program and the experimental facilities used to conduct the tests, and present the observed data in an organized form (apps. A through E) for the Space Shuttle Program. Although there are a number of noted observations made about some of the data throughout, it is beyond the scope of this report to draw any technical conclusions about what is presented. For the Return to Flight program, both external tank foam and ice were tested on RCC. This report covers the ice impact testing program, and the foam testing program is covered in reference 3. Although this report is largely comprehensive in outlining the details and procedures of the actual testing, a complete description can be obtained in the Orbiter RCC Flat Panel Impact Testing Plan (ref. 4).

Test Program

Program Objectives

Initially, the objective of the ice impact test program was to establish projectile velocities for high- and low-density ice types at a fixed size and shape that initiate the threshold of visual damage on simply supported 6- by 6-in. and 6- by 12-in. flat RCC panels at impact angles of 90° and 45°. However, as shuttle program requirements evolved, the focus changed to include establishing thresholds for damage detectable by nondestructive evaluation (NDE) with ultrasound and pulse thermography. In addition, RCC panel deformations were to be measured with a three-dimensional image correlation (digital photogrammetry) deformation measurement system throughout the entire spectrum of impact velocities for each test series. Observations made during each test were used to corroborate the validity of LS–DYNA deformation and damage RCC and projectile constitutive models to reliably predict actual or potential threats to the Space Shuttle Orbiter.

Test Series Description

The external tank ice impact testing was divided into five series: high-density ice on 6- by 6-in. panels at 90° and 45° impact angles, high-density ice on 6- by 12-in. panels at 90° and 45° impact angles, and low-density ice on 6- by 6-in. panels at a 90° impact angle.

Each RCC flat panel was visually inspected before and after each impact test to provide an indication of coating loss (spalling) due to the impact event. A second objective of this visual examination was to provide guidance for how to proceed with NDE inspection, which was performed on all posttest panels along with studio digital photography.

Success Criteria

A GRC quality assurance (QA) officer was present and provided QA and configuration control for all tests. The QA officer verified all test plan requirement compliance and ensured that the resulting test data sheets were accurate and complete and that all success criteria were met for each test.

Each individual test was deemed successful provided that the projectile remained intact upon exit of the gun barrel and prior to impact on the RCC target panel and that interpretable high-speed digital video was acquired from the Vision Research Phantom (Vision Research, Inc.) cameras for velocity and deformation measurements. In addition, it was highly desirable that each of the following parameters were met:

- All projectile impact velocity parameters called for in this plan were kept within ±20 ft/s (as measured from digital high-speed video)
- Projectile impacted the expected target area within 0.25 in.
- Projectile rotational motion at impact was ≤5°, as determined by engineering review of video imagery after each shot
- Vacuum of 0.2±0.1 psi was maintained in test chamber for each test
- Load cell response data was not compromised by any extraneous vibratory loads independent of the projectile impact event

Test Facilities

All of the Level 2 RCC impact tests were conducted in the large vacuum gun (fig. 1) at the NASA GRC Ballistic Impact Laboratory in Cleveland, Ohio. The large vacuum gun is a single-stage compressed helium type with a 0.33 ft^3 pressure vessel. Barrels from 12 to 25 ft long, and inner diameters of 1.25 to 1.5 in., were fit to the chamber, depending on the velocity and projectile requirements for each test.

The large vacuum chamber has an inside dimension of 5 by 4 by 4 ft. It currently has provisions for 16 instrumentation feedthroughs. Viewing access ports on the front, side, top, and back allow for photo instrumentation with high-speed digital cameras. Four 120-V feedthroughs provide power for high-intensity lighting inside the chamber required for the high-speed digital imagery. The barrels for the large vacuum gun protrude into the vacuum chamber via a plate attachment that creates a circular opening with an o-ring seal to the chamber. Each barrel (with its own plate attachment) used with the vacuum chambers fits snugly against the o-ring to seal it with the chamber itself. This gun utilizes a Mylar (DuPont) burst disk system to release the helium propellant gas. The burst disk is in contact with an electronically heated nichrome wire, which melts the Mylar, releasing the propellant. Impact tests are conducted by simultaneously drawing a vacuum in the vacuum chamber and behind the projectile, to avoid pulling the projectile down the gun barrel prior to shooting.

Experimental Fixtures

Panel fixtures and mounts made from aluminum were fabricated for use in the large vacuum chamber to hold the RCC panels at 90° and 45° to the axis of the gun barrel. The construction was designed to be massive, as well as stiff, to minimize structural ringing due to the impacts, which could adversely affect load cell and deformation data. Figure 2 shows the panel fixture and mounts of the inside of the large vacuum chamber in its 45° configuration, with the lighting system on and the high-speed cameras in place. The side of the panel fixture, shown in figures 3 and 4, is called out in the photograph.

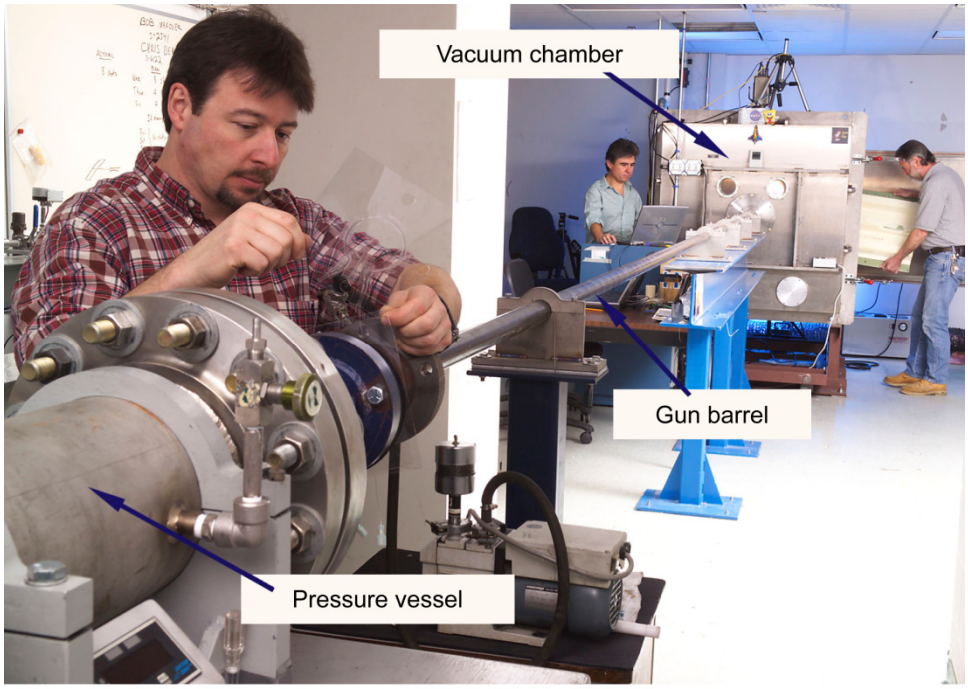

Figure 1.—Large vacuum gun with 2-in. barrel.

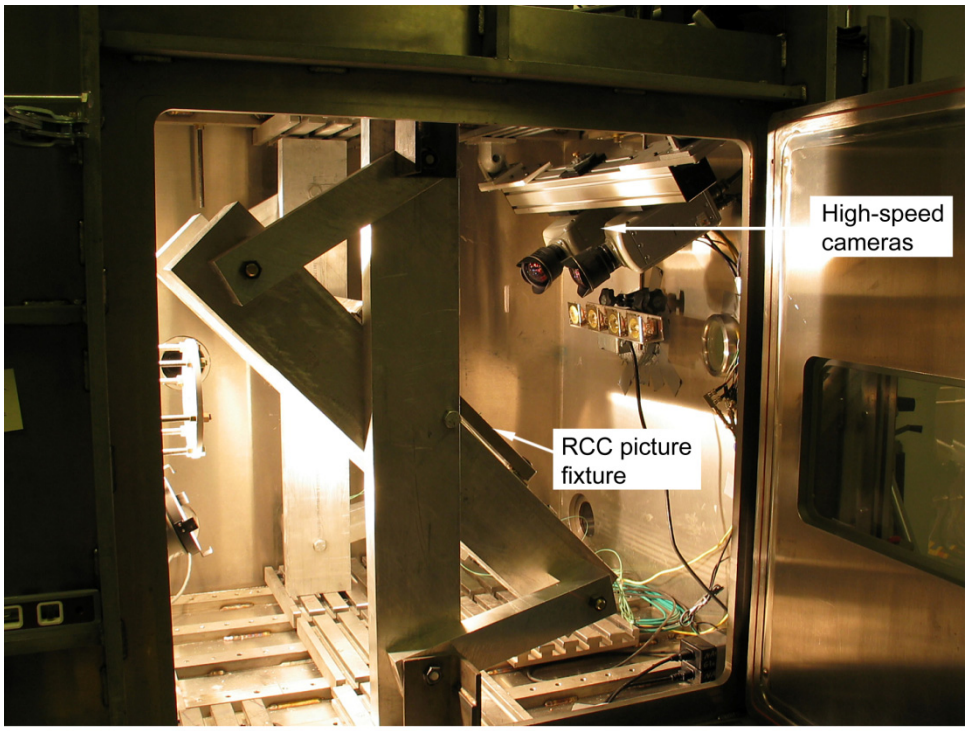

Figure 2.—Reinforced carbon-carbon (RCC) flat panel fixture assembly mounted in a large vacuum chamber for 45° impact tests.

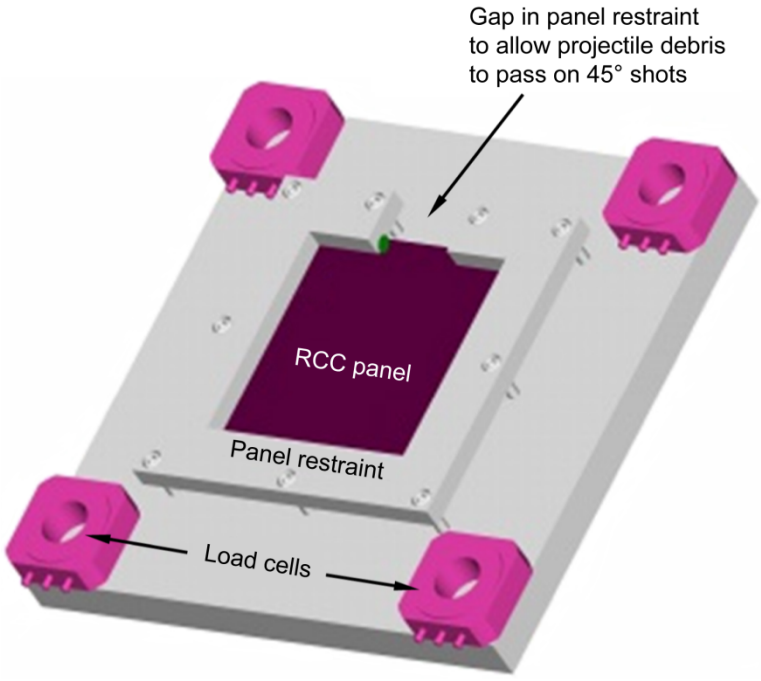

Figure 3.—Overview of reinforced carbon-carbon (RCC) flat panel holder fixture with load cells at corners (depicted upside down from actual testing orientation).

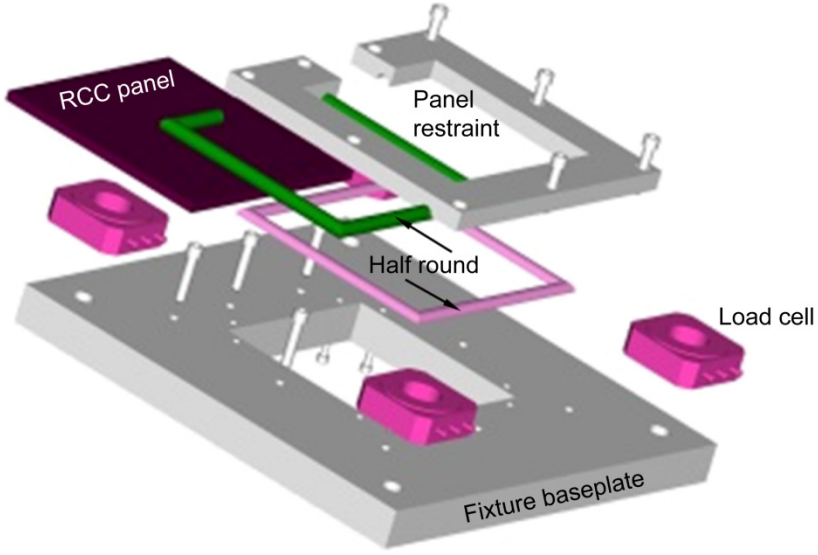

Figure 4.—Exploded view of reinforced carbon-carbon (RCC) flat panel holder fixture (depicted upside down from actual testing orientation).

Alignment of the test article with respect to the gun barrel shot line was accomplished through the use of a center-bore laser alignment tool inserted in the barrel such that the laser beam represented the centerpoint axis of the gun. The beam projected onto the test targets and was used to establish the correct fixture alignments and aim points for any given test conditions.

Two panel fixtures were fabricated to accommodate the 6- by 6-in. and 6- by 12-in. RCC panels. Figures 3 and 4 depict the 6- by 6-in. fixture with a panel in assembled and exploded views, respectively. Load cells, discussed in the next section, are shown at the corners of the fixture. The 6- by 6-in. panels were simply supported on all four edges in their mounts by being clamped in the frame between half-round aluminum bar stock around the complete perimeter of the panels and secured by nine bolts torqued to 8 in.-lb using a calibrated torque wrench. This torque limit was established with a study to establish the safe clamping pressure without crushing the RCC material or coating. The 6- by 12-in. panels were only restrained (simply supported) on the 6-in. edges at the same torque limit. The frames were designed to contact the RCC panels just inside of each panel edge. Hence, the actual distance between the centerlines of the half-round aluminum bar supports was 5 7/8 $in.^2$ for the 6- by 6-in. frame, and 11 7/8 in. for the 6- by 12-in. frame.

Instrumentation and Data Acquisition System

Load-time histories in three directions (one axial or normal and two shear to the panel face) were acquired from four piezoelectric three-axis load cells for each test by using load cells mounted in the fixture used to hold the flat panels. The fixture had a load cell mounted at each corner of the target panels shown in figures 3 and 4. Measurements taken from the load cells were averaged and filtered to obtain force time histories of each impact event.

The load cells were Kistler Model 9067 piezoelectric three-axis load washers (Kistler). They have a measurement range of ±10 000 lb in the normal axis and ±4500 lb in two shear directions. The load cell sensitivities are 17 picocoulomb/lb in the normal direction and 35 picocoulomb/lb in the shear direction. At the onset of the test program, the full usefulness of the load cell data had yet to be identified, and it was recorded for each test because it was relatively straightforward to do so. However, because of the complex dynamic response of the overall large vacuum gun test structure, the load cell data did not accurately represent the impact loads on the RCC and ultimately were not used for validating the LS–DYNA models. Consequently, load cell data are not presented or discussed further in this report.

Accelerometers were attached at several locations on the test frame in the large vacuum gun to identify and resolve potential response anomalies from the impact tests as well as quantify the degree of movement that the test frame experienced. Fortunately, there were no anomalies that arose during the entire ice test series, and the test frame displacements were within an expected range.

The application of strain gages to the RCC panels was considered initially as the plan for this test program was being developed; however, it was determined that strain gage data on RCC could be misleading and of low quality. This was established through laboratory level tests, which indicated that strain gages produce erratic data largely due to the craze cracking of the silicon carbide (SiC) coating on the panels. The full-field three-dimensional deformation measurements taken with the ARAMIS system (discussed below) ultimately provided full-field strain data that was of high value to the validation effort.

Two data acquisition systems were utilized to record signals from the load cells and accelerometers during testing: The first was a Spectral Dynamics model VX2805D 8-channel, 16-bit, 5-Msample/s/ channel system with signal conditioning capabilities. The second was an IOtech WaveBook 516E, 16-bit, 1-Msample/s system with eight analog input channels, eight strain gage conditioning channels, and eight ICP sensor channels. Dual-mode Kistler model 5010B charge amps were used to power the load cells.

High-Speed Cameras

High-speed digital Phantom cameras were used to document each impact test. For the majority of the program, both Phantom 5 and Phantom 7 cameras from Vision Research (ref. 5) were used and for a

select number of tests, Photron (ref. 6) FASTCAMS were used. The cameras measured projectile velocity and captured the damage and deformation dynamics resulting in each test in addition to being utilized with the three-dimensional displacement measurement system. Typically, five high-speed cameras would document one of these impact tests.

Various resolutions and frame rates were used depending on the requirements for each test as there is a direct tradeoff between frame rates and image resolution with the Phantom cameras. Higher frame rates result in lower resolution images. Typically frame rates of around 29 000 frames per second or more were used during these tests at resolutions of 256 by 256 or 256 by 128 pixels. It was a test goal to have exposure times of 2 to 20 μs (driven by light and viewing angle) to try to limit motion blur to 2 pixels.

The Phantom cameras record a continuous 1- to 2-s loop on an internal memory chip until stopped and do not require a trigger system to start recording. They are triggered manually to stop data acquisition at the sound of the gun blast, thus capturing the impact event in its entirety. Once the cameras were triggered, all of the recorded information was downloaded to laptop computers. All high-speed video captured in this test program has been archived by the Shuttle Program at JSC and is easily accessible for viewing to the interested reader (contacts: Justin Kerr or Jim Hyde).

Optical Full-Field Three-Dimensional Displacement Image Correlation Measurement System

Deformation and computed strains of the back side (opposite of the impact side) of the RCC panels were obtained using the ARAMIS system built by GOM mbH (ref. 7) acquired from Trilion Optical Test Systems (refs. 8 to 10). ARAMIS is a three-dimensional image correlation photogrammetry system that captures full-field displacement measurements under static, quasi-static, and ballistic impact loading.

The system works off image pairs taken simultaneously with two Phantom 7 cameras set up on a fixed beam, which viewed the back of the RCC panels undergoing impact. The image pairs were taken at 37.17 increments (~27 000 frames/s). The camera pair was set up outside the large vacuum chamber for the 90° impact tests and inside the chamber for the 45° tests. Inside mounting was necessary for the 45° tests to optimize the view of the panel backs. The outside mount configuration is shown in figure 5.

Figure 5.—ARAMIS Three-Dimensional Deformation/Strain Measurement System shown with static camera assembly setup at large vacuum-gun viewing ports. Inset in lower right corner depicts paint pattern on the back of a reinforced carbon-carbon panel.

In order for the ARAMIS system to make its measurements, a painted speckle or spot pattern must be applied to the field area of interest. The back side of each panel was painted before the impact testing was performed. Testing was performed on small samples of RCC that were painted for use with the ARAMIS system. A scanning electron microscope was used to confirm that the paint did not excessively wick into the RCC panels and potentially change the RCC material performance and NDE techniques or flash thermography, and ultrasound tests revealed no adverse interference or artifacts due to the speckled paint pattern on the back side of the panels. The speckled pattern can be seen on the postimpact photographs in the appendices of this report. As the test program proceeded, an optimum paint pattern was adapted going from a "spatter" pattern to a pattern spray painted through a uniform stencil. This accounts for the two types of patterns seen in the photographs. The paint patterns were created by applying paint to the back of each test panel in two layers. The first layer is white paint that has a high reflectivity rating followed by black spray paint applied in a random speckle pattern or through the stencil. The inset in the lower right-hand corner of figure 5 shows the uniform paint pattern on the back of an RCC panel.

Using photogrammetric principles, the three-dimensional coordinates of the surface of the specimen can be calculated precisely from observing the paint pattern from two known points of view. On the basis of the three-dimensional coordinates, the three-dimensional displacements, the strains, and shape of the specimen were calculated with a high degree of accuracy and resolution. The results can be rapidly postprocessed after each test and visualized in similar fashion to finite element results. Three types of ARAMIS output are presented in the appendices of this report: displacement cross sections at various times on a panel, centerpoint displacements as a function of time, and a full-field color displacement fringe plot at maximum displacement of each panel. An example of these plots is shown in figure 6.

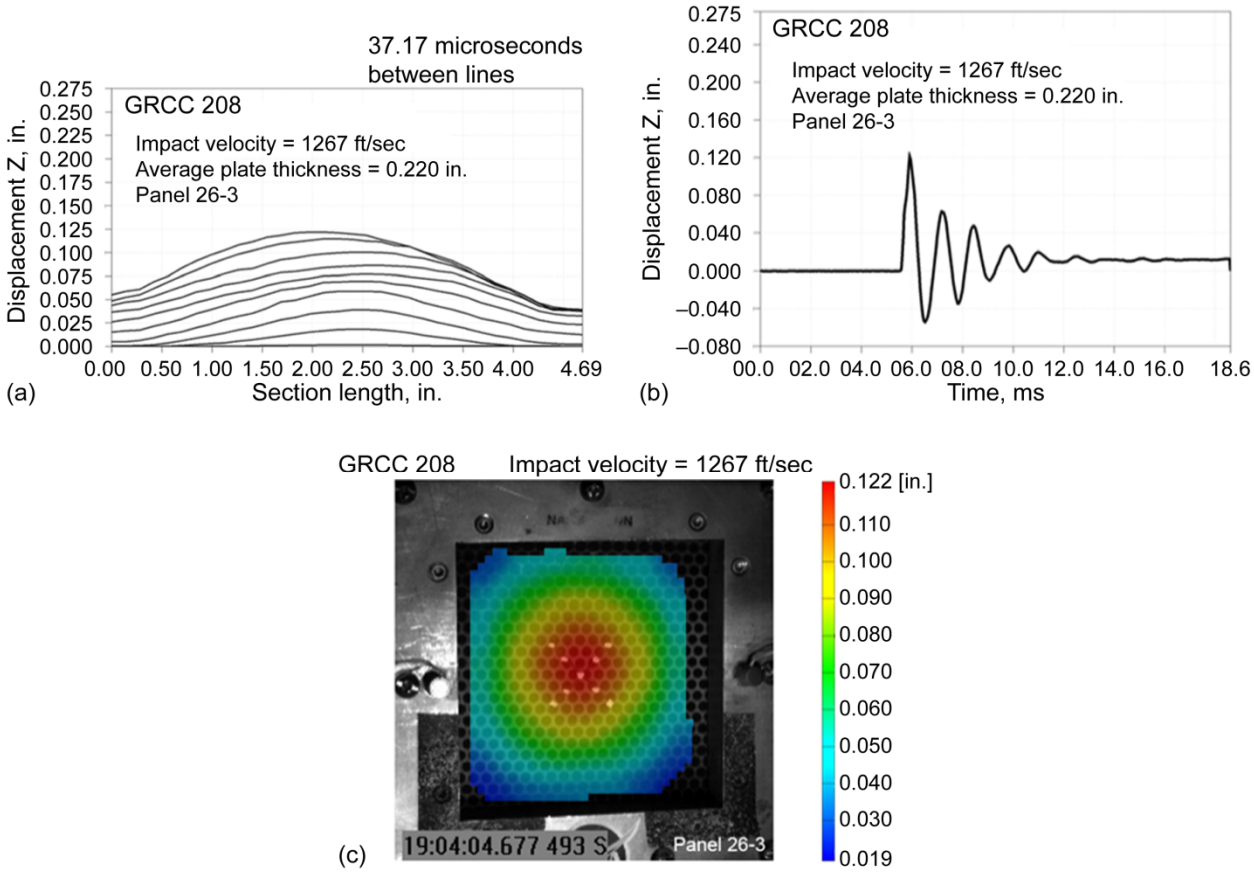

Figure 6.—Example output plots from the ARAMIS displacement measurement system. (a) Displacement countour plot. (b) Centerpoint displacement plot. (c) Displacement fringe plot.

Velocity Measurement

Posttest evaluation of the high-speed Phantom camera video established impact velocities for each test as well as provided verification of projectile integrity and orientation in flight.

To set up for obtaining projectile velocities, a camera was mounted orthogonal to the path of the projectile and a calibration bar was seated in the end gun barrel and projected into the test chamber along the centerline axis of the barrel. The calibration bar had precisely machined markings 0.5 in. apart on a section the same diameter as the ice projectiles to be shot. Given this device with known markings in the same plane of the projectile's motion, the relationship between physical distance in the plane of the projectile's trajectory and camera screen pixels was determined. The impact velocity of a projectile in a given test was then calculated from the following equation:

$$V_p = \mathrm{SF} \times \mathrm{PIX} \times \frac{\mathrm{FR}}{\mathrm{NF}}$$

where V_p is the velocity of the projectile, SF is the scaling factor in units of length per pixel, PIX is the number of pixels a mark on the projectile travels in a given number of frames (NF), and FR is the frame rate.

Pretest and Posttest RCC Panel Observations

Material Pedigrees

RCC Panel Pedigree and Fabrication

The RCC material used in this ice impact test program was obtained from Lockheed Martin Missiles and Fire Control in Dallas, Texas, through the Shuttle Program Office. Typically, the material was provided as-manufactured in 12- by 12-in. panels, with full traceability documentation, and cut to 6- by 6-in. or 6- by 12-in. sizes at Southern Research Institute (SRI) in Birmingham, Alabama. The cut plan for the panels is discussed in appendix C of reference 4. In addition, it should be noted that because of material loss during the cutting process, the panels were delivered to GRC nominally at 5.9 by 5.9 in. and 5.9 by 11.9 in. but are referred to in whole numbers for easier referencing. SRI supported a significant number of engineering efforts relating to the RCC material studies. Much of this work was complimentary and of great use to the LS–DYNA RCC constitutive model development.

Final reports from two of these studies may be of noteworthy interest to those reading this report. "Silicon Carbide Thickness Measurements of Various RCC Panels and Plates" (ref. 11) provides further detail on the panels tested in this report. "Correlation of RCC Substrate Properties" (ref. 12) reveals more on the weighted contributions of substrate RCC properties to the overall properties of coated RCC panels. In addition, it should be noted that significant work also was performed to obtain static and dynamic mechanical properties of the RCC material and is presented in references 13 and 14.

RCC material pedigrees to be used in this test program were identified through shipping documents that accompanied the deliveries to GRC. Reference to relevant shipping documents was recorded by the quality officer for each test to ensure traceability. For the purpose of identifying test panels, each flat panel was labeled with the unique identifier relating to the 12- by 12-in. parent panel and then assigned an additional number identifying the order in which it was cut from the parent panel. The application of this numbering scheme can be seen in the tables at the beginning of each appendix under the first column labeled "Test No." Expanding upon this, a test number identifier was assigned to each test which incorporated the assigned panel numbers. It included the test number (counted sequentially), the angle of impact, and the projectile material. An example of the flat panel test identification is given in figure 7. This example identifies the first impact test in the RCC impact testing was performed on subpanel 1 cut from parent T8015 and shot with BX–265 at a 90° impact angle. It should be noted that the NASA GRC

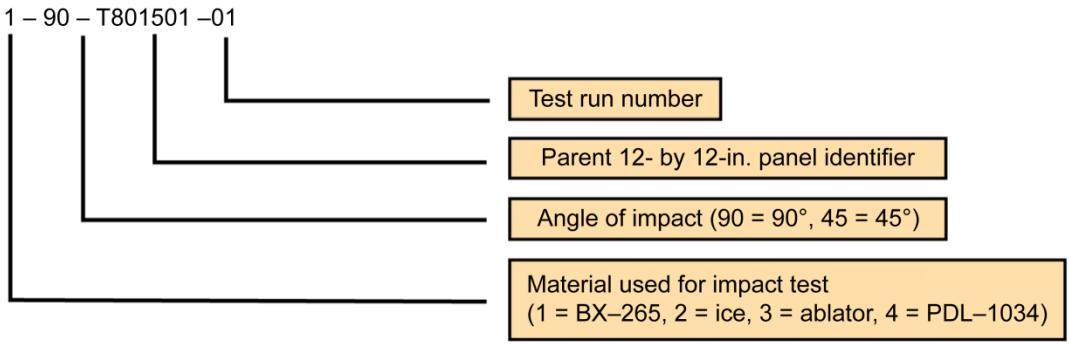

Figure 7.—Test numbering scheme for reinforced carbon-carbon flat panel impact tests.

Ballistic Impact Laboratory maintained its own test numbering scheme along with the aforementioned one. Test numbers were assigned sequentially after the prefix GRCC. It is presented in the appendices for clarity and completeness as the numbering used for the data archives follows this format.

Ice Pedigree and Fabrication

In the planning stages of the Level 2 ice impact tests, it was established that two types of ice would be used for projectiles. High-density ice or "hard" ice and a lower density ice or "soft" ice. Ice can form on the external tank with a wide latitude of densities and character. The assumption was that high-density ice would provide a worst case from a potential damage perspective to the RCC, and the soft ice would represent a more typical density observed to form on the external tank.

The hard ice was clear (no air bubbles) ice manufactured by Ice Culture, Inc. in Hensall, Ontario, Canada. Ice Culture, which traditionally manufactures ice sculptures for entertainment events, was chosen as the vendor because of their ability to manufacture cylindrical ice projectiles to within NASA's specifications using a computer numerically controlled milling machine. Each hard ice cylindrical projectile was nominally 1.66 in. long by 0.67 in. in diameter at a nominal density of 57.3 lb/ft^3.

The soft ice cylindrical projectiles were manufactured at JSC using shaved ice. These projectiles were 1.9 in. long by 0.8 in. in diameter at an average density of 37.3 lb/ft^3. The cylinders were made by "shaving" typical freezer ice in a children's snow cone machine in a controlled freezer room. For each piece, approximately 9.5 g of shaved ice was tapped into cylindrical molds, cut to projectile dimensions, with a mandrel (tapping in incremental amounts of the ice over several steps) to obtain as uniform density as possible. The individuals involved with the procedures and manufacture of these projectiles perfected their abilities to repeatedly deliver high-quality test articles within specifications for the ballistic and materials testing.

Ice can form in a very wide variety of types and structures, hence, detailed characterization of all ice specimens used for this test program was performed to ensure consistency from projectile to projectile. This was done under NASA contract at Dartmouth University in Hanover, New Hampshire. In the case of hard ice, both single-crystal and poly-crystal ice specimens were selected for testing from hundreds of specimens sent to them from Ice Culture. As seen in the testing documents, the majority of projectiles were poly-crystal. In addition to impact test projectiles, Dartmouth also screened ice specimens for mechanical properties tests to develop and validate the LS–DYNA models. References 25 through 28 and 13 provide details of the ice characterization and model development efforts to the interested reader.

Digital Photography

Digital photographs were taken of the front, back, and all four edges of each RCC panel both before and after impact testing to document any changes in the panel condition after testing. All of the posttest

images are presented in this report for each panel. Both pretest and posttest images have been archived in digital form by the Shuttle Program and are easily accessible to the interested reader (contacts: Justin Kerr or Jim Hyde). In addition, these photographs have been all assigned GRC C-numbers (seen in the lower right-hand corner of the appendices images) and will remain in the GRC archives, accessible through the GRC Imaging Technology Center.

Nondestructive Evaluation

NDE was performed on each RCC panel before and after testing to baseline the specimens and to evaluate the damage due to impact. The NDE not only characterized any damage due to the impact testing, but the findings from each panel's evaluation helped define the parameters of the panel testing to follow. All NDE outlined in this report was performed by the NDE group at GRC. Two NDE methods will be utilized for this program: pulse or flash thermography, and through-transmission ultrasound.

Pulse, or flash, thermography involves the heating of a specimen with a short duration pulse of energy and monitoring the transient thermal response of the surface of the specimen with an infrared camera. The thermal energy on the surface conducts into the cooler interior of the sample. In turn, there is a reduction of the surface temperature over time. This surface cooling will occur in a uniform manner as long as the material properties are consistent throughout the specimen. Subsurface defects that possess different material properties (e.g., thermal conductivity, density, or heat capacity) will affect the flow of heat in that particular region. This resistance in the conductive path causes a different cooling rate at the surface directly above the defect, when compared to the surrounding, defect-free material. The change in the subsurface conduction is seen as a nonuniform surface temperature profile as a function of time. Since the method depends on the interaction of the defect with the advancing thermal front, defects that are located at greater depths will show up later. Because of lateral diffusion, deeper defects will tend to have less contrast than near-surface flaws. Therefore, the critical flaw size capability of a thermographic inspection system is a function of the defect size, depth, and the material properties of the component being tested. Analysis of thermographic data involves examination of images based on the temperature-time data or derivatives calculated from the original data sets. Anomalous areas can then be identified based on deviations in the cooling behavior. Figure 8 (right) shows the thermal imaging setup used to conduct pulse thermography with an example output image.

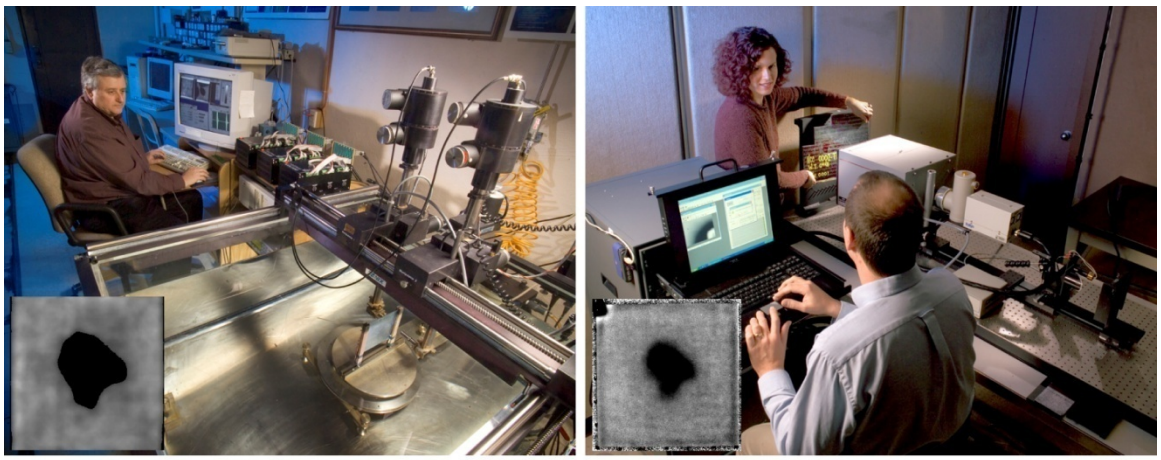

Figure 8.—Nondestructive evaluation facilities at Glenn Research Center: through-transmission ultrasonic immersion tank with reinforced carbon-carbon panel undergoing scanning (left) and thermal imaging setup to perform pulse thermography (right). Insets in the left corners of each photo depict sample output from each technique.

Through-transmission ultrasonic inspection utilizes two transducers, placed on opposite sides of a material for interrogation. One transducer sends an ultrasonic pulse through the material where it is received by the second. In scanning mode, the transducer pair is moved across the area of interest, and an image based on the amplitude of the received waveform is generated. Defects and other significant variations will result in the additional attenuation and scattering of the ultrasonic signal as it passes through the material, thus reducing the signal amplitude. Flaws are located in the image based on this decrease in signal amplitude. Minimum flaw resolution is a function of the wavelength of the ultrasonic signal flaw orientation. Resolution, in general, increases with increasing frequency. Figure 8 (left) shows the immersion ultrasonic tank and relevant hardware to perform the through-transmission ultrasonic inspection with a sample image.

Through-transmission ultrasound evaluation will require that the RCC panels be immersed in water during the scanning process. Each RCC panel was weighed before each scan and then vacuum dried until the after-scan weight is that of the initial weight to ensure that all water absorbed from the immersion was removed from the panel. The vacuum drying process was accomplished referencing SRI standard specification for drying RCC panels. This specification used 180 °F heat while pulling a vacuum of approximately 10^{-3} torr. The weight of the flat panel was monitored until stabilization occurred.

Testing Summaries

Below are brief summaries of the ice impact test program as organized into impact angle and ice projectile type. Comprehensive data sets reside in each of the six appendices in the back of this report.

High-Density Ice on 6- by 6-in. Reinforced Carbon-Carbon (RCC) Panels at 90° Impact Angle (Appendix A)

Twenty shots were conducted in this test series with impact velocities ranging from 240 to 641 ft/s. Sixteen of the tests used poly-crystal ice projectiles and four with single-crystal projectiles. The RCC material for this test series was tested in the as-manufactured condition.

High-Density Ice on 6- by 6-in. Reinforced Carbon-Carbon (RCC) Panels at 45° Impact Angle (Appendix B)

Thirteen shots were conducted in this test series with impact velocities ranging from 429 to 858 ft/s. All projectiles used poly-crystal ice. The RCC material for this test series was tested in the as-manufactured condition.

High-Density Ice on 6- by 12-in. Reinforced Carbon-Carbon (RCC) Panels at 90° Impact Angle (Appendix C)

Five shots were conducted in this test series with impact velocities ranging from 265 to 616 ft/s. All shots used poly-crystal ice projectiles with the exception of the first test in the series that was single-crystal. The RCC material for this test series was tested in the as-manufactured condition. All of the 6- by 12-in. panel tests were only simply supported on two ends. As a consequence, the wave propagation in these panels were dramatically different and less controlled and damped than in the 6- by 6-in. panels, which were supported on all four edges. The impact response of the 6- by 12-in. panels showed additional modes of vibration that are identified in the ARAMIS data presented in the appendix.

High-Density Ice on 6- by 12-in. Reinforced Carbon-Carbon (RCC) Panels at 45° Impact Angle (Appendix D)

Six shots were conducted in this test series with impact velocities ranging from 493 to 809 ft/s. All shots used poly-crystal ice projectiles. The RCC material for this test series was tested in the as-manufactured condition. All of the 6- by 12-in. panel tests were only simply supported on two ends. As a consequence, the wave propagation in these panels were dramatically different and less controlled and damped than in the 6- by 6-in. panels which were supported on all four edges. The impact response of the 6- by 12-in. panels showed additional modes of vibration which are identified in the ARAMIS data presented in the appendix.

Low-Density Ice on 6- by 6-in. Reinforced Carbon-Carbon (RCC) Panels at 90° Impact Angle (Appendix E)

Ten shots were conducted in this test series on nine RCC panels with impact velocities ranging from 431 to 612 ft/s. Panel 64–3 was shot twice in GRCC144 and GRCC151. This was a consequence of the panel being deemed "undamaged" in GRCC144 making it available for additional testing. The RCC material for this test series was tested in the as-manufactured condition. Low-density ice projectiles, manufactured at JSC, were used for each of these 10 tests.

Concluding Remarks

The Level 2 reinforced carbon-carbon (RCC) flat panel impact test program at the NASA Glenn Research Center Ballistic Impact Laboratory was successfully completed on time supporting NASA's Return to Flight with the STS–114 mission. The data in the appendices of this report present the results from 54 ice projectile impact tests, which were used to demonstrate the validity of ice and RCC models developed and implemented in the LS–DYNA impact analysis program. As a point of interest, the final validation step of the LS–DYNA models was through correlation with observations from follow-on full-scale orbiter wing leading edge and nose cap impact tests performed at Southwest Research Institute (SwRI).

In preparation for the STS–114 launch, virtually hundreds of analyses with LS–DYNA were performed to establish certified impact damage thresholds for RCC thermal protection systems on the orbiter helping to recertify the shuttle system for flight. For the interested reader, references 15 through 25 provide additional details on much of the analysis development process with LS–DYNA, and references 26 through 28 highlight the efforts performed to evaluate ice impacts on RCC. Reference 3 is the companion report that provides all of the postimpact test data on the RCC panels from the external tank foam test program.

Appendixes

Data from the external tank foam impact tests are presented in the following five appendixes (A through E) as follows:

Appendix A—High-Density Ice Impact Testing at 90° Angle on 6- by 6-in. Reinforced Carbon-Carbon (RCC) Flat Panels
Appendix B—High-Density Ice Impact Testing at 45° Angle on 6- by 6-in. Reinforced Carbon-Carbon (RCC) Flat Panels
Appendix C—High-Density Ice Impact Testing at 90° Angle on 6- by 12-in. Reinforced Carbon-Carbon (RCC) Flat Panels
Appendix D—High-Density Ice Impact Testing at 45° Angle on 6- by 12-in. Reinforced Carbon-Carbon (RCC) Flat Panels
Appendix E—Low-Density Ice Impact Testing at 90° Angle on 6- by 6-in. Reinforced Carbon-Carbon Flat Panels

In each appendix, the data are organized in the following fashion:

1. A table summarizing the appendix test series.
2. Baseline and posttest imagery from ultrasound and thermography nondestructive evaluations arranged in order of ascending impact velocities. (It should be noted that in the thermography imagery, black spots appear in the upper left or right corners of the panels. This is an artifact of the fixturing to hold the panels during evaluation.)
3. Displacement contours output from ARAMIS showing the displacements along a cross-sectional line on the back of the panels at uniform increments of time as the panels were impacted. Note the sectional line for the 6- by 12-in. panels were taken along the long edge of the panels.
4. Displacement trace plots output from ARAMIS of the panel centerpoints as a function of time.
5. ARAMIS full-field color fringe plots taken from the point of maximum displacement of the panel resulting from the impact. (Note that in some of these plots, coating loss on the back side of the panels obscured ARAMIS from measuring accurate displacements. In these cases, the plots shown were selected just before or after failure of the panels. Knowing maximum displacement for a panel subject to failure is less meaningful for analysis correlation since the structure of the panel is compromised.)
6. High-resolution digital photography of each panel show front, back, and edge composite views as well as isometric views of both front and back of each panel.

Appendix A.—High-Density Ice Impact Testing at 90° Angle on 6- by 6-in. Reinforced Carbon-Carbon (RCC) Flat Panels

Notable Observations From the Appendix A Test Series

1. The last four panels tested in this series (GRCC 139, 141, 142, and 143) were tested with single-crystal ice.
2. ARAMIS data existed for nearly all ice impact tests, but are not presented when considered to be uninterpretable.

Appendix A Test Series

High Density Poly-Crystal Ice 90 Degree Impact Test Parameters on 6" x 6" Reinforced Carbon-Carbon Panels													
Test No.	Glenn Test Reference Number	Impact Velocity (ft/sec)	Panel ID Number	Average Panel Thickness (inches)	Visual Damage Observations	Mass of panel before test (grams)	Mass of panel after test (grams)	Projectile Mass (g)	Projectile Length (in)	Projectile Diameter (in)	Projectile Density lb_m/ft^3	Test Date	Projectile ID Number
2-90-164-12	GRCC078	240	16-4	0.217	No significant indications	201.18	201.61	8.800	1.661	0.662	58.638	10/19/04	Ice: 11-PX-2
2-90-132-02	GRCC067	290	13-2	0.225	No significant indications	204.70	204.95	8.940	1.662	0.667	58.646	10/15/04	Ice: 11-PX-3
2-90-133-03	GRCC068	438	13-3	0.223	Coating loss on back (2 chips)	202.12	202.78	8.940	1.662	0.675	57.264	10/18/04	Ice: 11-PX-6
2-90-162-10	GRCC075	471	16-2	0.220	No significant indications	202.78	203.35	8.950	1.663	0.669	58.326	10/19/04	Ice: 11-PX-15
2-90-161-09	GRCC074	474	16-1	0.222	No significant indications	200.91	201.55	8.880	1.660	0.671	57.629	10/19/04	Ice: 11-PX-11
2-90-141-05	GRCC070	486	14-1	0.221	Back side coating loss	199.87	200.24	8.910	1.664	0.673	57.342	10/18/04	Ice: 11-PX-9
2-90-452-28	GRCC115	489	45-2	0.223	Backside damage/coating loss	210.24	210.79	8.48	1.66	0.658	57.229	11/4/04	Ice: 13-PX-24
2-90-163-11	GRCC077	490	16-3	0.220	No significant indications	199.18	199.75	8.900	1.658	0.668	58.349	10/19/04	Ice: 11-PX-16
2-90-143-07	GRCC072	495	14-3	0.223	Backside damage/coating loss	202.33	202.32	8.960	1.663	0.671	58.043	10/19/04	Ice: 11-PX-10
2-90-144-08	GRCC073	495	14-4	0.223	Coating loss on back-chips	204.45	205.16	8.960	1.663	0.665	59.095	10/19/04	Ice: 11-PX-5
2-90-204-26	GRCC113	498	20-4	0.220	Front and Back side damage	201.10	199.76	8.71	1.66	0.666	57.378	11/4/04	Ice: 13-PX-18
2-90-453-29	GRCC116	501	45-3	0.222	Front and back side damage	212.96	212.44	8.74	1.662	0.668	57.162	11/4/04	Ice: 13-PX-23
2-90-451-27	GRCC114	509	45-1	0.222	Backside damage	211.52	211.24	8.55	1.655	0.662	57.179	11/4/04	Ice: 13-PX-22
2-90-134-04	GRCC069	511	13-4	0.220	Front/back coating loss	204.05	203.55	8.970	1.659	0.668	58.773	10/18/04	Ice: 11-PX-13
2-90-142-06	GRCC071	517	14-2	0.220	Front/back coating loss	201.71	197.65	8.970	1.659	0.674	57.731	10/19/04	Ice: 11-PX-12
2-90-131-01	GRCC066	641	13-1	0.220	Hole thru center of panel	202.81	190.44	9.02	1.66	0.67	58.888	10/15/04	Ice: 11-PX-7
High Density Single Crystal Ice 90 Degree Impact Test Parameters on 6" x 6" Reinforced Carbon-Carbon Panels													
2-90-642-02	GRCC141	484	64-2	0.229	Front crack/backside coating loss	206.72	207.02	8.51	1.661	0.665	56.195	1/13/05	Ice: 13-SX-8
2-90-651-03	GRCC142	517	65-1	0.236	Front crack/back side damage	207.96	208.18	8.46	1.662	0.662	56.338	1/13/05	Ice: 13-SX-5
2-90-652-04	GRCC143	528	65-2	0.230	Front/back coating loss	205.57	205.24	8.55	1.661	0.663	56.800	1/13/05	Ice: 13-SX-2
2-90-641-01	GRCC139	589	64-1	0.233	Hole thru sample	206.63	193.05	8.5	1.663	0.66	56.914	1/13/05	Ice: 13-SX-10

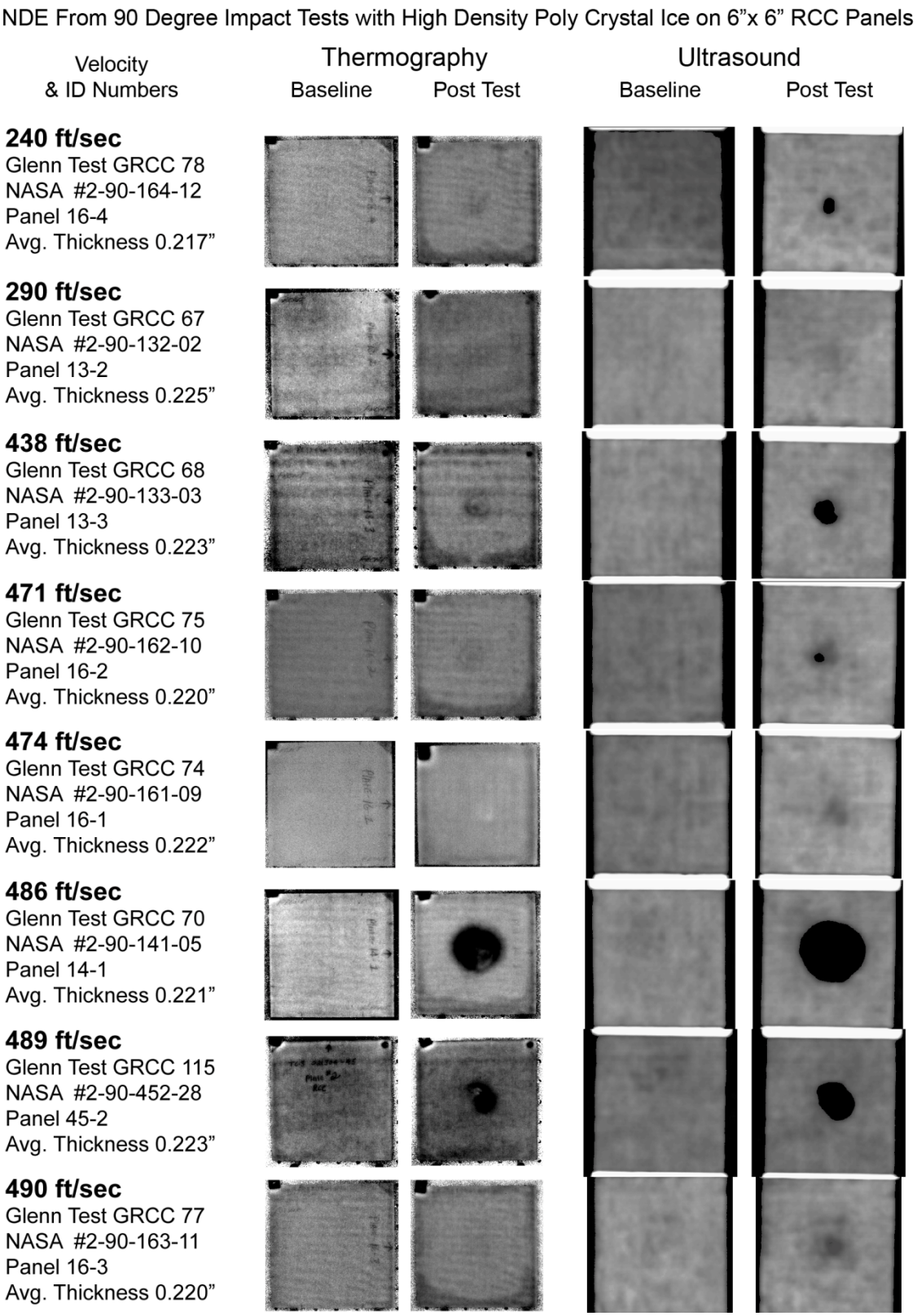

Figure A1–1.—Pulse thermography and ultrasound post impact pre- and posttest images of reinforced carbon-carbon 6- by 6-in. flat panels impacted with high-density poly-crystal ice cylinders (nominally 0.66 in. in diameter by 1.66 in.) at a 90° angle.

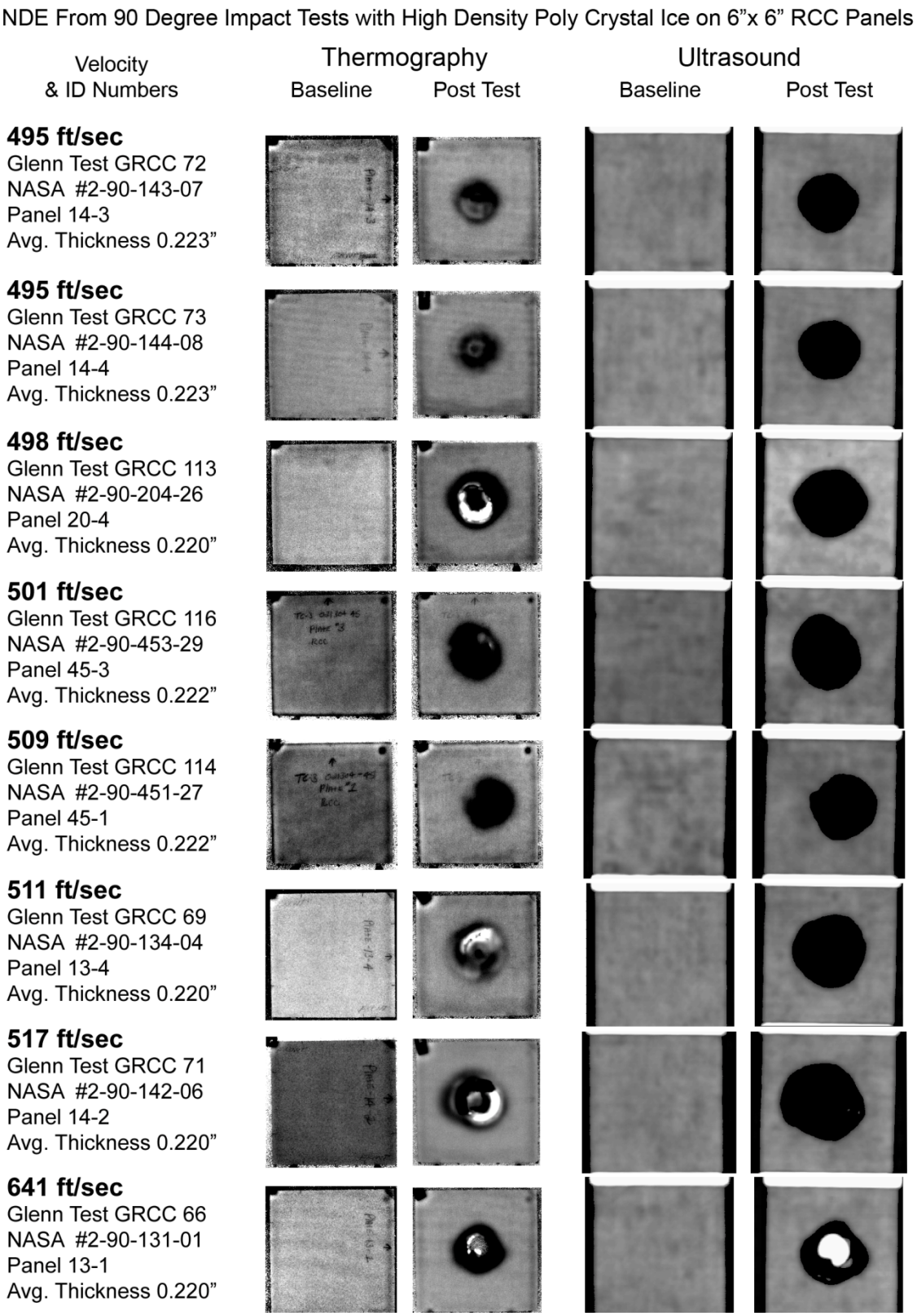

Figure A1–2.—Pulse thermography and ultrasound post impact pre- and posttest images of reinforced carbon-carbon 6- by 6-in. flat panels impacted with high-density poly-crystal ice cylinders (nominally 0.66 in. in diameter by 1.66 in.) at a 90° angle.

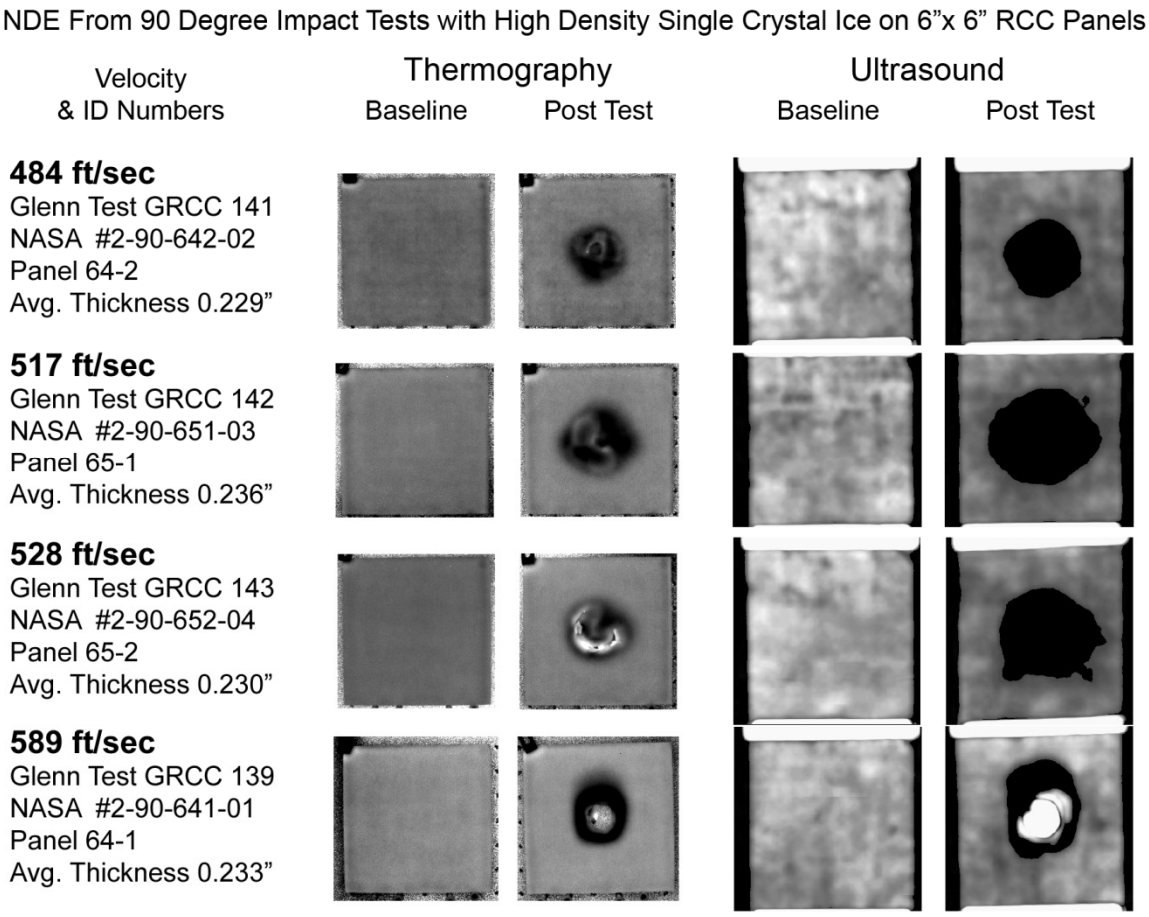

Figure A1–3.—Pulse thermography and ultrasound post impact pre- and posttest images of reinforced carbon-carbon 6- by 6-in. flat panels impacted with high-density poly-crystal ice cylinders (nominally 0.66 in. in diameter by 1.66 in.) at a 90° angle.

Aramis Displacement Contours from 90 Degree Impact Tests with High Density Poly-Crystal Ice on 6”x 6” RCC Panels

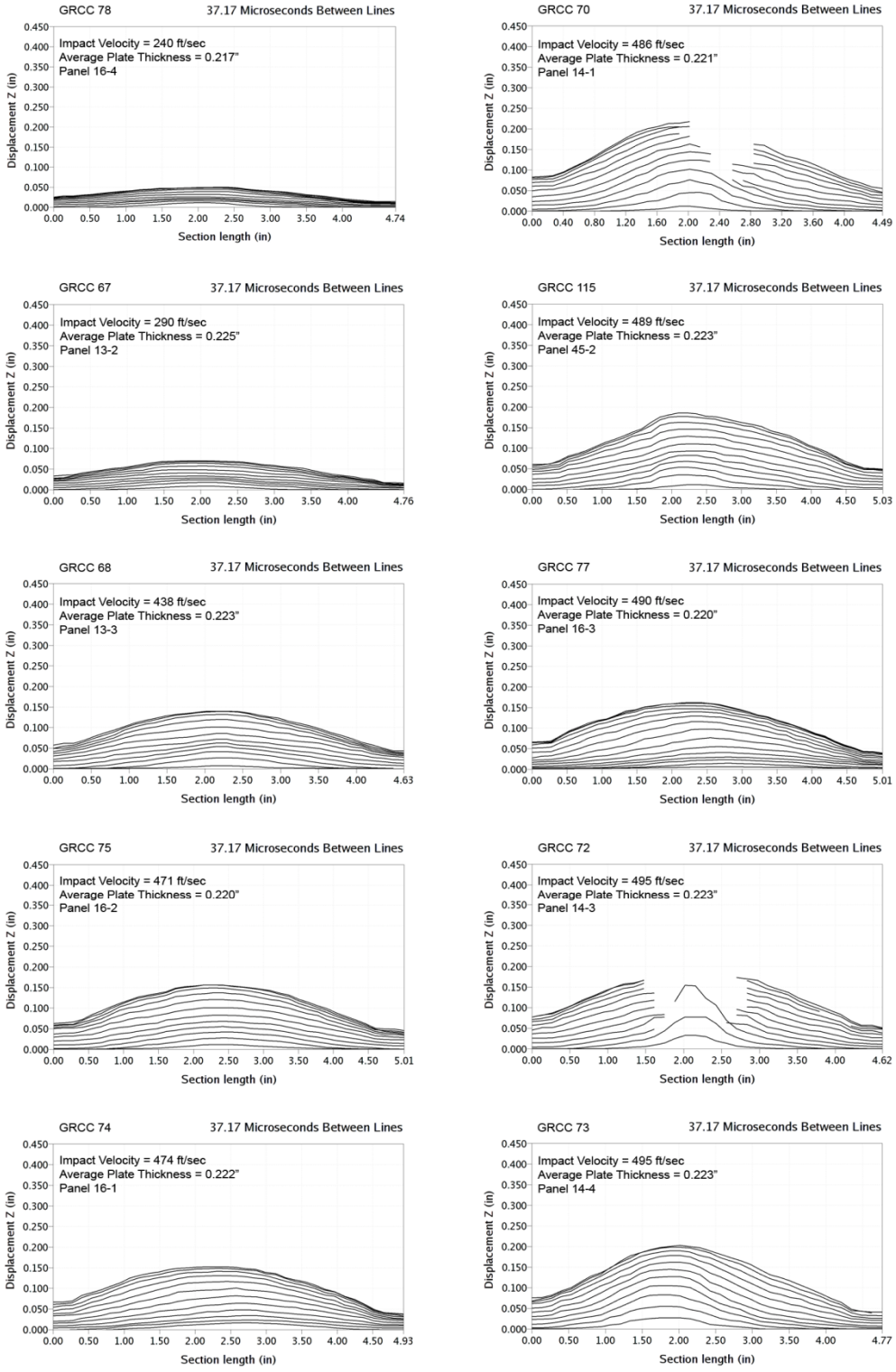

Figure A2–1.—ARAMIS out-of-plane deformation contours across centerline of 6- by 6-in. reinforced carbon-carbon flat panels measured at 37 μs increments undergoing impact with high-density poly-crystal ice cylinders (nominally 0.66 in. in diameter by 1.66 in.) at a 90° angle.

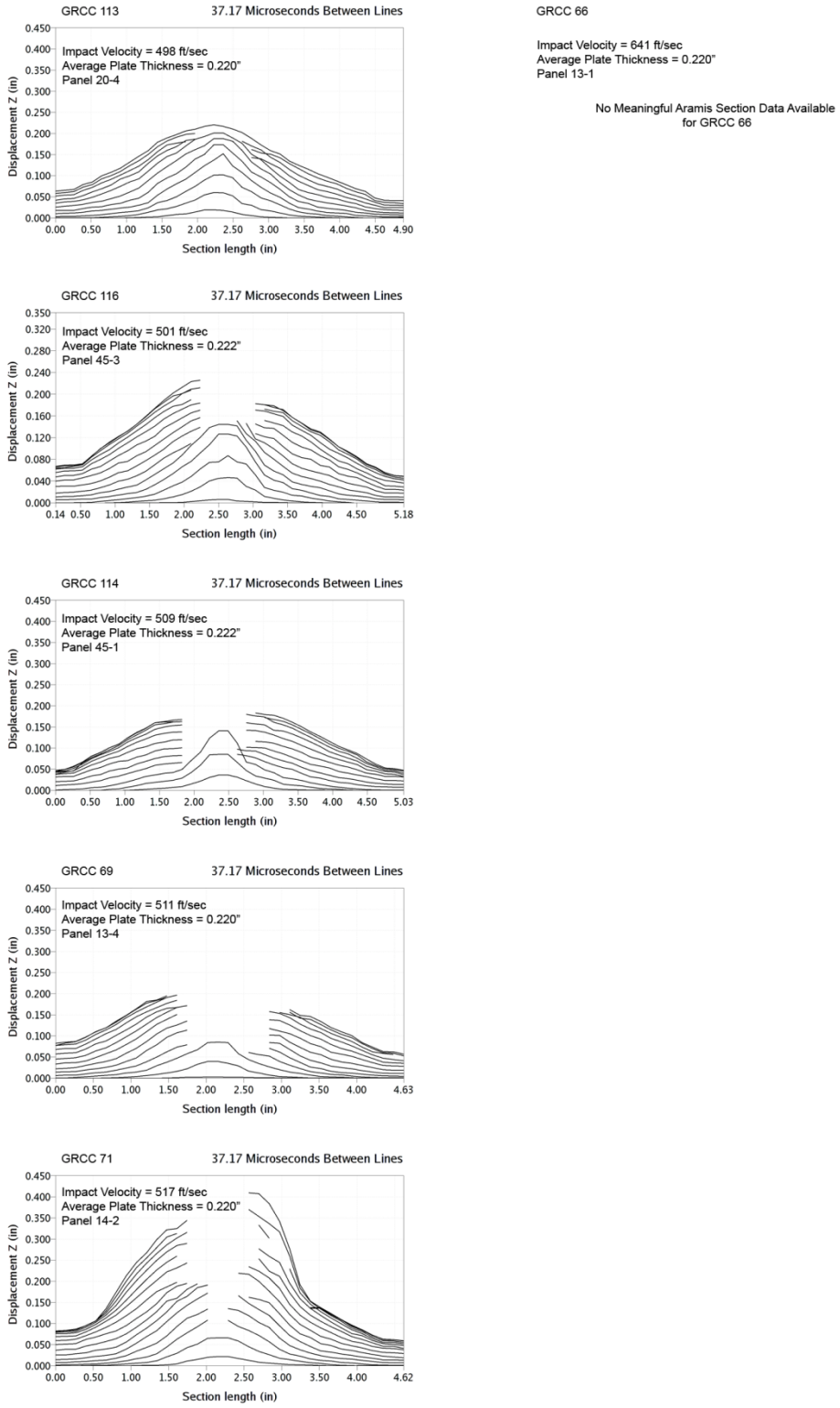

Figure A2–2.—ARAMIS out-of-plane deformation contours across centerline of 6- by 6-in. reinforced carbon-carbon flat panels plotted at 37 μs increments undergoing impact with high-density poly-crystal ice cylinders (nominally 0.66 in. in diameter by 1.66 in.) at a 90° angle.

Aramis Displacement Contours from 90 Degree Impact Tests with High Density Single Crystal Ice on 6”x 6” RCC Panels

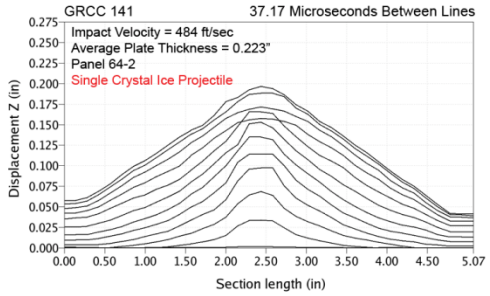

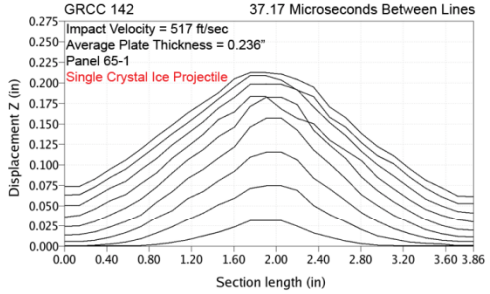

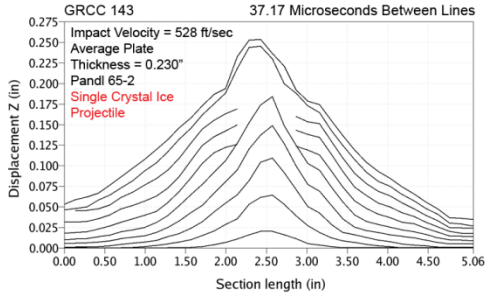

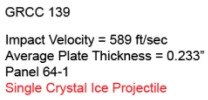

No Meaningful Aramis Section Data
Generated for GRCC 139

Figure A2–2.—Concluded.

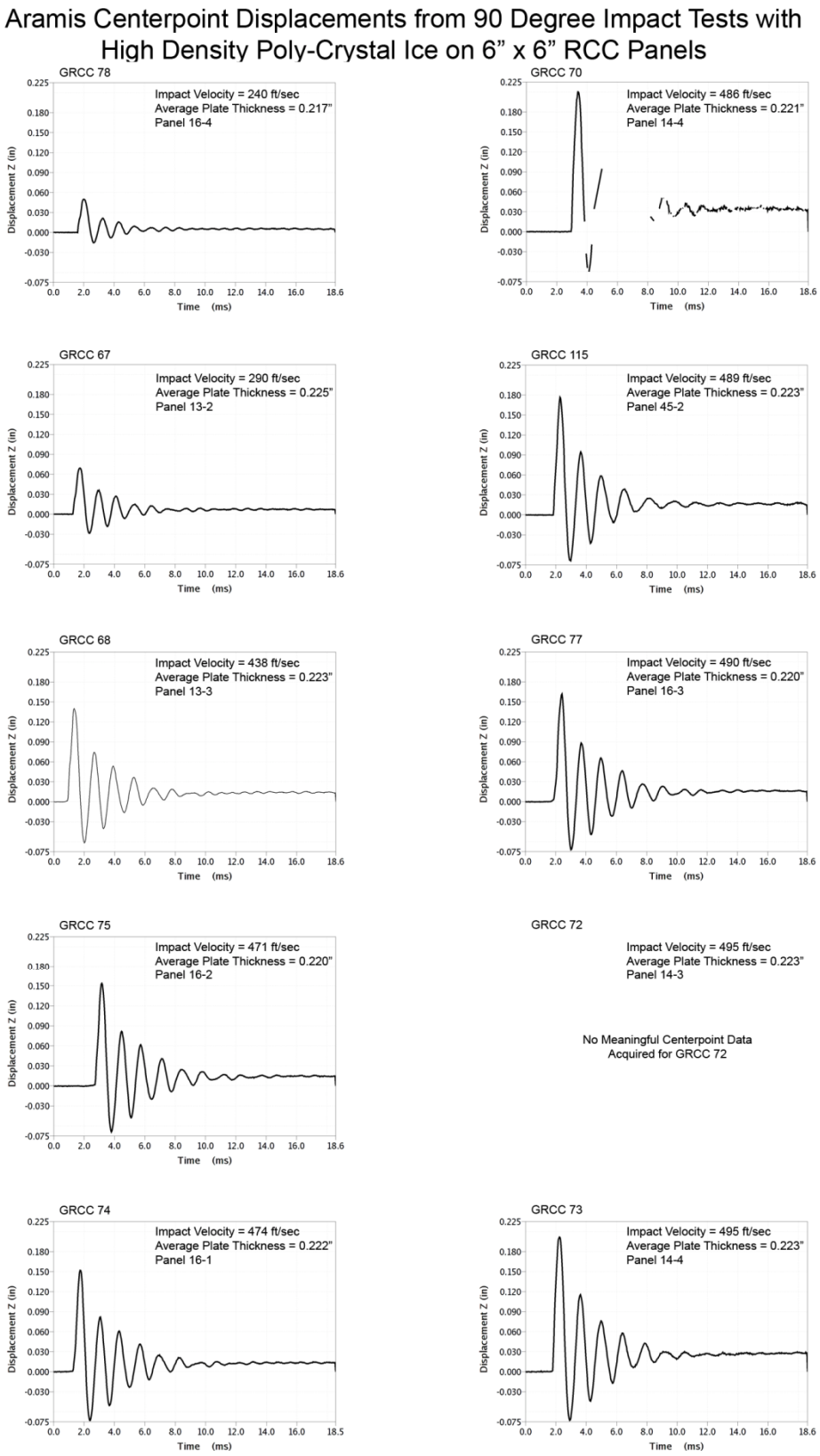

Figure A3–1.—ARAMIS centerpoint out-of-plane deformation vs. time of 6- by 6-in. reinforced carbon-carbon flat panels impacted with high-density poly-crystal ice cylinders (nominally 0.66 in. in diameter by 1.66 in.) at a 90° angle.

Figure A3–2.—ARAMIS centerpoint out-of-plane deformation versus time of 6- by 6-in. reinforced carbon-carbon flat panels impacted with high-density poly-crystal ice cylinders (nominally 0.66 in. in diameter by 1.66 in.) at a 90° angle.

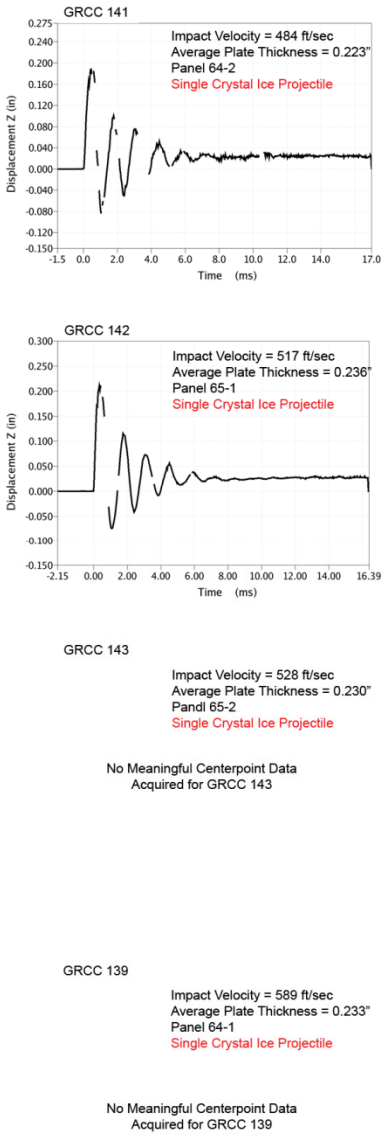

Figure A3–3.—ARAMIS centerpoint out-of-plane deformation versus time of 6- by 6-in. reinforced carbon-carbon flat panels impacted with high-density single-crystal ice cylinders (nominally 0.66 in. in diameter by 1.66 in.) at a 90° angle.

Aramis Maximum Displacement Fringe Plots from 90 Degree Impact Tests with High Density Poly-Crystal Ice on 6” x 6” RCC Panels

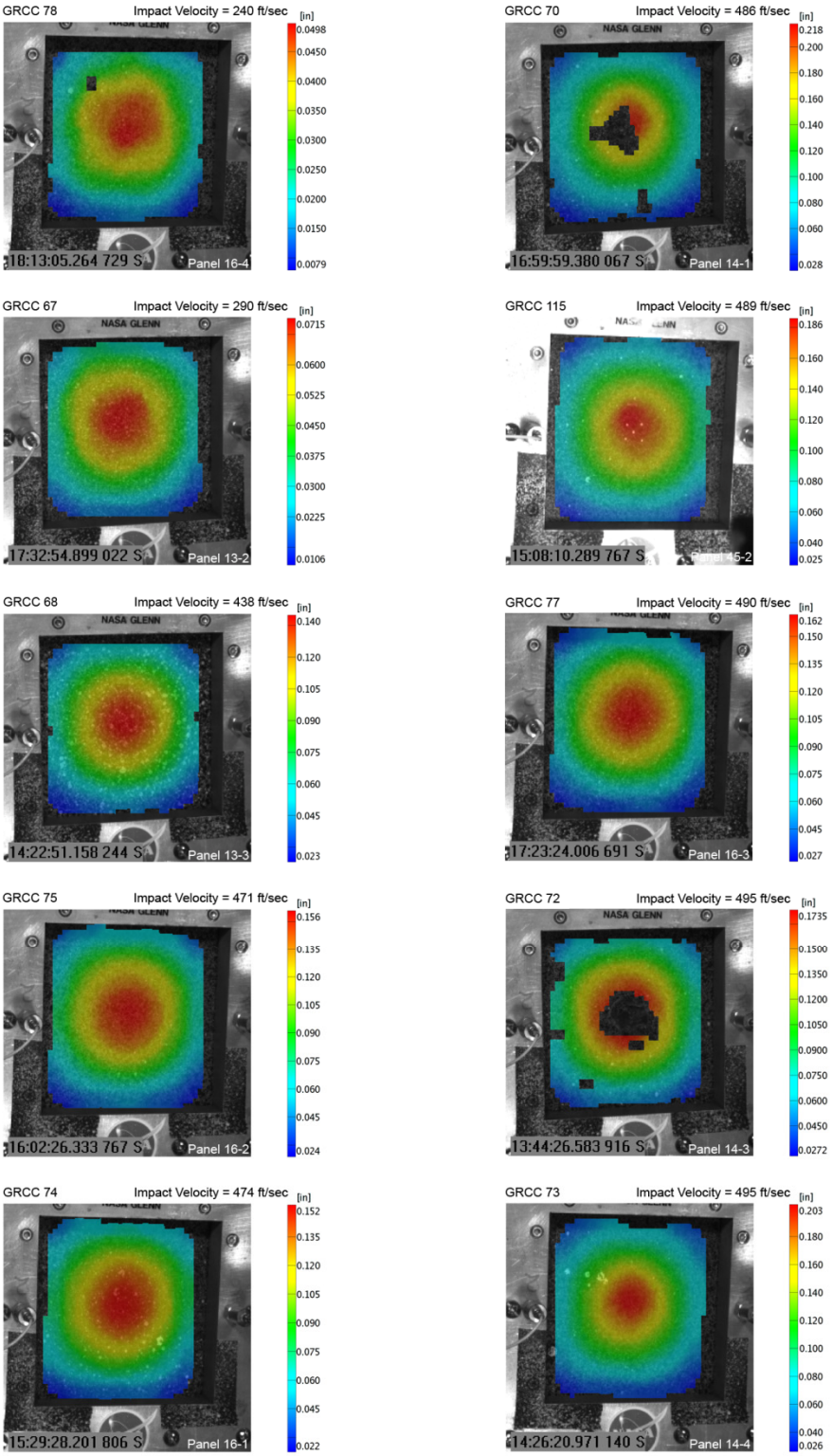

Figure A4–1.—ARAMIS color fringe plots depicting maximum deformation prior to material failure of 6- by 6-in. reinforced carbon-carbon flat panels as they undergo impact with high-density poly-crystal ice cylinders (nominally 0.66 in. in diameter by 1.66 in.) at a 90° angle.

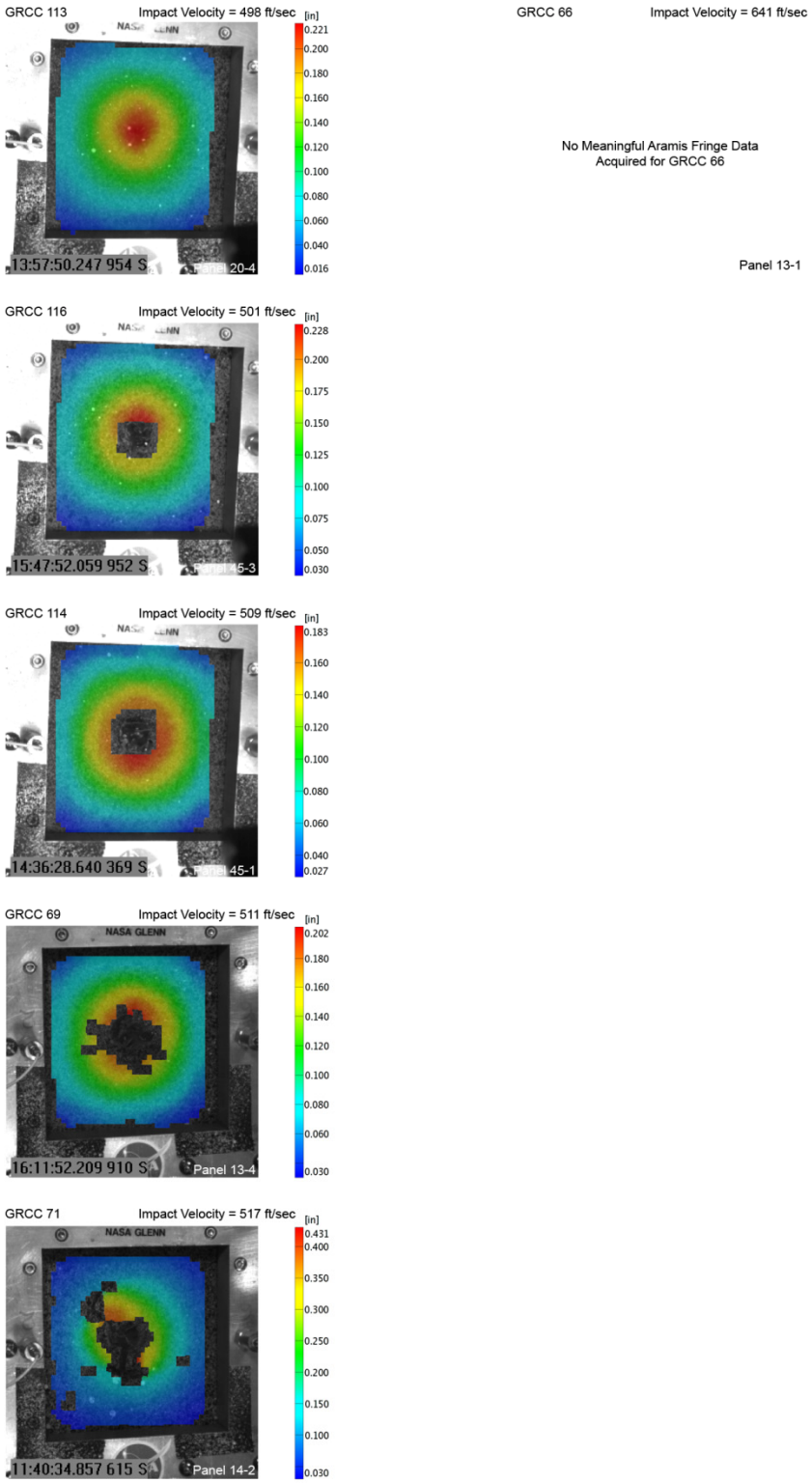

Figure A4–2.—ARAMIS color fringe plots depicting maximum deformation prior to material failure of 6- by 6-in. reinforced carbon-carbon flat panels as they undergo impact with high-density poly-crystal ice cylinders (nominally 0.66 in. in diameter by 1.66 in.) at a 90° angle.

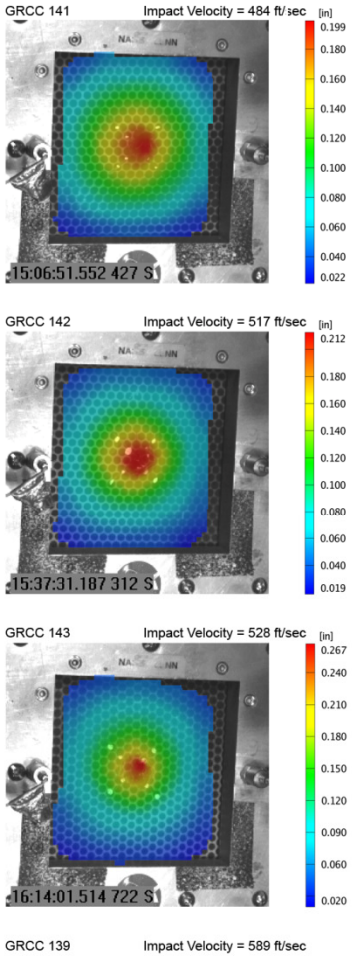

Figure A4–2.—ARAMIS color fringe plots depicting maximum deformation prior to material failure of 6- by 6-in. reinforced carbon-carbon flat panels as they undergo impact with high-density single-crystal ice cylinders (nominally 0.66 in. in diameter by 1.66 in.) at a 90° angle.

Figure A5–1.—Edges and faces of panel 16-4 at 240 ft/s with a high-density, poly-crystal ice cylinder (nominally 0.66 in. in diameter by 1.66 in.) at 90° impact angle. Test GRCC 78.

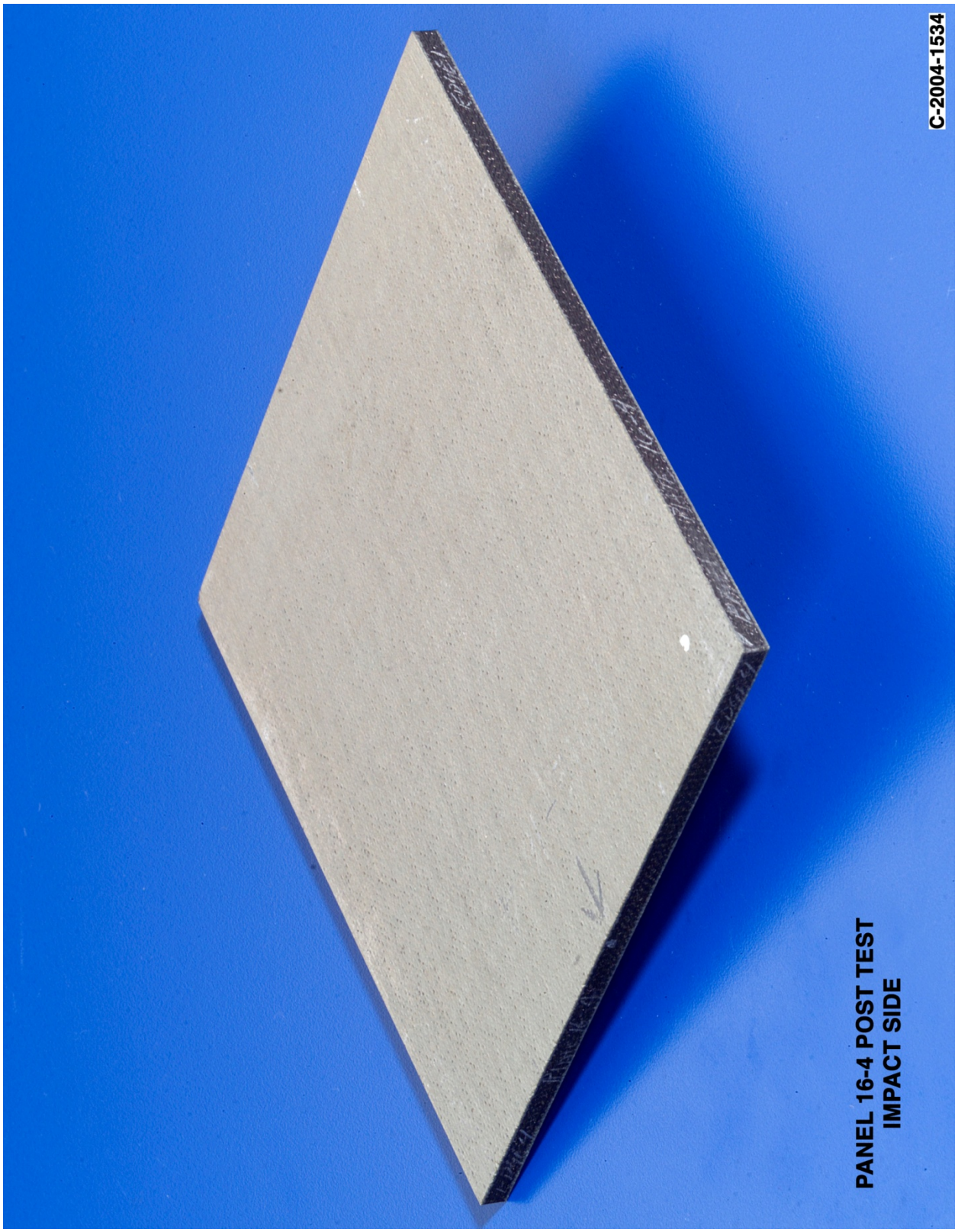

Figure A5–2.—Front (impact side) of panel 16-4 at 240 ft/s with a high-density, poly-crystal ice cylinder (nominally 0.66 in. in diameter by 1.66 in.) at 90° impact angle. Test GRCC 78.

Figure A5–3.—Back face of panel 16-4 at 240 ft/s with a high-density, poly-crystal ice cylinder (nominally 0.66 in. in diameter by 1.66 in.) at 90° impact angle. Test GRCC 78.

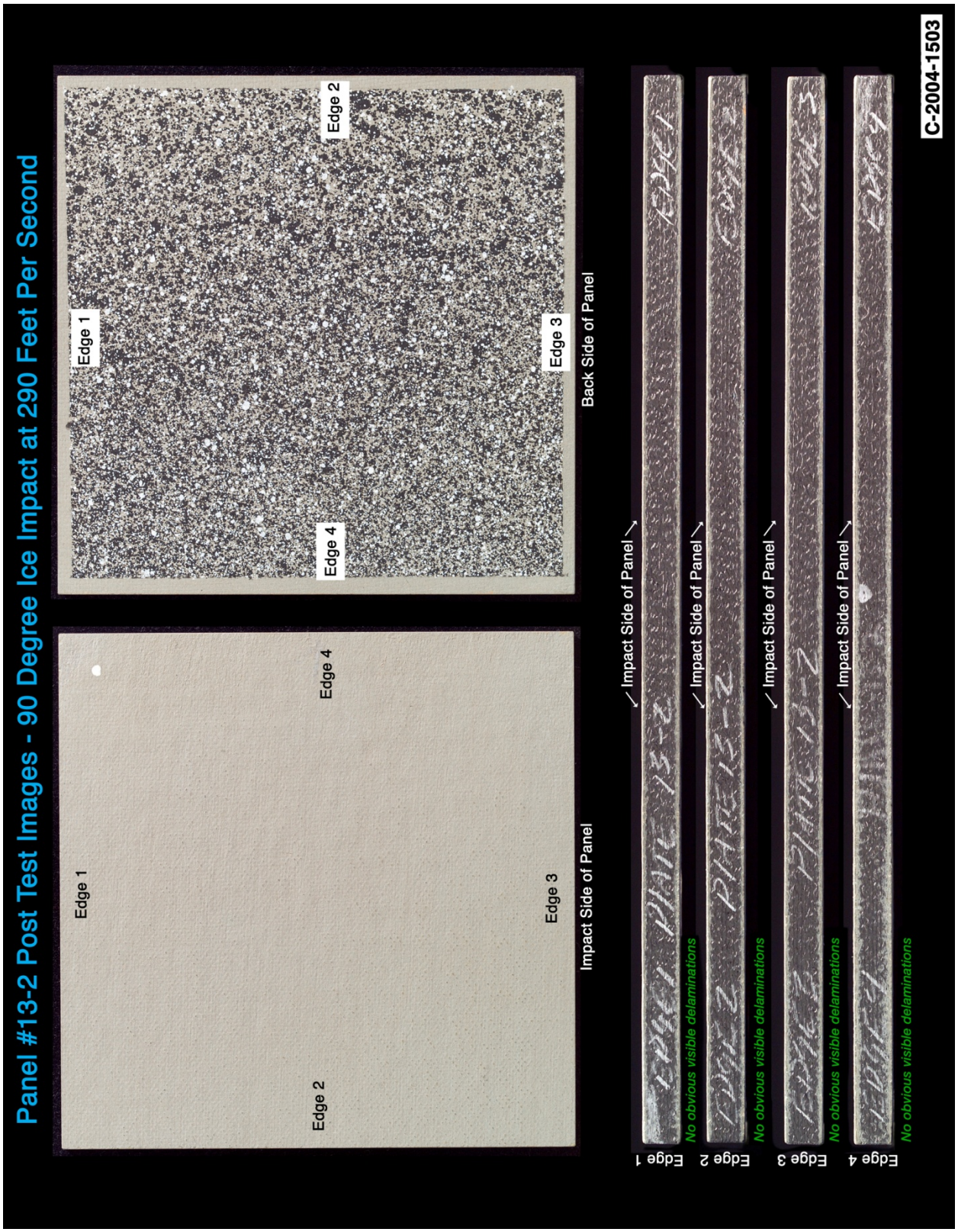

Figure A6–1.—Edges and faces of panel 13-2 at 290 ft/s with a high-density, poly-crystal ice cylinder (nominally 0.66 in. in diameter by 1.66 in.) at 90° impact. Test GRCC 67.

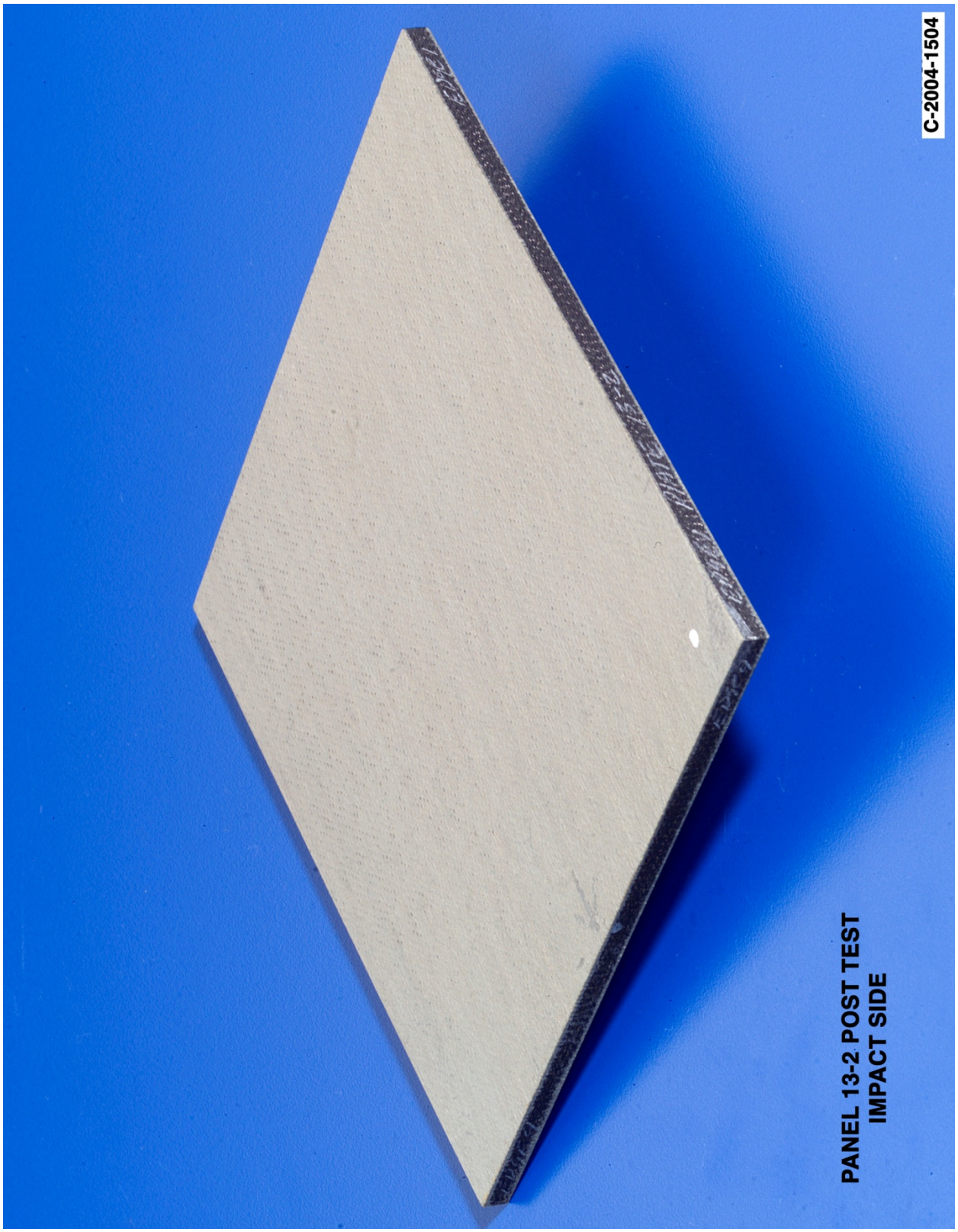

Figure A6–2.—Front (impact side) of panel 13-2 at 290 ft/s with a high-density, poly-crystal ice cylinder (nominally 0.66 in. in diameter by 1.66 in.) at 90° impact angle. Test GRCC 67.

Figure A6–3.—Back face of panel 13-2 at 290 ft/s with a high-density, poly-crystal ice cylinder (nominally 0.66 in. in diameter by 1.66 in.) at 90° impact angle. Test GRCC 67.

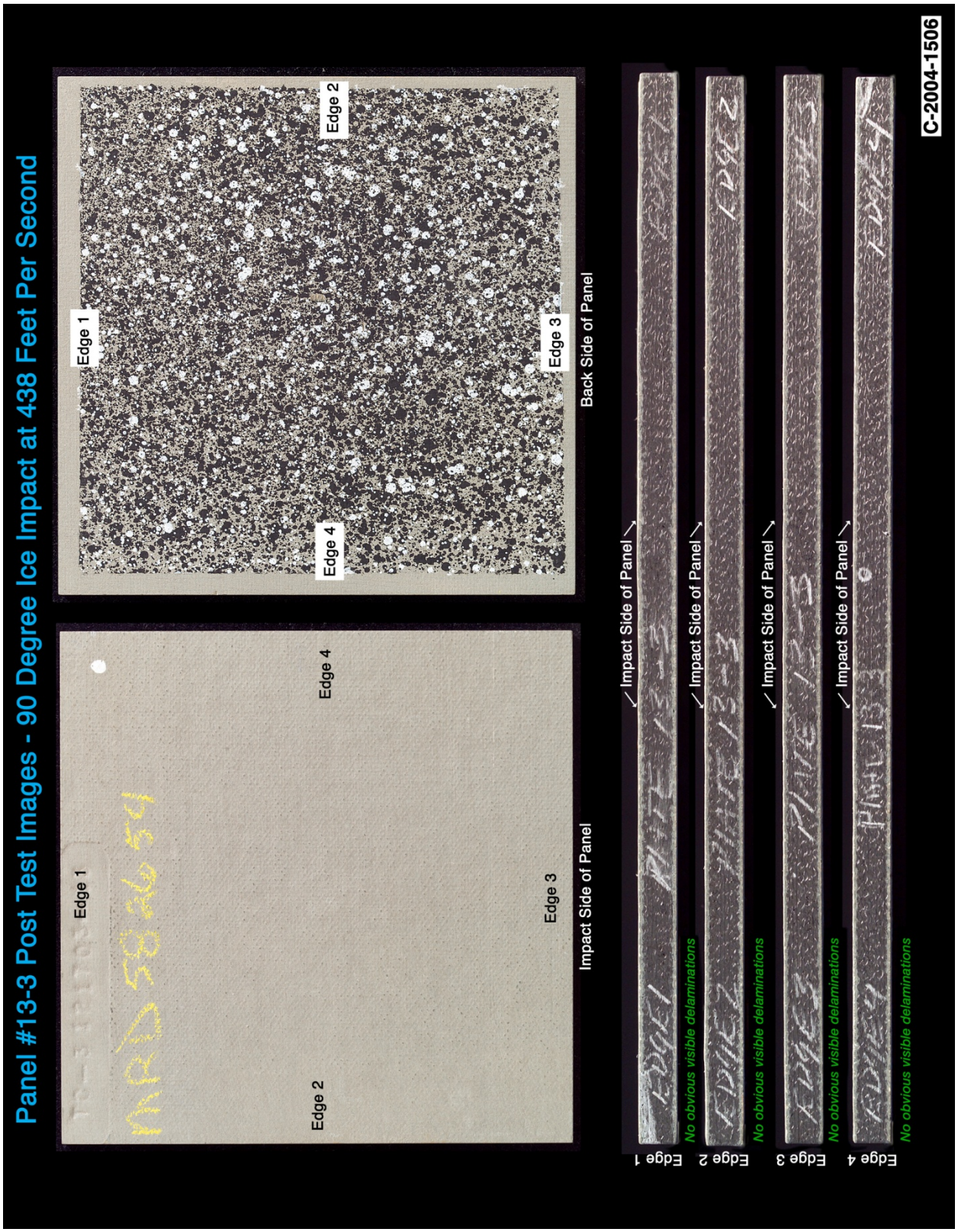

Figure A7–1.—Edges and faces of panel 13-3 at 438 ft/s with a high-density, poly-crystal ice cylinder (nominally 0.66 in. in diameter by 1.66 in.) at 90° impact. Test GRCC 68.

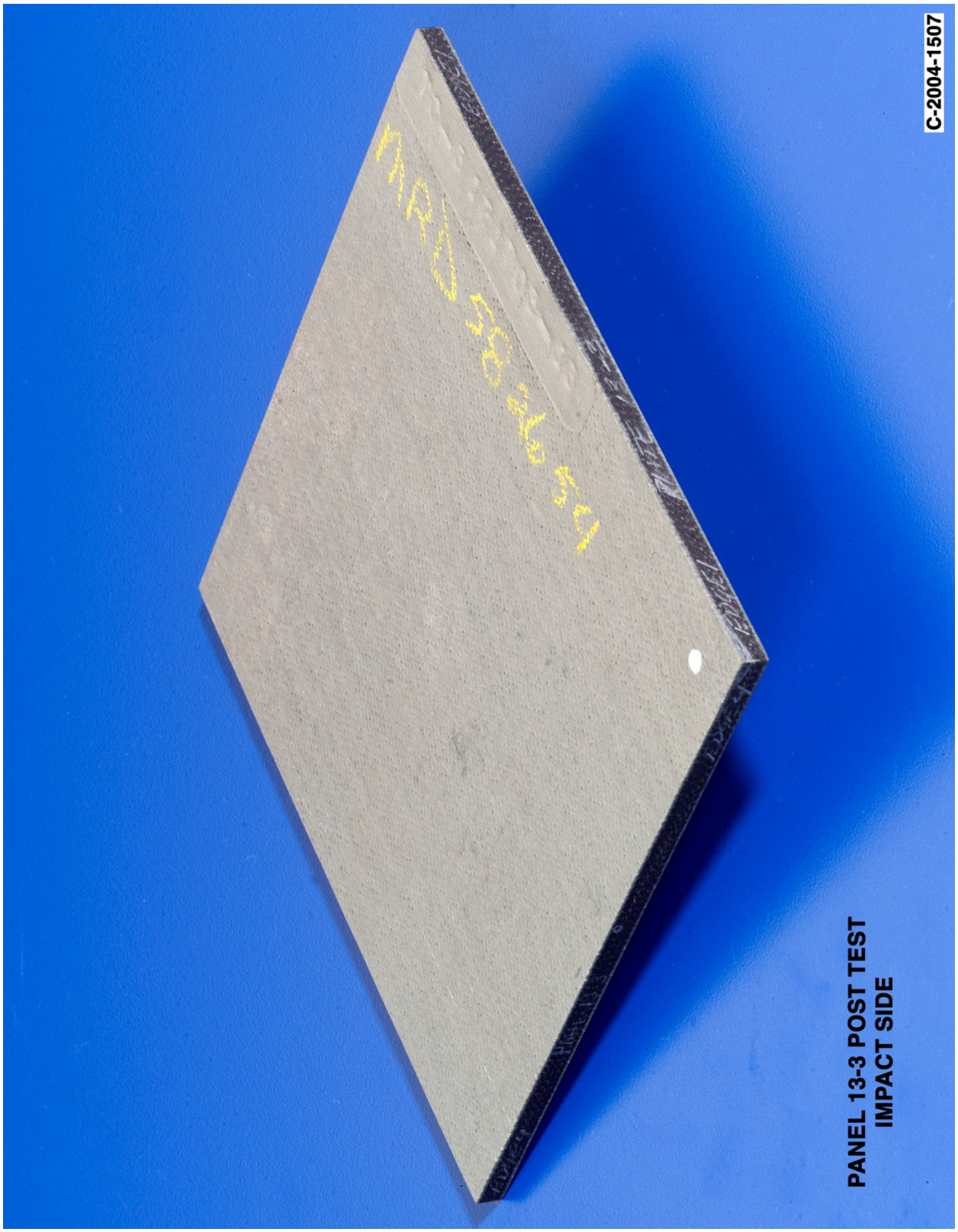

Figure A7–2.—Front (impact side) of panel 13-3 at 438 ft/s with a high-density, poly-crystal ice cylinder (nominally 0.66 in. in diameter by 1.66 in.) at 90° impact angle. Test GRCC 68.

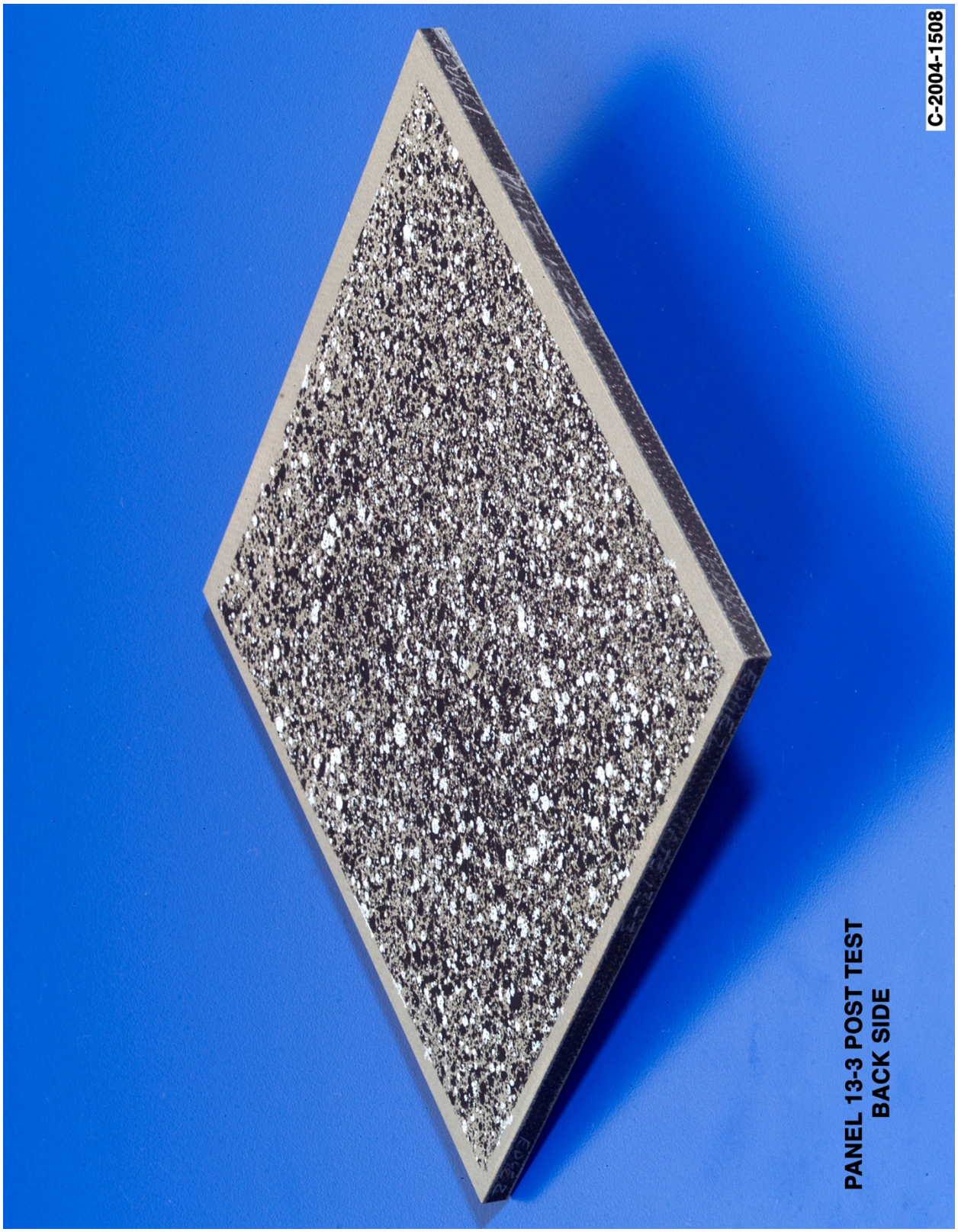

Figure A7–3.—Back face of panel 13-3 at 438 ft/s with a high-density, poly-crystal ice cylinder (nominally 0.66 in. in diameter by 1.66 in.) at 90° impact angle. Test GRCC 68.

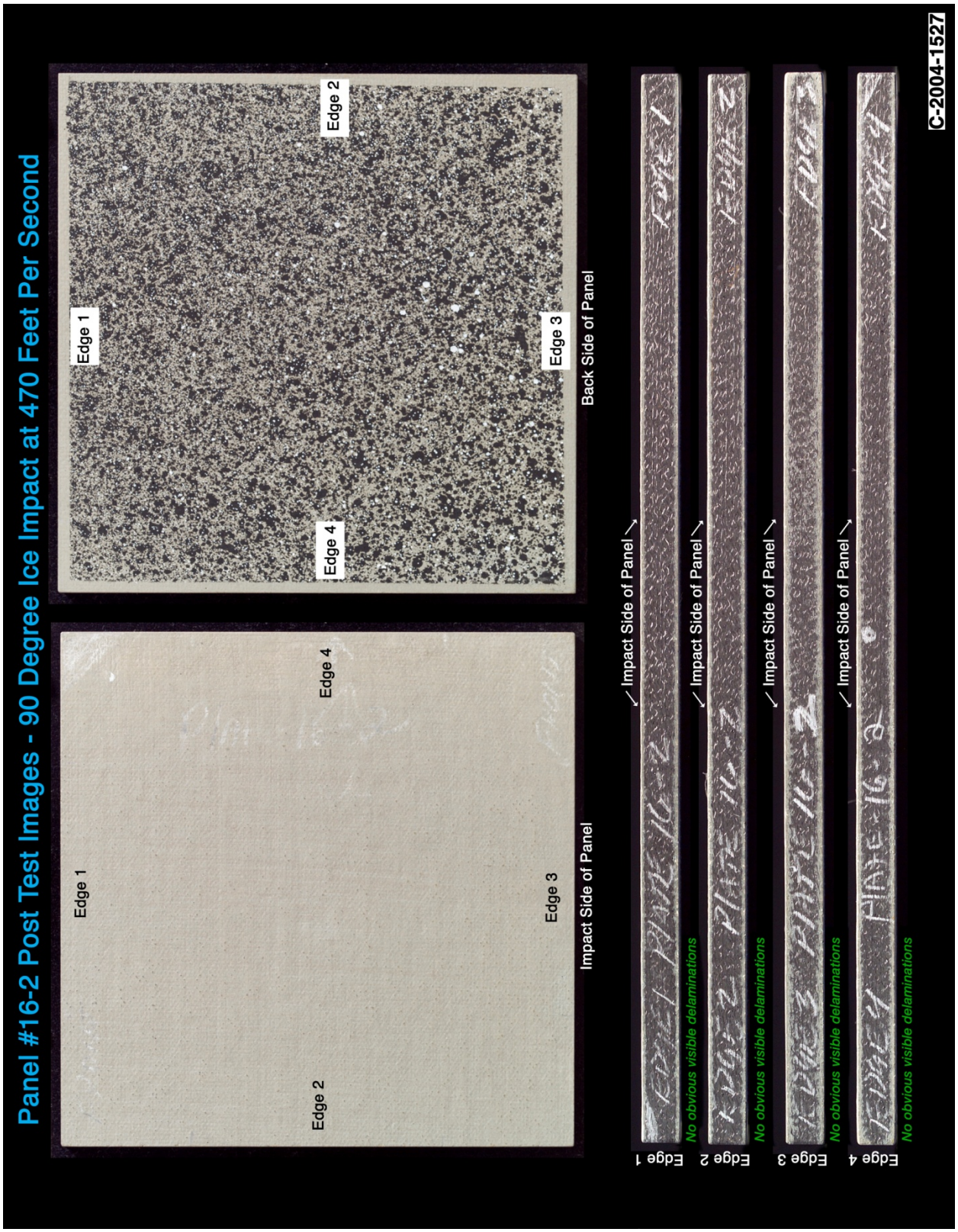

Figure A8–1.—Edges and faces of panel 16-2 at 470 ft/s with a high-density, poly-crystal ice cylinder (nominally 0.66 in. in diameter by 1.66 in.) at 90° impact. Test GRCC 75.

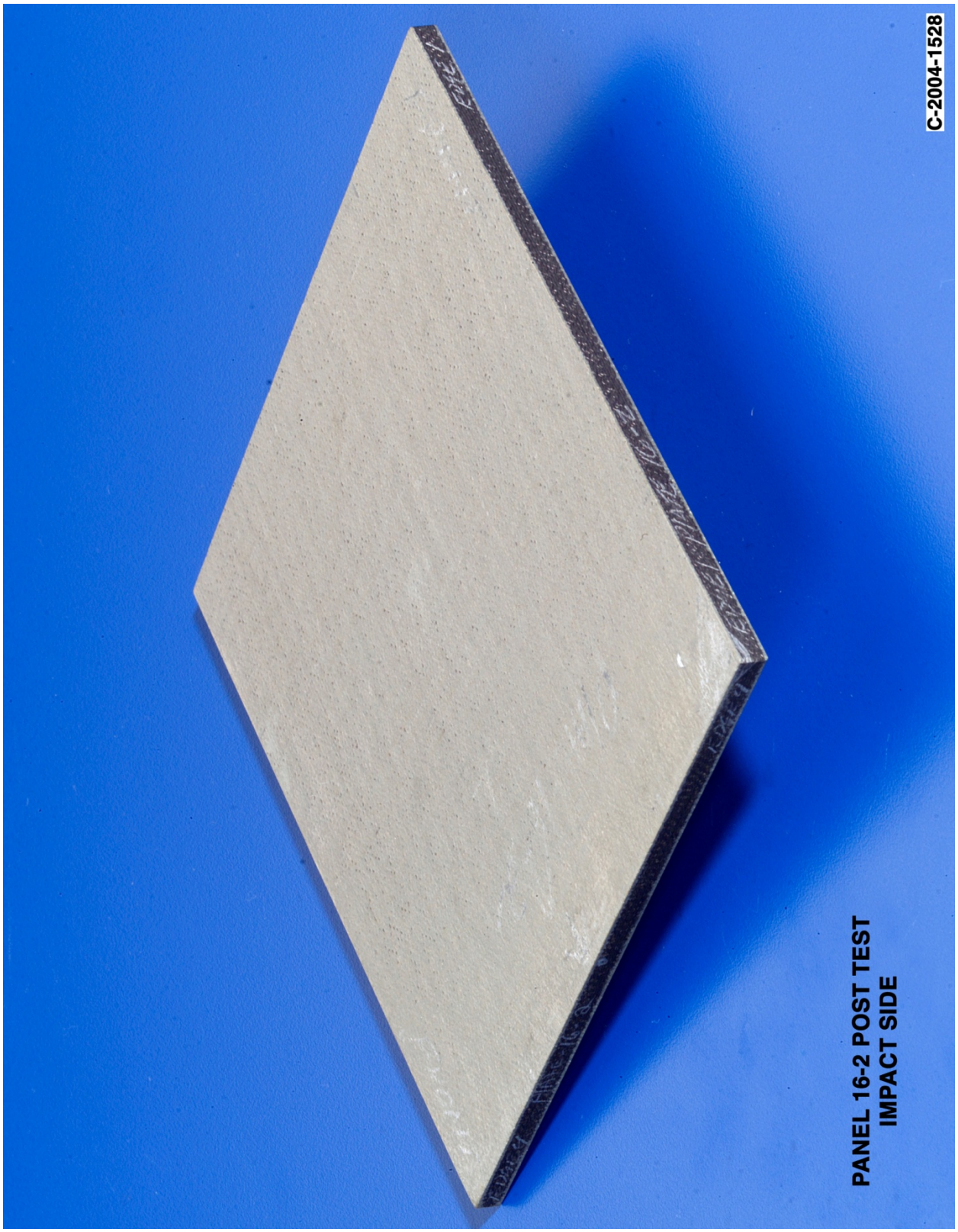

Figure A8–2.—Front (impact side) of panel 16-2 at 470 ft/s with a high-density, poly-crystal ice cylinder (nominally 0.66 in. in diameter by 1.66 in.) at 90° impact angle. Test GRCC 75.

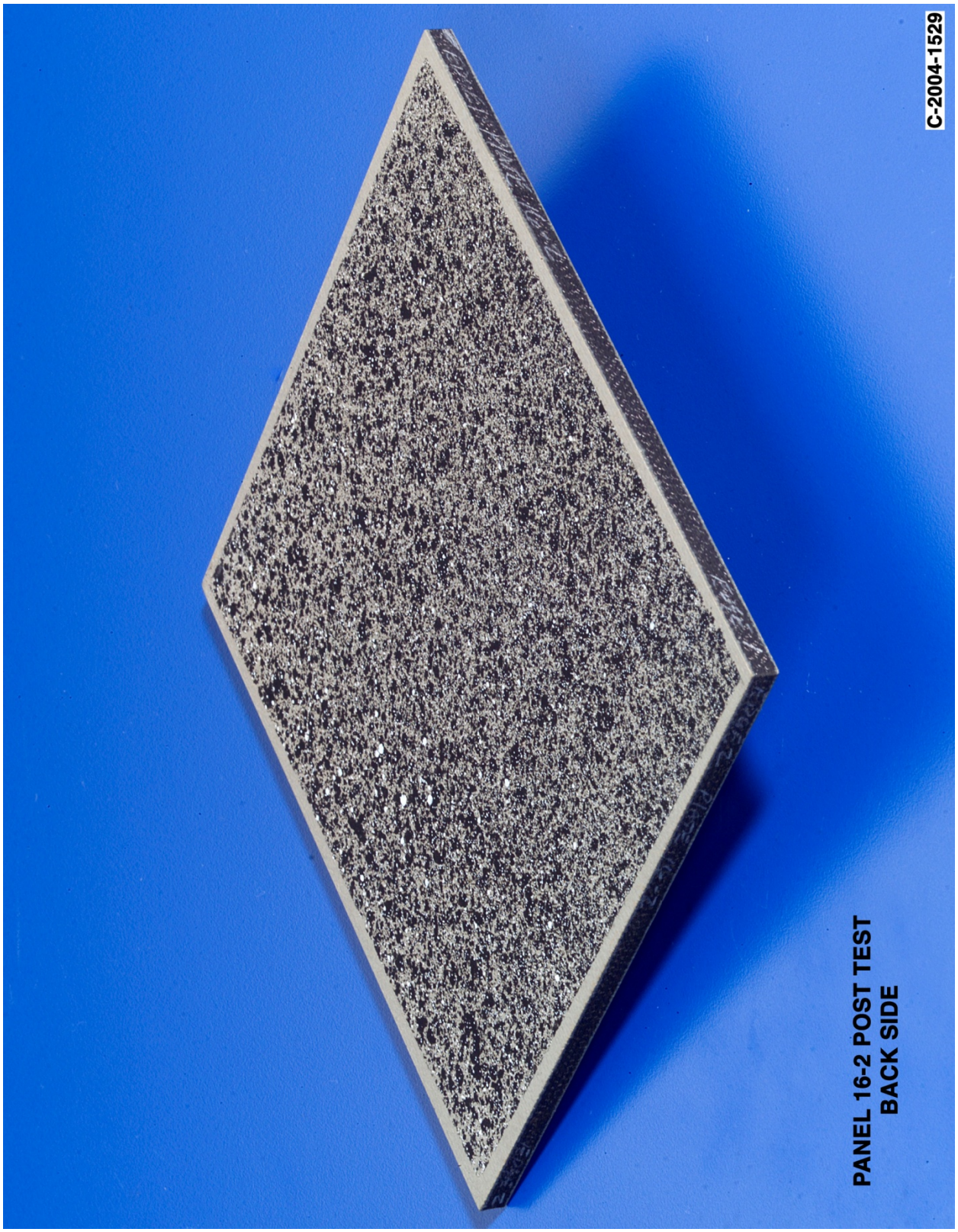

Figure A8–3.—Back face of panel 16-2 at 470 ft/s with a high-density, poly-crystal ice cylinder (nominally 0.66 in. in diameter by 1.66 in.) at 90° impact angle. Test GRCC 75.

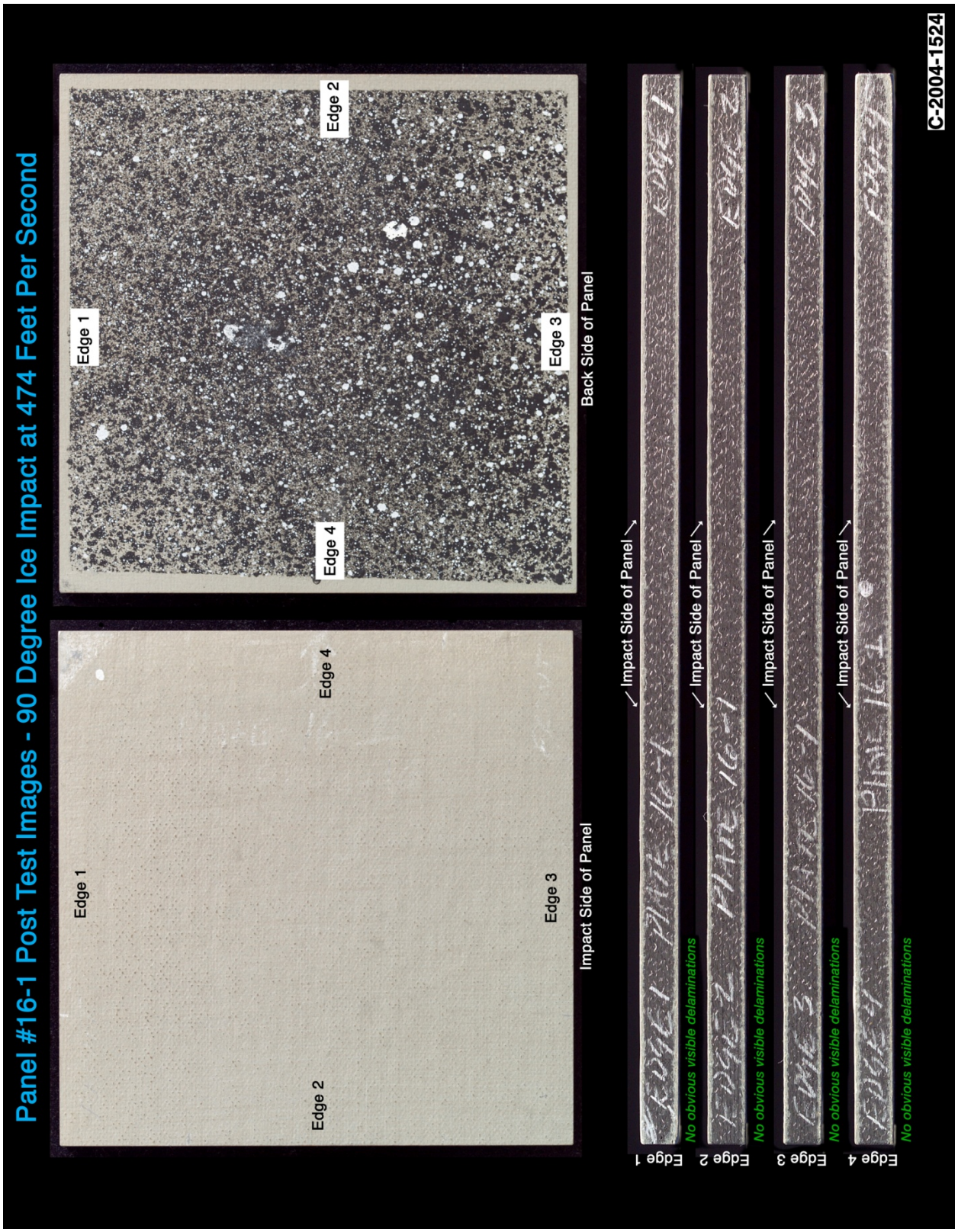

Figure A9–1.—Edges and faces of panel 16-1 at 474 ft/s with a high-density, poly-crystal ice cylinder (nominally 0.66 in. in diameter by 1.66 in.) at 90° impact. Test GRCC 74.

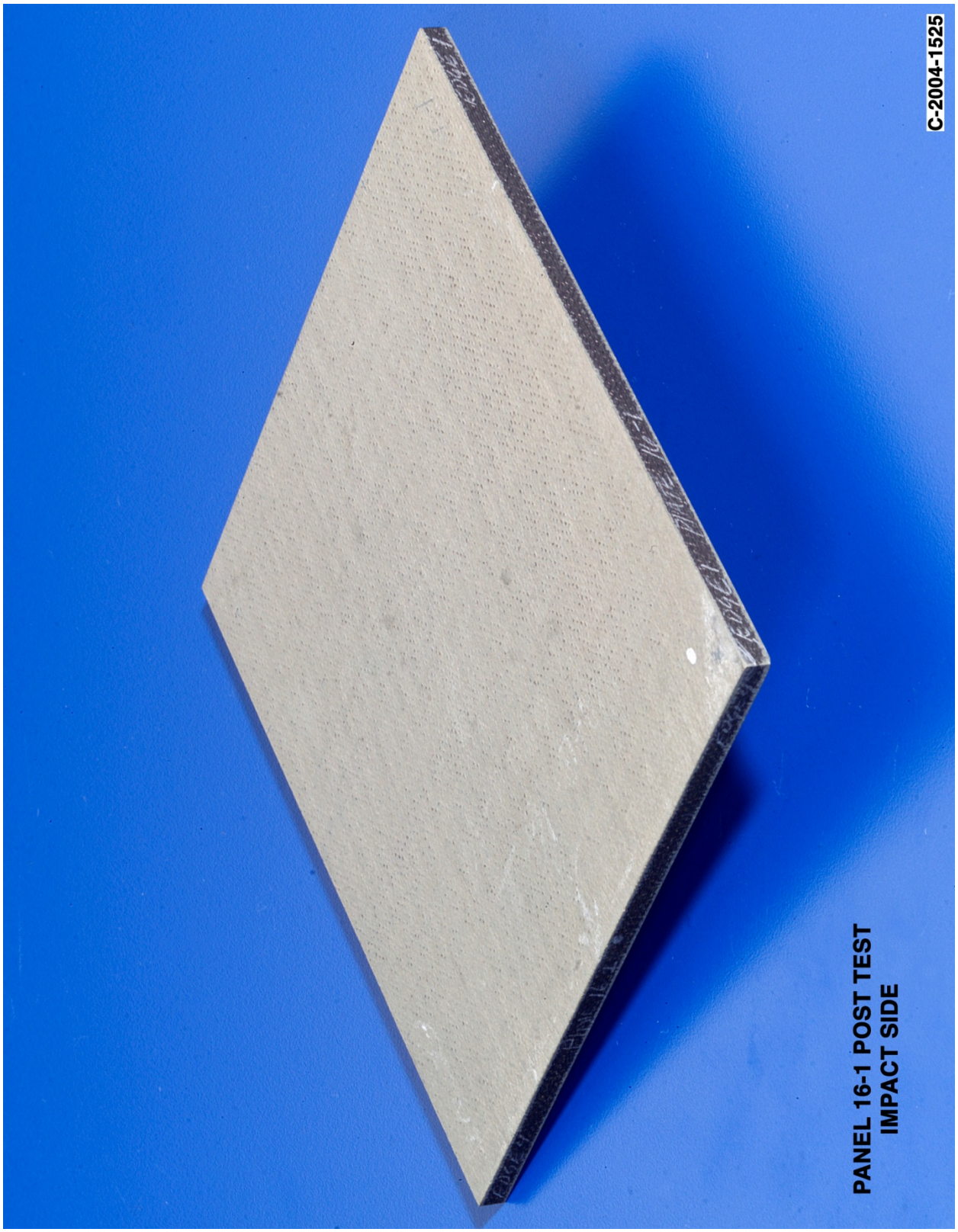

Figure A9–2.—Front (impact side) of panel 16-1 at 474 ft/s with a high-density, poly-crystal ice cylinder (nominally 0.66 in. in diameter by 1.66 in.) at 90° impact angle. Test GRCC 74.

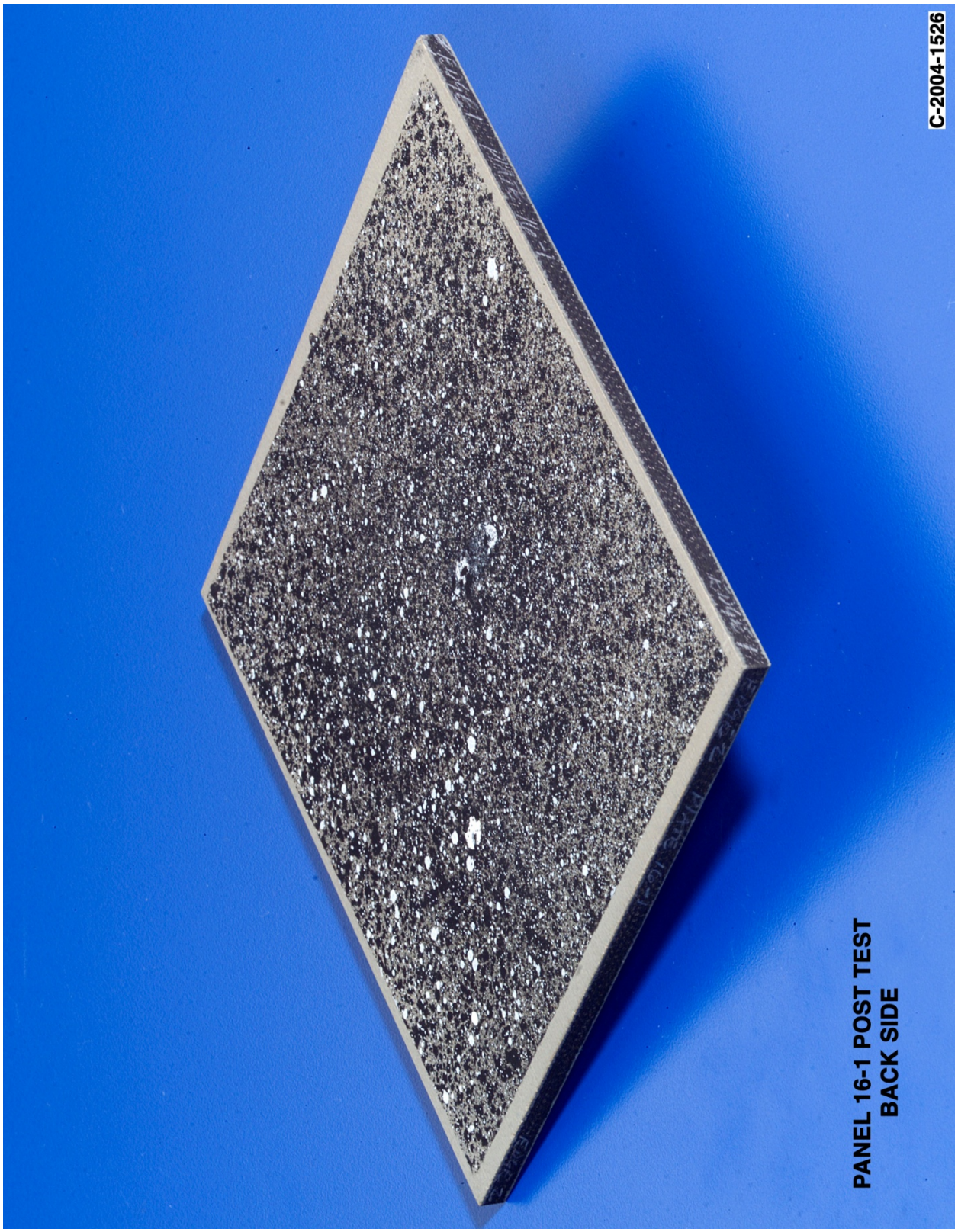

Figure A9–3.—Back face of panel 16-1 at 474 ft/s with a high-density, poly-crystal ice cylinder (nominally 0.66 in. in diameter by 1.66 in.) at 90° impact angle. Test GRCC 74.

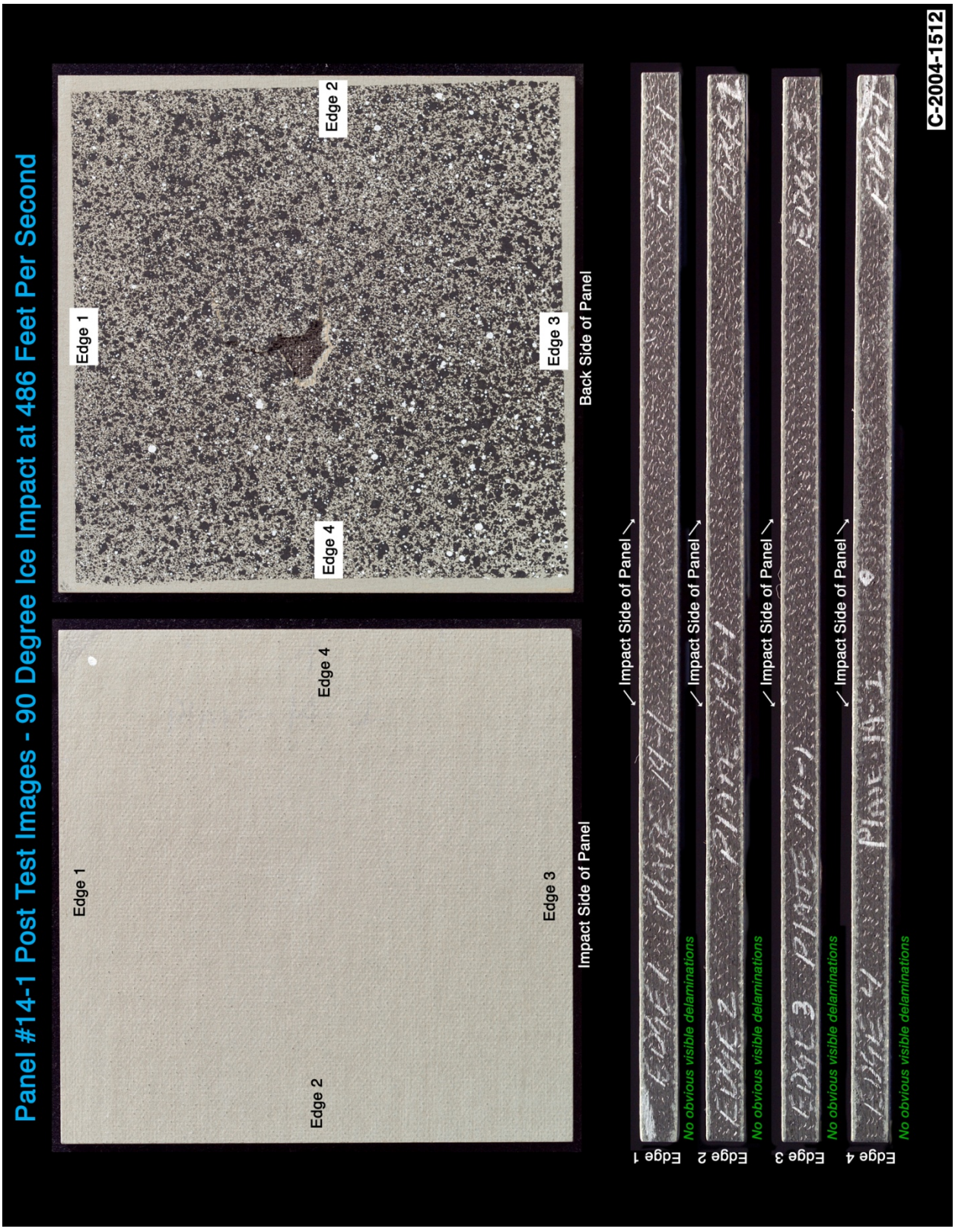

Figure A10–1.—Edges and faces of panel 14-1 at 486 ft/s with a high-density, poly-crystal ice cylinder (nominally 0.66 in. in diameter by 1.66 in.) at 90° impact. Test GRCC 70.

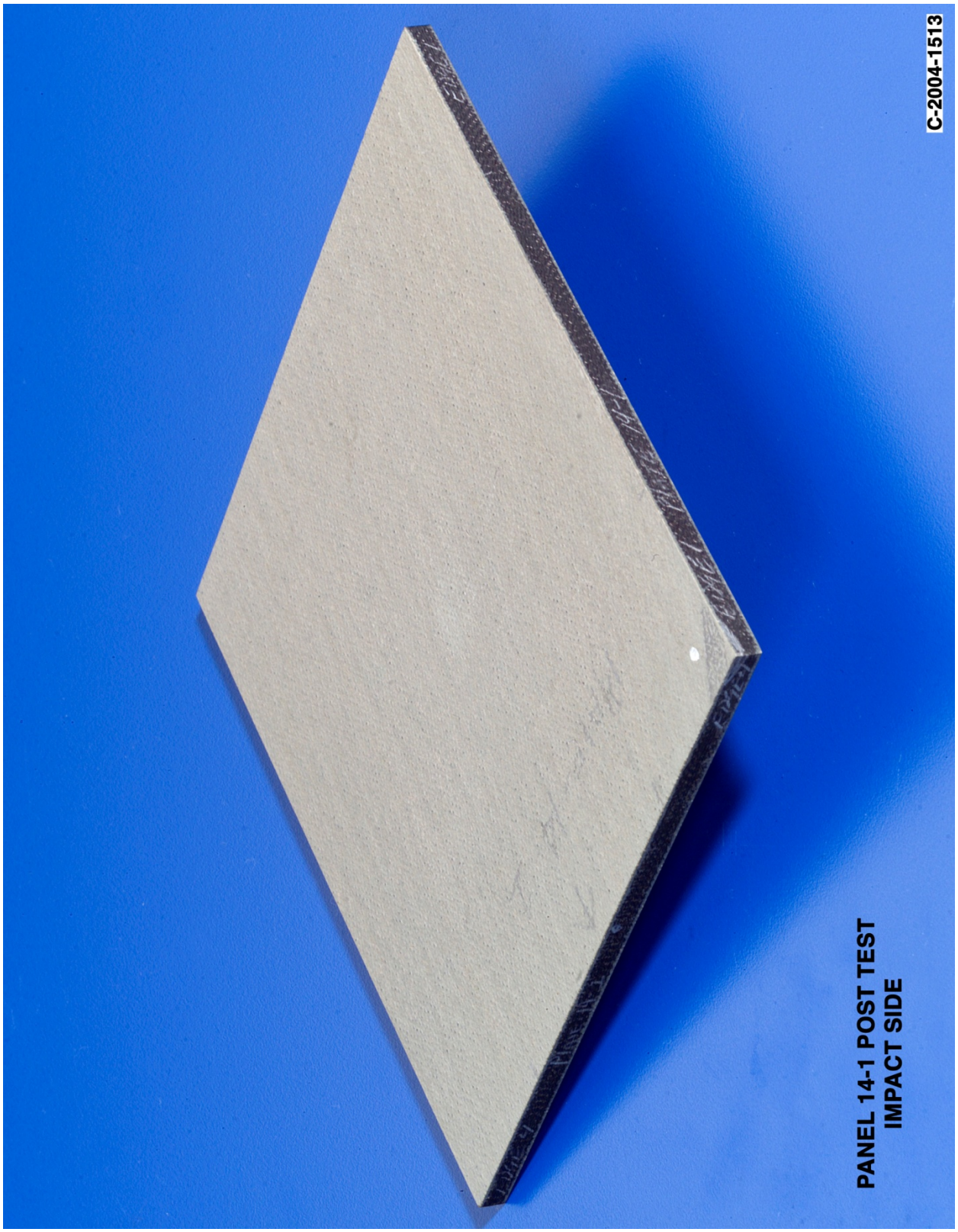

Figure A10–2.—Front (impact side) of panel 14-1 at 486 ft/s with a high-density, poly-crystal ice cylinder (nominally 0.66 in. in diameter by 1.66 in.) at 90° impact angle. Test GRCC 70.

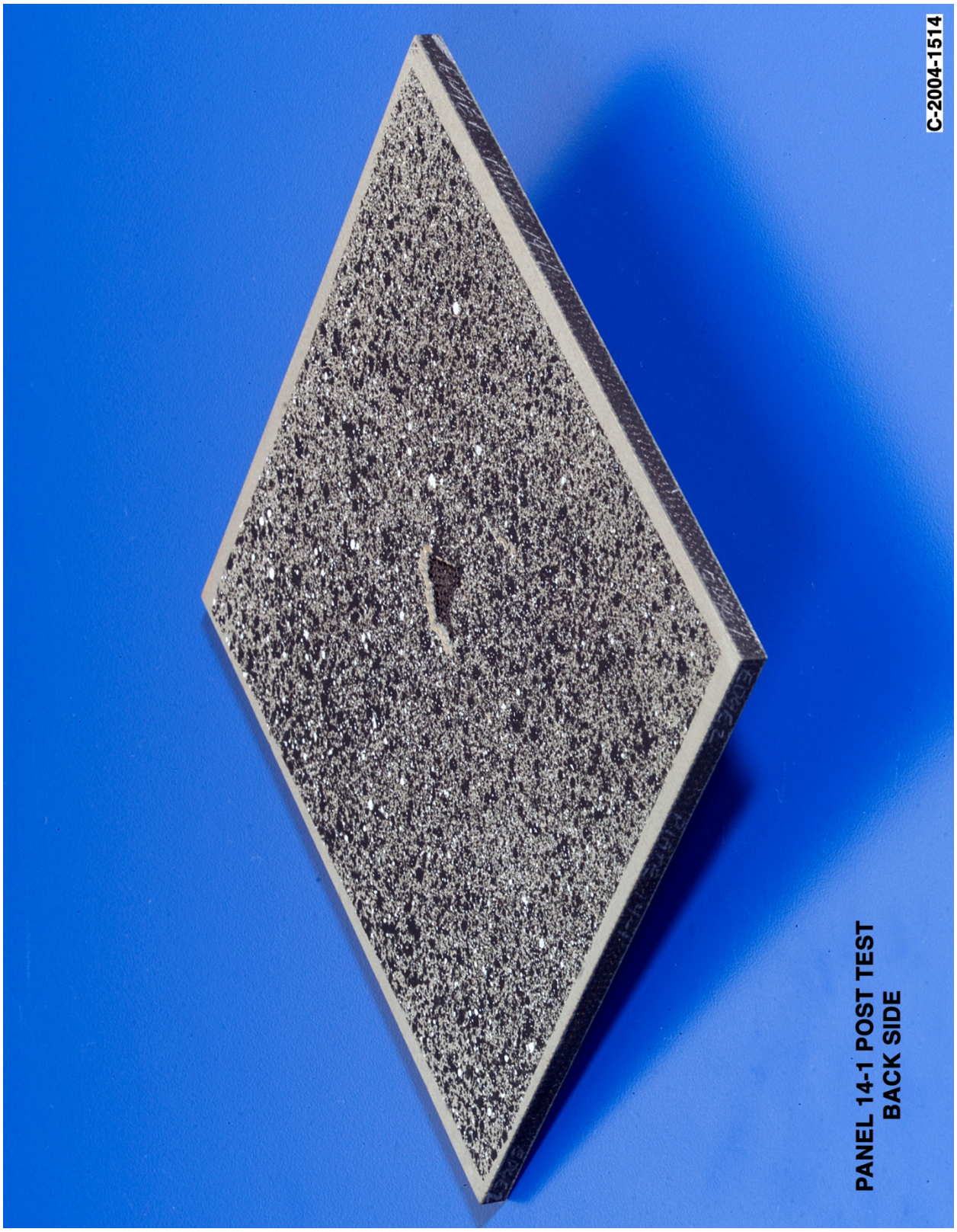

Figure A10–3.—Back face of panel 14-1at 486 ft/s with a high-density, poly-crystal ice cylinder (nominally 0.66 in. in diameter by 1.66 in.) at 90° impact angle. Test GRCC 70.

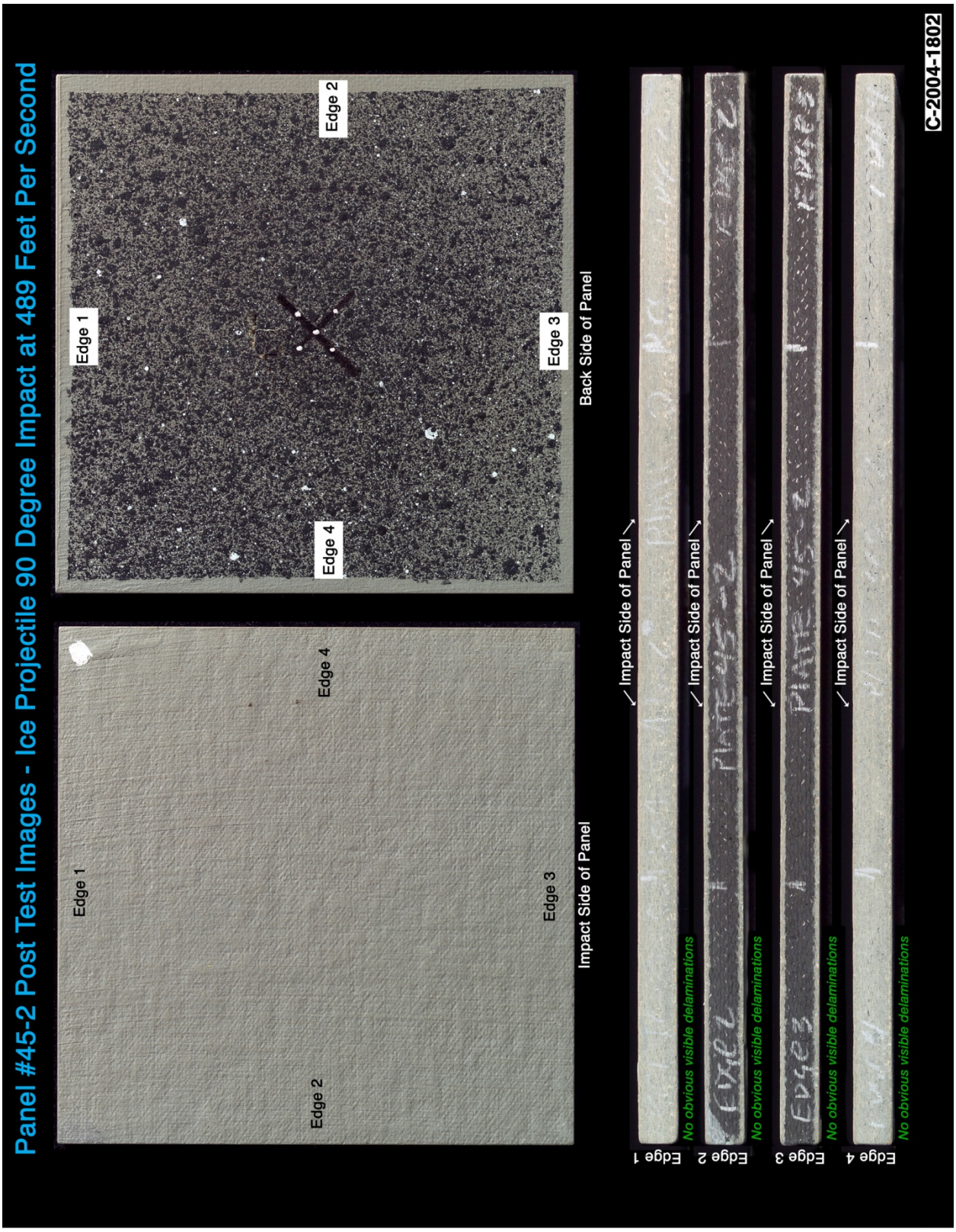

Figure A11–1.—Edges and faces of panel 45-2 at 489 ft/s with a high-density, poly-crystal ice cylinder (nominally 0.66 in. in diameter by 1.66 in.) at 90° impact. Test GRCC 115.

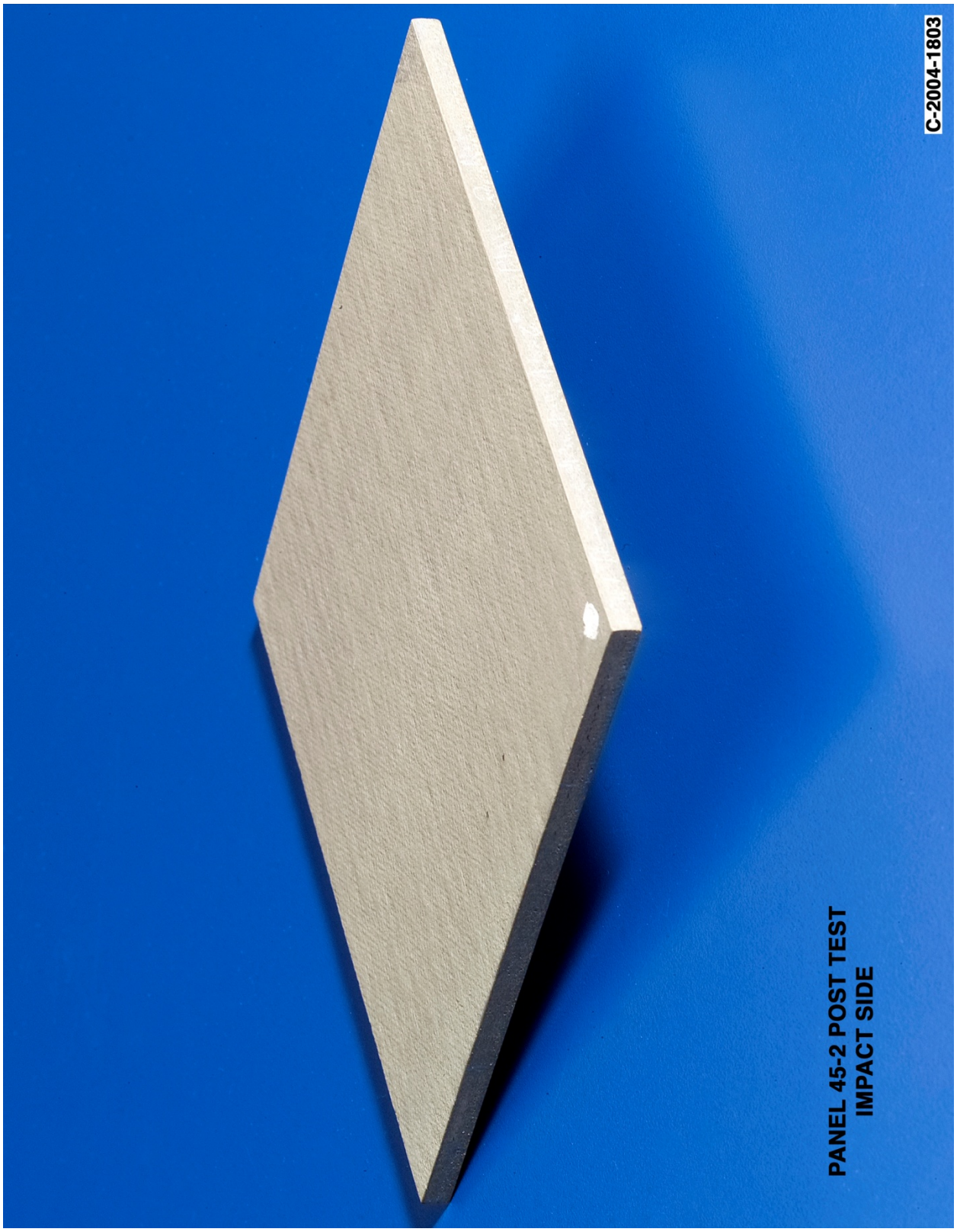

Figure A11–2.—Front (impact side) of panel 45-2 at 489 ft/s with a high-density, poly-crystal ice cylinder (nominally 0.66 in. in diameter by 1.66 in.) at 90° impact angle. Test GRCC 115.

Figure A11–3.—Back face of panel 45-2 at 489 ft/s with a high-density, poly-crystal ice cylinder (nominally 0.66 in. in diameter by 1.66 in.) at 90° impact angle. Test GRCC 115.

Figure A12–1.—Edges and faces of panel 16-3 at 490 ft/s with a high-density, poly-crystal ice cylinder (nominally 0.66 in. in diameter by 1.66 in.) at 90° impact. Test GRCC 77.

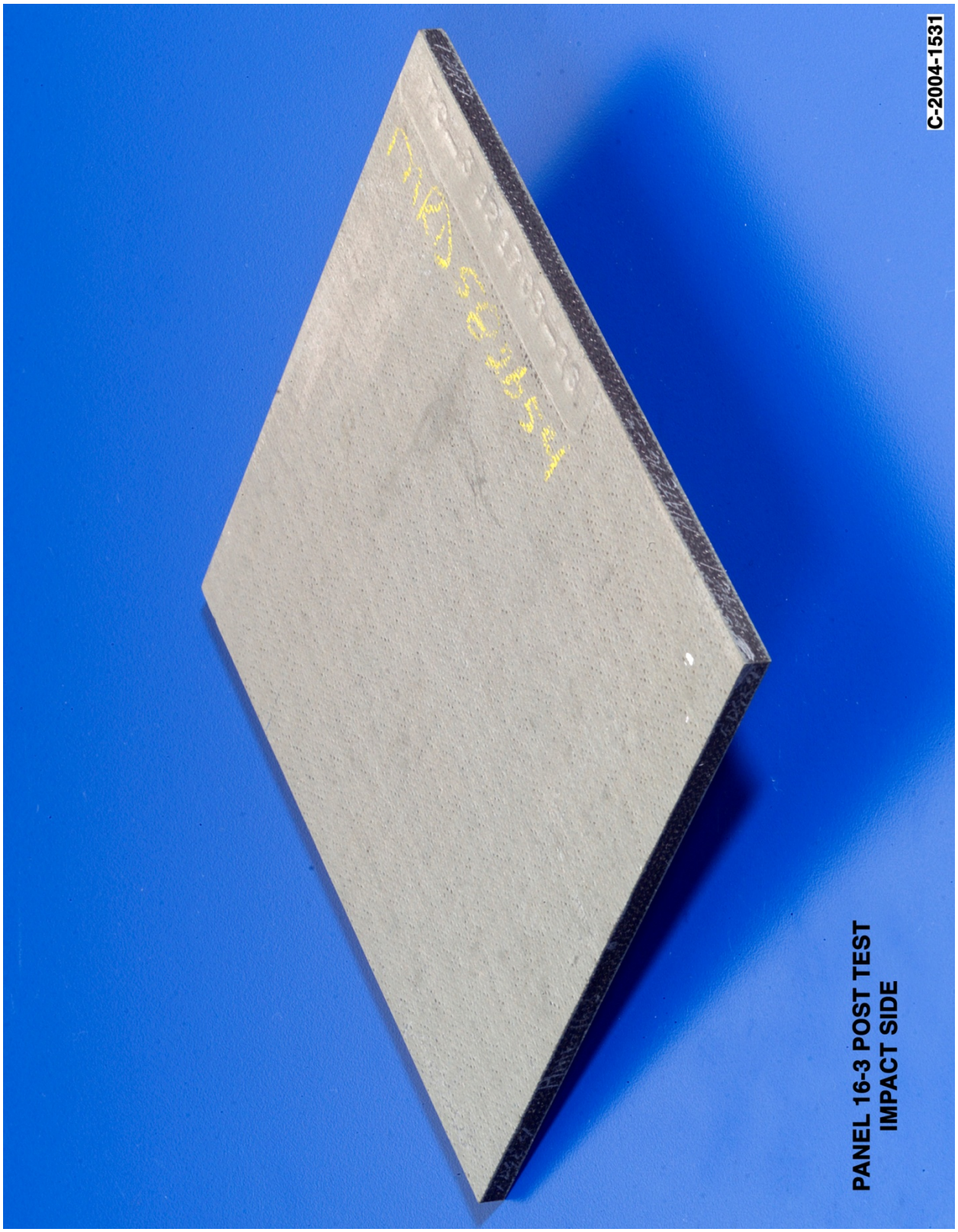

Figure A12–2.—Front (impact side) of panel 16-3 at 490 ft/s with a high-density, poly-crystal ice cylinder (nominally 0.66 in. in diameter by 1.66 in.) at 90° impact angle. Test GRCC 77.

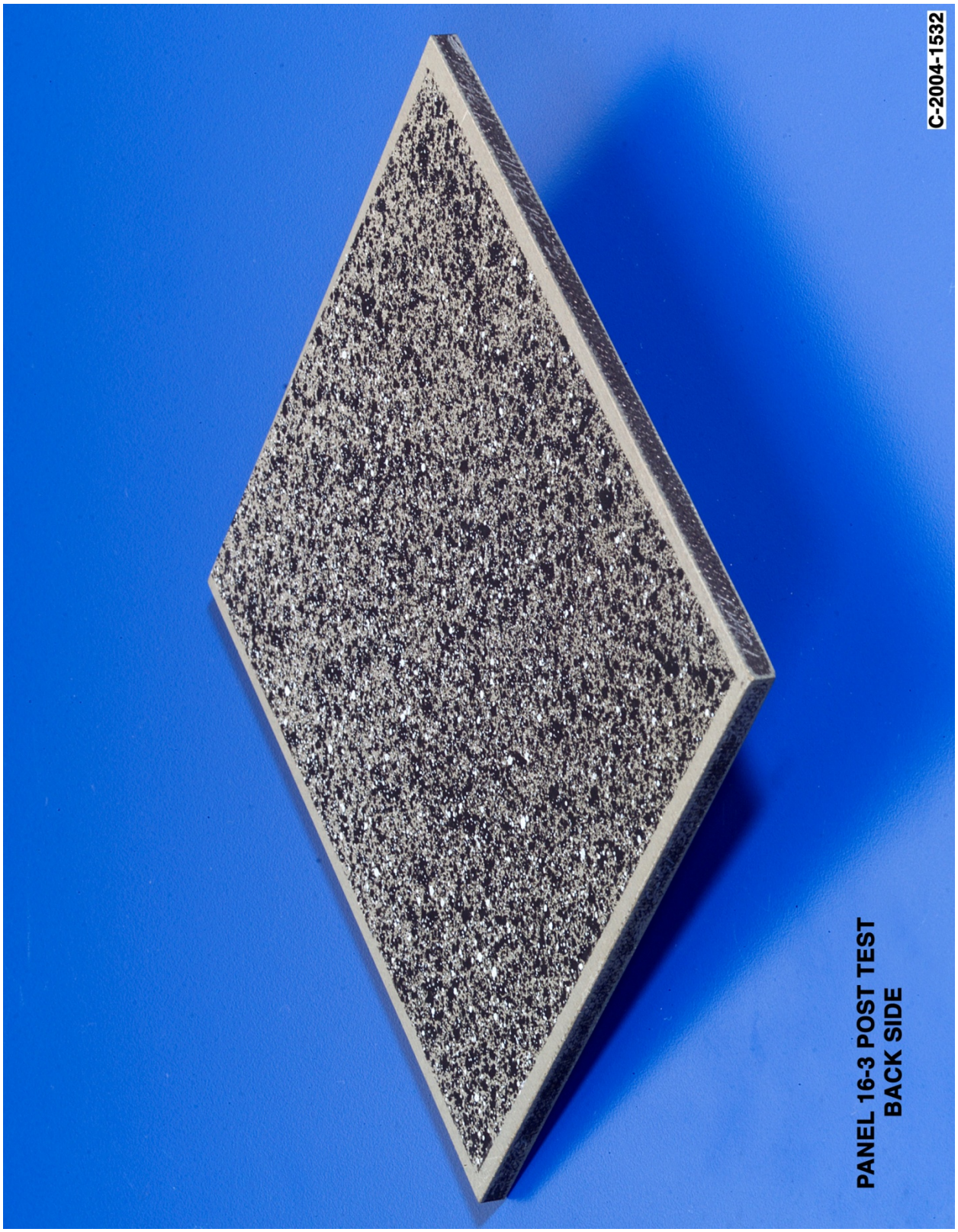

Figure A12–3.—Back face of panel 16-3 at 490 ft/s with a high-density, poly-crystal ice cylinder (nominally 0.66 in. in diameter by 1.66 in.) at 90° impact angle. Test GRCC 77.

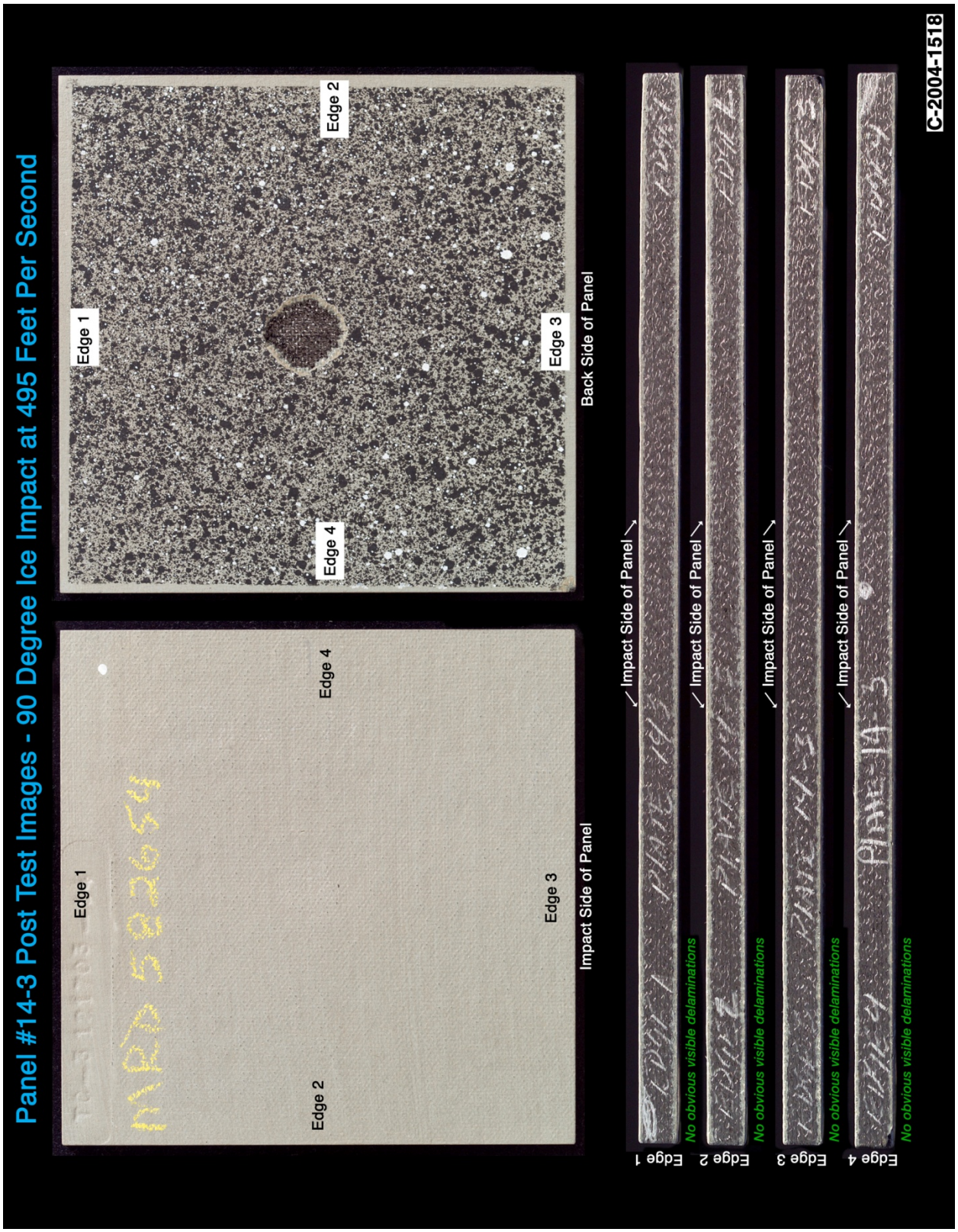

Figure A13–1.—Edges and faces of panel 14-3 at 495 ft/s with a high-density, poly-crystal ice cylinder (nominally 0.66 in. in diameter by 1.66 in.) at 90° impact. Test GRCC 72.

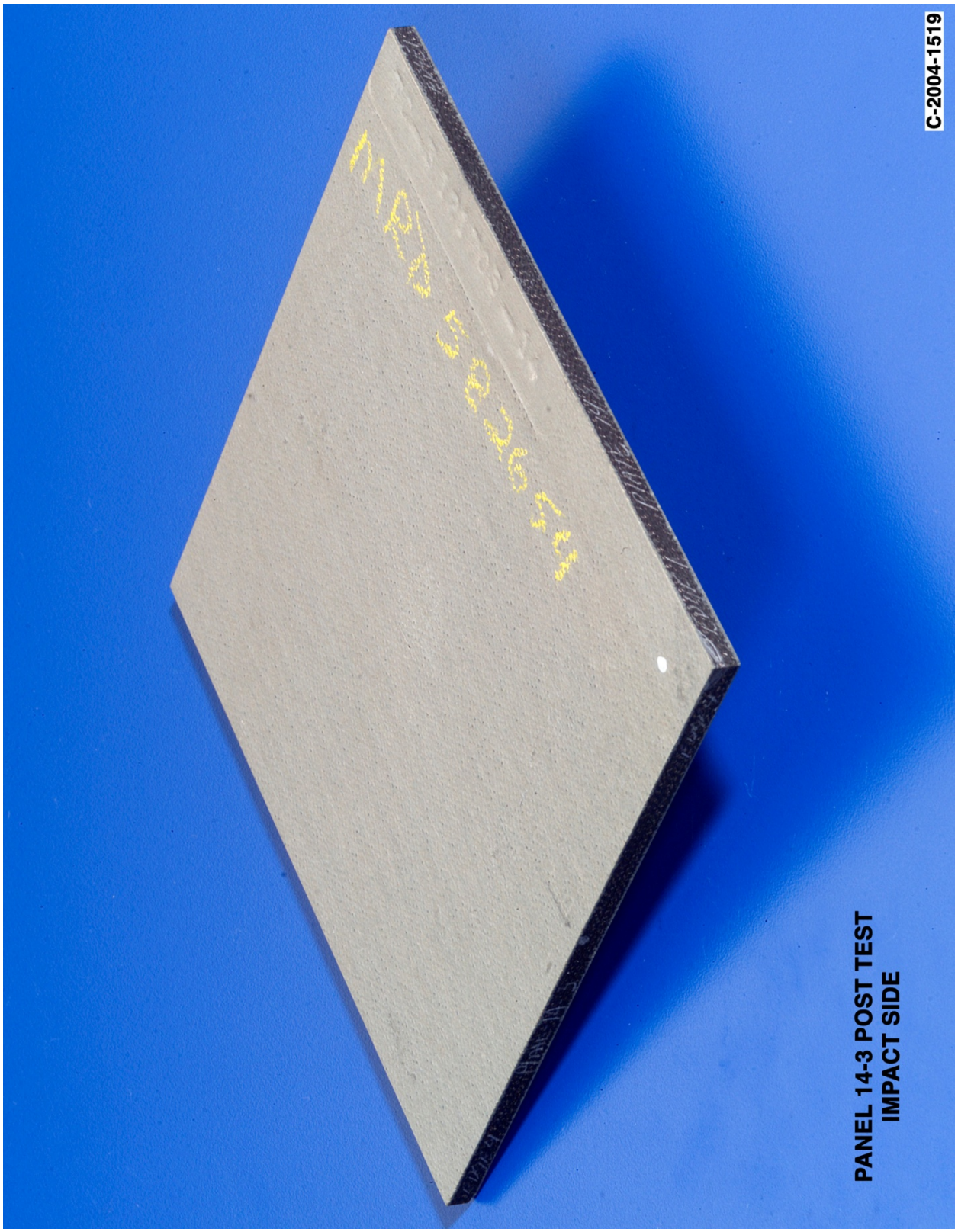

Figure A13–2.—Front (impact side) of panel 14-3 at 495 ft/s with a high-density, poly-crystal ice cylinder (nominally 0.66 in. in diameter by 1.66 in.) at 90° impact angle. Test GRCC 72.

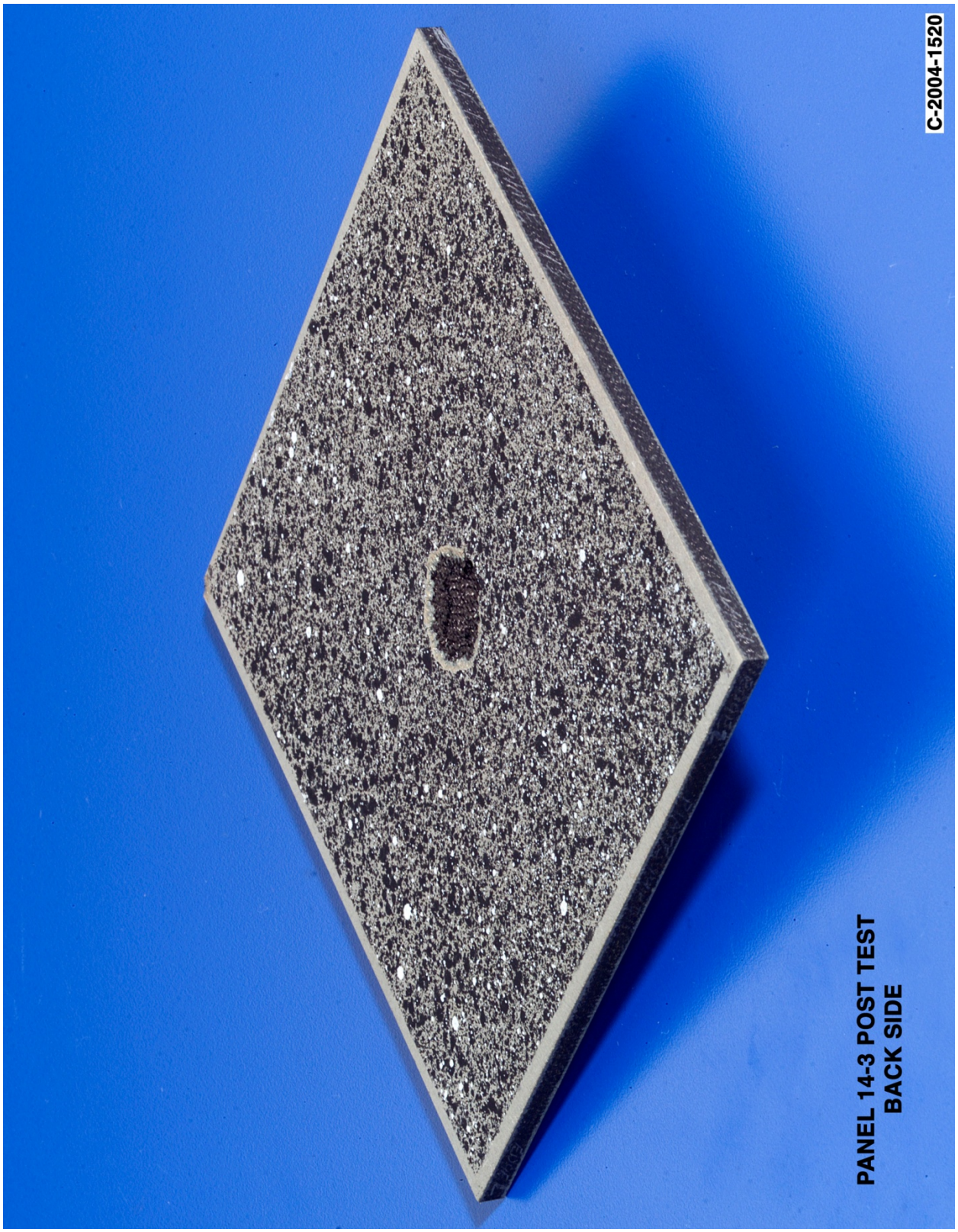

Figure A13–3.—Back face of panel 14-3 at 495 ft/s with a high-density, poly-crystal ice cylinder (nominally 0.66 in. in diameter by 1.66 in.) at 90° impact angle. Test GRCC 72.

Figure A14–1.—Edges and faces of panel 14-4 at 495 ft/s with a high-density, poly-crystal ice cylinder (nominally 0.66 in. in diameter by 1.66 in.) at 90° impact. Test GRCC 73.

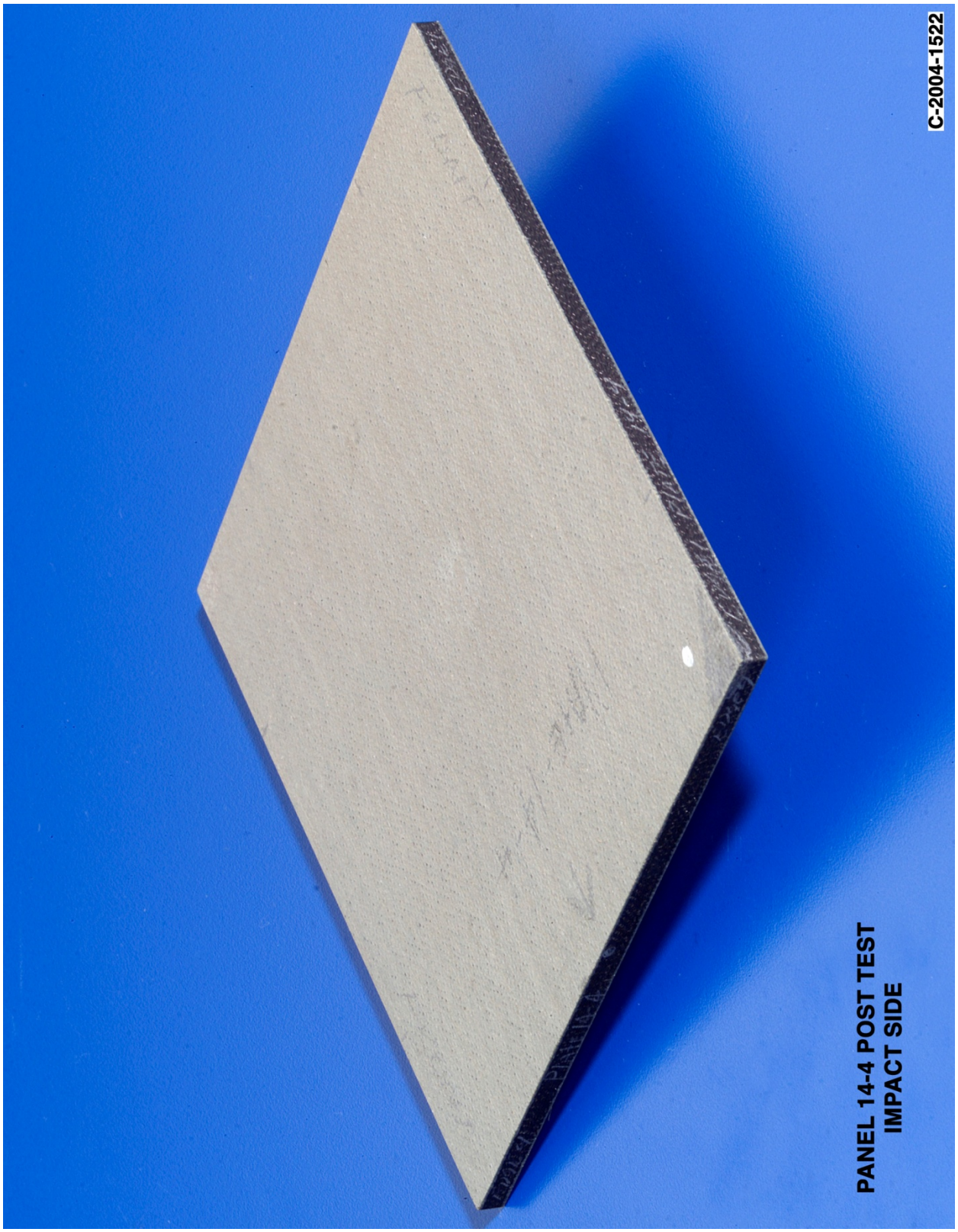

Figure A14–2.—Front (impact side) of panel 14-4 at 495 ft/s with a high-density, poly-crystal ice cylinder (nominally 0.66 in. in diameter by 1.66 in.) at 90° impact angle. Test GRCC 73.

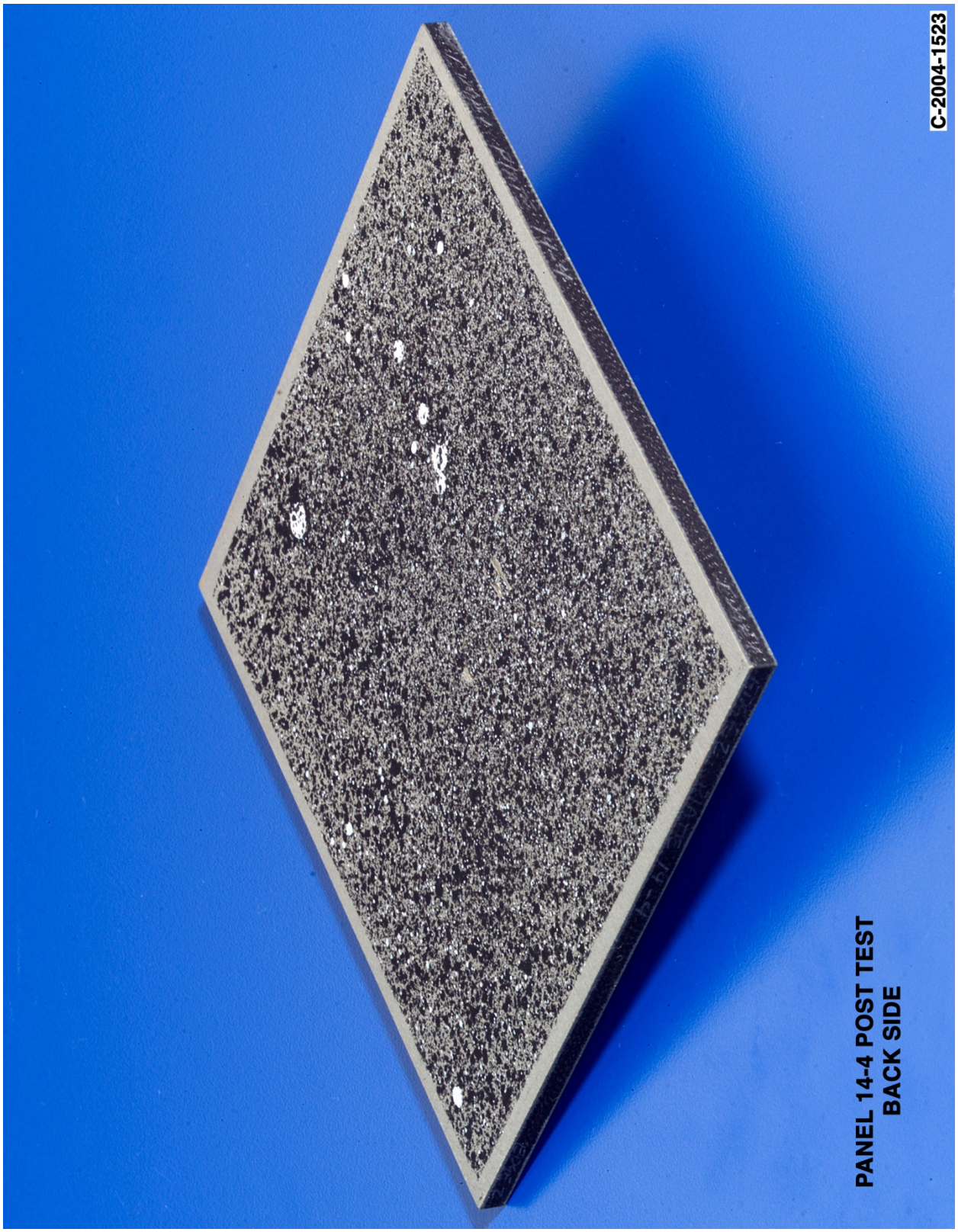

Figure A14–3.—Back face of panel 14-4 at 495 ft/s with a high-density, poly-crystal ice cylinder (nominally 0.66 in. in diameter by 1.66 in.) at 90° impact angle. Test GRCC 73.

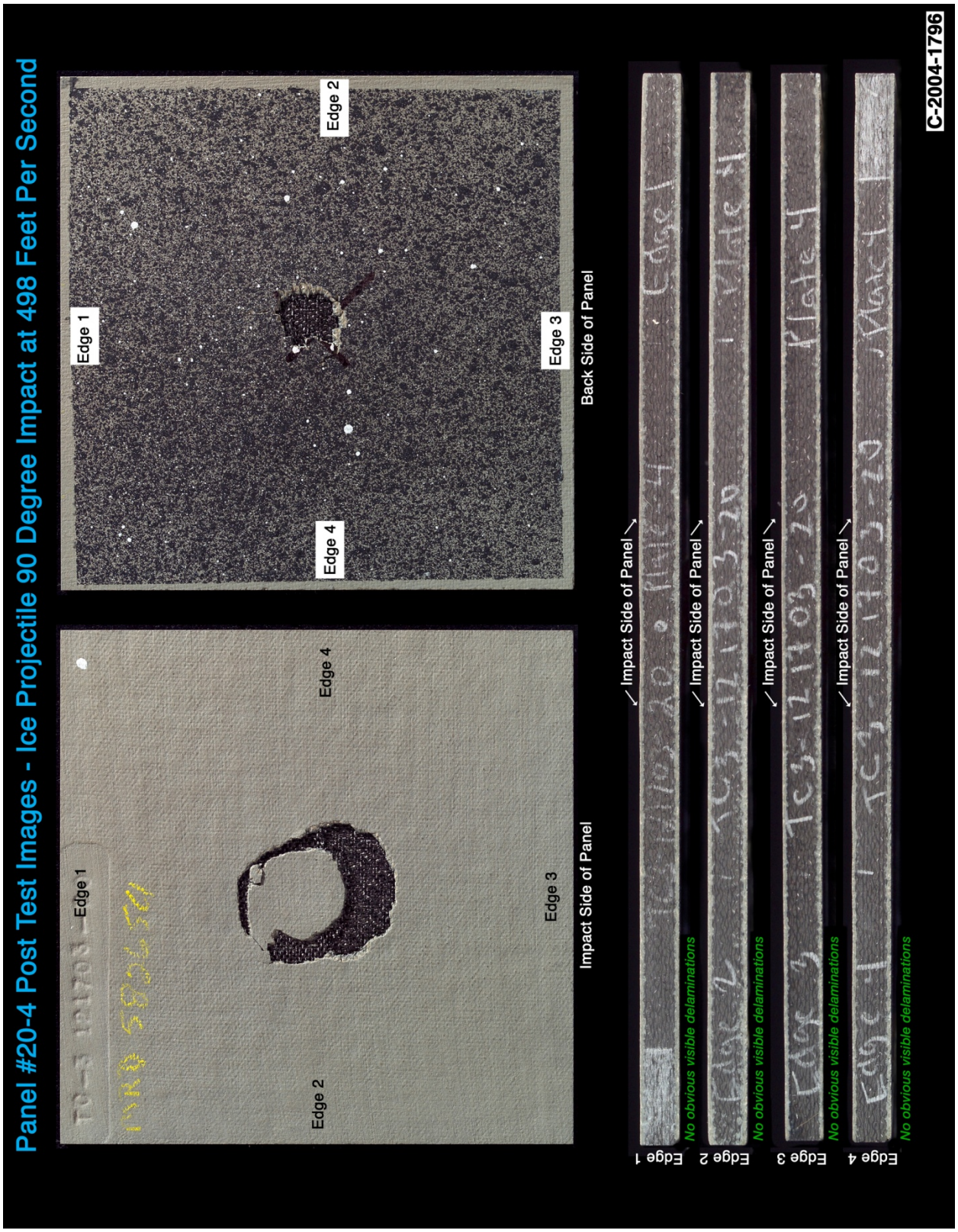

Figure A15–1.—Edges and faces of panel 20-4 at 498 ft/s with a high-density, poly-crystal ice cylinder (nominally 0.66 in. in diameter by 1.66 in.) at 90° impact. Test GRCC 113.

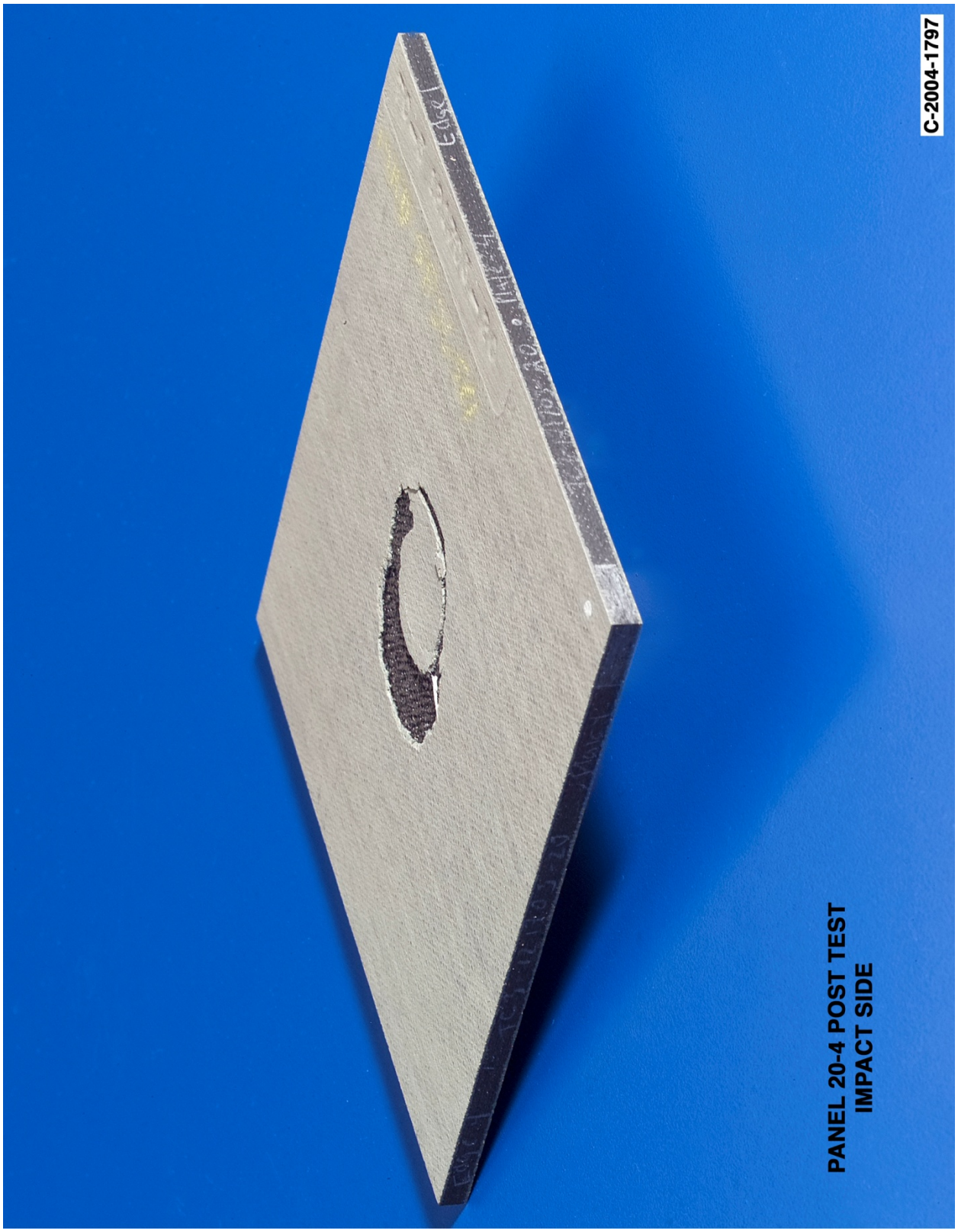

Figure A15–2.—Front (impact side) of panel 20-4 at 498 ft/s with a high-density, poly-crystal ice cylinder (nominally 0.66 in. in diameter by 1.66 in.) at 90° impact angle. Test GRCC 113.

Figure A15–3.—Back face of panel 20-4 at 498 ft/s with a high-density, poly-crystal ice cylinder (nominally 0.66 in. in diameter by 1.66 in.) at 90° impact angle. Test GRCC 113.

Figure A16–1.—Edges and faces of panel 45-3 at 501 ft/s with a high-density, poly-crystal ice cylinder (nominally 0.66 in. in diameter by 1.66 in.) at 90° impact. Test GRCC 116.

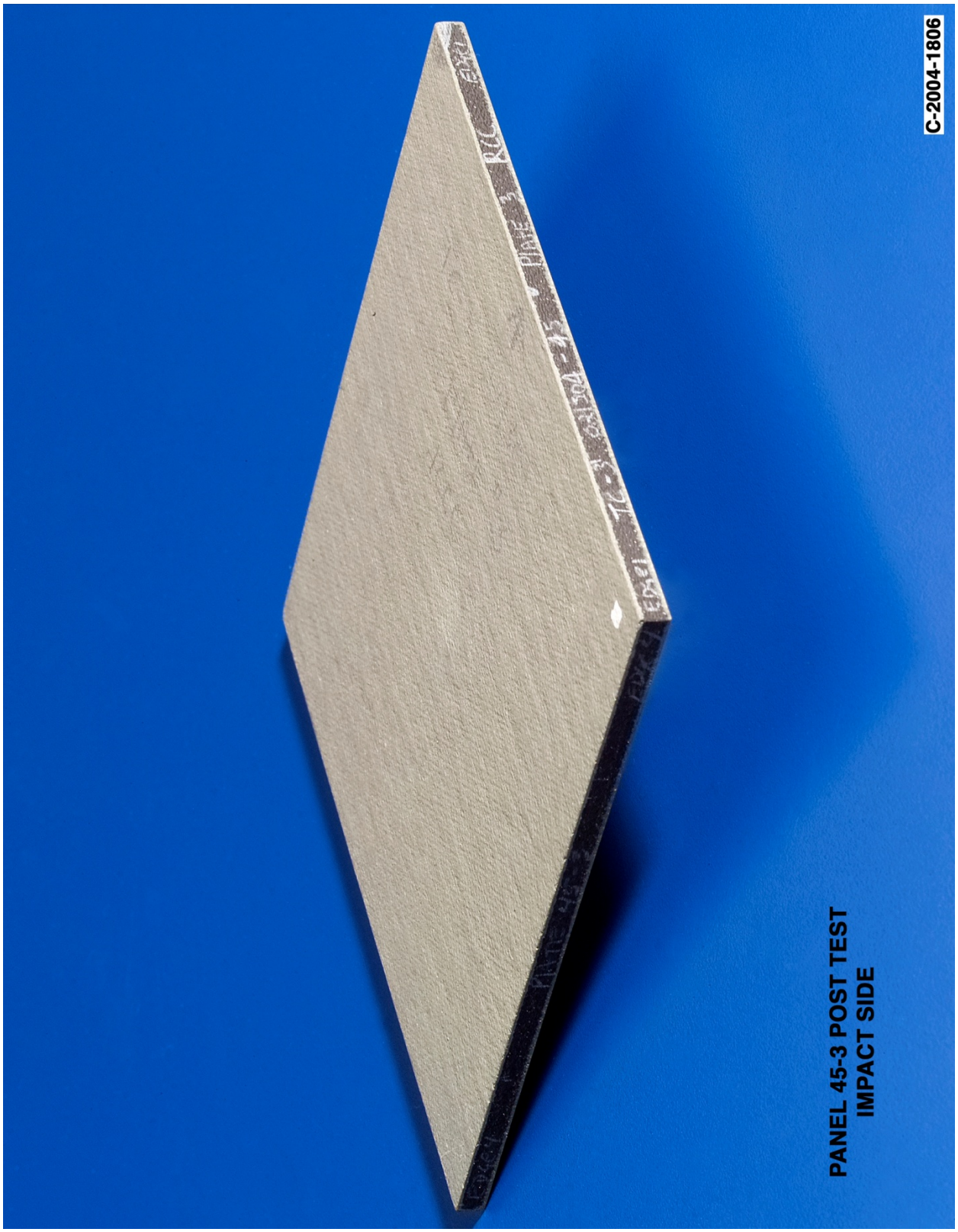

Figure A16–2.—Front (impact side) of panel 45-3 at 501 ft/s with a high-density, poly-crystal ice cylinder (nominally 0.66 in. in diameter by 1.66 in.) at 90° impact angle. Test GRCC 116.

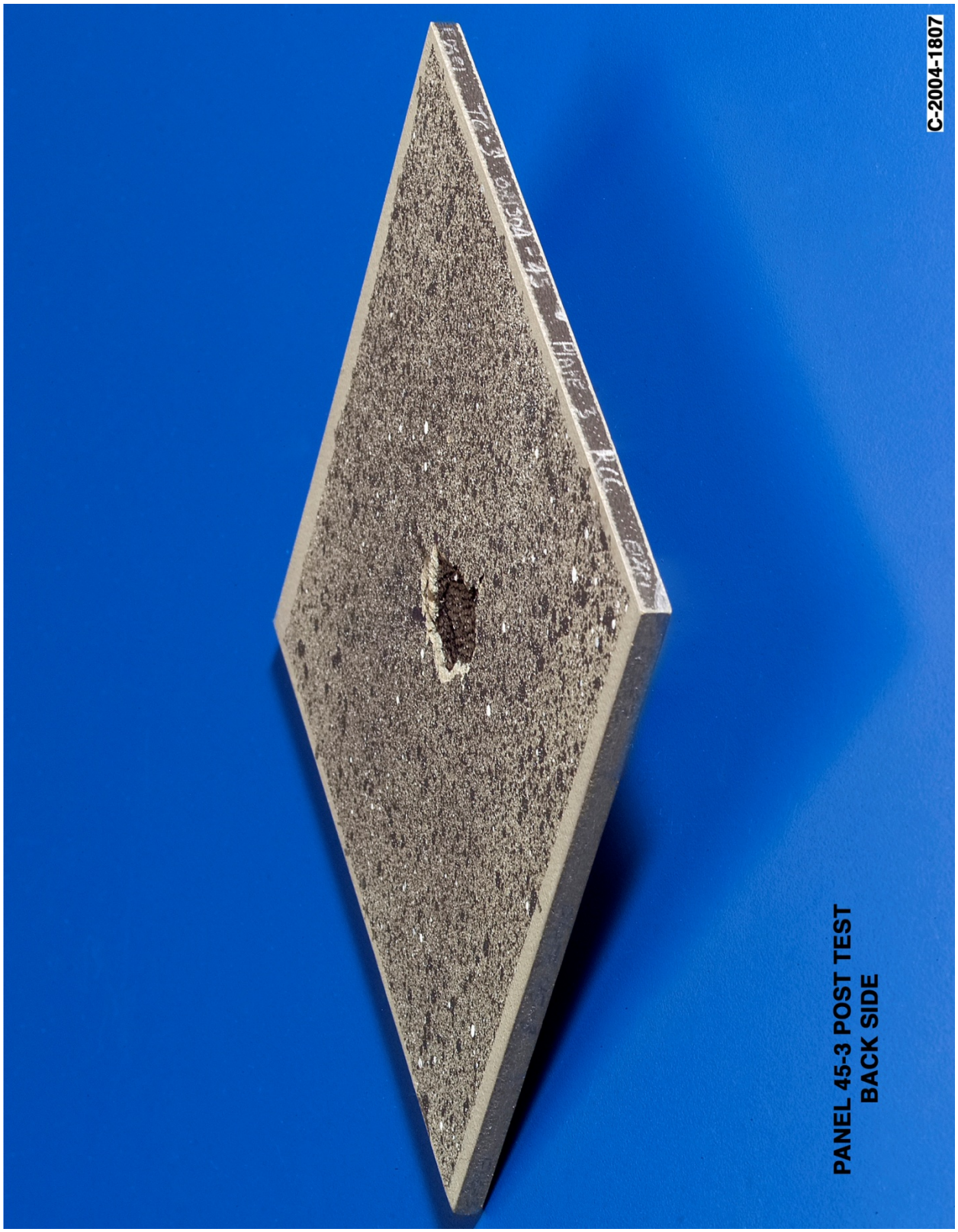

Figure A16–3.—Back face of panel 45-3 at 501 ft/s with a high-density, poly-crystal ice cylinder (nominally 0.66 in. in diameter by 1.66 in.) at 90° impact angle. Test GRCC 116.

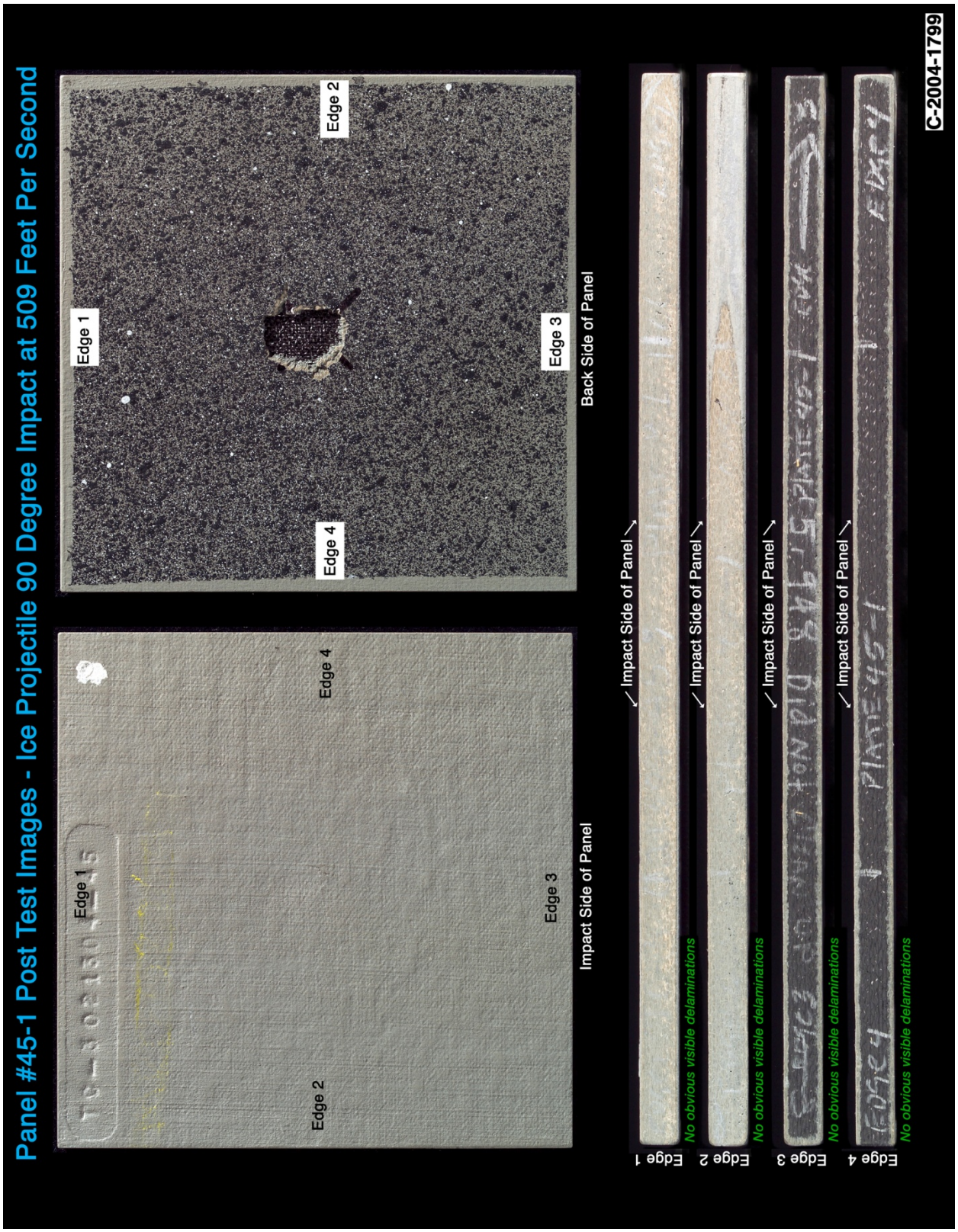

Figure A17–1.—Edges and faces of panel 45-1 at 509 ft/s with a high-density, poly-crystal ice cylinder (nominally 0.66 in. in diameter by 1.66 in.) at 90° impact. Test GRCC 114.

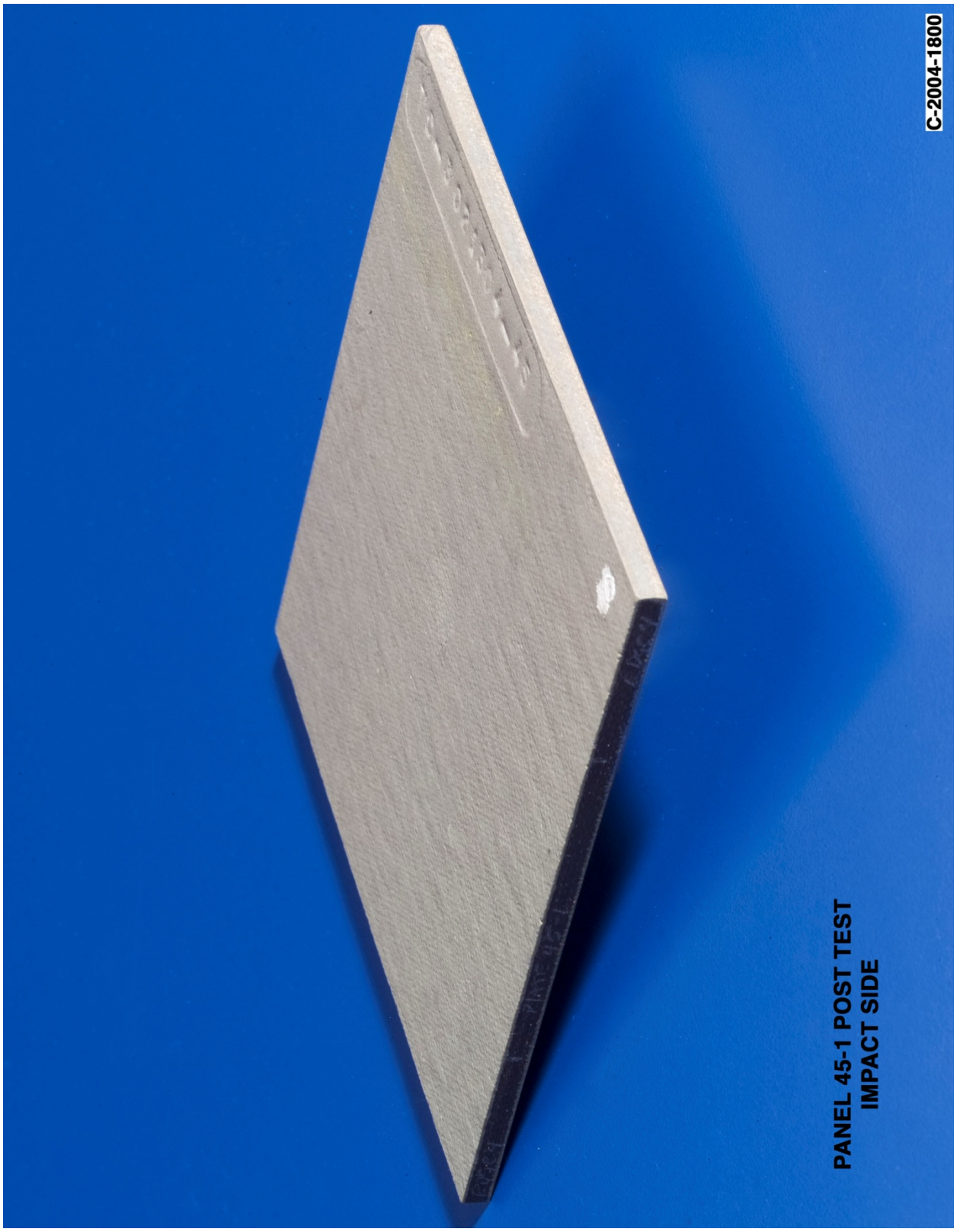

Figure A17–2.—Front (impact side) of panel 45-1 at 509 ft/s with a high-density, poly-crystal ice cylinder (nominally 0.66 in. in diameter by 1.66 in.) at 90° impact angle. Test GRCC 114.

Figure A17–3.—Back face of panel 45-1 at 509 ft/s with a high-density, poly-crystal ice cylinder (nominally 0.66 in. in diameter by 1.66 in.) at 90° impact angle. Test GRCC 114.

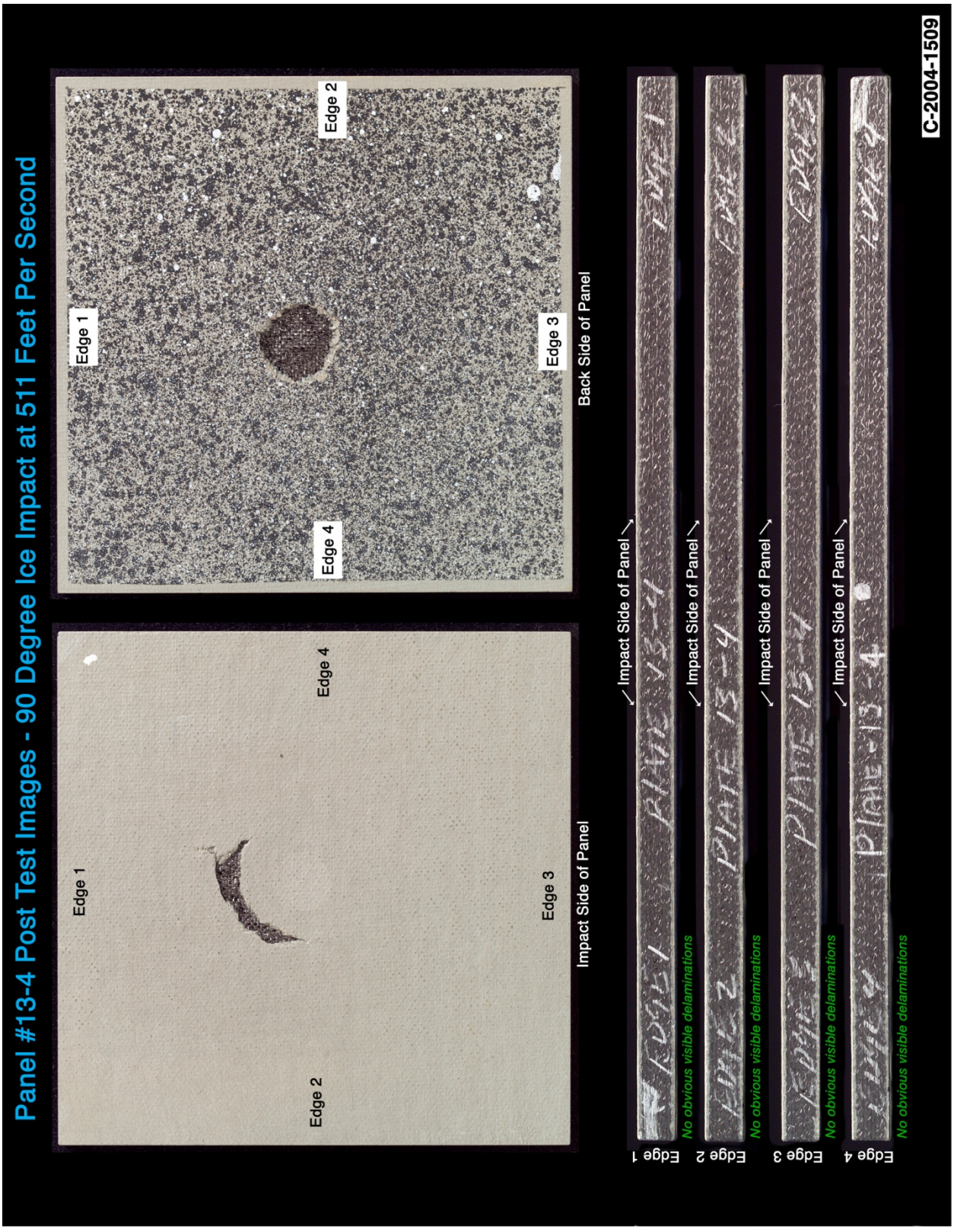

Figure A18–1.—Edges and faces of panel 13-4 at 511 ft/s with a high-density, poly-crystal ice cylinder (nominally 0.66 in. in diameter by 1.66 in.) at 90° impact. Test GRCC 69.

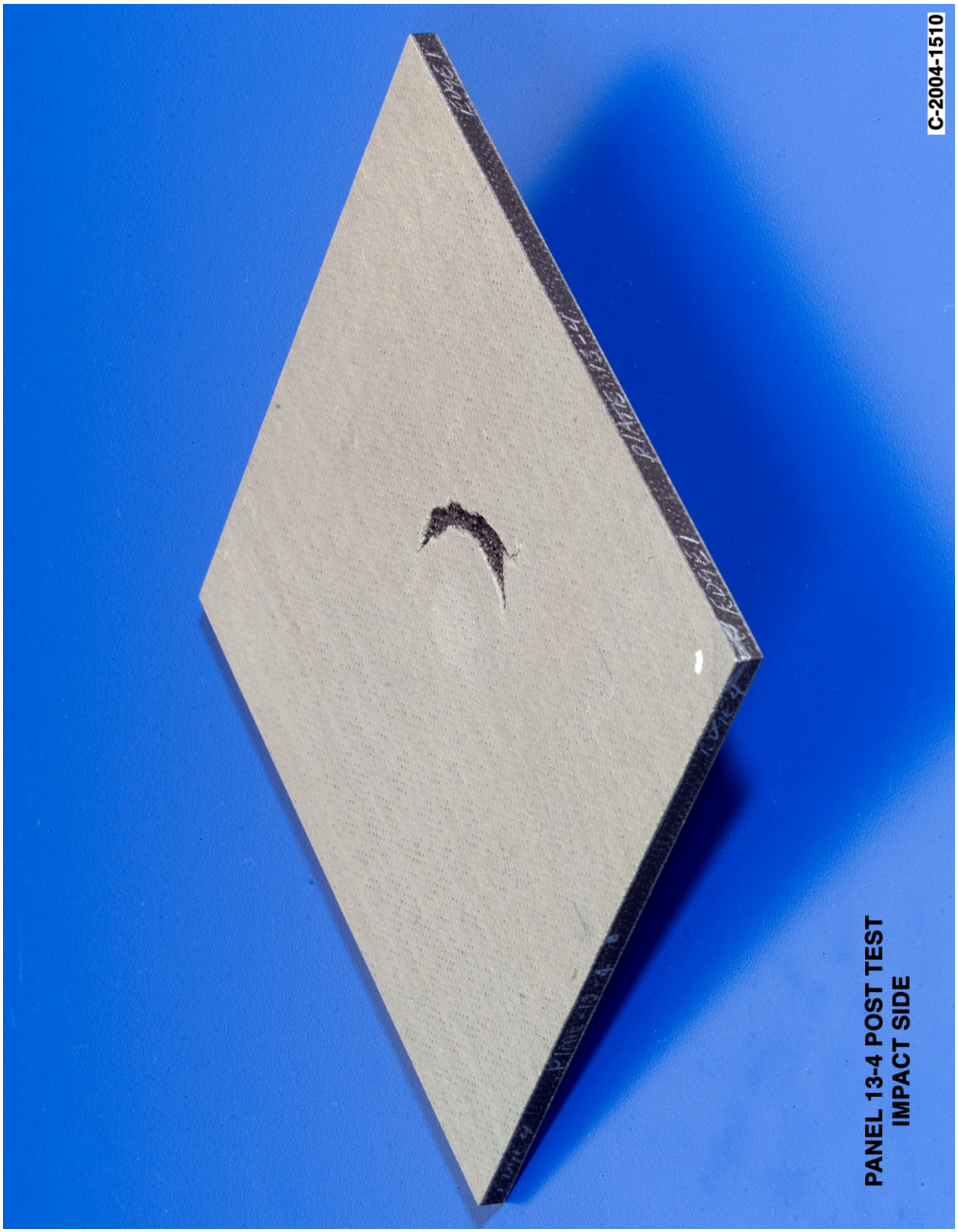

Figure A18–2.—Front (impact side) of panel 13-4 at 511 ft/s with a high-density, poly-crystal ice cylinder (nominally 0.66 in. in diameter by 1.66 in.) at 90° impact angle. Test GRCC 69.

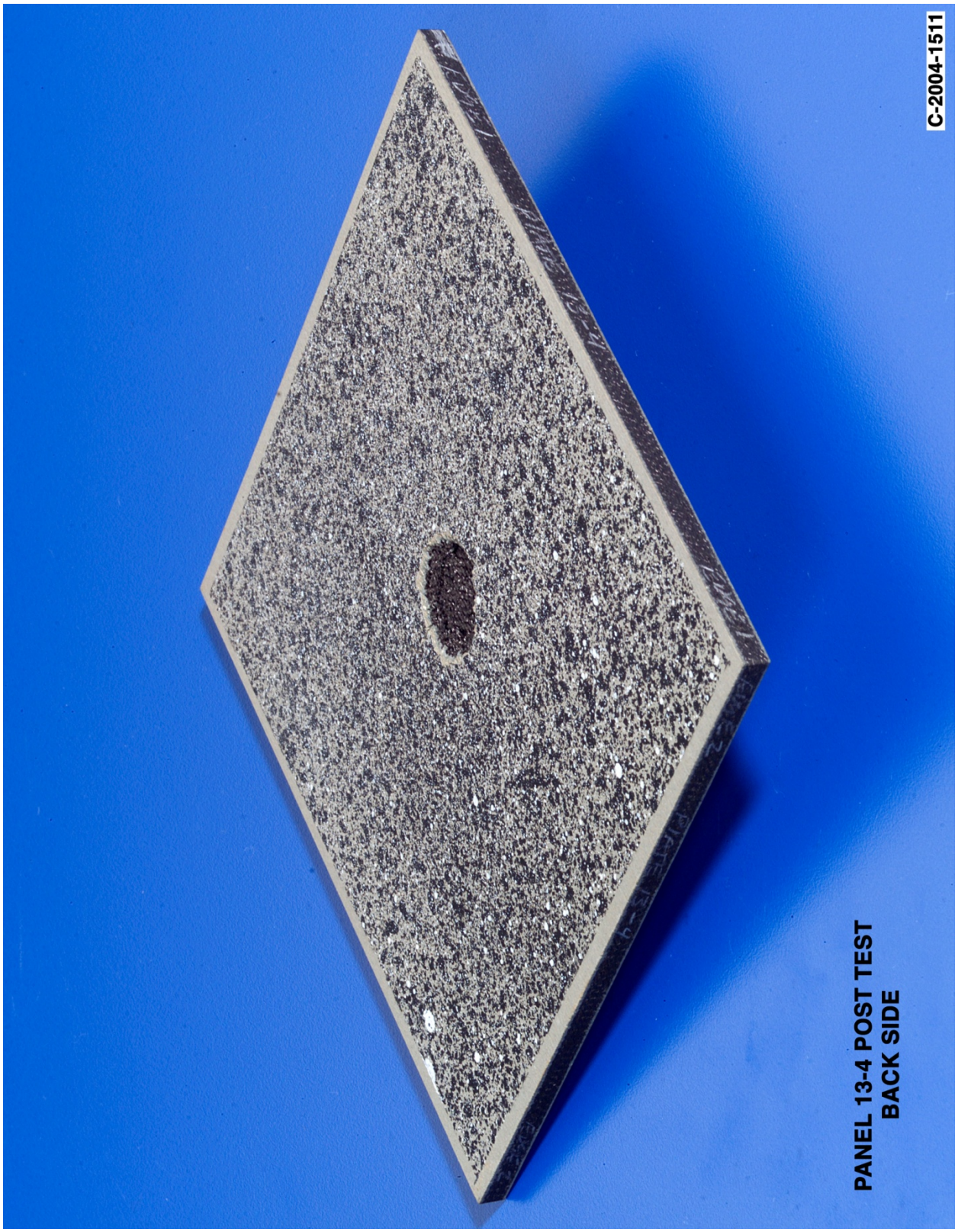

Figure A18–3.—Back face of panel 13-4 at 511 ft/s with a high-density, poly-crystal ice cylinder (nominally 0.66 in. in diameter by 1.66 in.) at 90° impact angle. Test GRCC 69.

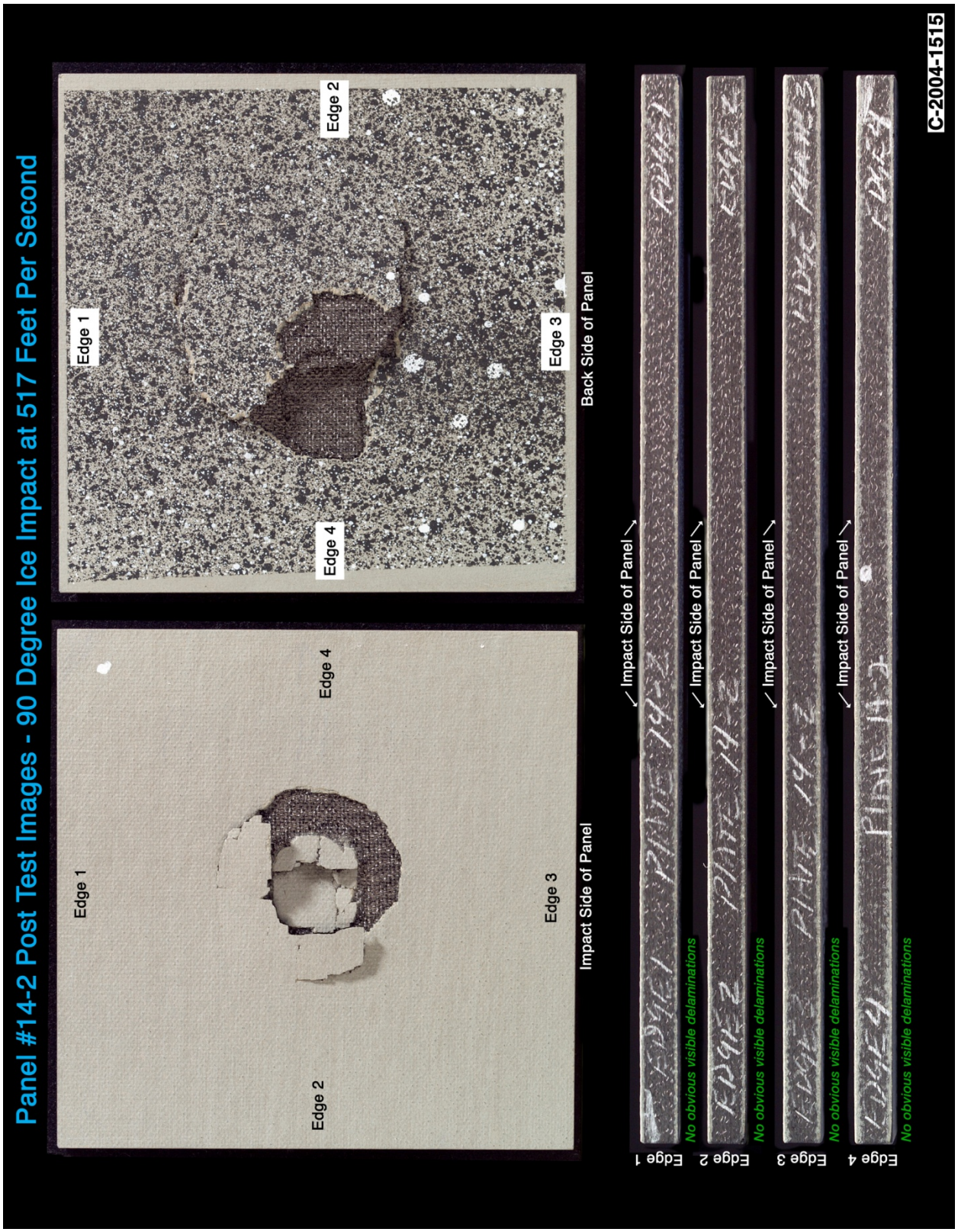

Figure A19–1.—Edges and faces of panel 14-2 at 517 ft/s with a high-density, poly-crystal ice cylinder (nominally 0.66 in. in diameter by 1.66 in.) at 90° impact. Test GRCC 71.

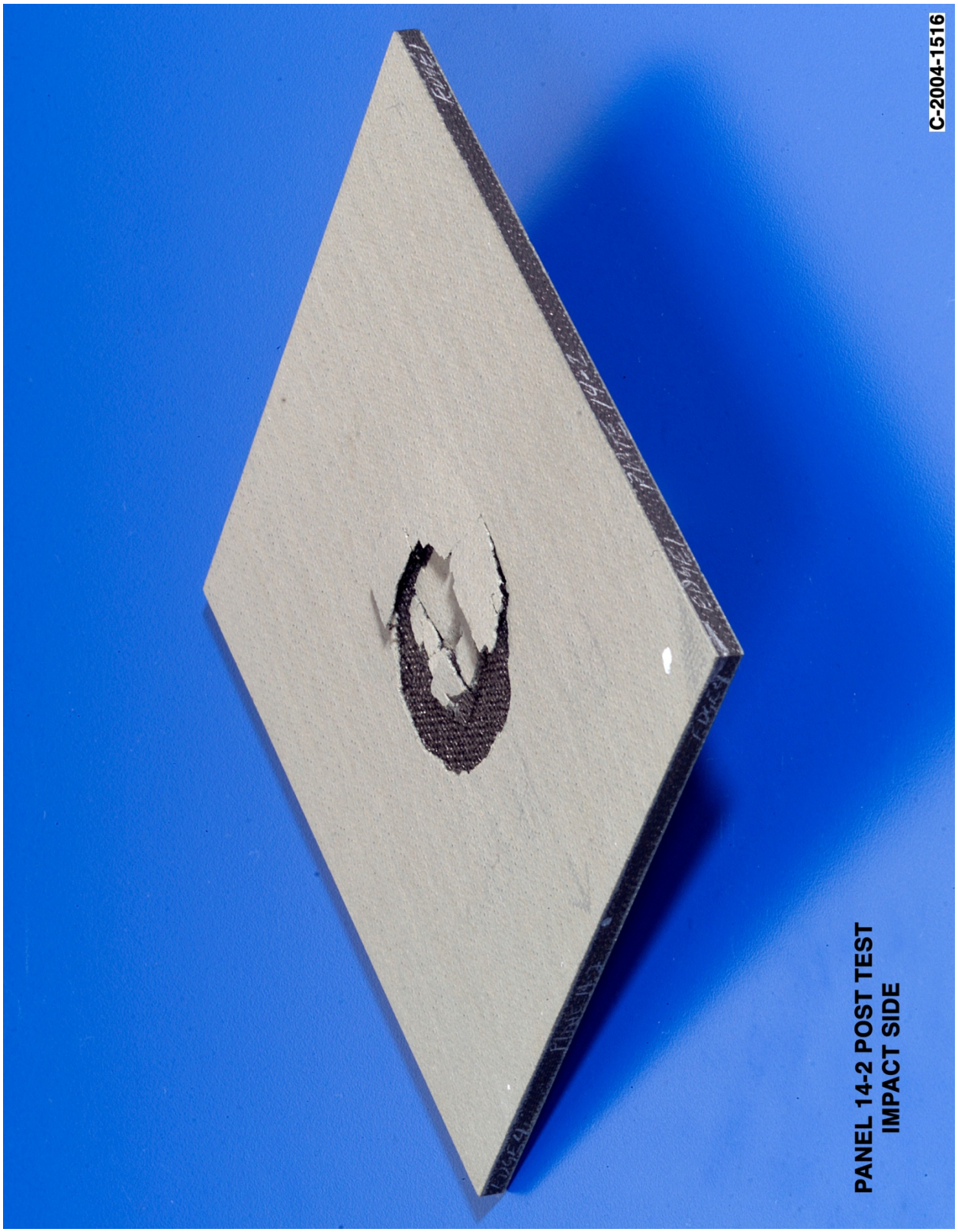

Figure A19–2.—Front (impact side) of panel 14-2 at 517 ft/s with a high-density, poly-crystal ice cylinder (nominally 0.66 in. in diameter by 1.66 in.) at 90° impact angle. Test GRCC 71.

Figure A19–3.—Back face of panel 14-2 at 517 ft/s with a high-density, poly-crystal ice cylinder (nominally 0.66 in. in diameter by 1.66 in.) at 90° impact angle. Test GRCC 71.

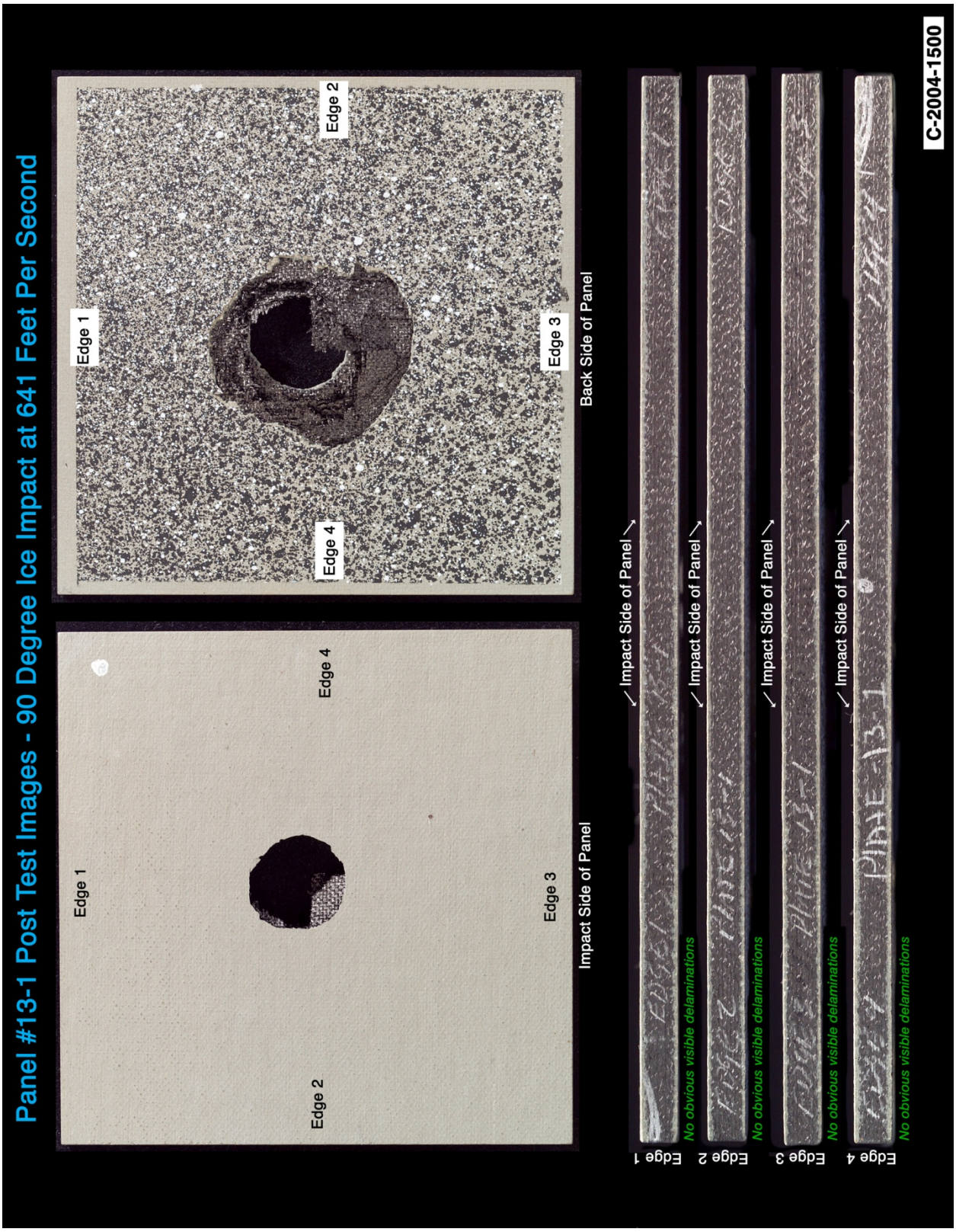

Figure A20–1.—Edges and faces of panel 13-1 at 641 ft/s with a high-density, poly-crystal ice cylinder (nominally 0.66 in. in diameter by 1.66 in.) at 90° impact. Test GRCC 66.

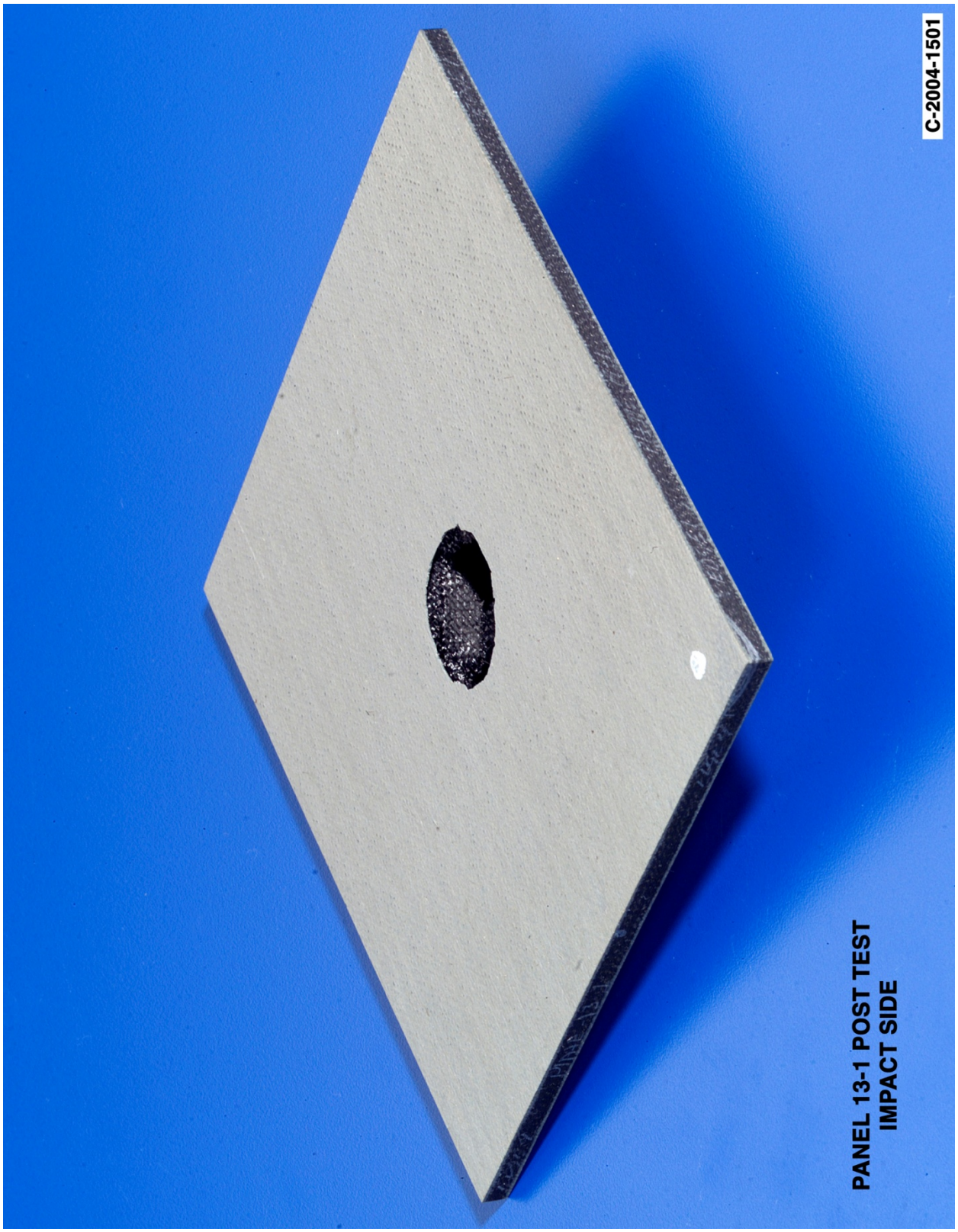

Figure A20–2.—Front (impact side) of panel 13-1 at 641 ft/s with a high-density, poly-crystal ice cylinder (nominally 0.66 in. in diameter by 1.66 in.) at 90° impact angle. Test GRCC 66.

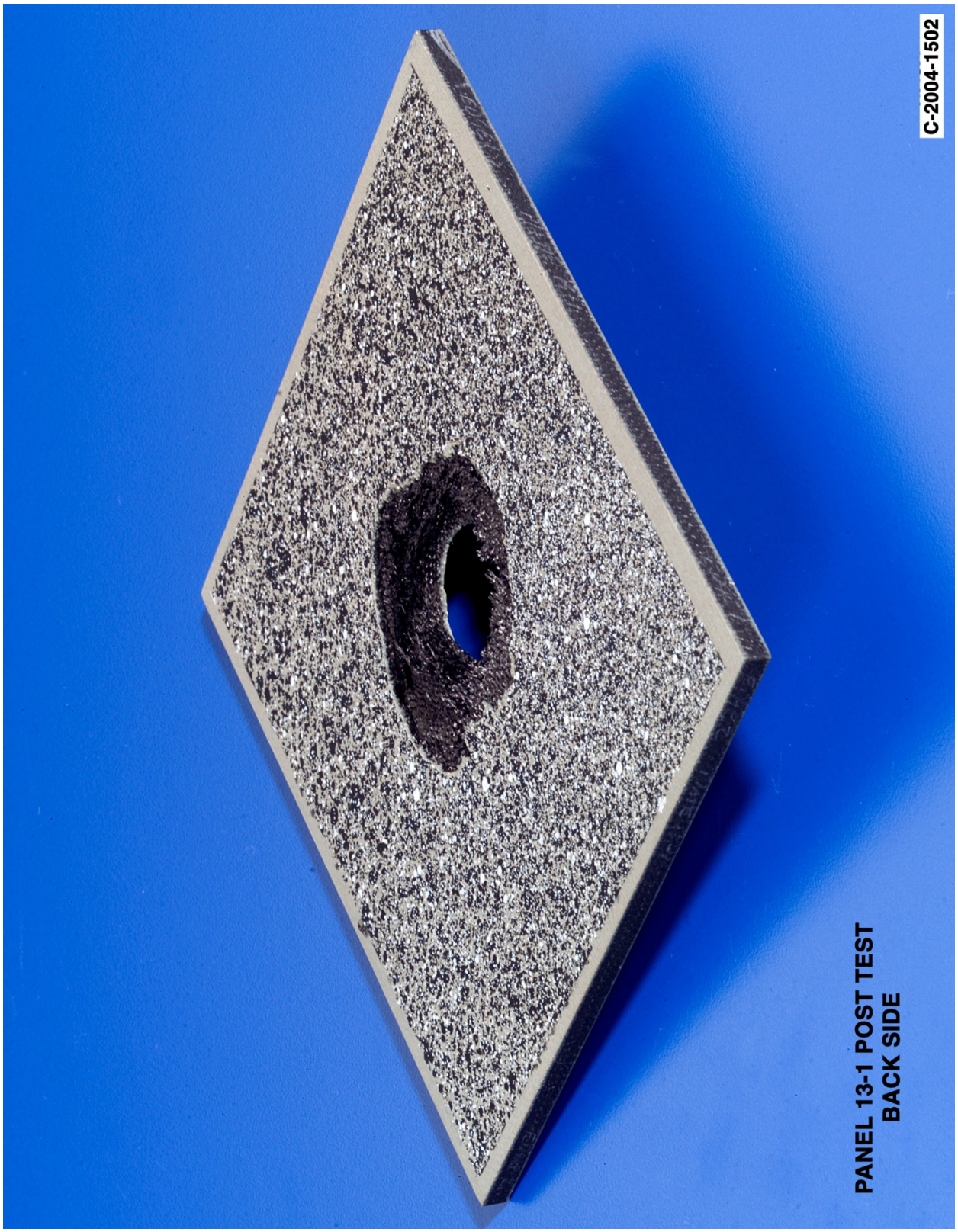

Figure A20–3.—Back face of panel 13-1 at 641 ft/s with a high-density, poly-crystal ice cylinder (nominally 0.66 in. in diameter by 1.66 in.) at 90° impact angle. Test GRCC 66.

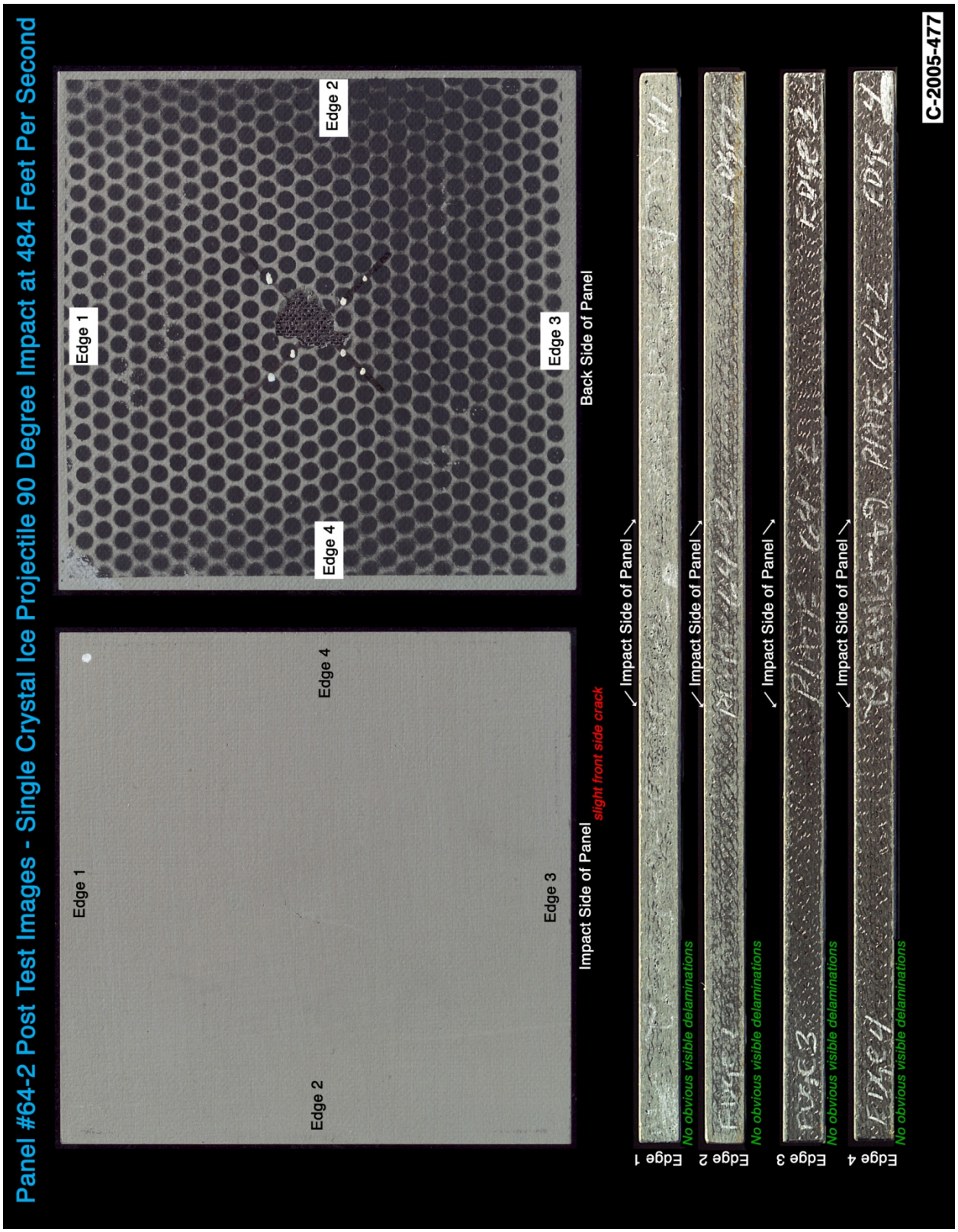

Figure A21–1.—Edges and faces of panel 64-2 at 484 ft/s with a high-density, single-crystal ice cylinder (nominally 0.66 in. in diameter by 1.66 in.) at 90° impact. Test GRCC 141.

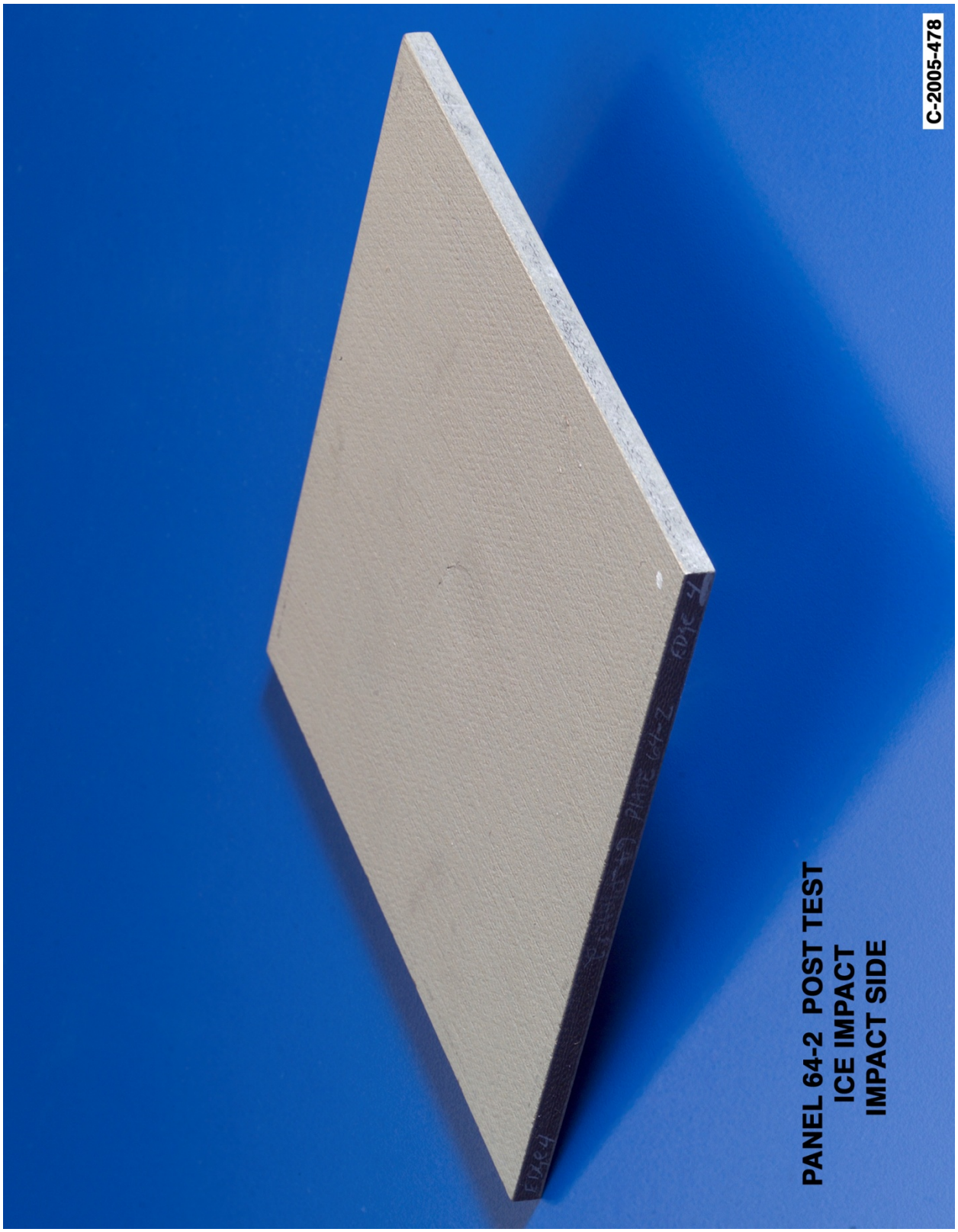

Figure A21–2.—Front (impact side) of panel 64-2 at 484 ft/s with a high-density, single-crystal ice cylinder (nominally 0.66 in. in diameter by 1.66 in.) at 90° impact angle. Test GRCC 141.

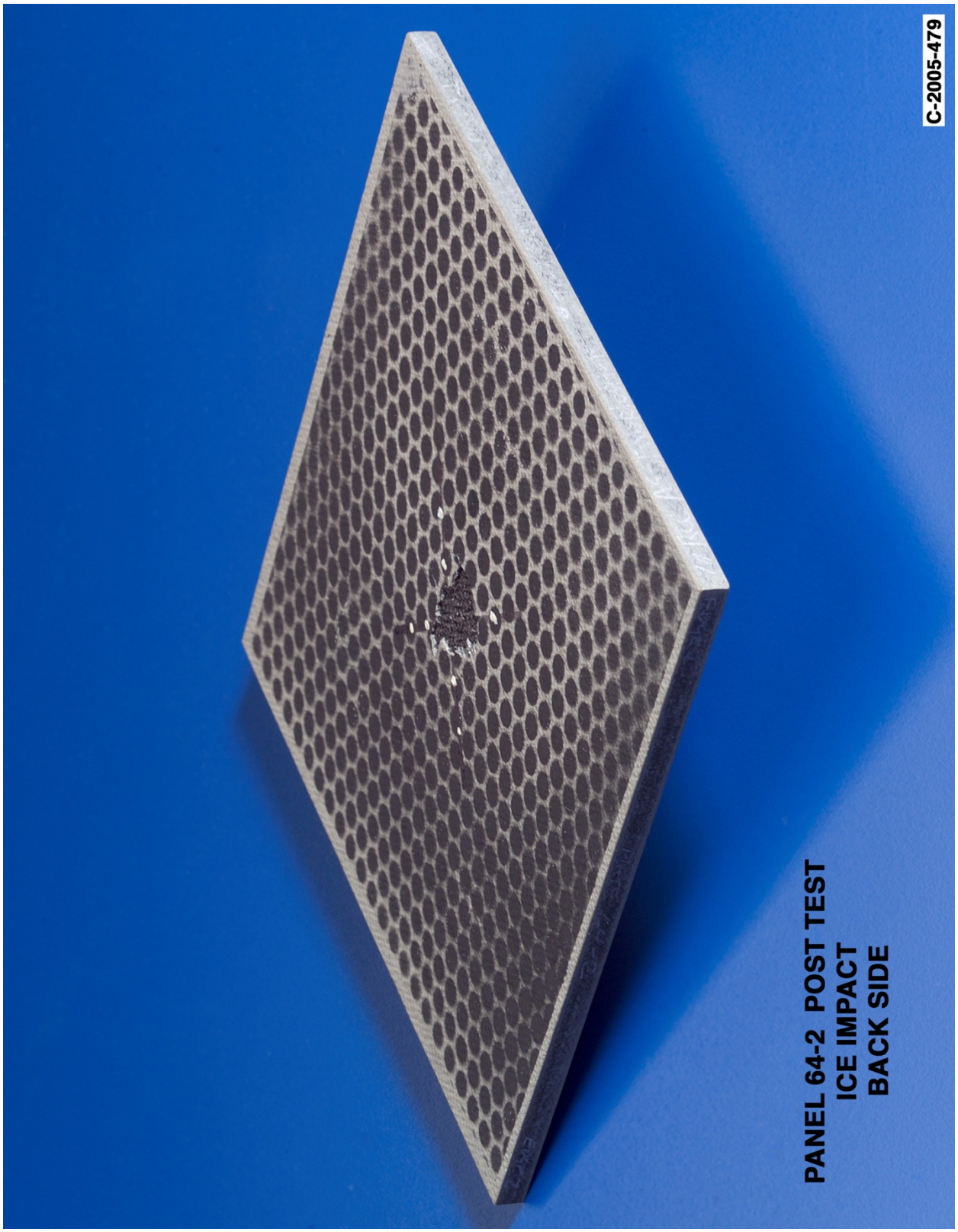

Figure A21–3.—Back face of panel 64-2 at 484 ft/s with a high-density, single-crystal ice cylinder (nominally 0.66 in. in diameter by 1.66 in.) at 90° impact angle. Test GRCC 141.

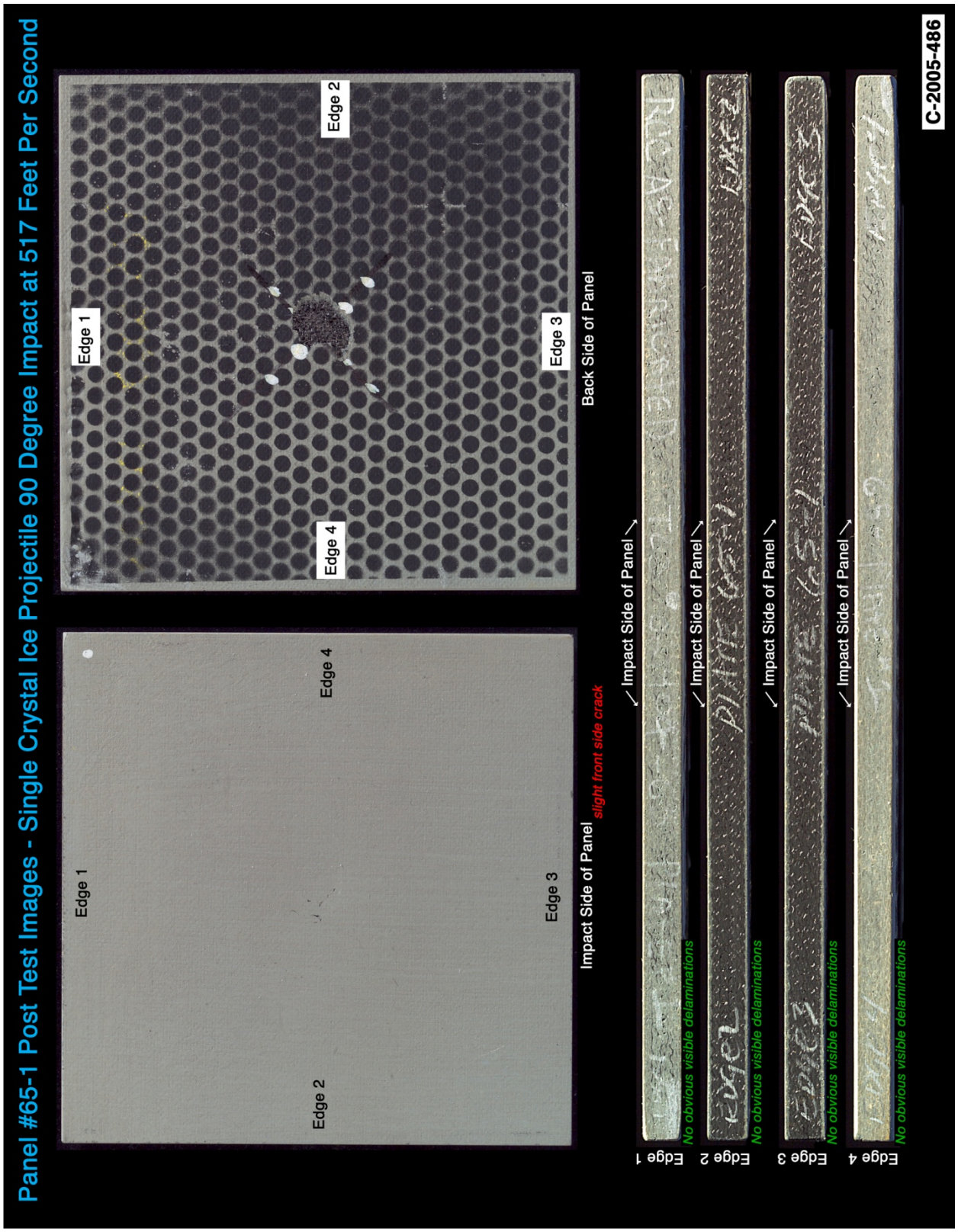

Figure A22–1.—Edges and faces of panel 65-1 at 517 ft/s with a high-density, single-crystal ice cylinder (nominally 0.66 in. in diameter by 1.66 in.) at 90° impact. Test GRCC 142.

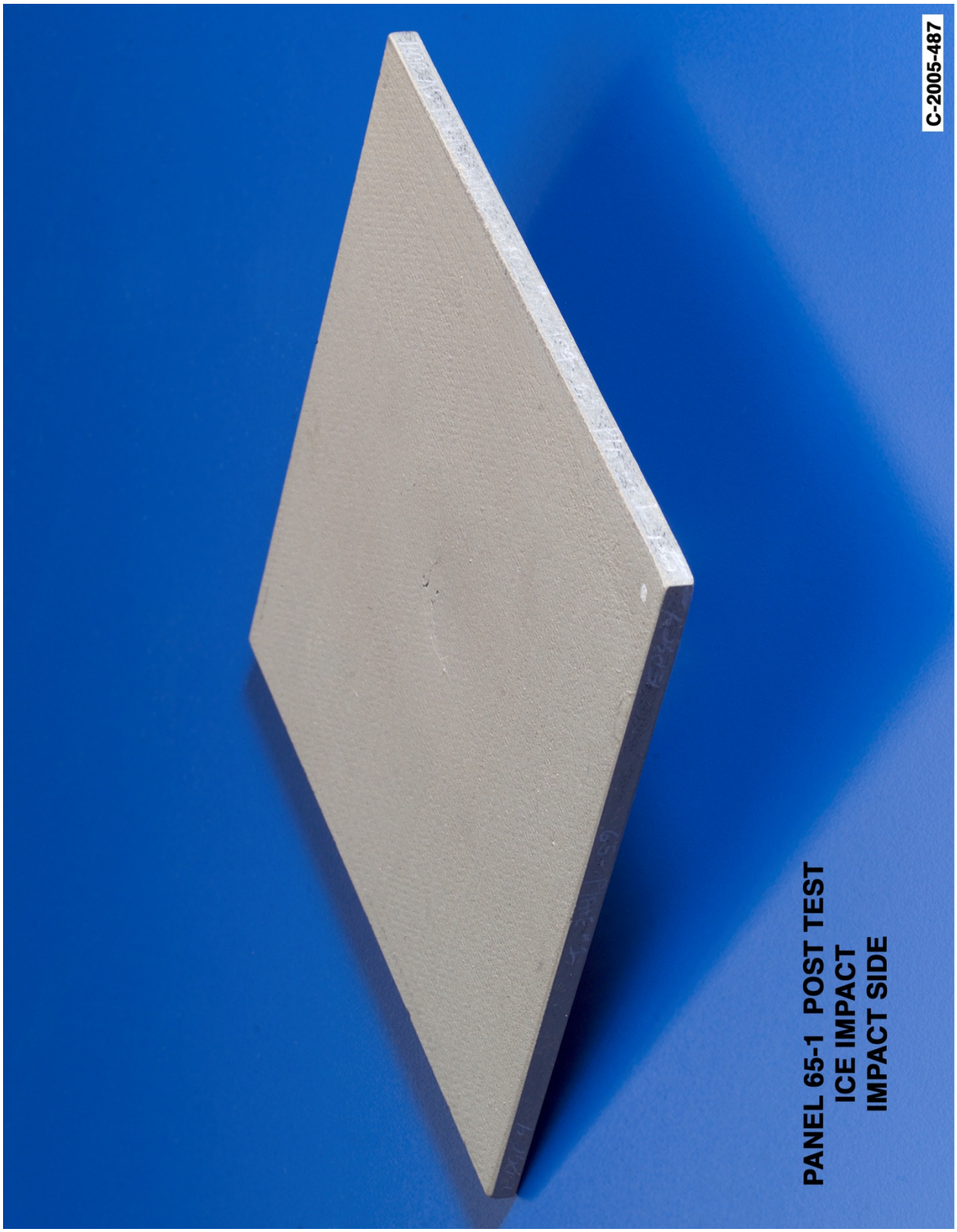

Figure A22–2.—Front (impact side) of panel 65-1 at 517 ft/s with a high-density, single-crystal ice cylinder (nominally 0.66 in. in diameter by 1.66 in.) at 90° impact angle. Test GRCC 142.

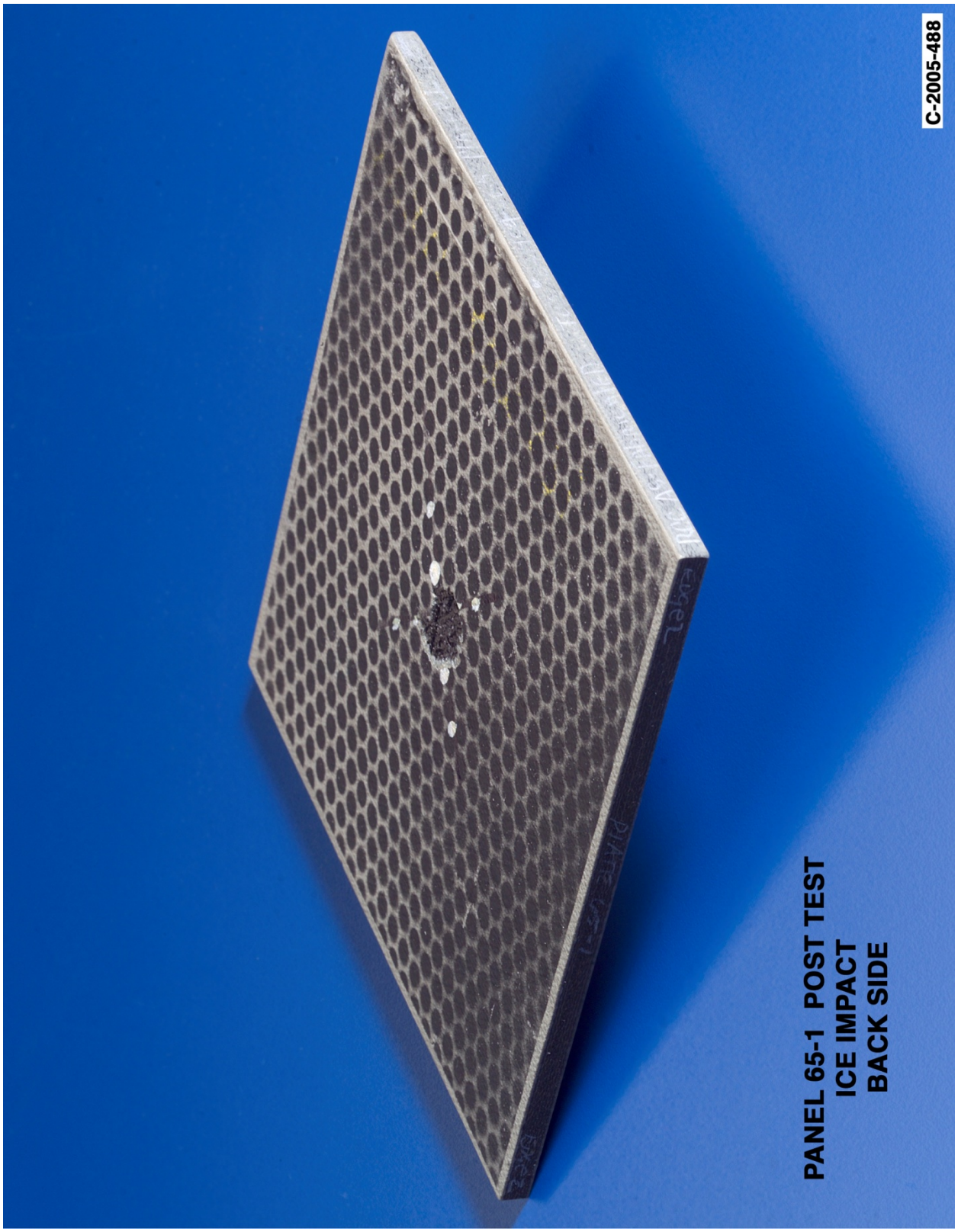

Figure A22–3.—Back face of panel 65-1 at 517 ft/s with a high-density, single-crystal ice cylinder (nominally 0.66 in. in diameter by 1.66 in.) at 90° impact angle. Test GRCC 142.

Figure A23–1.—Edges and faces of panel 65-2 at 528 ft/s with a high-density, single-crystal ice cylinder (nominally 0.66 in. in diameter by 1.66 in.) at 90° impact. Test GRCC 143.

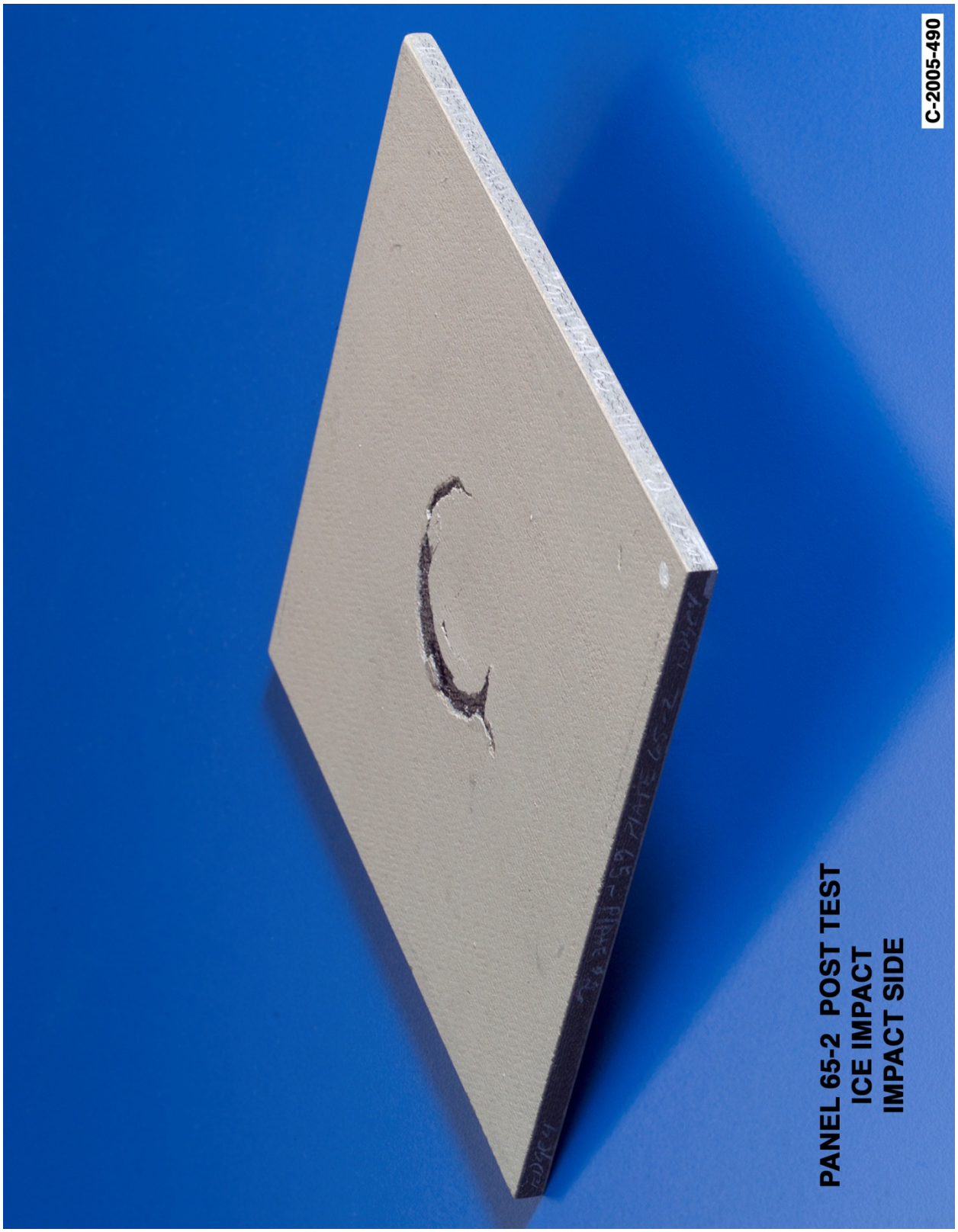

Figure A23–2.—Front (impact side) of panel 65-2 at 528 ft/s with a high-density, single-crystal ice cylinder (nominally 0.66 in. in diameter by 1.66 in.) at 90° impact angle. Test GRCC 143.

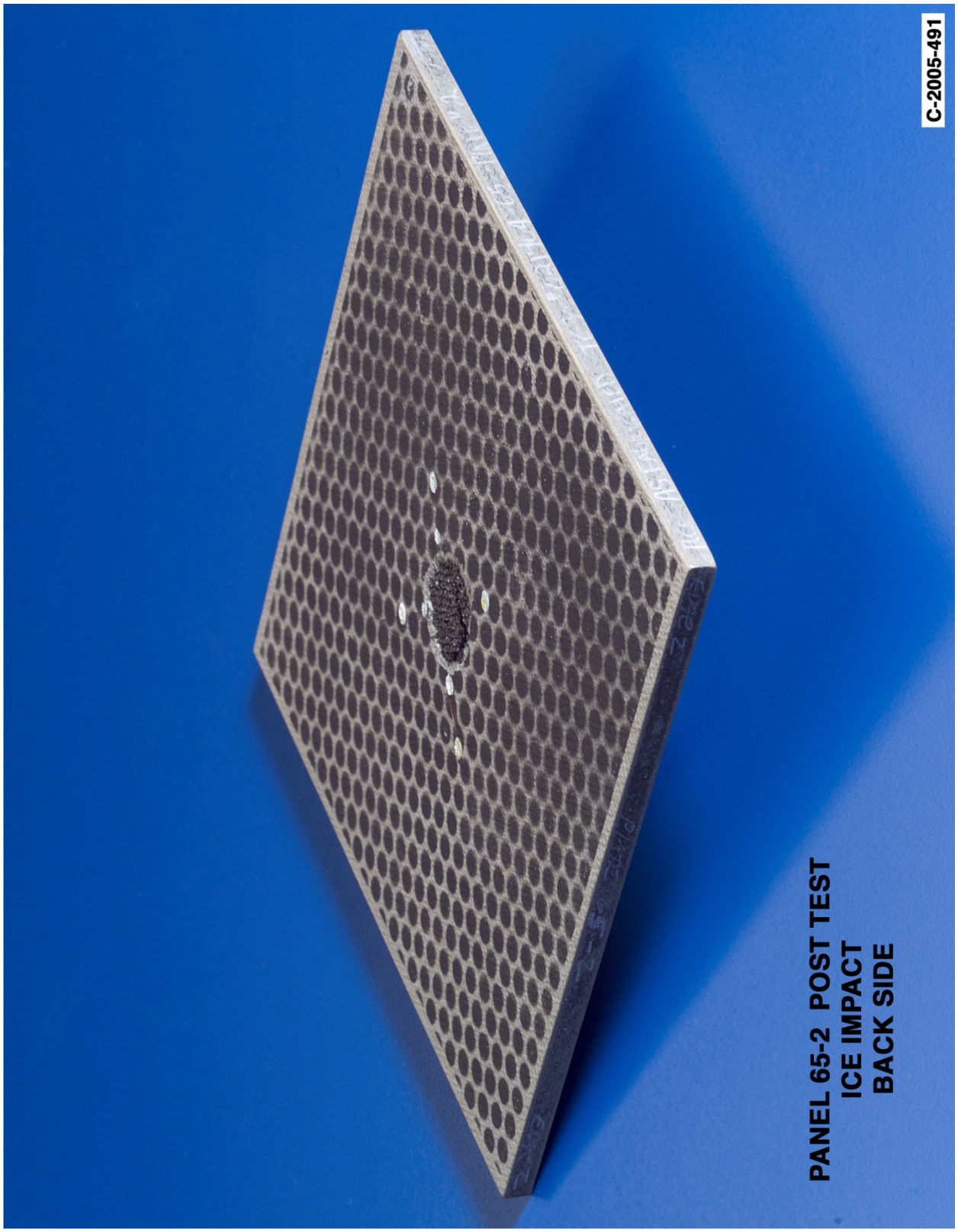

Figure A23–3.—Back face of panel 65-2 at 528 ft/s with a high-density, single-crystal ice cylinder (nominally 0.66 in. in diameter by 1.66 in.) at 90° impact angle. Test GRCC 143.

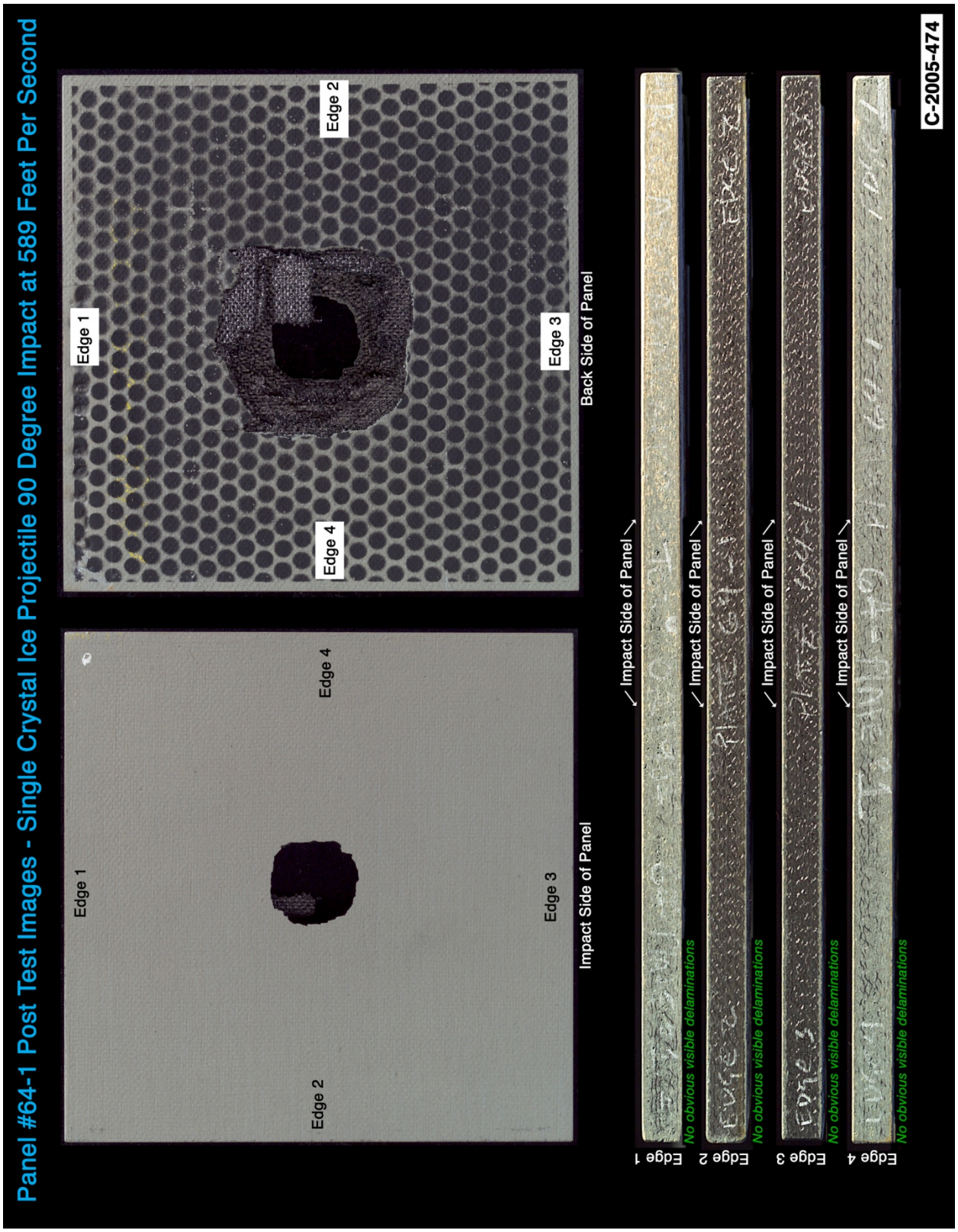

Figure A24–1.—Edges and faces of panel 64-1 at 589 ft/s with a high-density, single-crystal ice cylinder (nominally 0.66 in. in diameter by 1.66 in.) at 90° impact. Test GRCC 139.

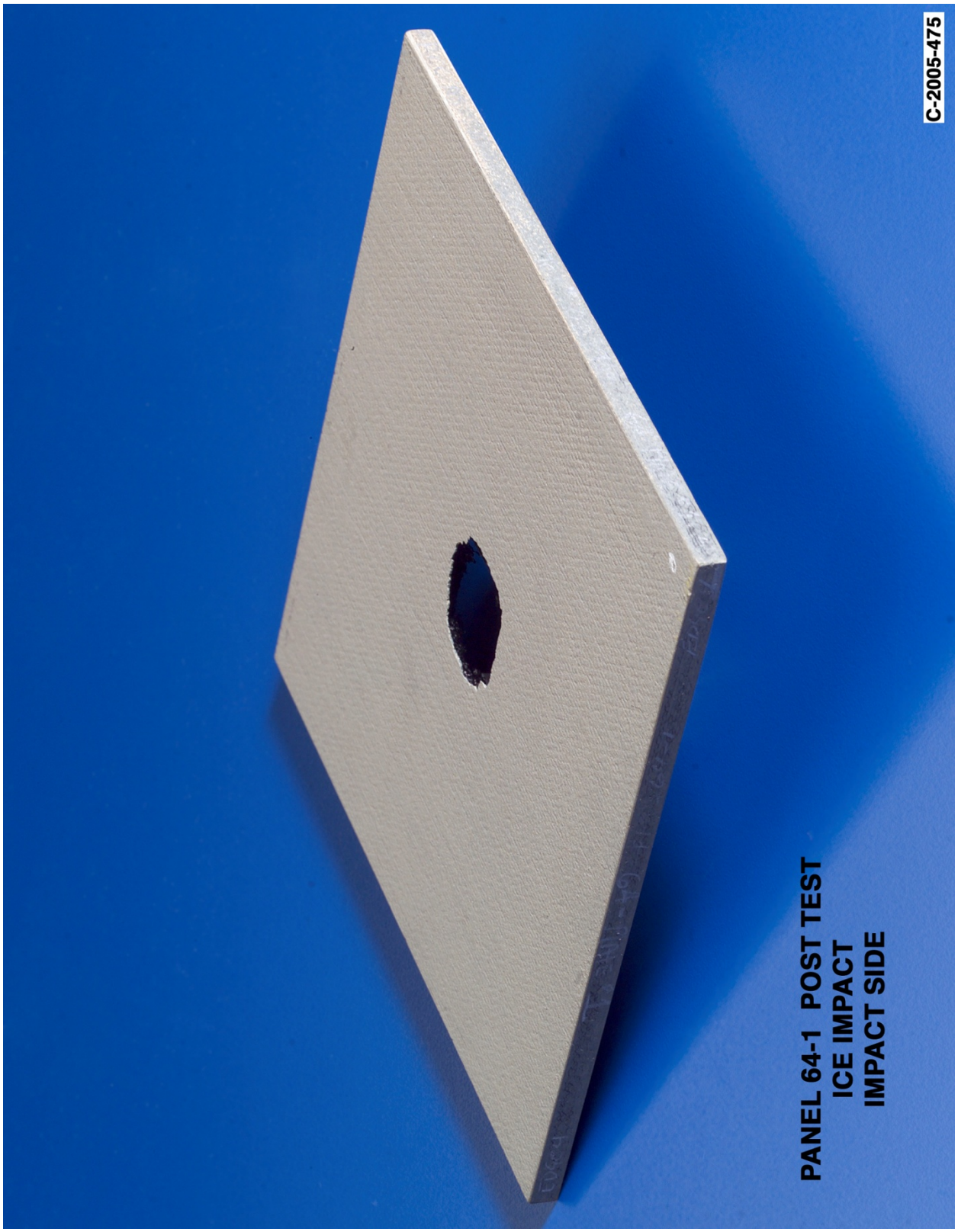

Figure A24–2.—Front (impact side) of panel 64-1 at 589 ft/s with a high-density, single-crystal ice cylinder (nominally 0.66 in. in diameter by 1.66 in.) at 90° impact angle. Test GRCC 139.

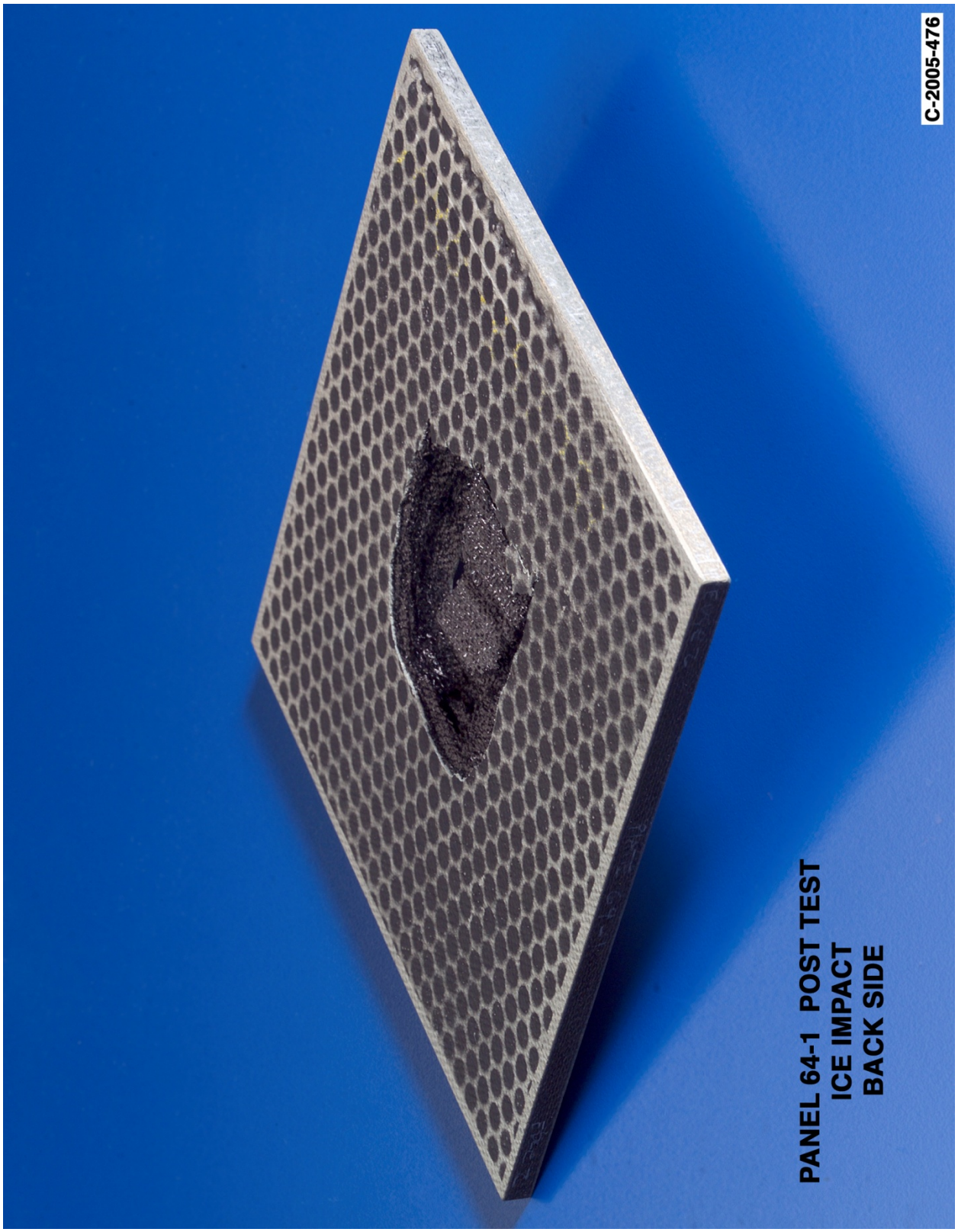

Figure A24–3.—Back face of panel 64-1 at 589 ft/s with a high-density, single-crystal ice cylinder (nominally 0.66 in. in diameter by 1.66 in.) at 90° impact angle. Test GRCC 139.

Appendix B.—Test Data

High-Density Ice Impact Testing at 45° Angle on 6- by 6-in. Reinforced Carbon-Carbon Flat Panels

Notable Observations From the Appendix B Test Series

1. ARAMIS data existed for nearly all ice impact tests but are not presented when considered to be uninterpretable.

Appendix B Test Series

High Density Ice 45 Degree Impact Test Parameters on 6" x 6" Reinforced Carbon-Carbon Panels

Test No.	Glenn Test Reference Number	Impact Velocity (ft/sec)	Panel ID Number	Average Panel Thickness (inches)	Visual Damage Observations	Mass of panel before test (grams)	Mass of panel after test (grams)	Projectile Mass (g)	Projectile Length (in)	Projectile Diameter (in)	Projectile Density lb_m/ft^3	Test Date	Projectile ID Number
2-45-192-14	GRCC098	429	19-2	0.218	Slight internal damage	203.33	203.66	8.600	1.662	0.662	57.271	10/29/04	Ice: 13-PX-5
2-45-193-15	GRCC099	607	19-3	0.217	No Visible damage	202.08	202.31	8.370	1.661	0.653	57.321	10/29/04	Ice: 13-PX-6
2-45-194-16	GRCC100	674	19-4	0.218	No Visible damage	204.39	204.67	8.550	1.660	0.661	57.179	10/29/04	Ice: 13-PX-7
2-45-181-17	GRCC101	777	18-1	0.218	Cracks on front and back	199.07	199.43	8.660	1.661	0.665	57.186	10/29/04	Ice: 13-PX-8
2-45-182-18	GRCC102	780	18-2	0.218	No visible damage	201.19	201.47	8.450	1.662	0.656	57.306	10/29/04	Ice: 13-PX-16
2-45-183-19	GRCC103	802	18-3	0.219	Small coating loss, cracks back	202.45	202.83	8.530	1.659	0.660	57.253	10/29/04	Ice: 13-PX-14
2-45-151-21	GRCC106	816	15-1	0.221	No indication found	201.65	202.00	8.500	1.660	0.659	57.190	11/2/04	Ice: 13-PX-12
2-45-203-25	GRCC110	819	20-3	0.220	Front and Back side damage	201.67	202.09	8.4	1.663	0.654	57.281	11/2/04	Ice: 13-PX-17
2-45-152-24	GRCC109	826	15-2	0.223	No indication found	202.60	202.91	8.450	1.662	0.656	57.306	11/2/04	Ice: 13-PX-9
2-45-184-20	GRCC105	830	18-4	0.217	Crack on front, coating loss back	201.04	201.29	8.580	1.663	0.661	57.276	11/2/04	Ice: 13-PX-15
2-45-201-23	GRCC108	830	20-1	0.224	Front and Back side damage	202.54	202.54	8.56	1.663	0.66	57.316	11/2/04	Ice: 13-PX-10
2-45-202-22	GRCC107	833	20-2	0.220	Front and Back side damage	202.63	201.69	8.75	1.661	0.668	57.262	11/2/04	Ice: 13-PX-11
2-45-191-13	GRCC083	858	19-1	0.218	Blew hole in panel	201.25	192.25	8.620	1.660	0.663	57.300	10/25/04	Ice: 13-PX-4

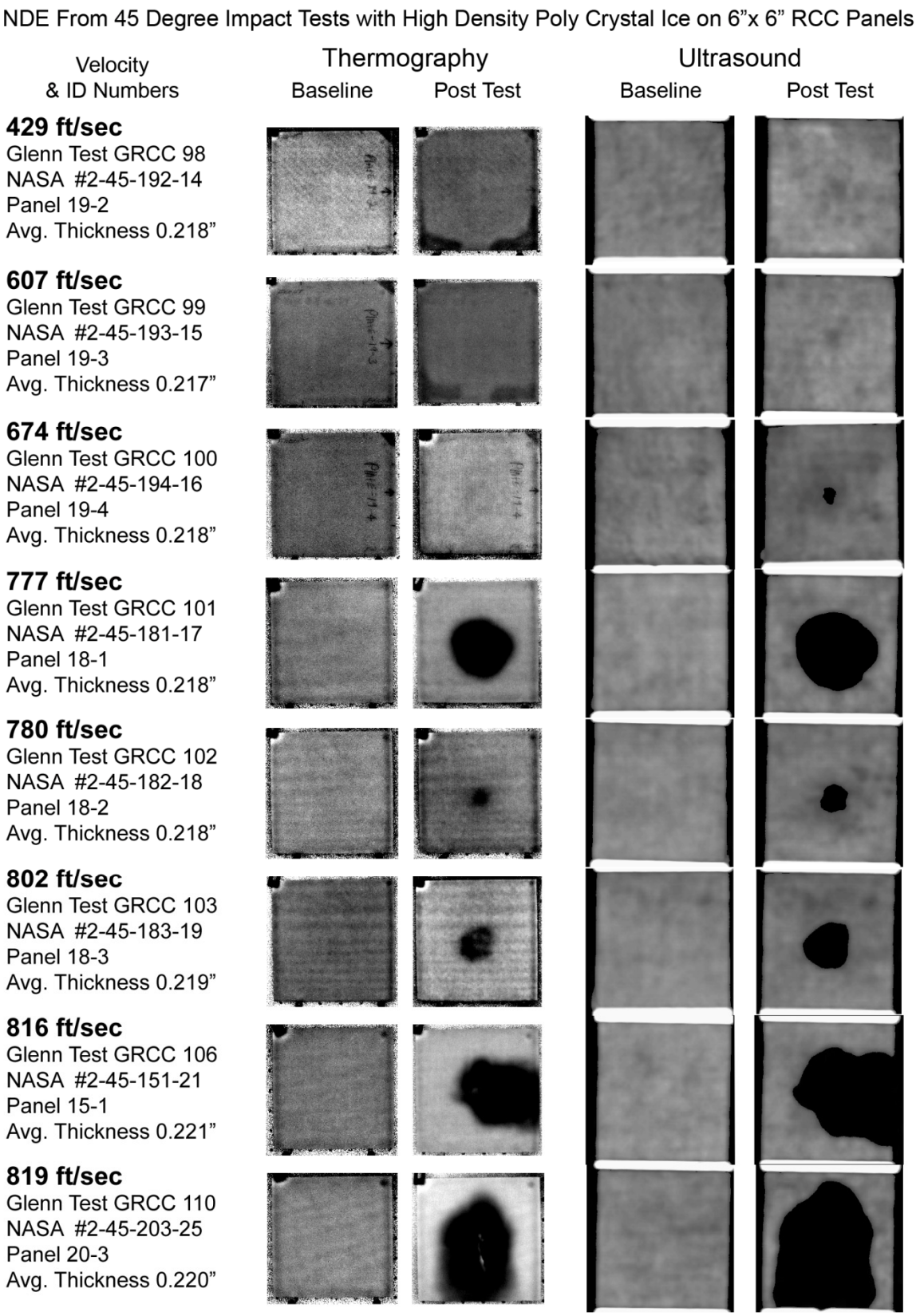

Figure B1–1.—Pulse thermography and ultrasound post impact pre- and posttest images of RCC 6- by 6-in. flat panels impacted with high-density ice cylinders (nominally 0.66 in. in diameter by 1.66 in.) at 45° angle.

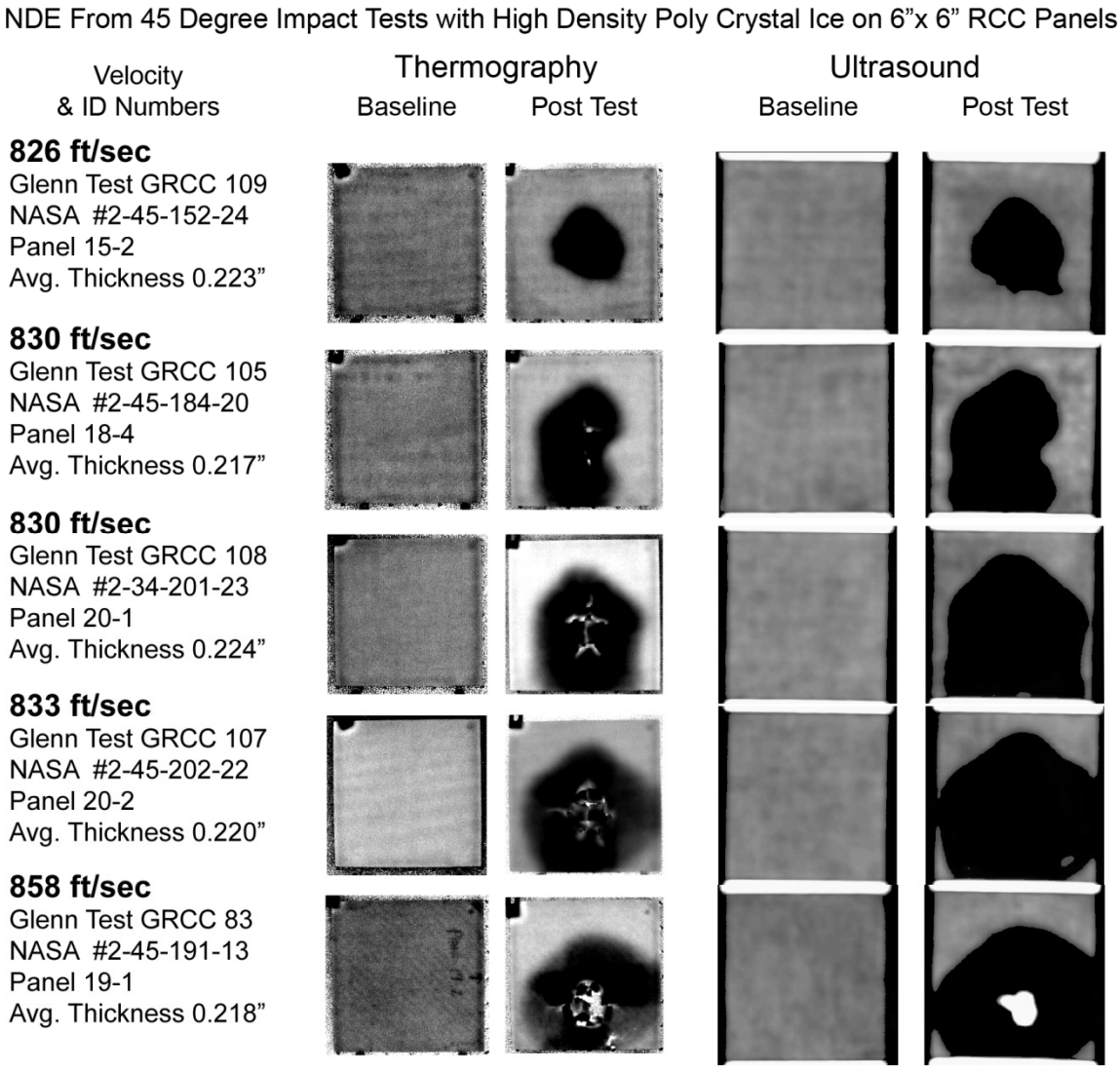

Figure B1–2.—Pulse thermography and ultrasound post impact pre- and posttest images of reinforced carbon-carbon 6- by 6-in. flat panels impacted with high-density ice cylinders (nominally 0.66 in. in diameter by 1.66 in.) at 45° angle.

Aramis Displacement Contours from 45 Degree Impact Tests with High Density Poly-Crystal Ice on 6”x 6” RCC Panels

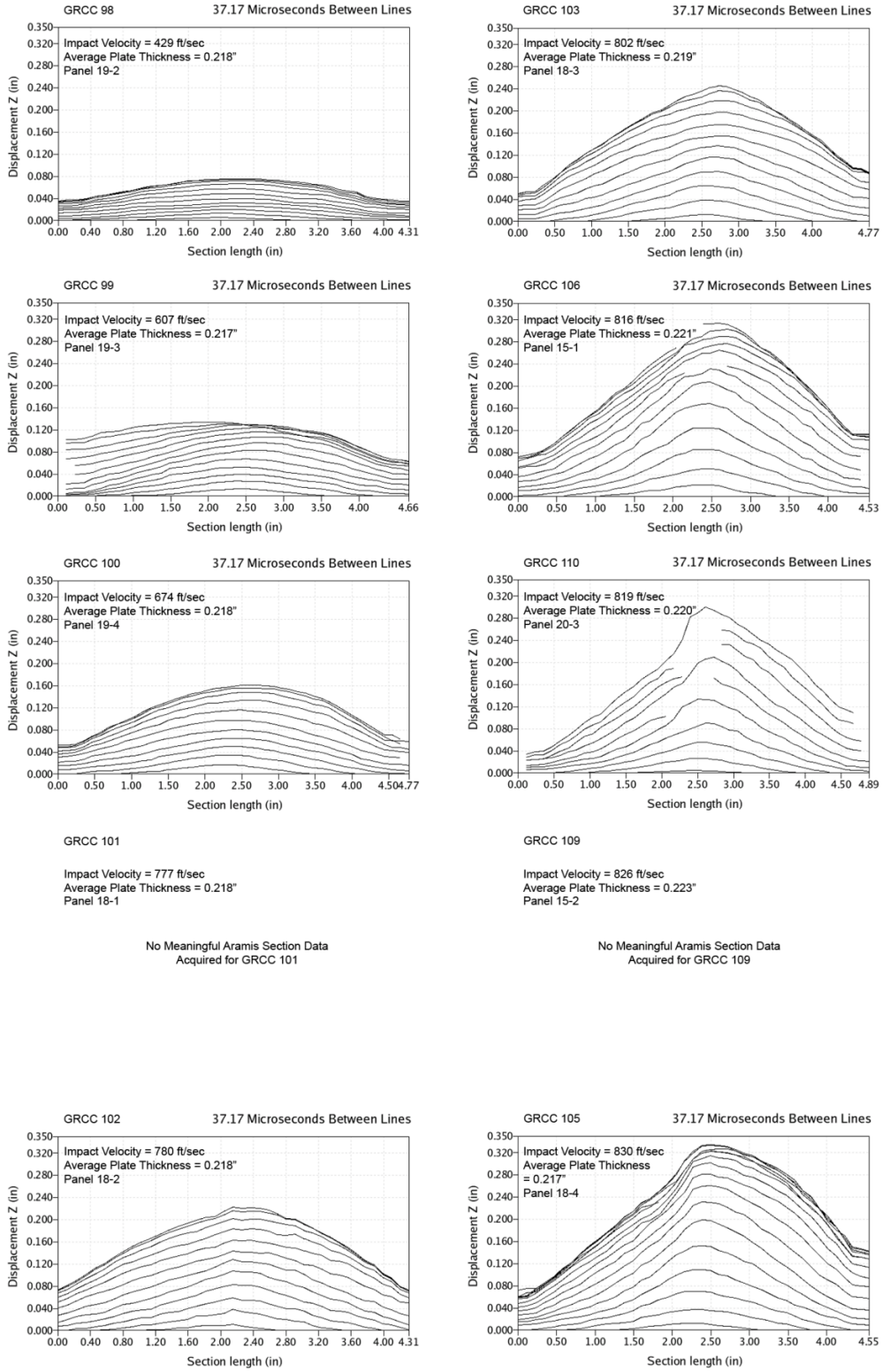

Figure B2–1.—ARAMIS out-of-plane deformation contours across centerline of 6- by 6-in. RCC flat panels measured at 37 μs increments undergoing impact with high-density ice cylinders (nominally 0.66 in. in diameter by 1.66 in.) at 45° angle.

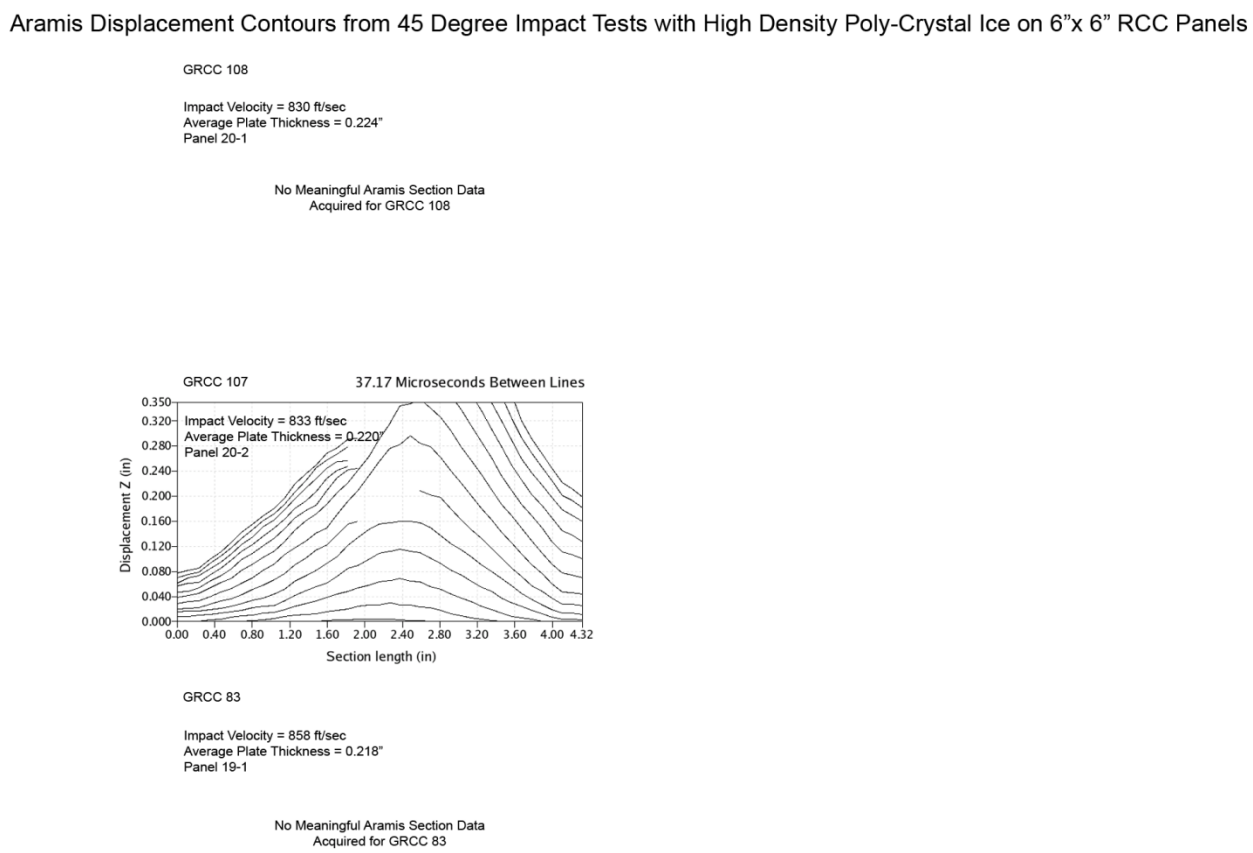

Figure B2–2.—ARAMIS out-of-plane deformation contours across centerline of 6- by 6-in. reinforced carbon-carbon flat panels plotted at 37 μs increments undergoing impact with high-density ice cylinders (nominally 0.66 in. in diameter by 1.66 in.) at 45° angle.

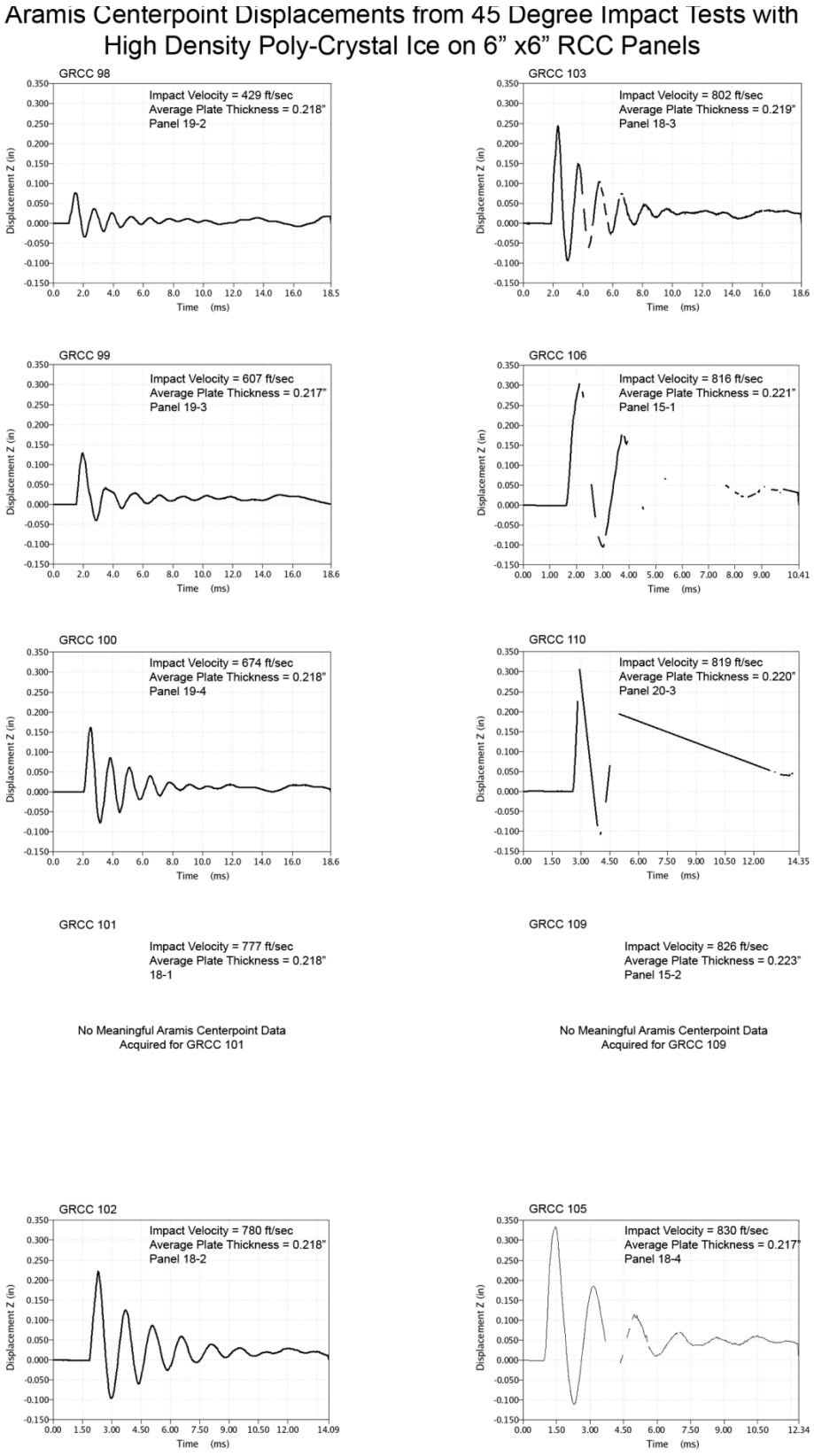

Figure B3–1.—ARAMIS centerpoint out-of-plane deformation vs. time of 6- by 6-in. reinforced carbon-carbon flat panels impacted with high-density ice cylinders (nominally 0.66 in. in diameter by 1.66 in.) at 45° angle.

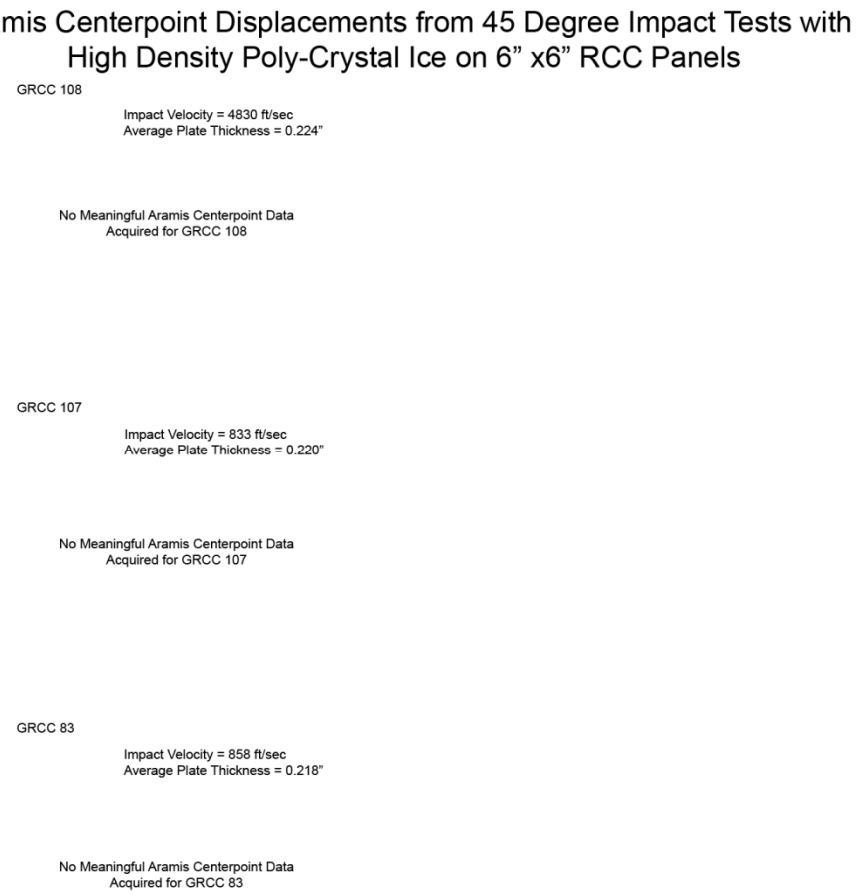

Figure B3–2.—ARAMIS centerpoint out-of-plane deformation versus time of 6- by 6-in. reinforced carbon-carbon flat panels impacted with high-density ice cylinders (nominally 0.66 in. in diameter by 1.66 in.) at 45° angle.

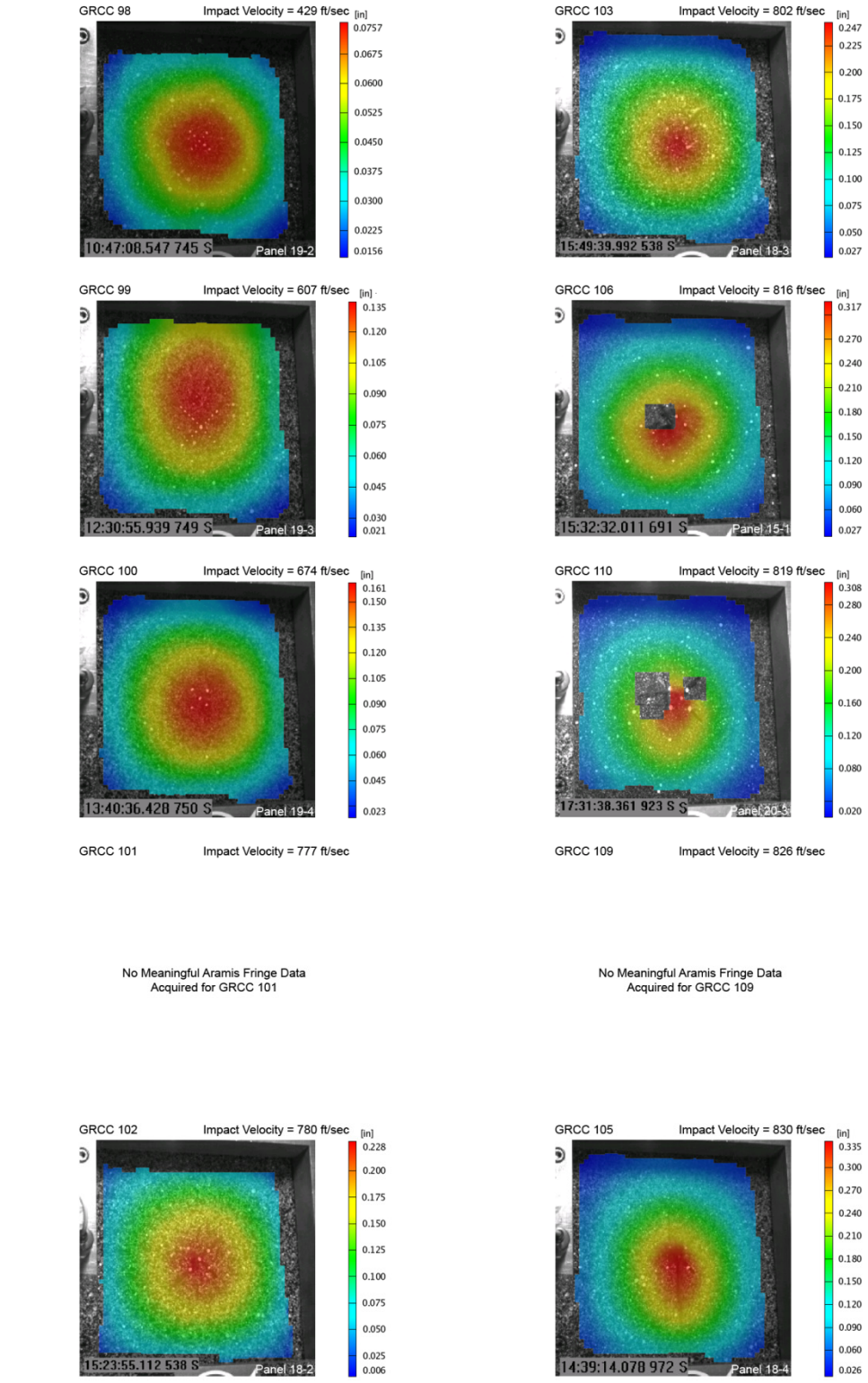

Figure B4–1.—ARAMIS color fringe plots depicting maximum deformation prior to material failure of 6- by 6-in. reinforced carbon-carbon flat panels as they undergo impact with high-density ice cylinders (nominally 0.66 in. in diameter by 1.66 in.) at 45° angle.

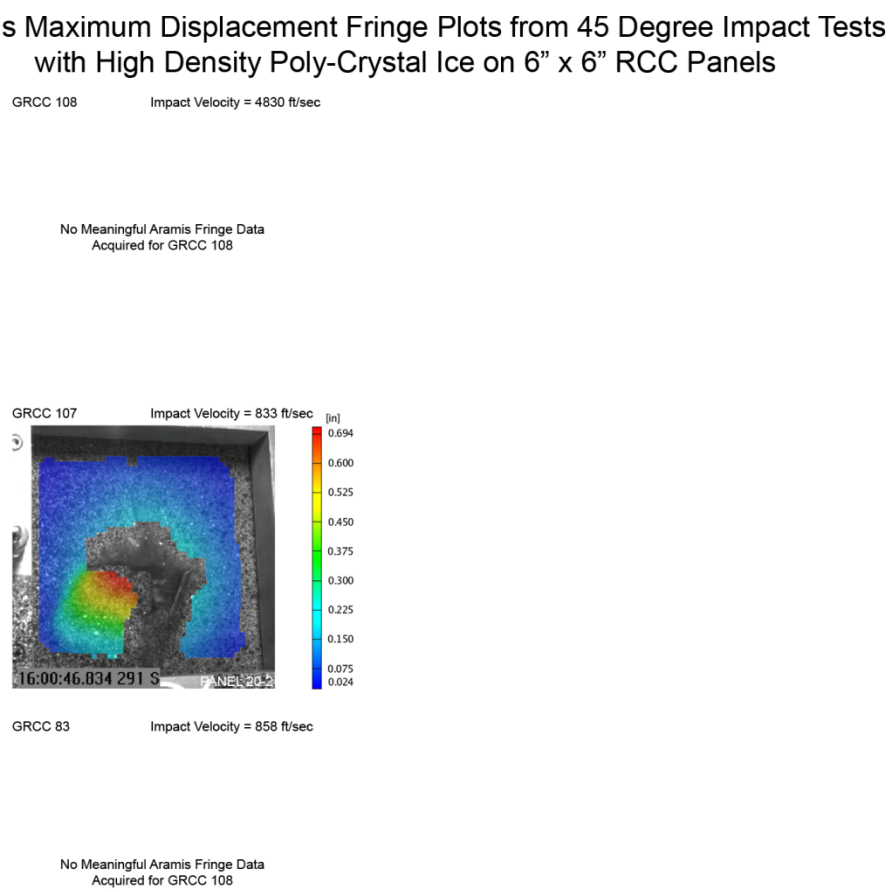

Figure B4–2.—ARAMIS color fringe plots depicting maximum deformation prior to material failure of 6- by 6-in. reinforced carbon-carbon flat panels as they undergo impact with high-density ice cylinders (nominally 0.66 in. in diameter by 1.66 in.) at 45° angle.

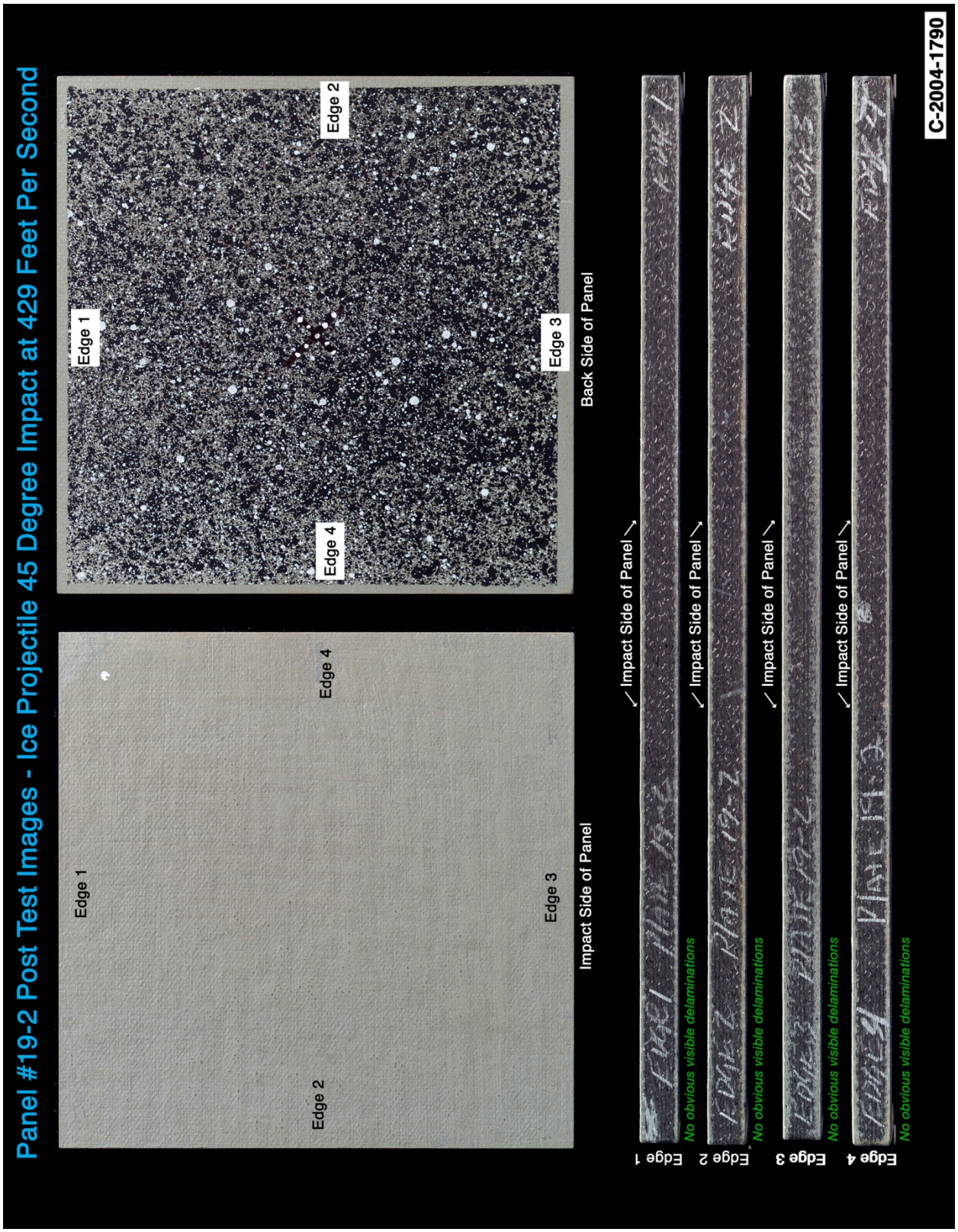

Figure B5–1.—Edges and faces of panel 19-2 at 429 ft/s with a high-density, poly-crystal ice cylinder (nominally 0.66 in. in diameter by 1.66 in.) at 45° impact angle. Test GRCC 98.

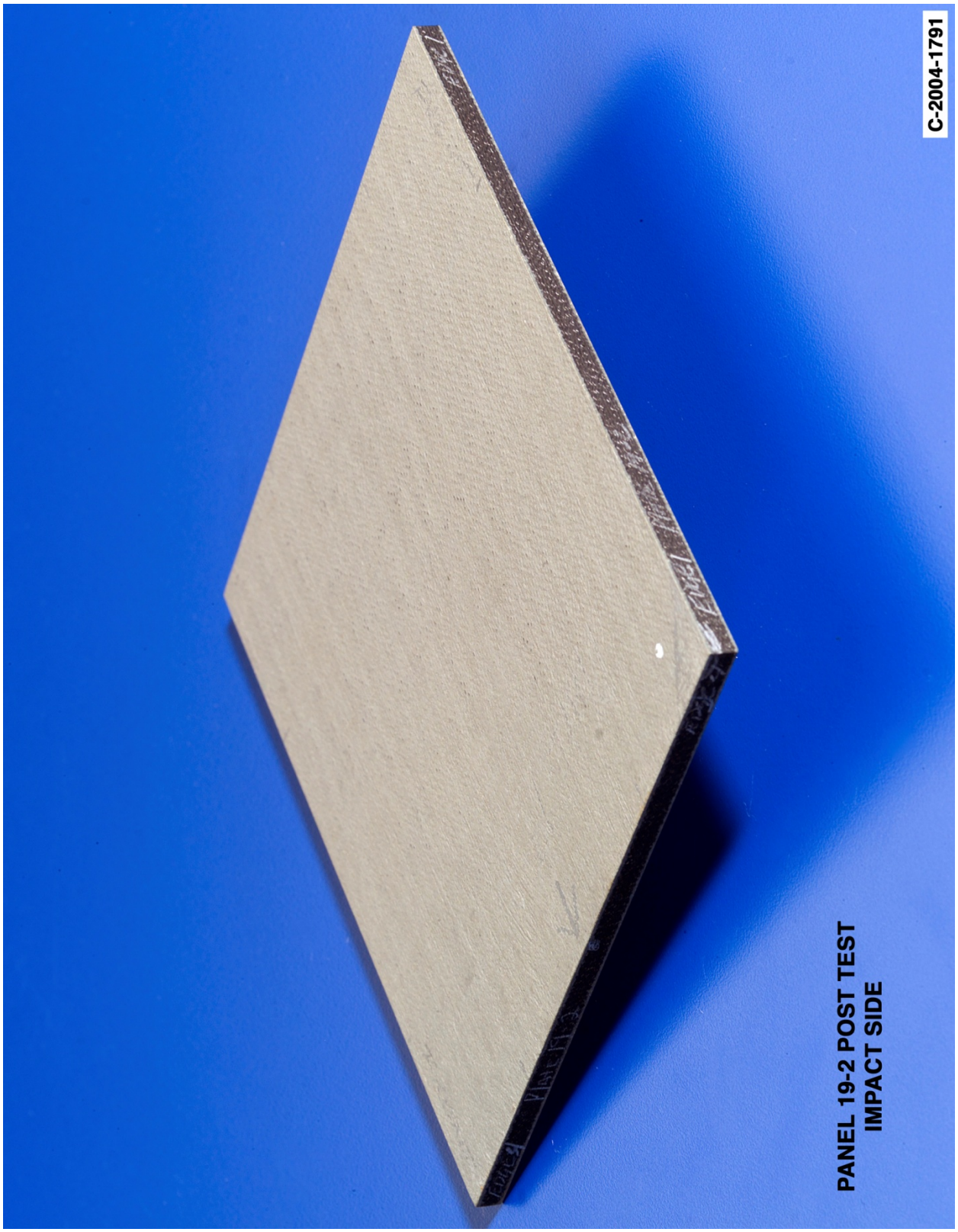

Figure B5–2.—Front (impact side) of panel 19-2 at 429 ft/s with a high-density, poly-crystal ice cylinder (nominally 0.66 in. in diameter by 1.66 in.) at 45° impact angle. Test GRCC 98.

Figure B5–3.—Back face of panel 19-2 at 429 ft/s with a high-density, poly-crystal ice cylinder (nominally 0.66 in. in diameter by 1.66 in.) at 45° impact angle. Test GRCC 98.

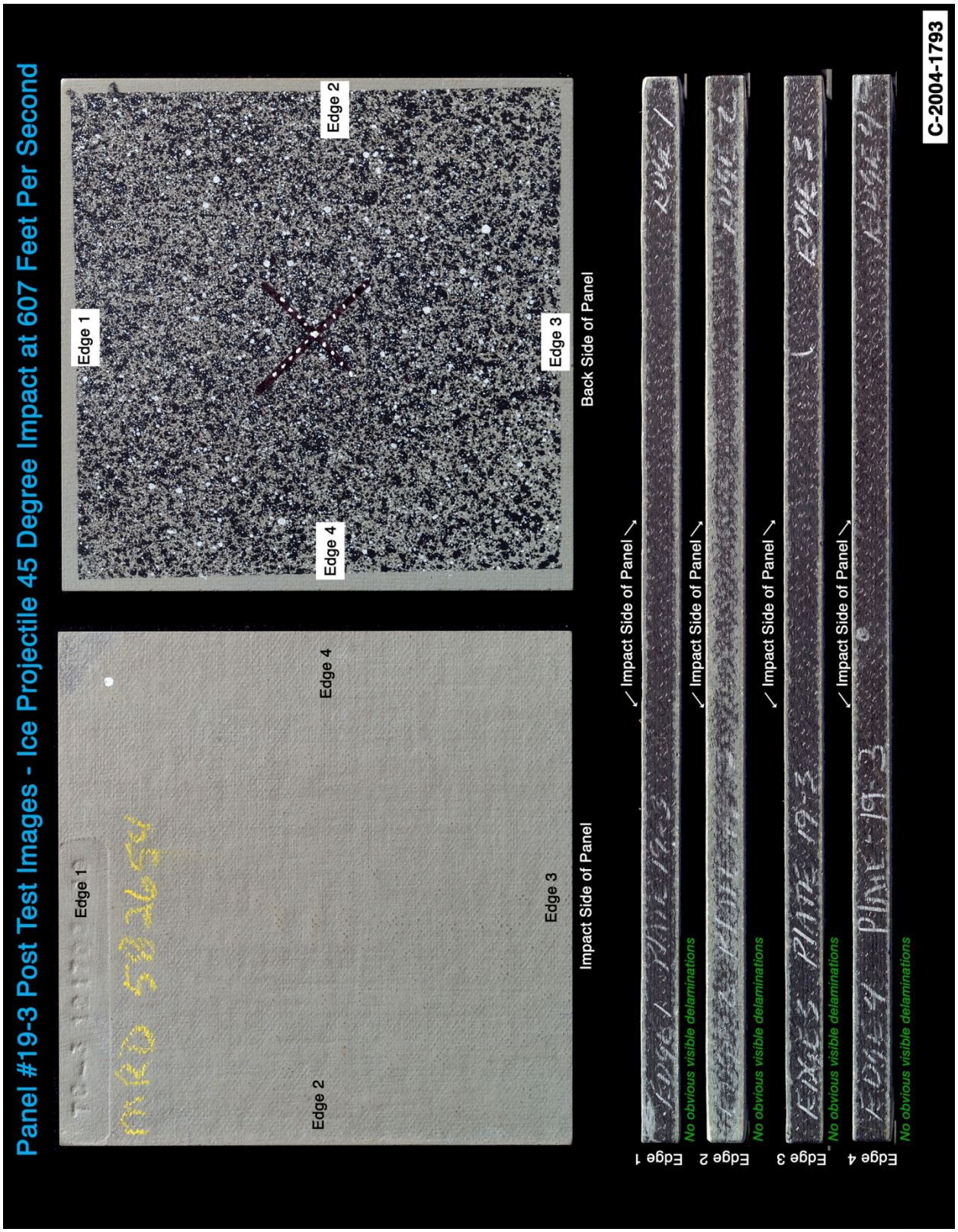

Figure B6–1.—Edges and faces of panel 19-3 at 607 ft/s with a high-density, poly-crystal ice cylinder (nominally 0.66 in. in diameter by 1.66 in.) at 45° impact. Test GRCC 99.

Figure B6–2.—Front (impact side) of panel 19-3 at 607 ft/s with a high-density, poly-crystal ice cylinder (nominally 0.66 in. in diameter by 1.66 in.) at 45° impact angle. Test GRCC 99.

Figure B6–3.—Back face of panel 19-3 at 607 ft/s with a high-density, poly-crystal ice cylinder (nominally 0.66 in. in diameter by 1.66 in.) at 45° impact angle. Test GRCC 99.

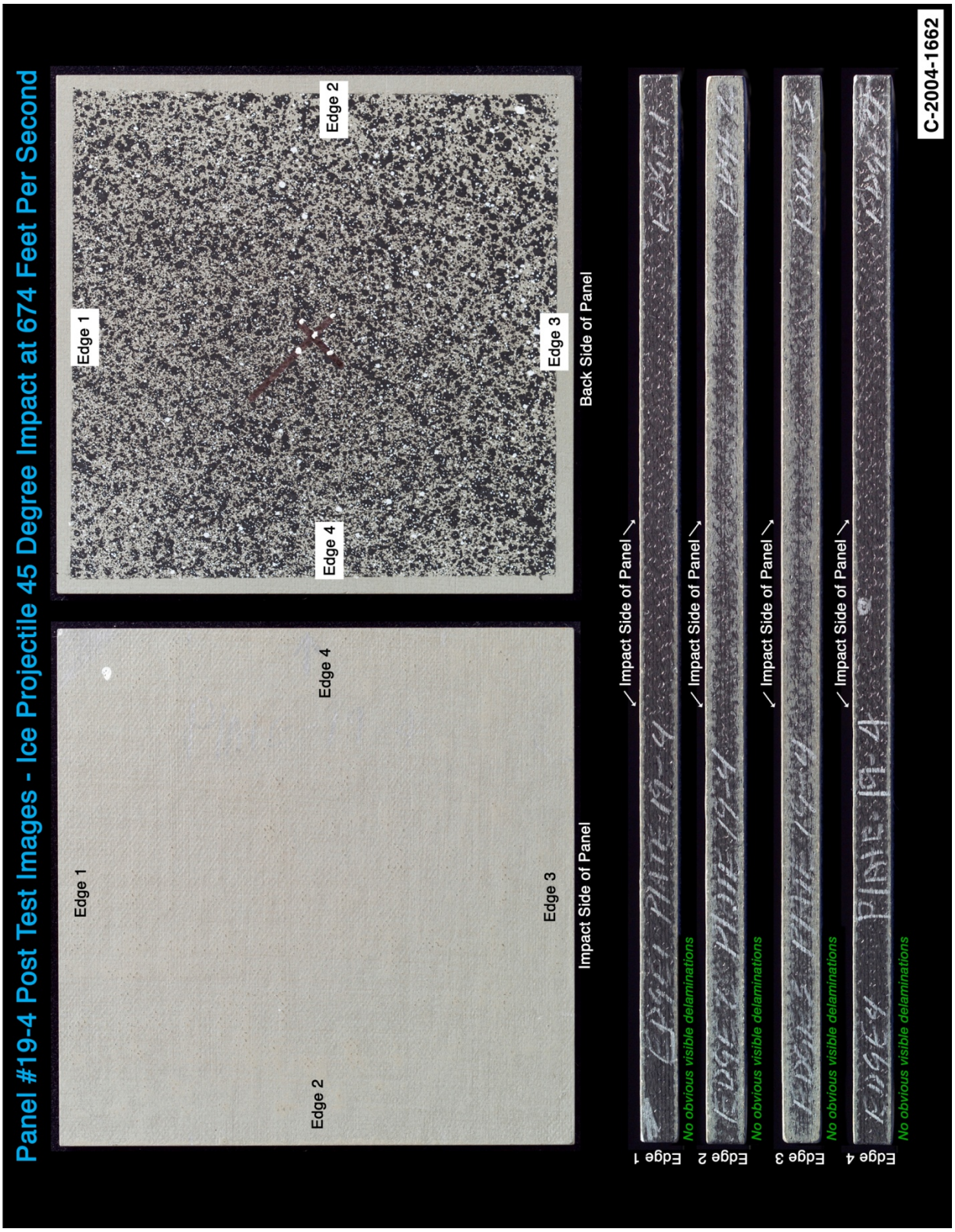

Figure B7–1.—Edges and faces of panel 19-4 at 674 ft/s with a high-density, poly-crystal ice cylinder (nominally 0.66 in. in diameter by 1.66 in.) at 45° impact. Test GRCC 100.

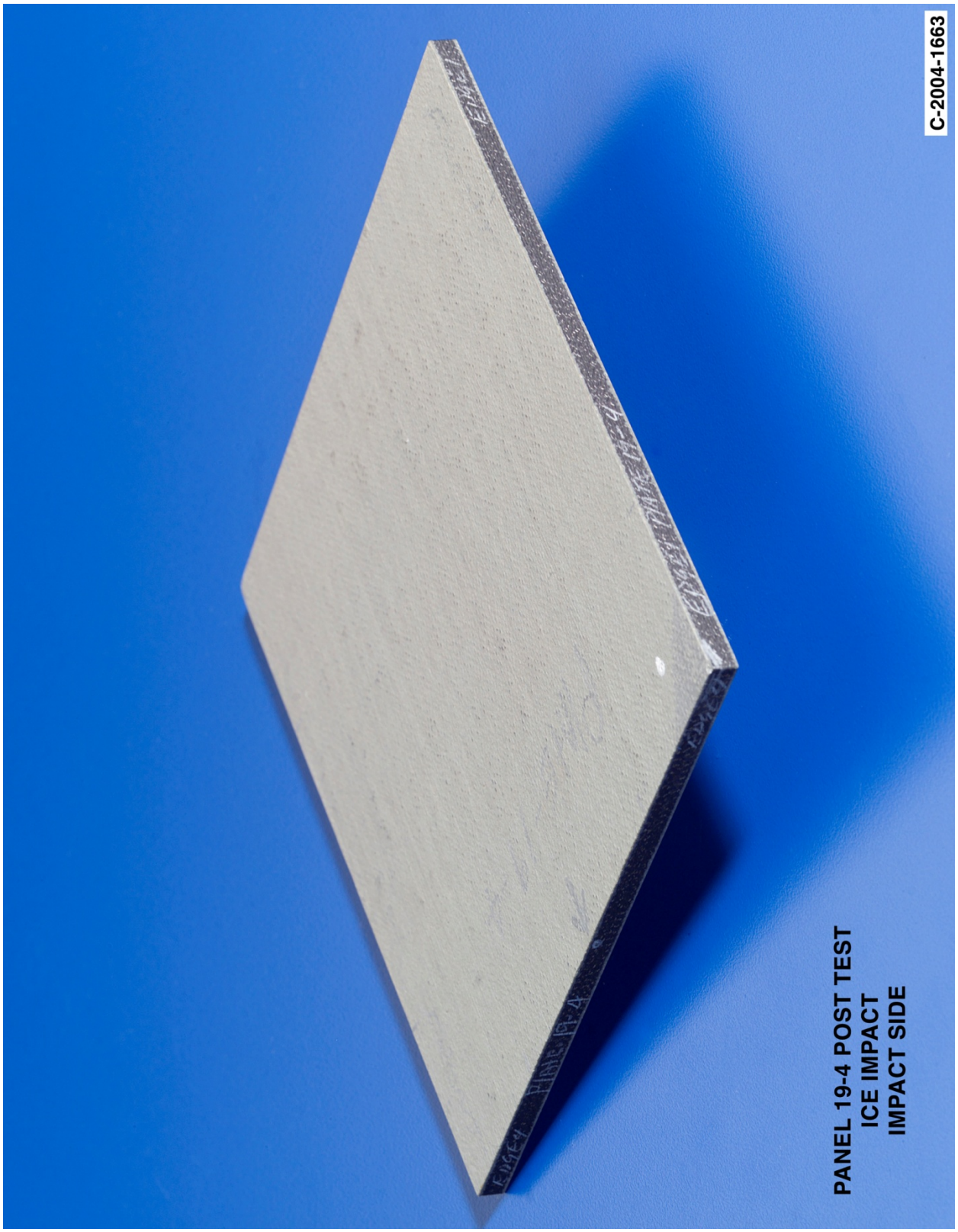

Figure B7–2.—Front (impact side) of panel 19-4 at 674 ft/s with a high-density, poly-crystal ice cylinder (nominally 0.66 in. in diameter by 1.66 in.) at 45° impact angle. Test GRCC 100.

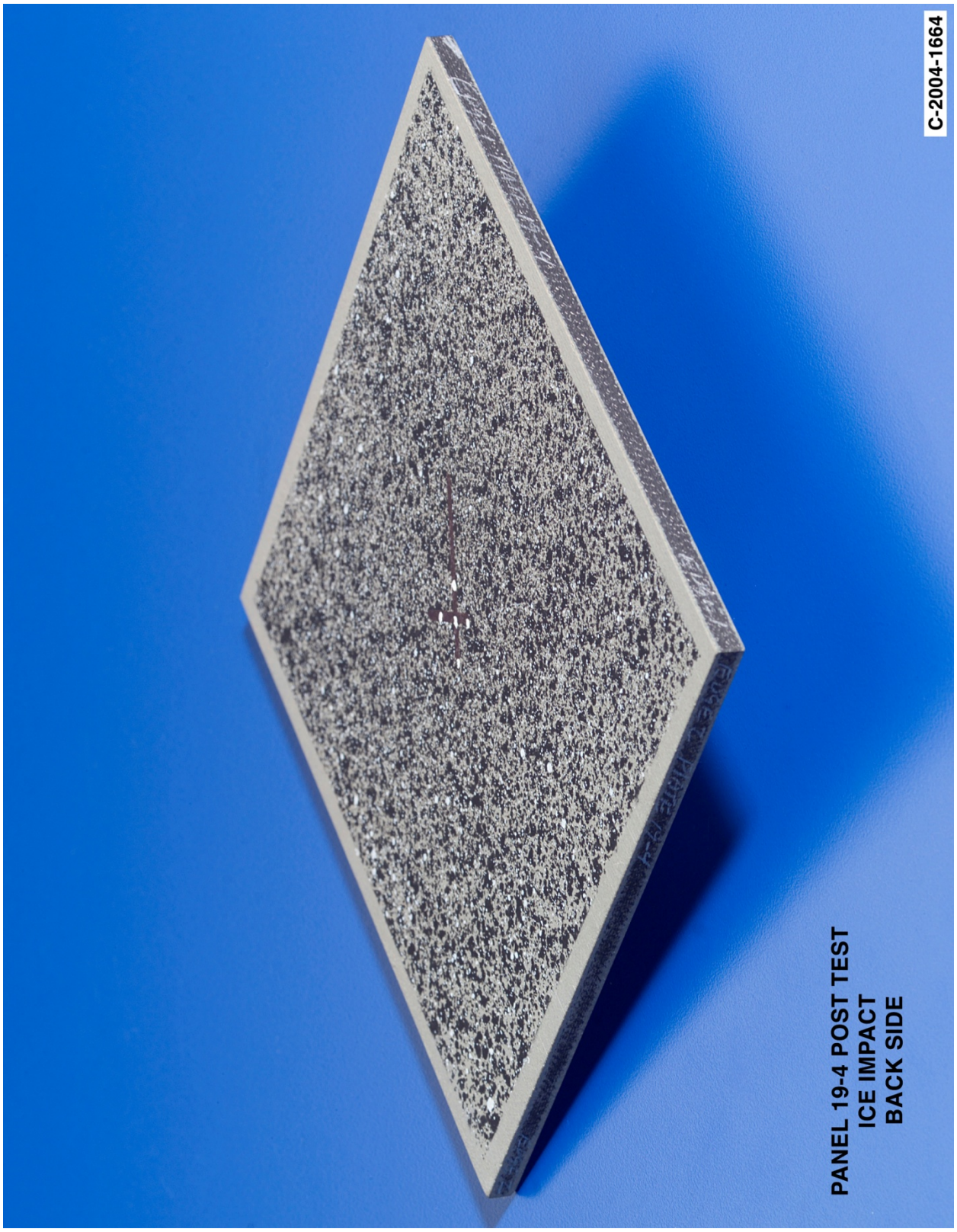

Figure B7–3.—Back face of panel 19-4 at 674 ft/s with a high-density, poly-crystal ice cylinder (nominally 0.66 in. in diameter by 1.66 in.) at 45° impact angle. Test GRCC 100.

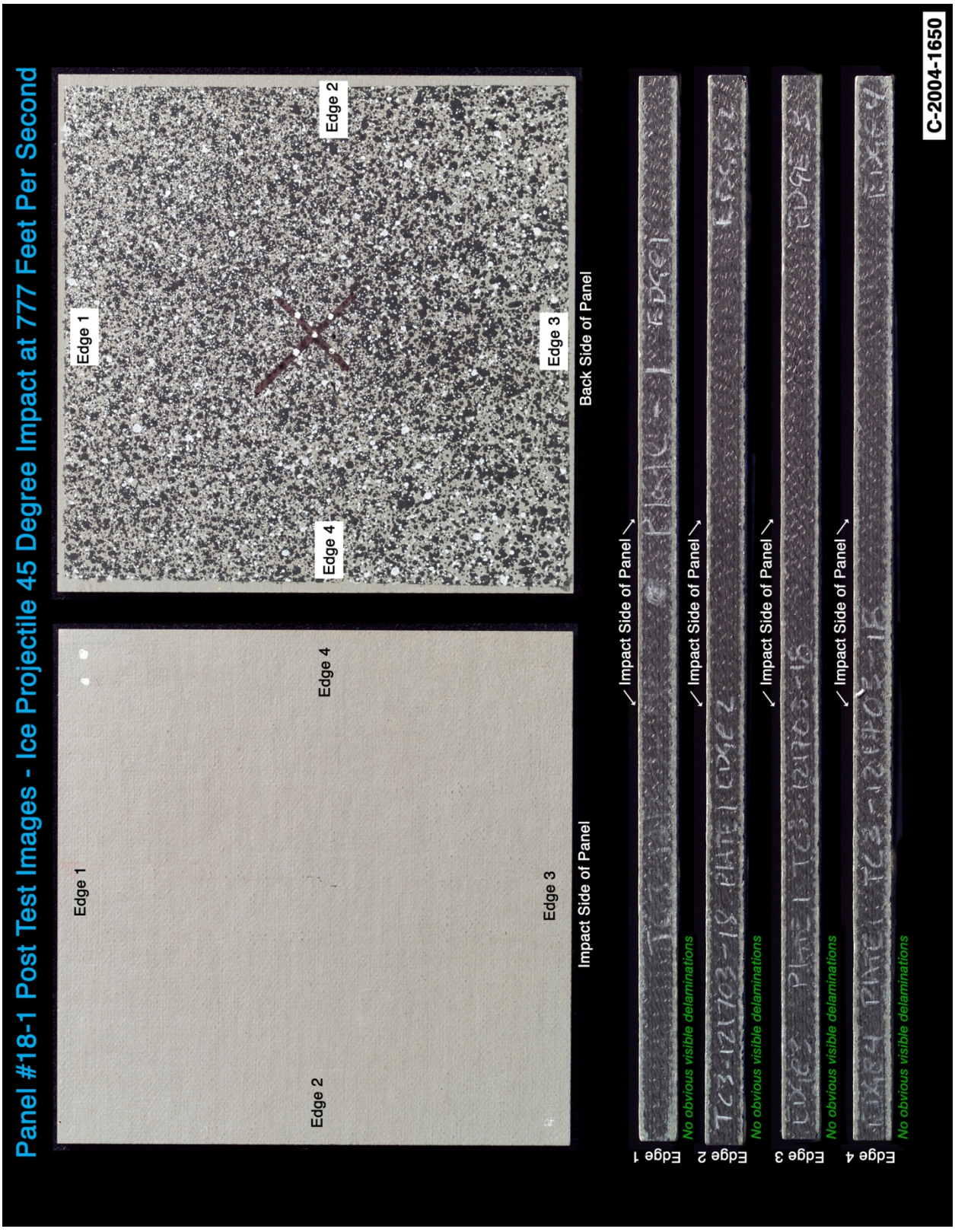

Figure B8–1.—Edges and faces of panel 18-1 at 777 ft/s with a high-density, poly-crystal ice cylinder (nominally 0.66 in. in diameter by 1.66 in.) at 45° impact. Test GRCC 101.

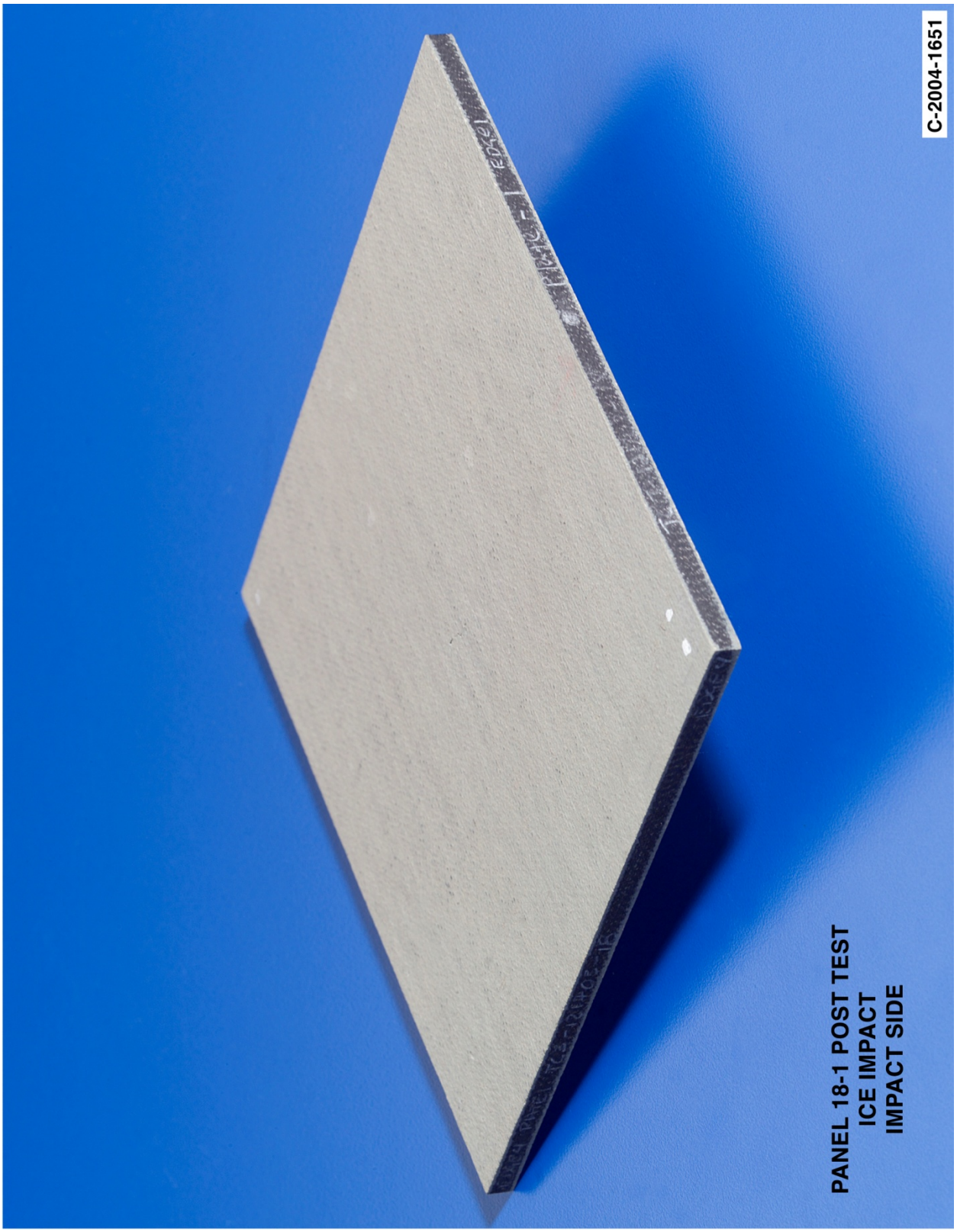

Figure B8–2.—Front (impact side) of panel 18-1 at 777 ft/s with a high-density, poly-crystal ice cylinder (nominally 0.66 in. in diameter by 1.66 in.) at 45° impact angle. Test GRCC 101.

Figure B8–3.—Back face of panel 18-1 at 777 ft/s with a high-density, poly-crystal ice cylinder (nominally 0.66 in. in diameter by 1.66 in.) at 45° impact angle. Test GRCC 101.

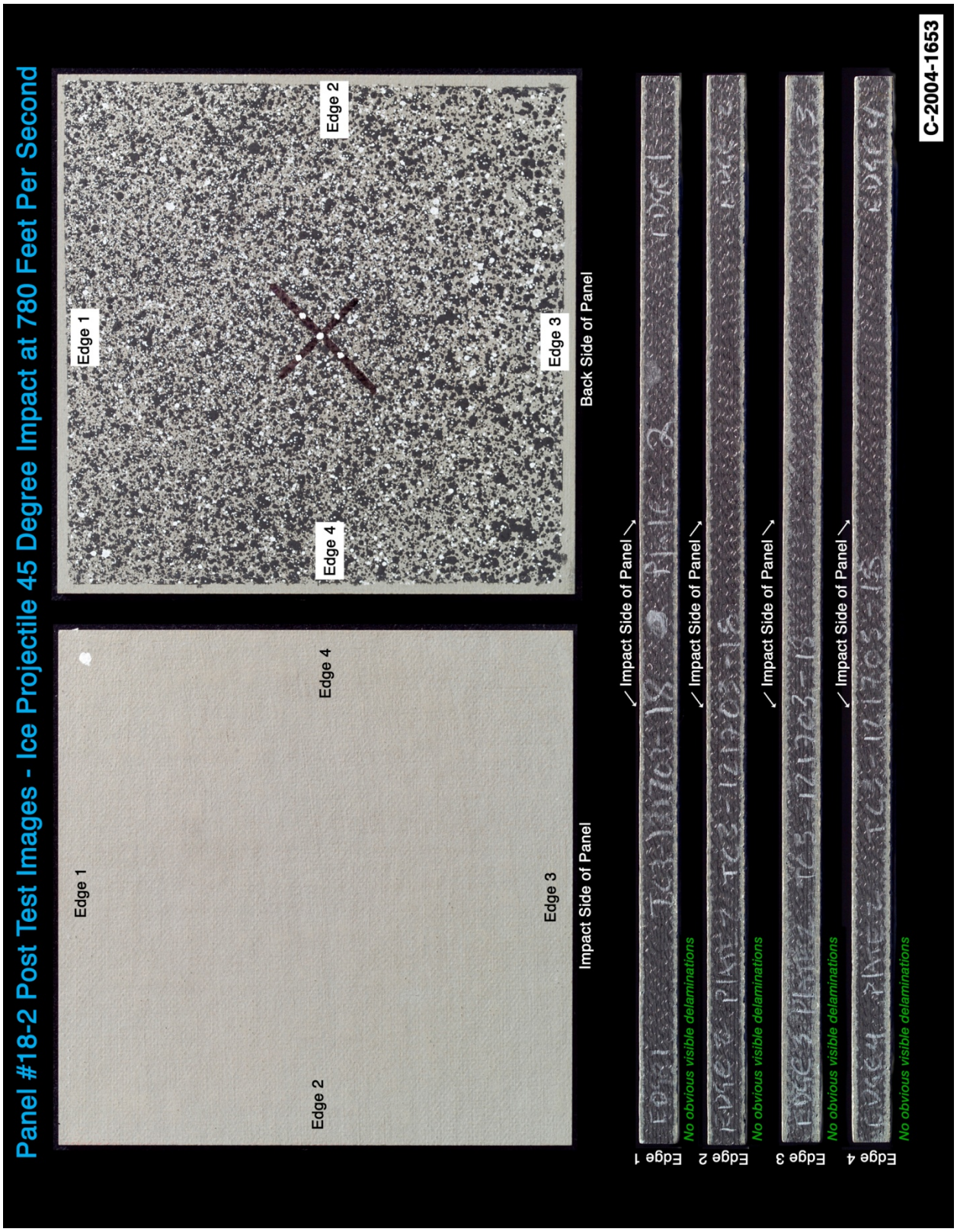

Figure B9–1.—Edges and faces of panel 18-2 at 780 ft/s with a high-density, poly-crystal ice cylinder (nominally 0.66 in. in diameter by 1.66 in.) at 45° impact. Test GRCC 102.

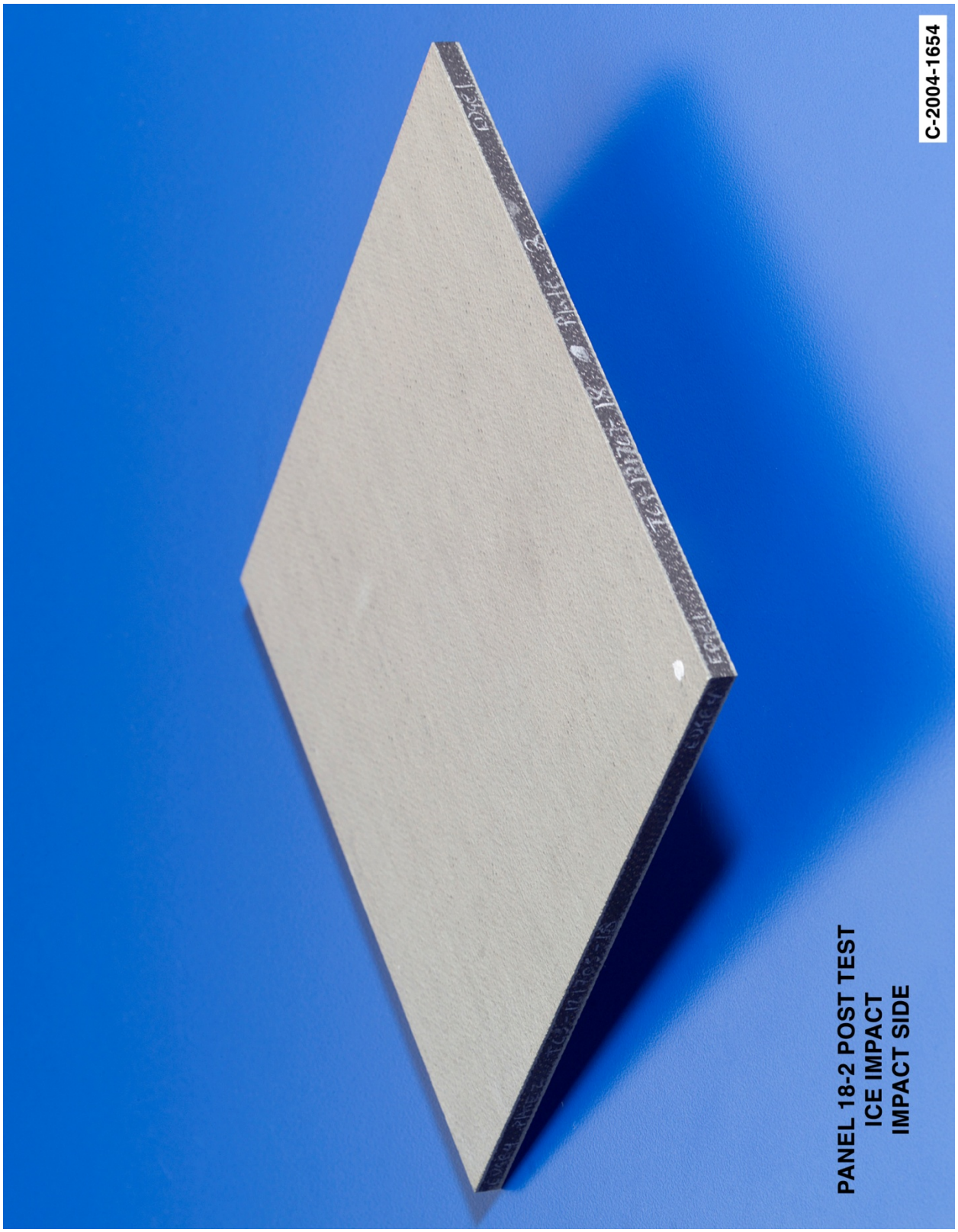

Figure B9–2.—Front (impact side) of panel 18-2 at 780 ft/s with a high-density, poly-crystal ice cylinder (nominally 0.66 in. in diameter by 1.66 in.) at 45° impact angle. Test GRCC 102.

Figure B9–3.—Back face of panel 18-2 at 780 ft/s with a high-density, poly-crystal ice cylinder (nominally 0.66 in. in diameter by 1.66 in.) at 45° impact angle. Test GRCC 102.

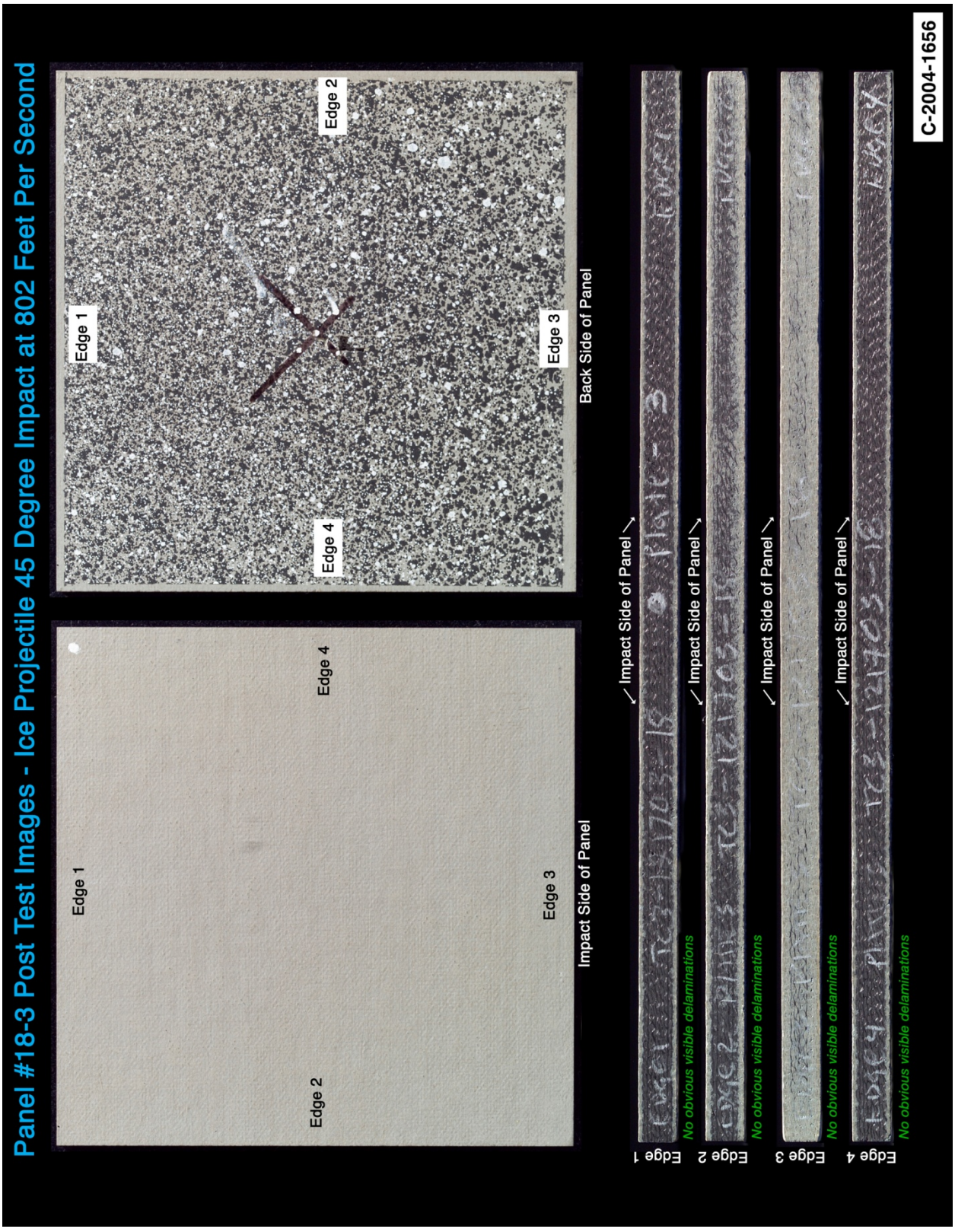

Figure B10–1.—Edges and faces of panel 18-3 at 802 ft/s with a high-density, poly-crystal ice cylinder (nominally 0.66 in. in diameter by 1.66 in.) at 45° impact. Test GRCC 103.

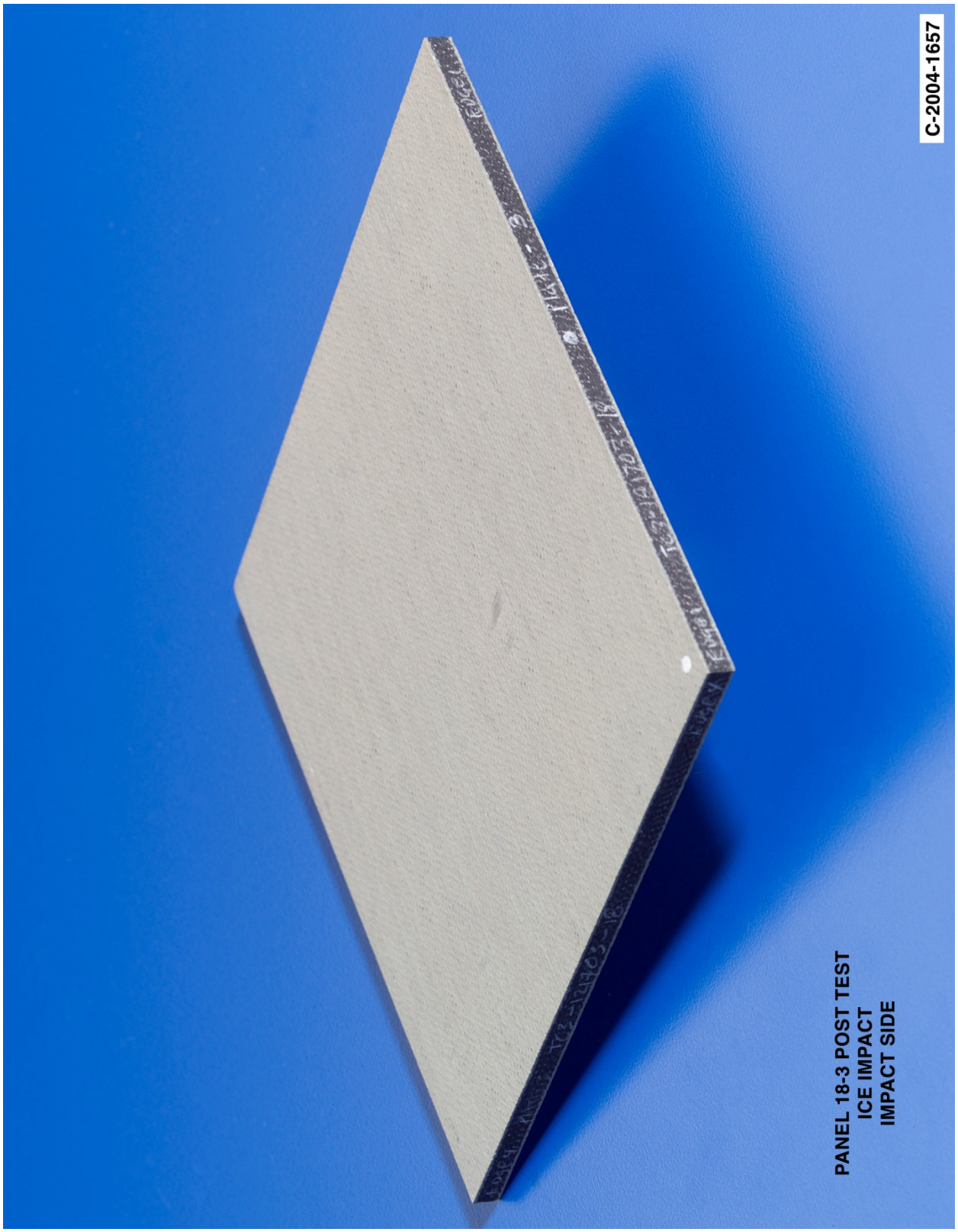

Figure B10–2.—Front (impact side) of panel 18-3 at 802 ft/s with a high-density, poly-crystal ice cylinder (nominally 0.66 in. in diameter by 1.66 in.) at 45° impact angle. Test GRCC 103.

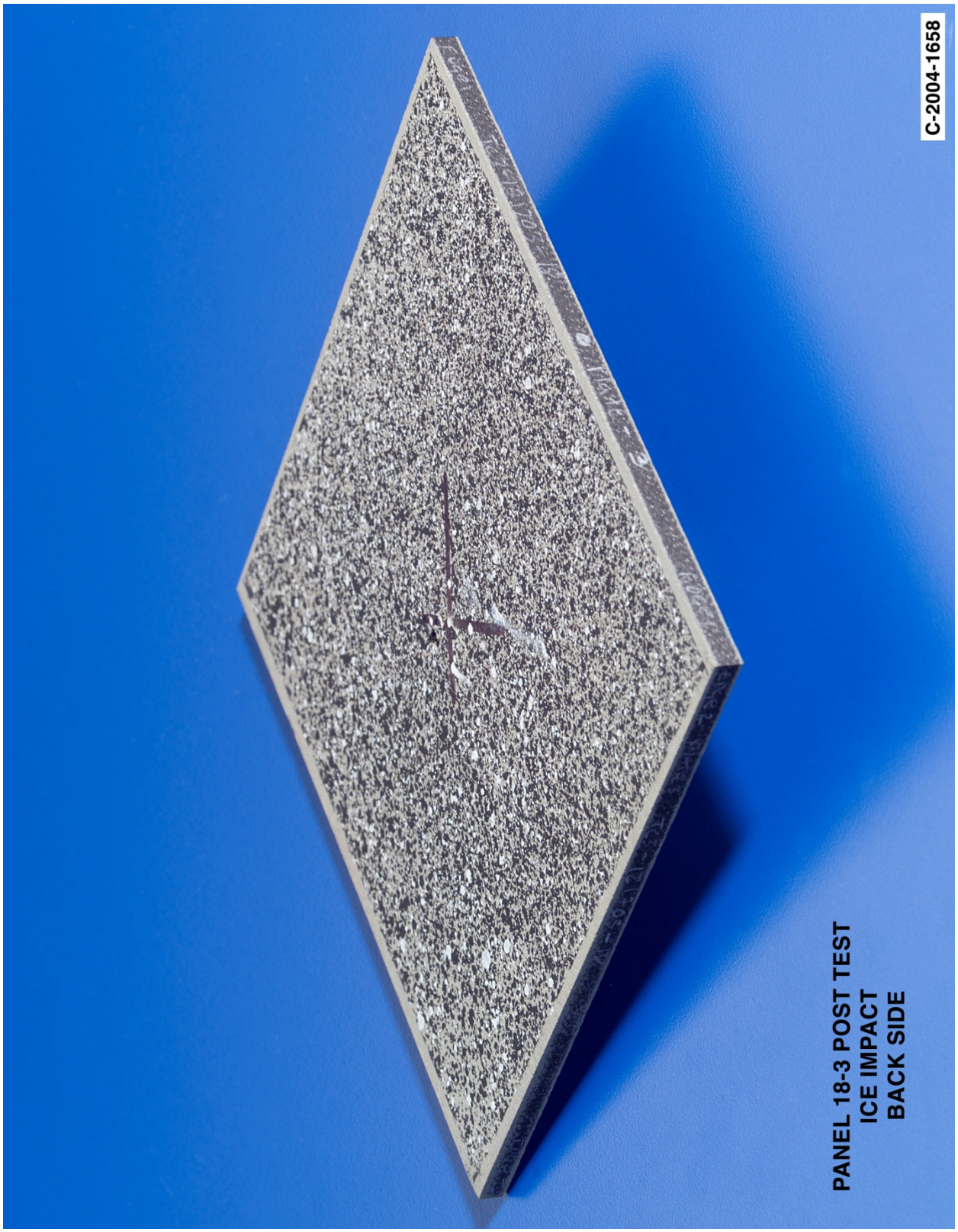

Figure B10–3.—Back face of panel 18-3 at 802 ft/s with a high-density, poly-crystal ice cylinder (nominally 0.66 in. in diameter by 1.66 in.) at 45° impact angle. Test GRCC 103.

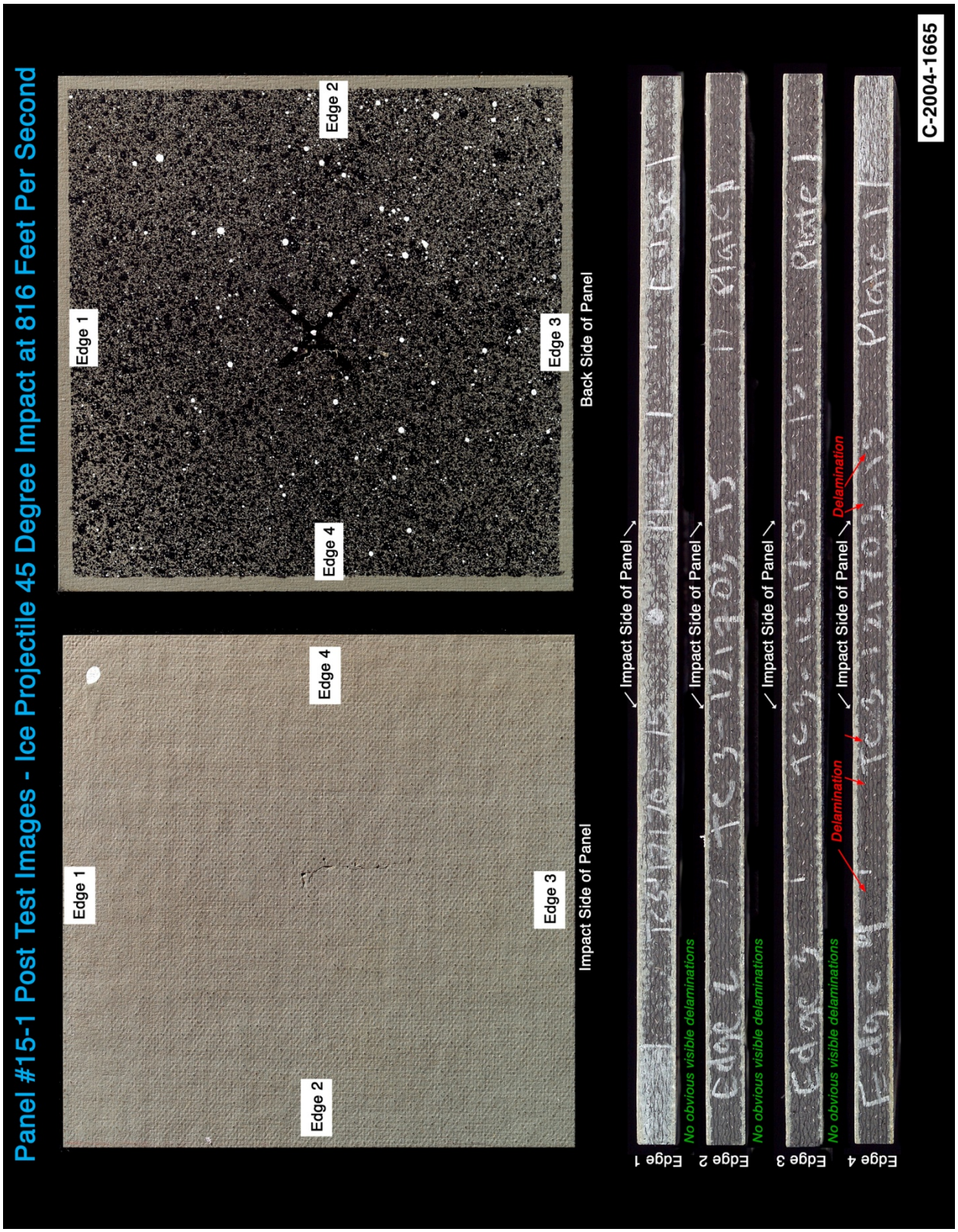

Figure B11–1.—Edges and faces of panel 15-1 at 816 ft/s with a high-density, poly-crystal ice cylinder (nominally 0.66 in. in diameter by 1.66 in.) at 45° impact. Test GRCC 106.

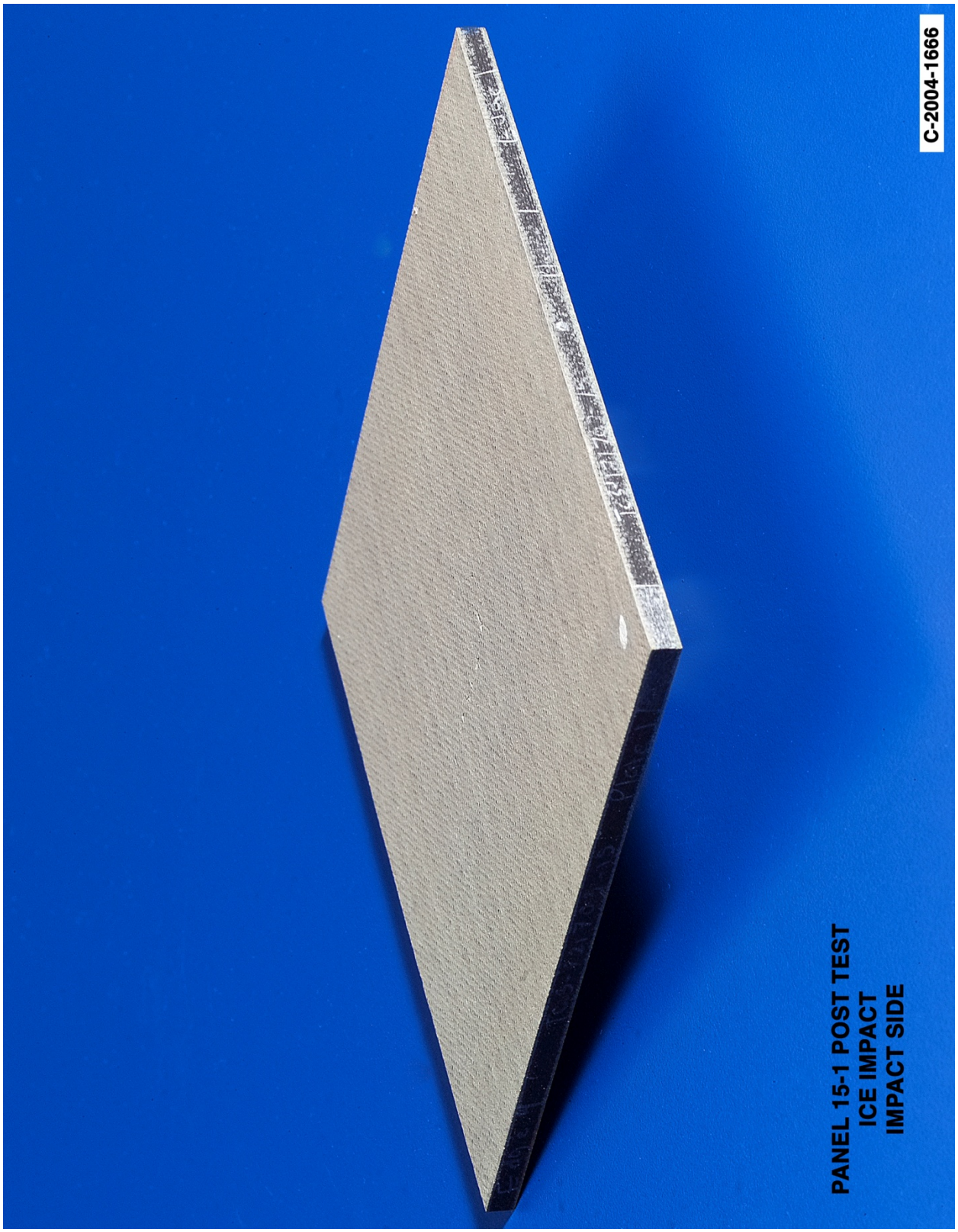

Figure B11–2.—Front (impact side) of panel 15-1 at 816 ft/s with a high-density, poly-crystal ice cylinder (nominally 0.66 in. in diameter by 1.66 in.) at 45° impact angle. Test GRCC 106.

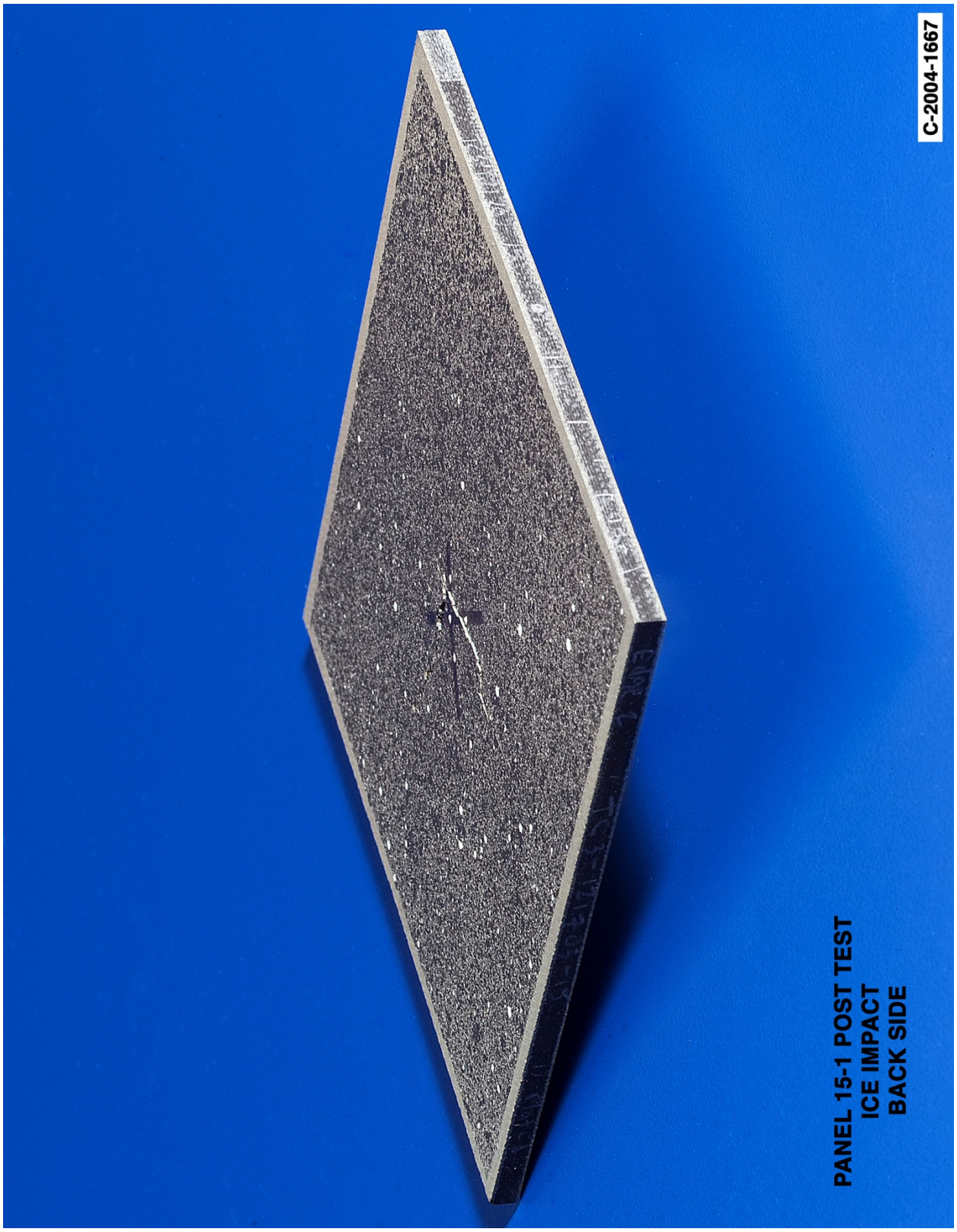

Figure B11–3.—Back face of panel 15-1 at 816 ft/s with a high-density, poly-crystal ice cylinder (nominally 0.66 in. in diameter by 1.66 in.) at 45° impact angle. Test GRCC 106.

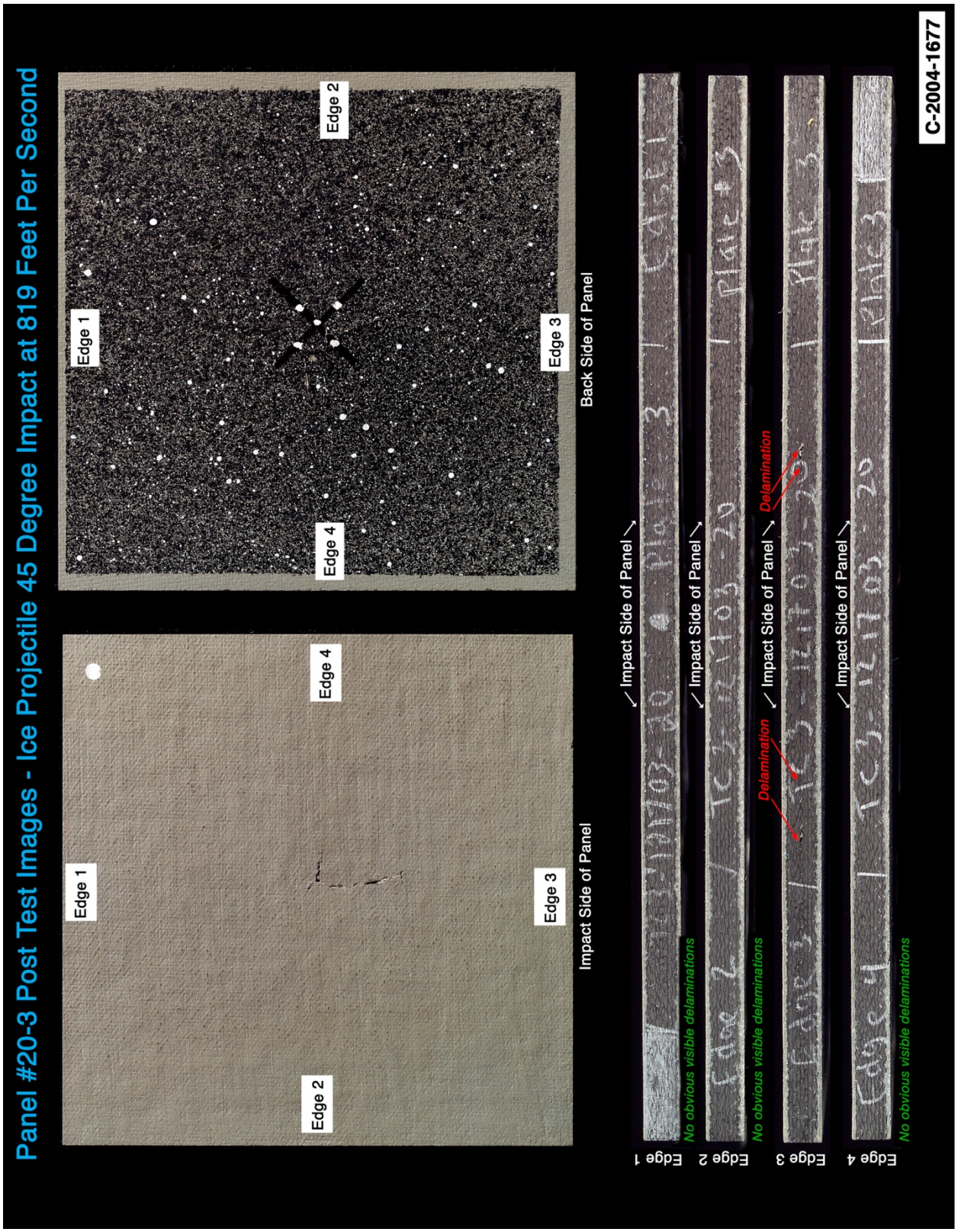

Figure B12–1.—Edges and faces of panel 20-3 at 819 ft/s with a high-density, poly-crystal ice cylinder (nominally 0.66 in. in diameter by 1.66 in.) at 45° impact. Test GRCC 110.

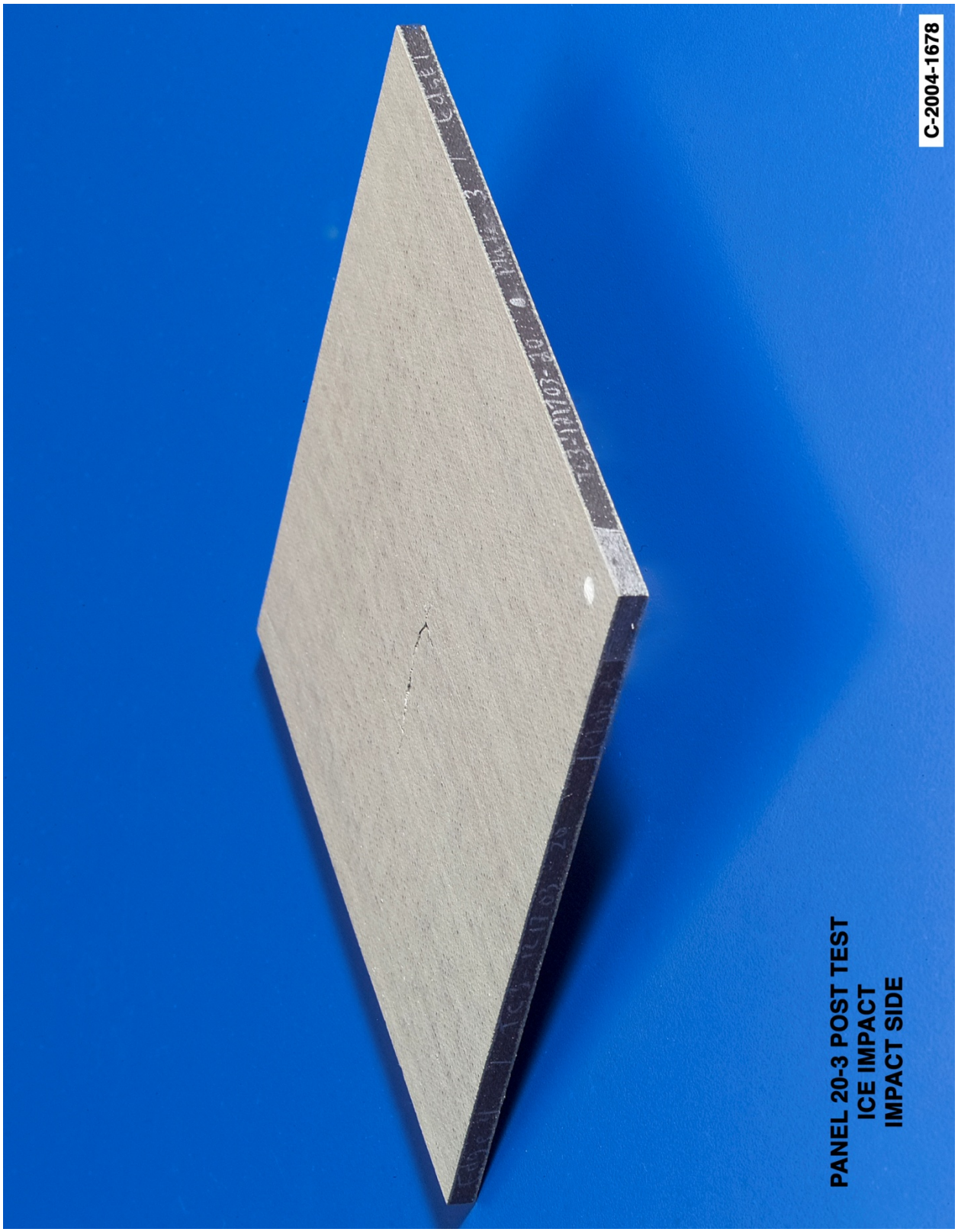

Figure B12–2.—Front (impact side) of panel 20-3 at 819 ft/s with a high-density, poly-crystal ice cylinder (nominally 0.66 in. in diameter by 1.66 in.) at 45° impact angle. Test GRCC 110.

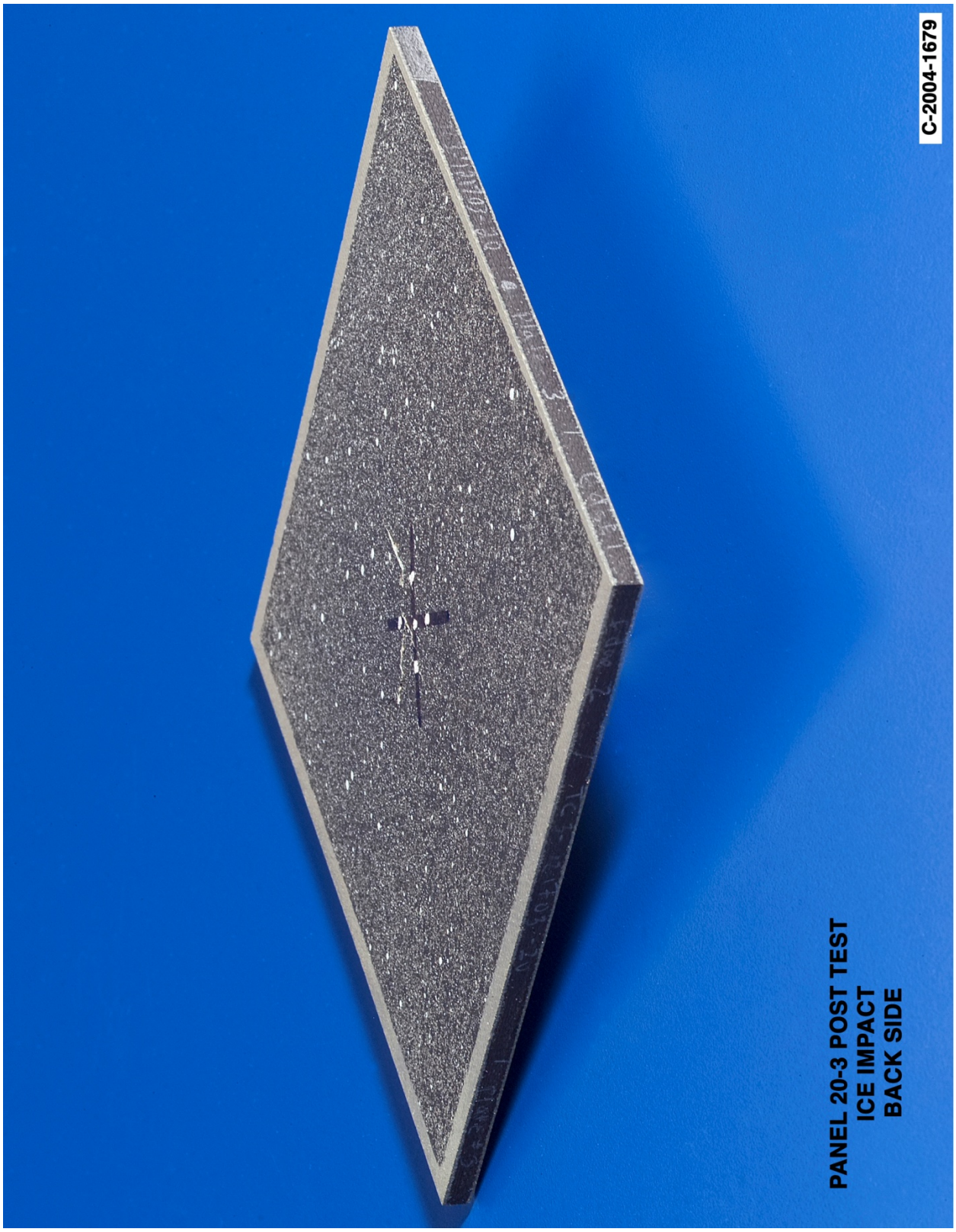

Figure B12–3.—Back face of panel 20-3 at 819 ft/s with a high-density, poly-crystal ice cylinder (nominally 0.66 in. in diameter by 1.66 in.) at 45° impact angle. Test GRCC 110.

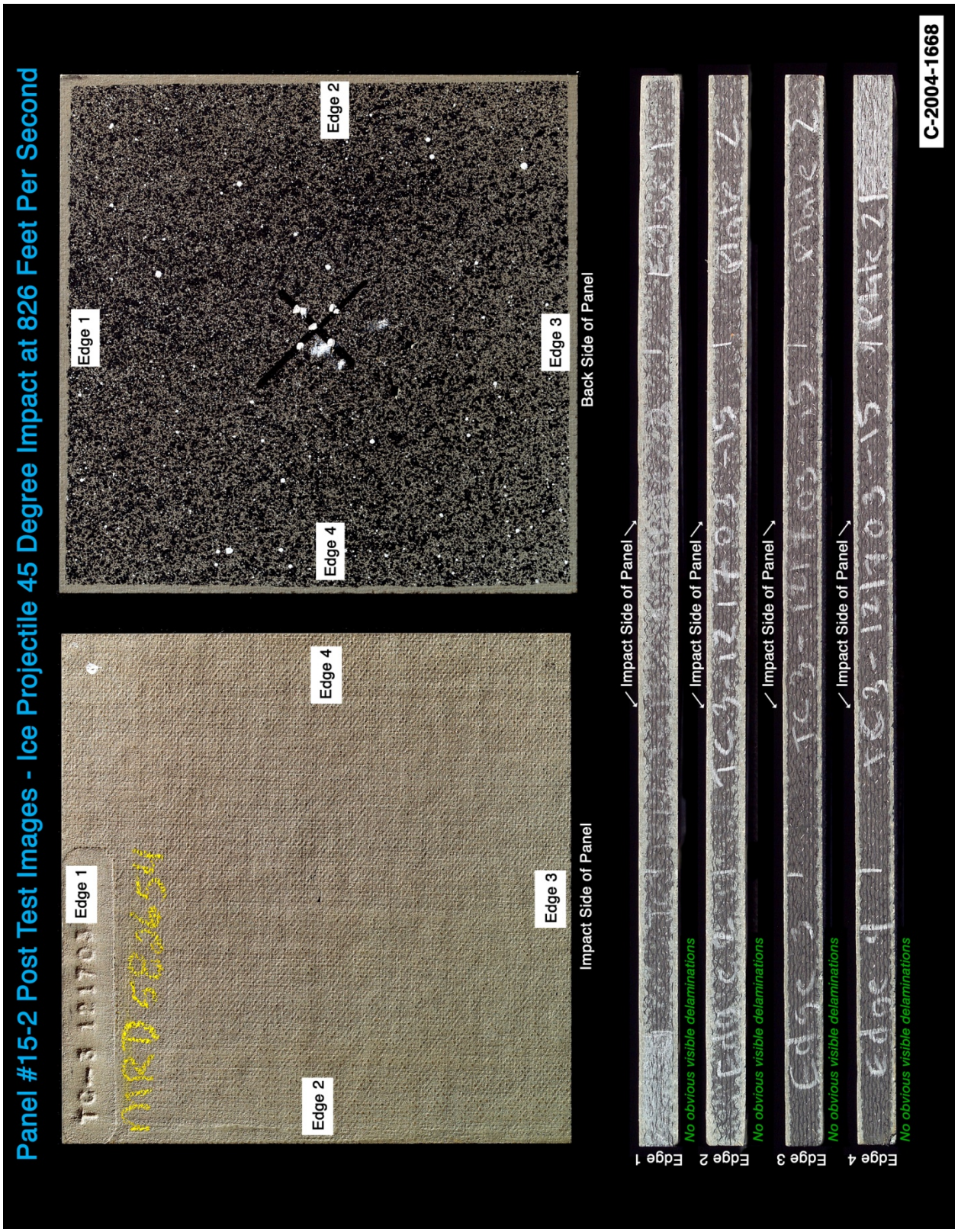

Figure B13–1.—Edges and faces of panel 15-2 at 826 ft/s with a high-density, poly-crystal ice cylinder (nominally 0.66 in. in diameter by 1.66 in.) at 45° impact. Test GRCC 109.

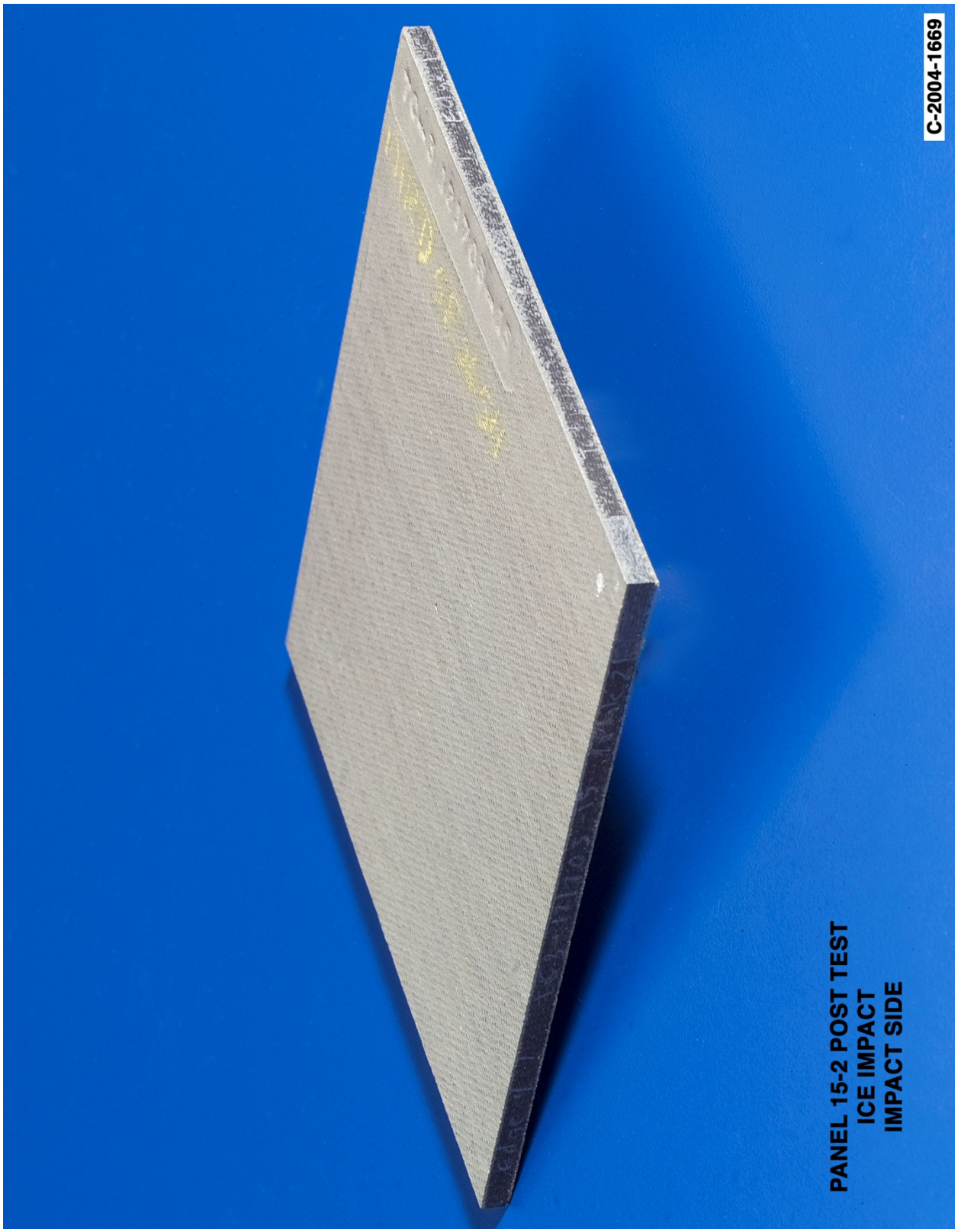

Figure B13–2.—Front (impact side) of panel 15-2 at 826 ft/s with a high-density, poly-crystal ice cylinder (nominally 0.66 in. in diameter by 1.66 in.) at 45° impact angle. Test GRCC 109.

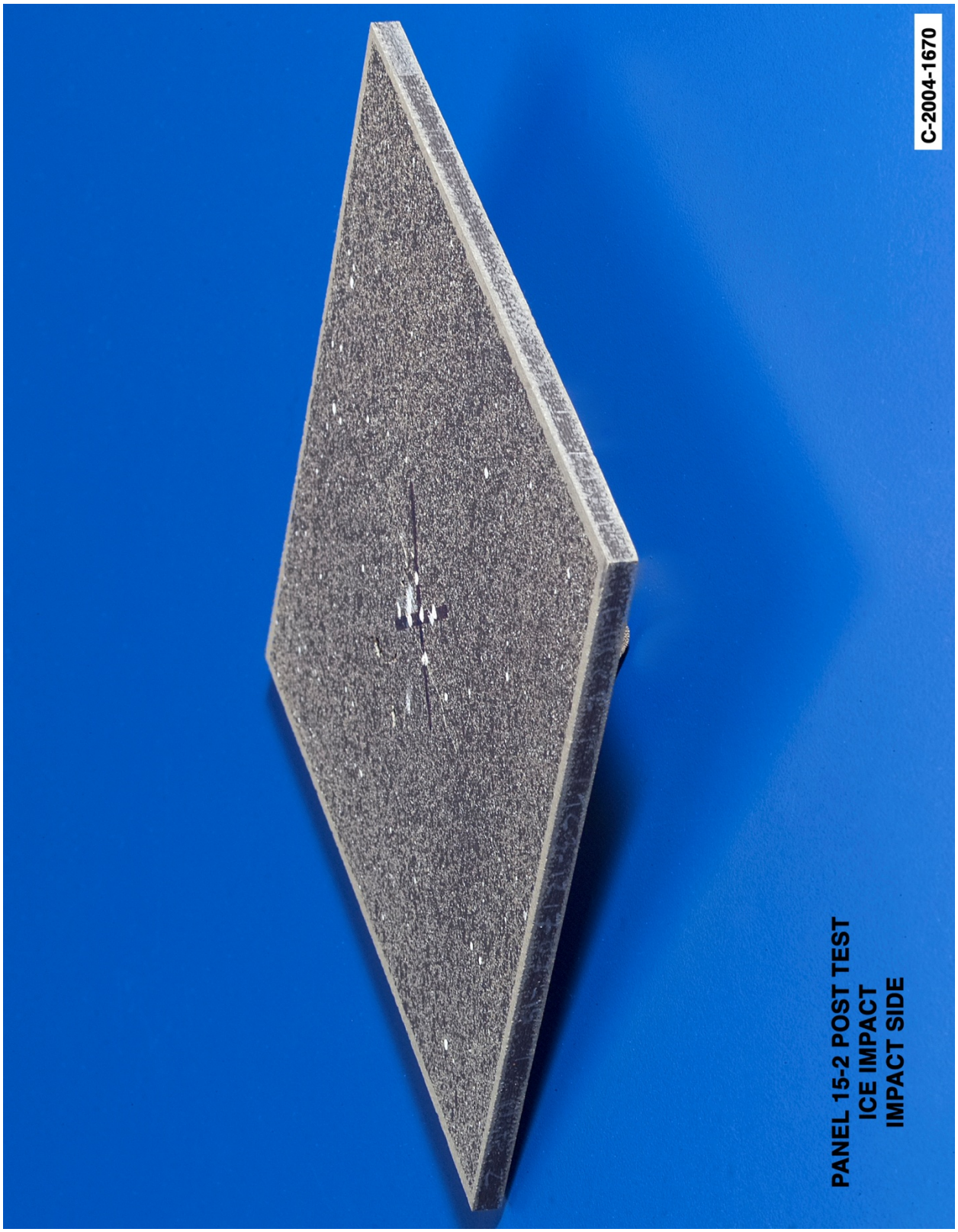

Figure B13–3.—Back face of panel 15-2 at 826 ft/s with a high-density, poly-crystal ice cylinder (nominally 0.66 in. in diameter by 1.66 in.) at 45° impact angle. Test GRCC 109.

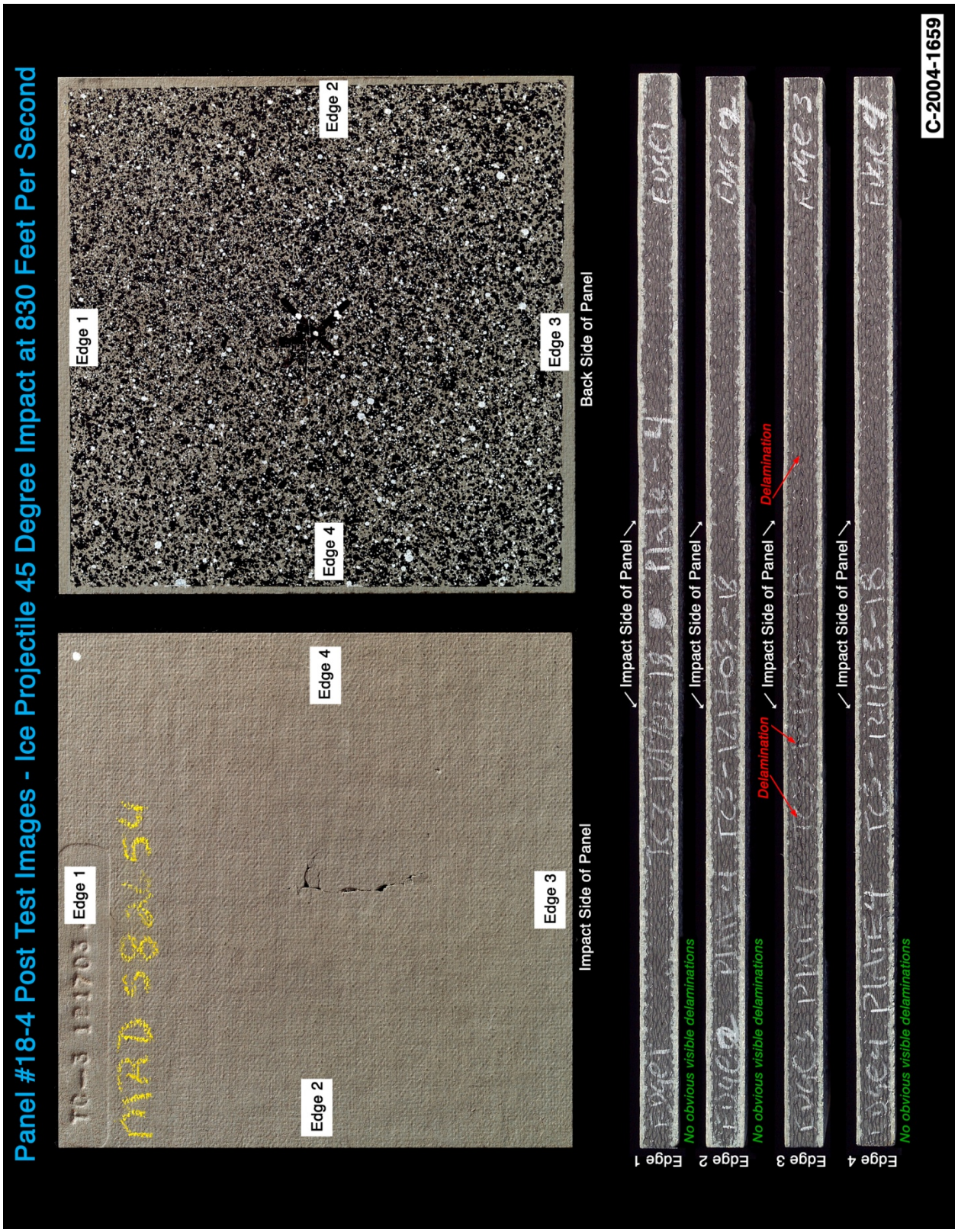

Figure B14–1.—Edges and faces of panel 18-4 at 830 ft/s with a high-density, poly-crystal ice cylinder (nominally 0.66 in. in diameter by 1.66 in.) at 45° impact. Test GRCC 105.

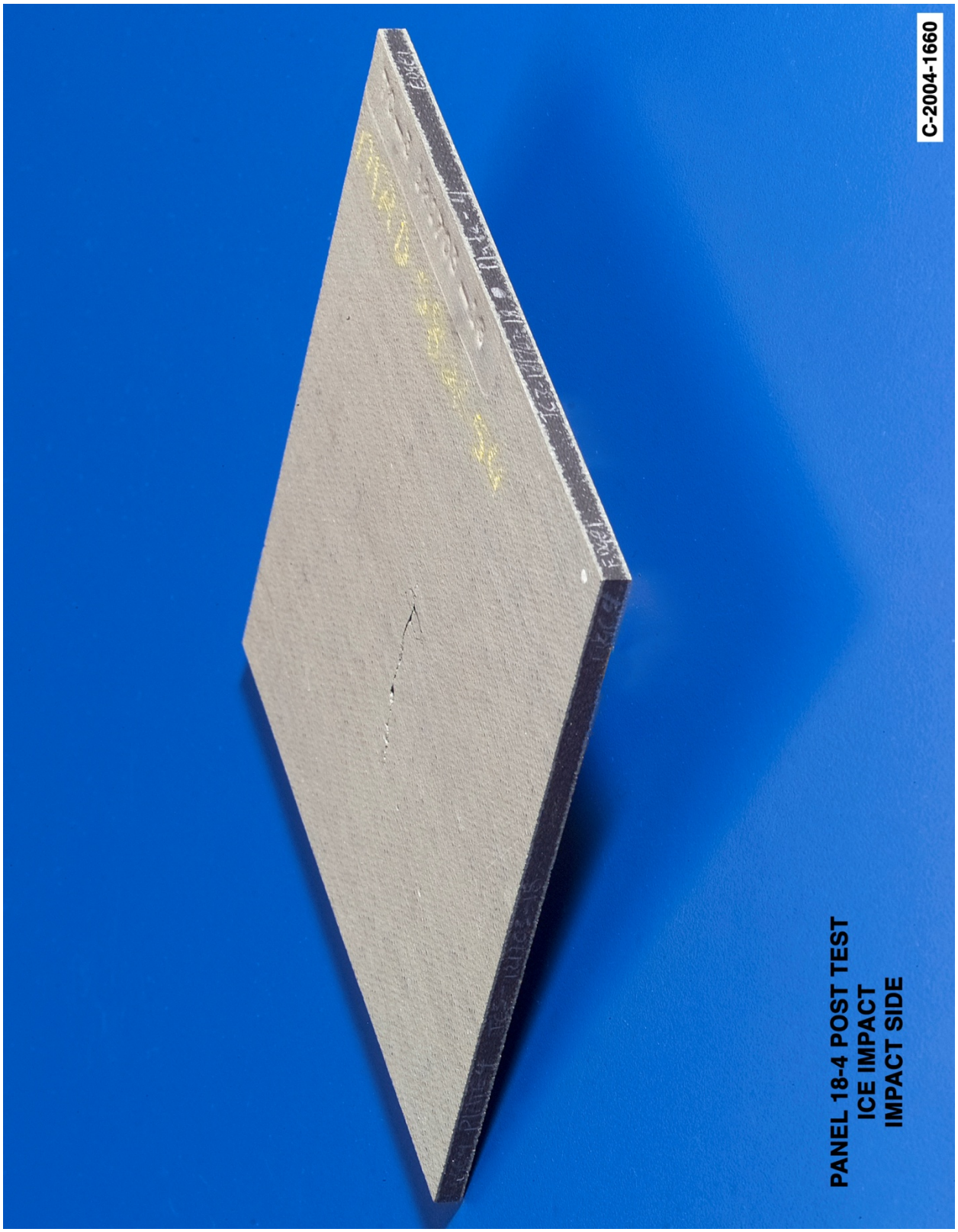

Figure B14–2.—Front (impact side) of panel 18-4 at 830 ft/s with a high-density, poly-crystal ice cylinder (nominally 0.66 in. in diameter by 1.66 in.) at 45° impact angle. Test GRCC 105.

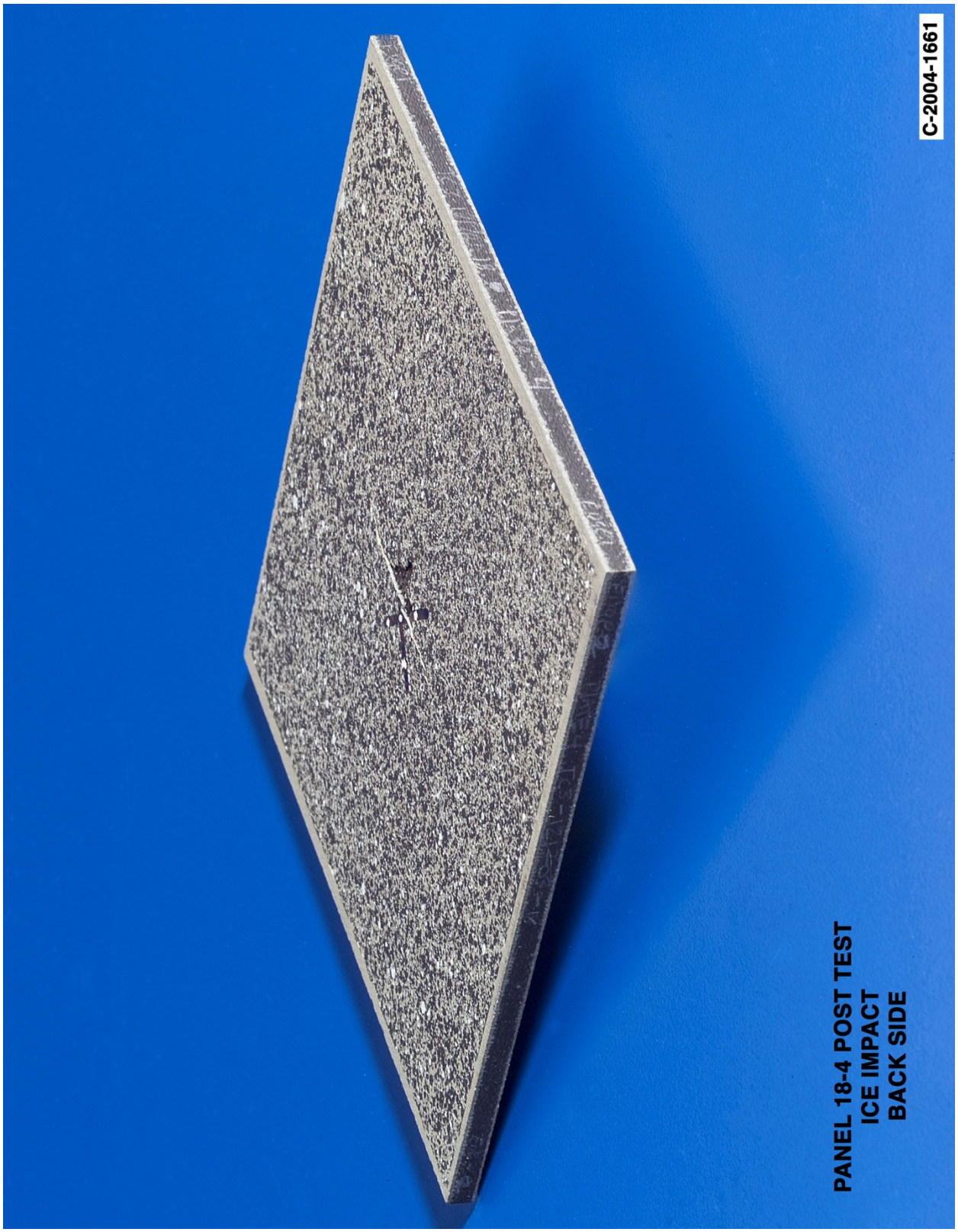

Figure B14–3.—Back face of panel 18-4 at 830 ft/s with a high-density, poly-crystal ice cylinder (nominally 0.66 in. in diameter by 1.66 in.) at 45° impact angle. Test GRCC 105.

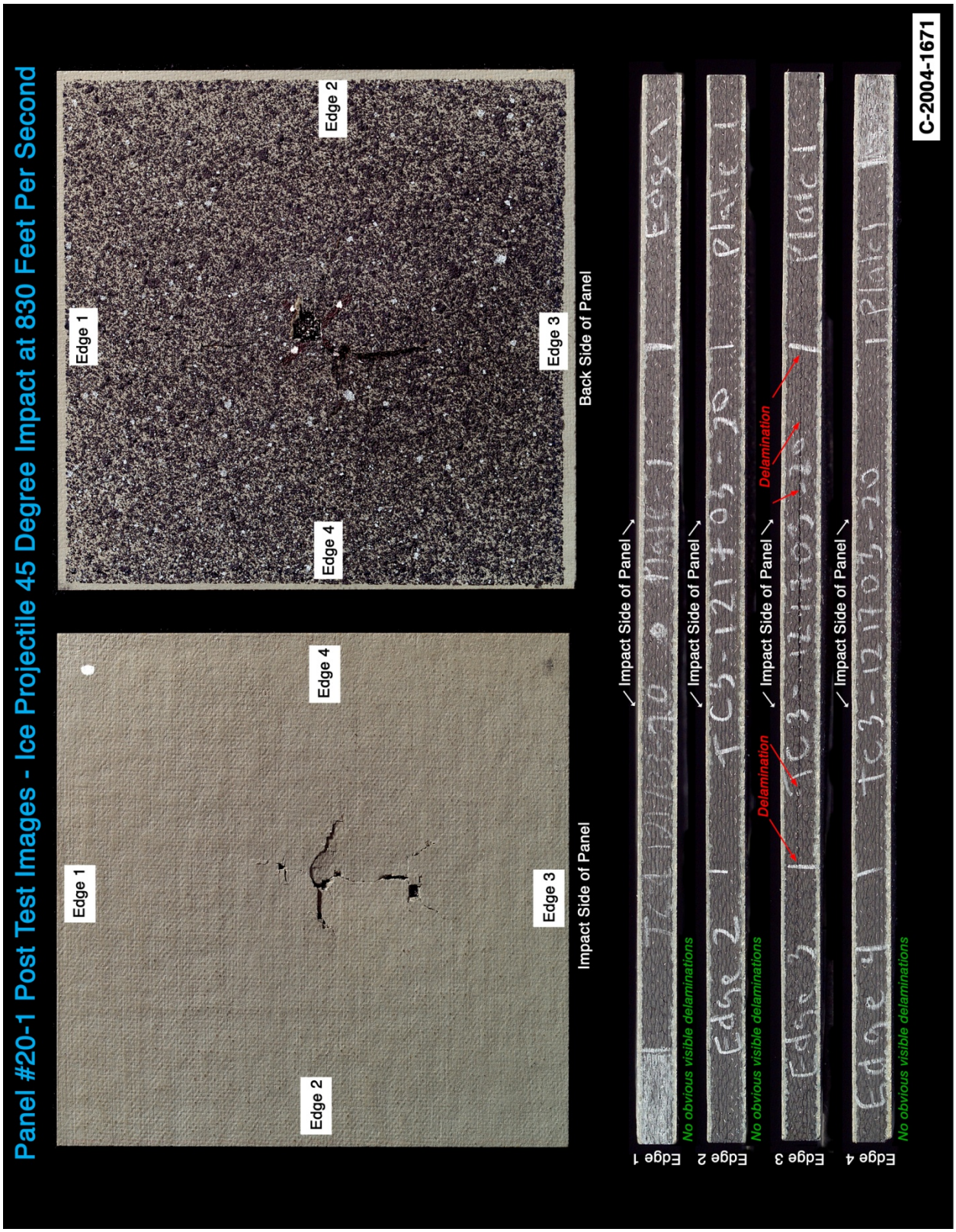

Figure B15–1.—Edges and faces of panel 20-1 at 830 ft/s with a high-density, poly-crystal ice cylinder (nominally 0.66 in. in diameter by 1.66 in.) at 45° impact. Test GRCC 108.

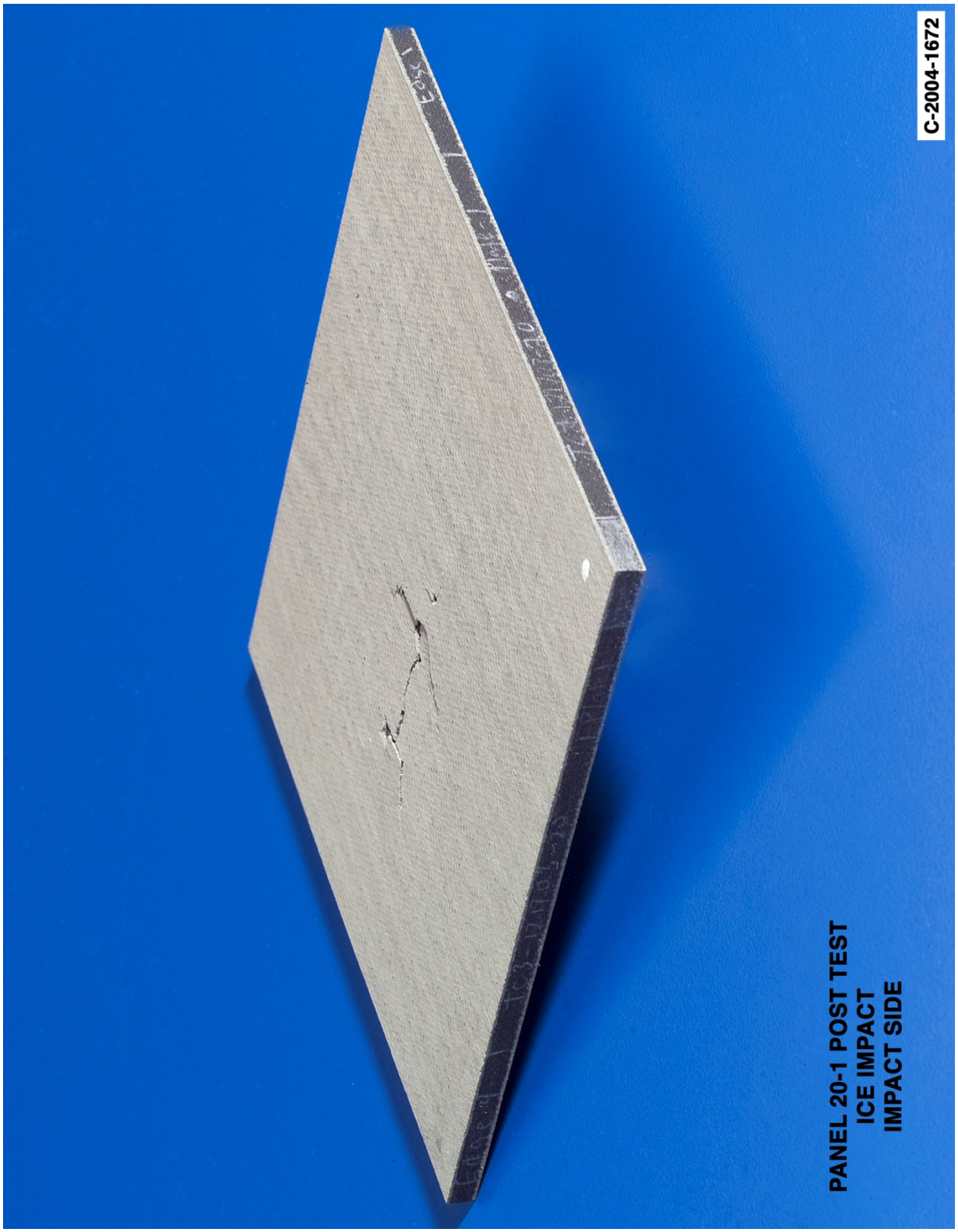

Figure B15–2.—Front (impact side) of panel 20-1 at 830 ft/s with a high-density, poly-crystal ice cylinder (nominally 0.66 in. in diameter by 1.66 in.) at 45° impact angle. Test GRCC 108.

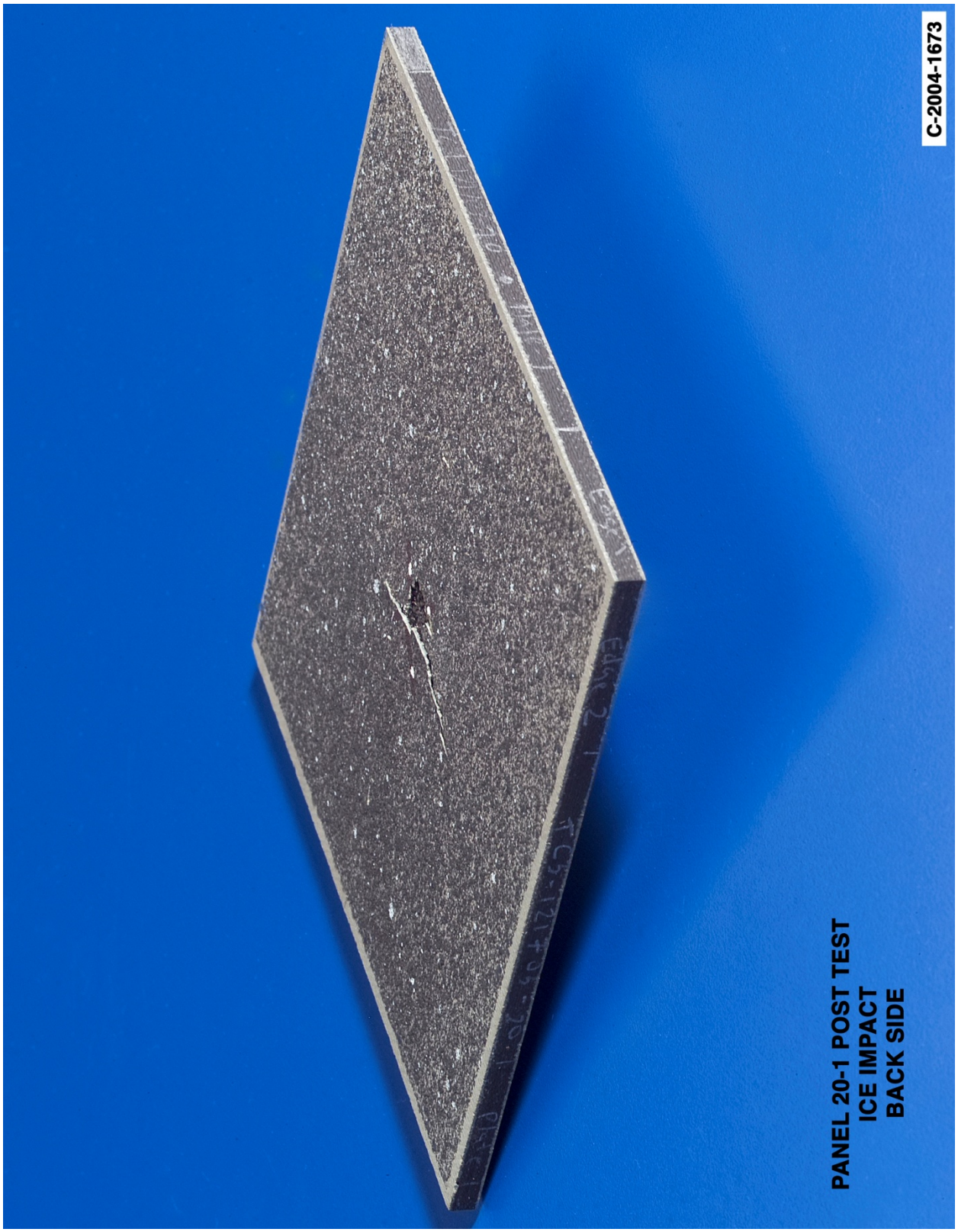

Figure B15–3.—Back face of panel 20-1 at 830 ft/s with a high-density, poly-crystal ice cylinder (nominally 0.66 in. in diameter by 1.66 in.) at 45° impact angle. Test GRCC 108.

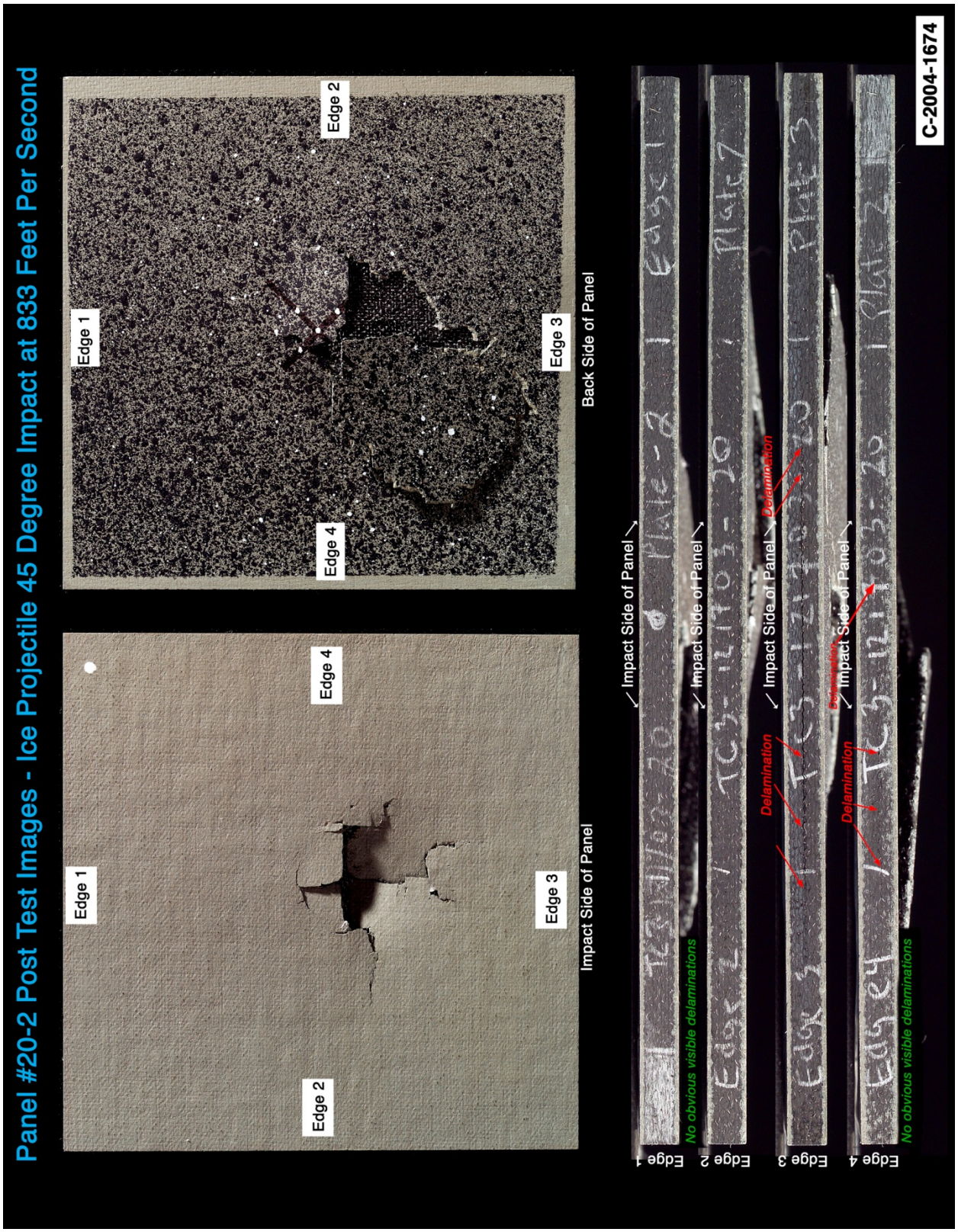

Figure B16–1.—Edges and faces of panel 20-2 at 833 ft/s with a high-density, poly-crystal ice cylinder (nominally 0.66 in. in diameter by 1.66 in.) at 45° impact. Test GRCC 107.

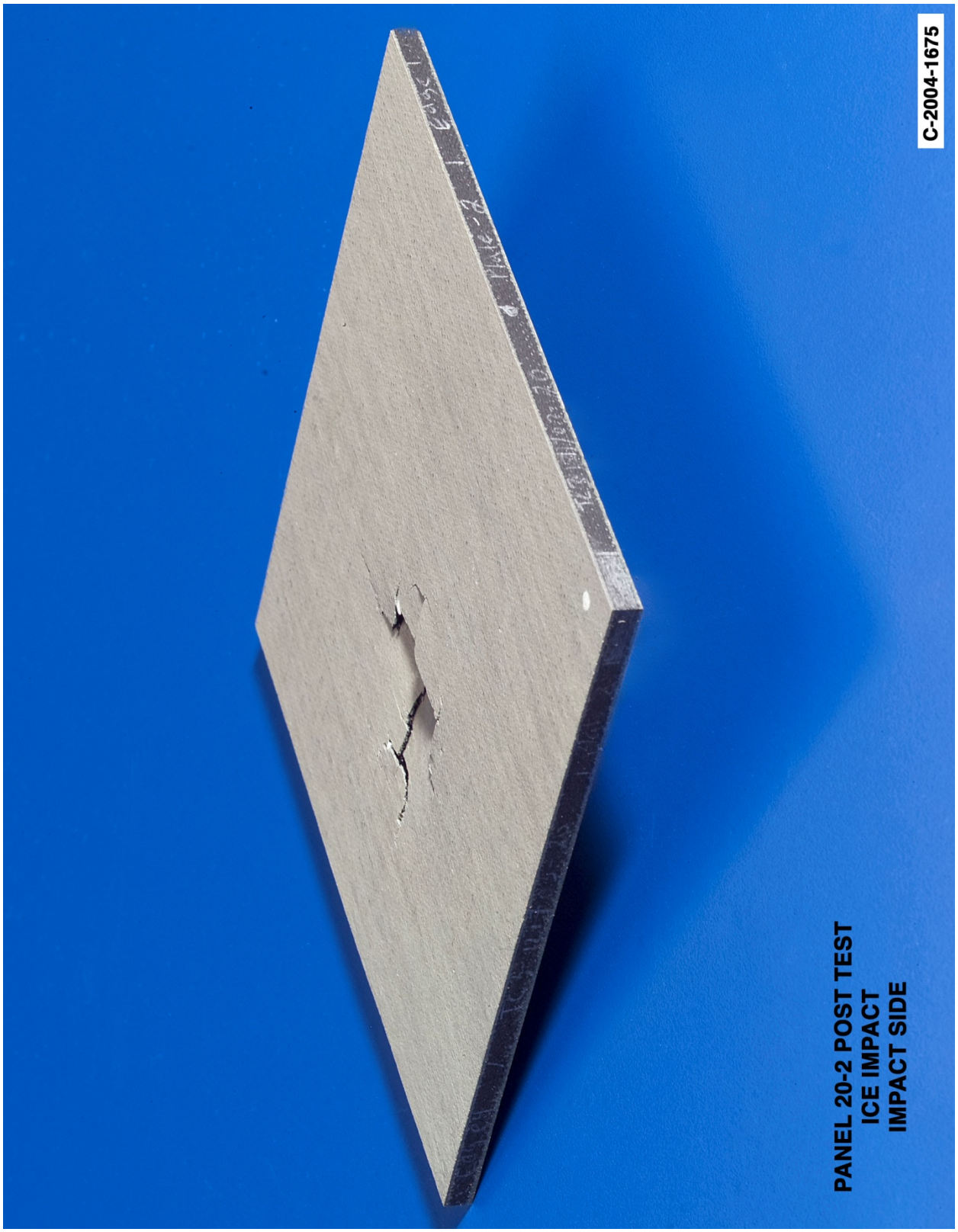

Figure B16–2.—Front (impact side) of panel 20-2 at 833 ft/s with a high-density, poly-crystal ice cylinder (nominally 0.66 in. in diameter by 1.66 in.) at 45° impact angle. Test GRCC 107.

Figure B16–3.—Back face of panel 20-2 at 833 ft/s with a high-density, poly-crystal ice cylinder (nominally 0.66 in. in diameter by 1.66 in.) at 45° impact angle. Test GRCC 107.

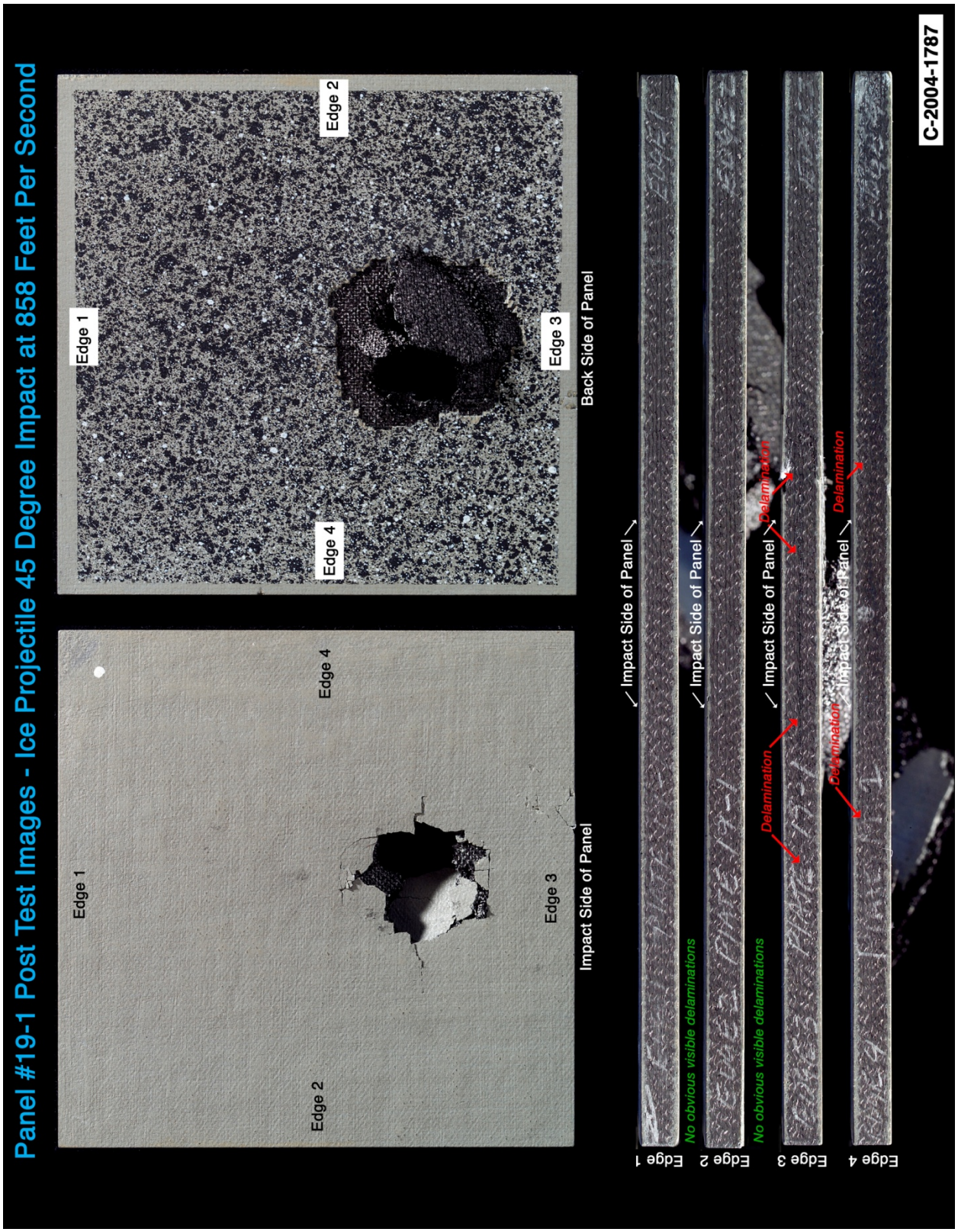

Figure B17–1.—Edges and faces of panel 19-1 at 858 ft/s with a high-density, poly-crystal ice cylinder (nominally 0.66 in. in diameter by 1.66 in.) at 45° impact. Test GRCC 83.

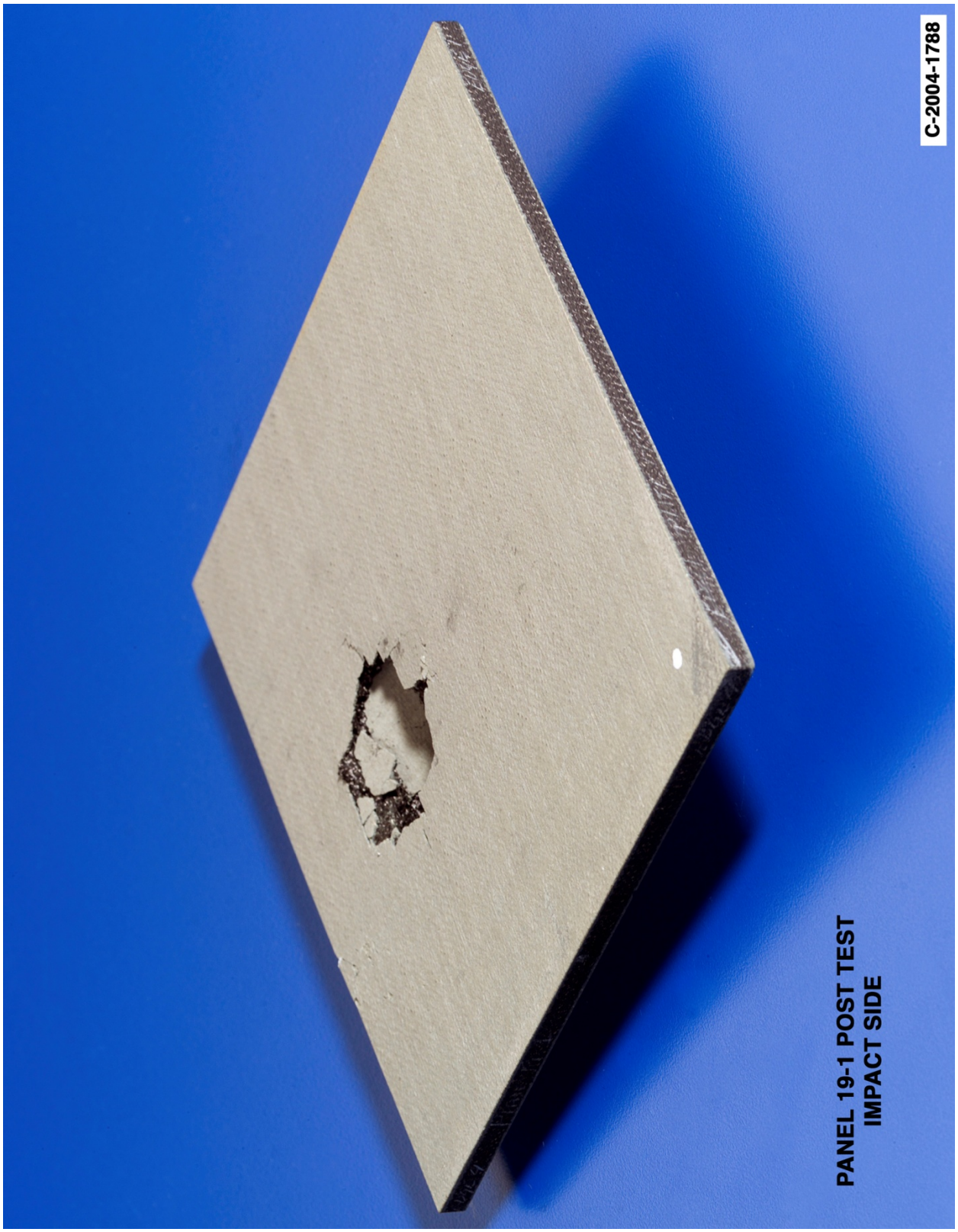

Figure B17–2.—Front (impact side) of panel 19-1 at 858 ft/s with a high-density, poly-crystal ice cylinder (nominally 0.66 in. in diameter by 1.66 in.) at 45° impact angle. Test GRCC 83.

Figure B17–3.—Back face of panel 19-1 at 858 ft/s with a high-density, poly-crystal ice cylinder (nominally 0.66 in. in diameter by 1.66 in.) at 45° impact angle. Test GRCC 83.

Appendix C.—High-Density Ice Impact Testing at 90° Angle on 6- by 12-in. Reinforced Carbon-Carbon (RCC) Flat Panels

Notable Observations From the Appendix C Test Series

1. ARAMIS data existed for nearly all ice impact tests but are not presented when considered to be uninterpretable.

Appendix C Test Series

High Density Ice 90 Degree Impact Test Parameters on 6" x 12" Reinforced Carbon-Carbon Panels													
Test No.	Glenn Test Reference Number	Impact Velocity (ft/sec)	Panel ID Number	Average Panel Thickness (inches)	Visual Damage Observations	Mass of panel before test (grams)	Mass of panel after test (grams)	Projectile Mass (g)	Projectile Length (in)	Projectile Diameter (in)	Projectile Density lb_m/ft^3	Test Date	Projectile ID Number
2-90-402-05	GRCC159	265	40-2	0.222	No Visible Damage	410.79	410.92	8.35	1.661	0.653	57.184	1/21/05	Ice: 13-SX-6
2-90-401-04	GRCC157	319	40-1	0.224	No apparent damage	412.18	412.12	8.59	1.659	0.662	57.308	1/20/05	Ice: 14-PX-22
2-90-382-03	GRCC156	350	38-2	0.222	Small chips off back side	413.50	413.33	8.68	1.661	0.665	57.318	1/20/05	Ice: 14-PX-21
2-90-153-01	GRCC154	398	15-3	0.221	Small chip on back	404.34	404.47	8.61	1.657	0.664	57.164	1/20/05	Ice: 14-PX-19
2-90-381-02	GRCC155	616	38-1	0.225	Blew hole thru panel	409.55	400.38	8.57	1.657	0.662	57.243	1/20/05	Ice: 14-PX-19

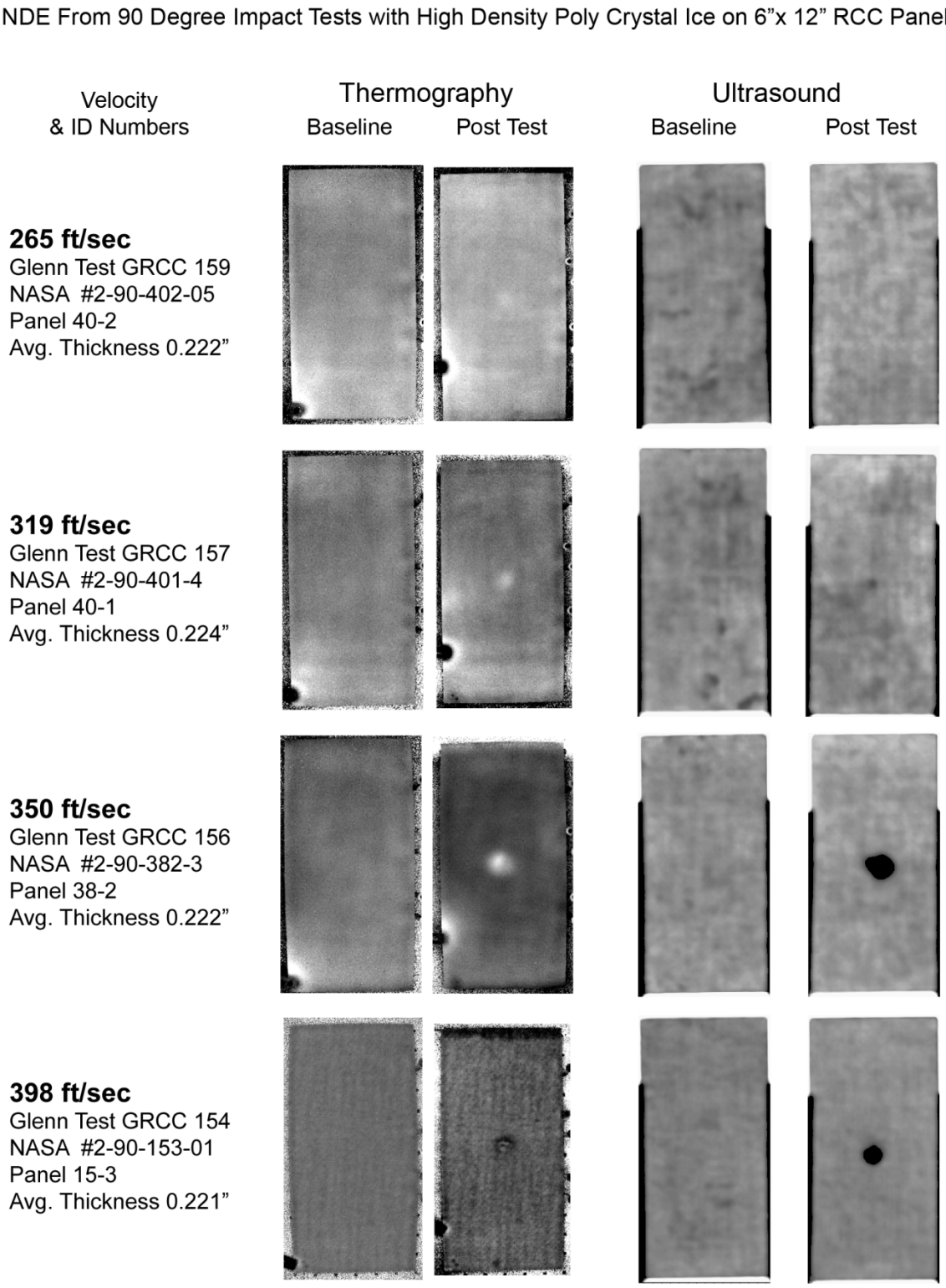

Figure C1–1.—Pulse thermography and ultrasound post impact pre- and posttest images of reinforced carbon-carbon 6- by 12-in. flat panels impacted with high-density poly-crystal ice cylinders (nominally 0.66 in. in diameter by 1.66 in.) at a 90° angle.

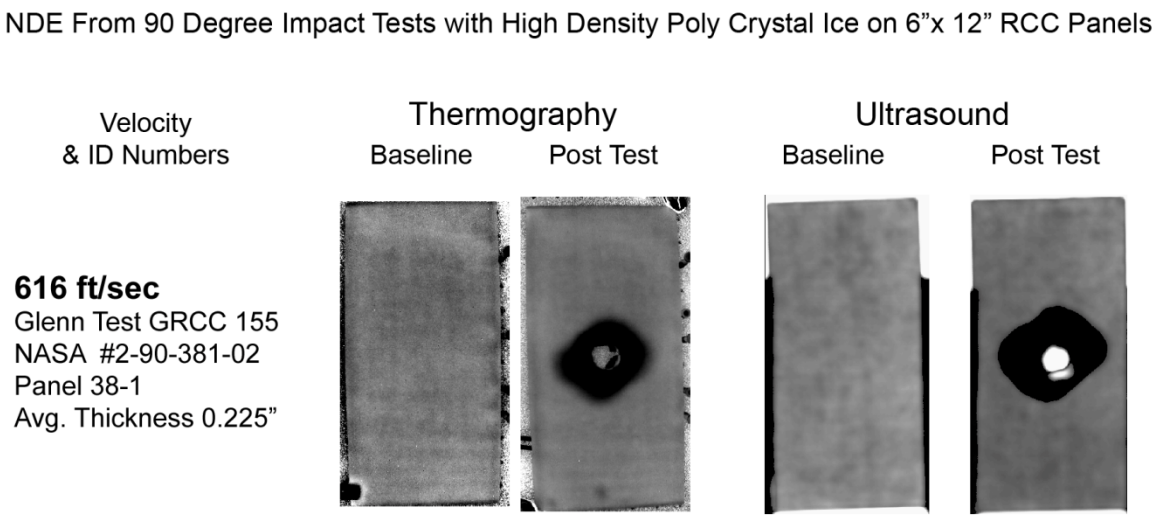

Figure C1–2.—Pulse thermography and ultrasound post impact pre- and posttest images of reinforced carbon-carbon 6- by 12-in. flat panels impacted with high-density poly-crystal ice cylinders (nominally 0.66 in. in diameter by 1.66 in.) at a 90° angle.

Aramis Displacement Contours from 90 Degree Impact Tests with High Density Poly-Crystal Ice on 6”x 12” RCC Panels

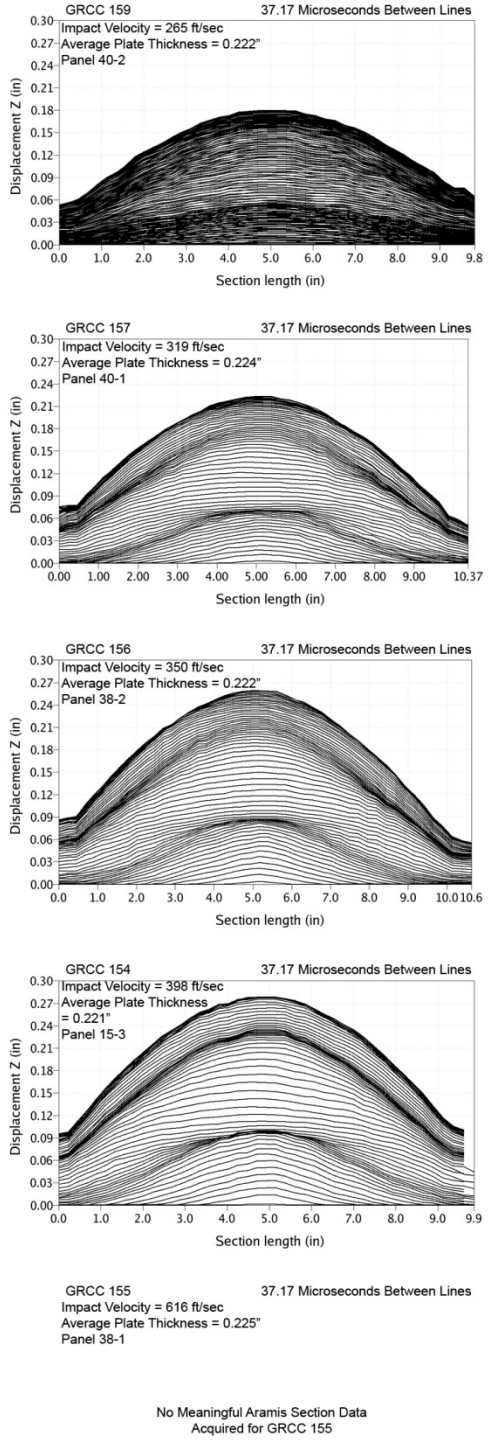

Figure C2–1.—ARAMIS out-of-plane deformation contours across centerline of 6- by 12-in. reinforced carbon-carbon flat panels measured at 37 μs increments undergoing impact with high-density poly-crystal ice cylinders (nominally 0.66 in. in diameter by 1.66 in.) at a 90° angle.

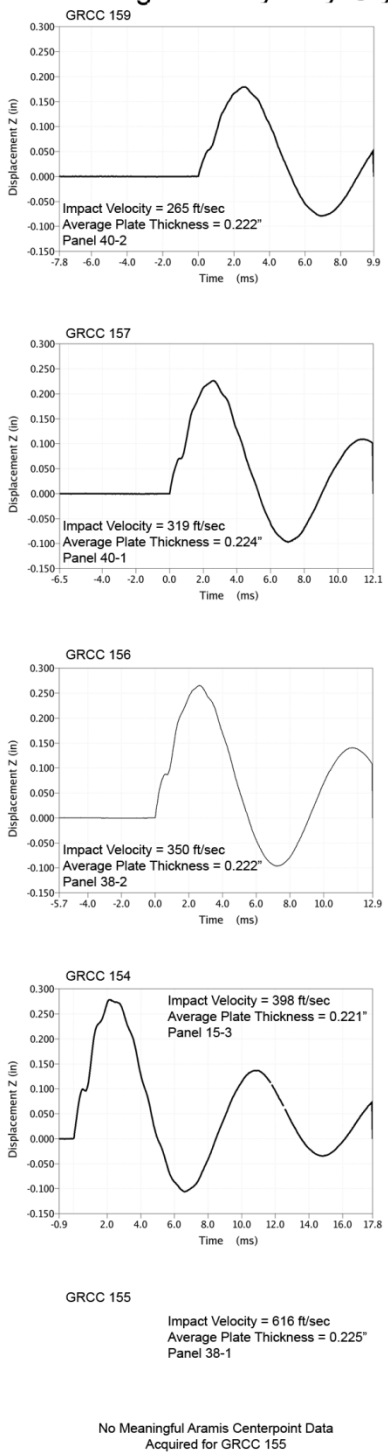

Figure C3–1.—ARAMIS centerpoint out-of-plane deformation vs. time of 6- by 12-in. reinforced carbon-carbon flat panels impacted with high-density poly-crystal ice cylinders (nominally 0.66 in. in diameter by 1.66 in.) at a 90° angle.

Aramis Maximum Displacement Fringe Plots from 90 Degree Impact Tests
with High Density Poly-crystal Ice on 6” x 12” RCC Panels

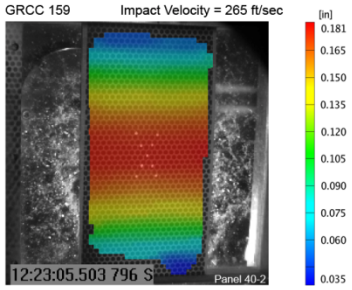

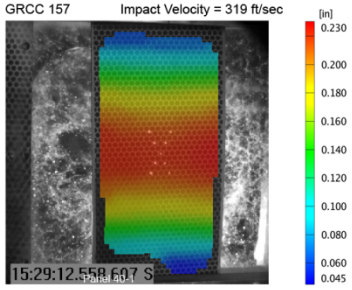

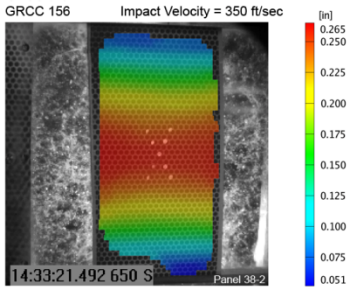

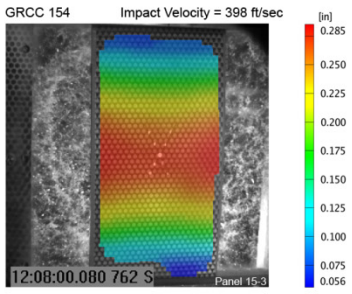

GRCC 155 Impact Velocity = 616 ft/sec

No Meaningful Aramis Fringe Data
Acquired for GRCC 155

Figure C4–1.—ARAMIS color fringe plots depicting maximum deformation prior to material failure of 6- by 12-in. reinforced carbon-carbon flat panels as they undergo impact with high-density poly-crystal ice cylinders (nominally 0.66 in. in diameter by 1.66 in.) at a 90° angle.

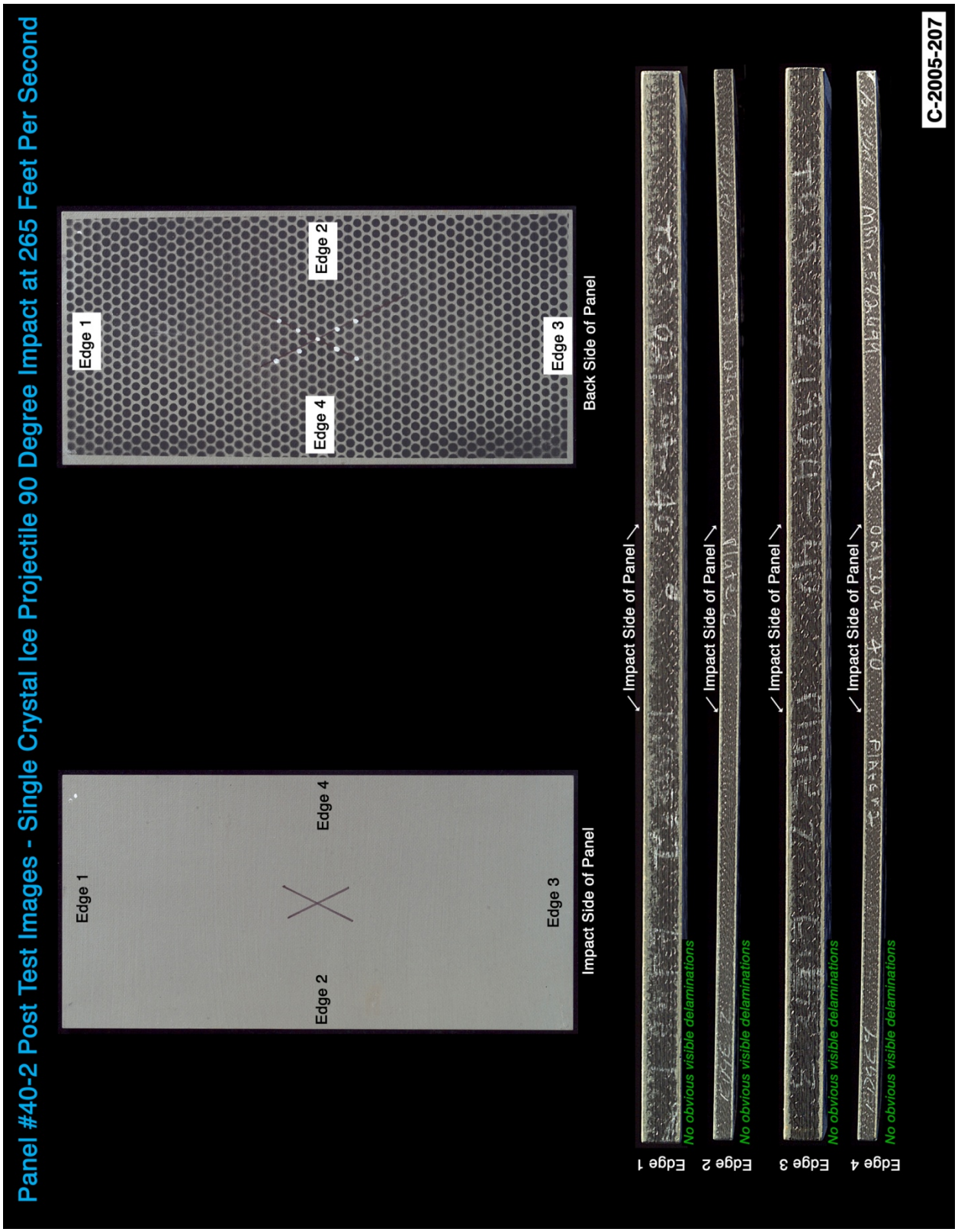

Figure C5–1.—Edges and faces of panel 40-2 at 265 ft/s with a high-density, single-crystal ice cylinder (nominally 0.66 in. in diameter by 1.66 in.) at 90° impact angle. Test GRCC 159.

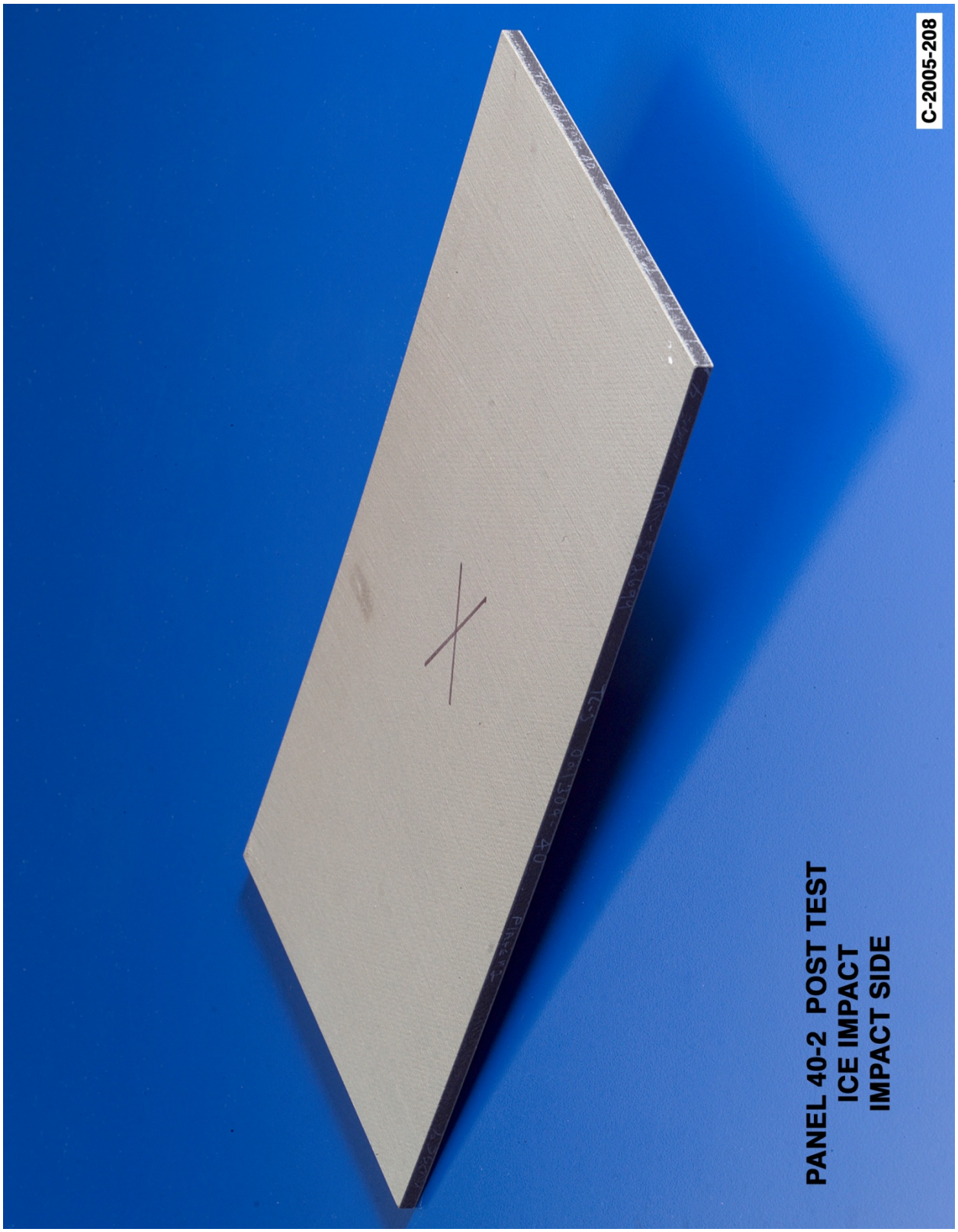

Figure C5–2.—Front (impact side) of panel 40-2 at 265 ft/s with a high-density, single-crystal ice cylinder (nominally 0.66 in. in diameter by 1.66 in.) at 90° impact angle. Test GRCC 159.

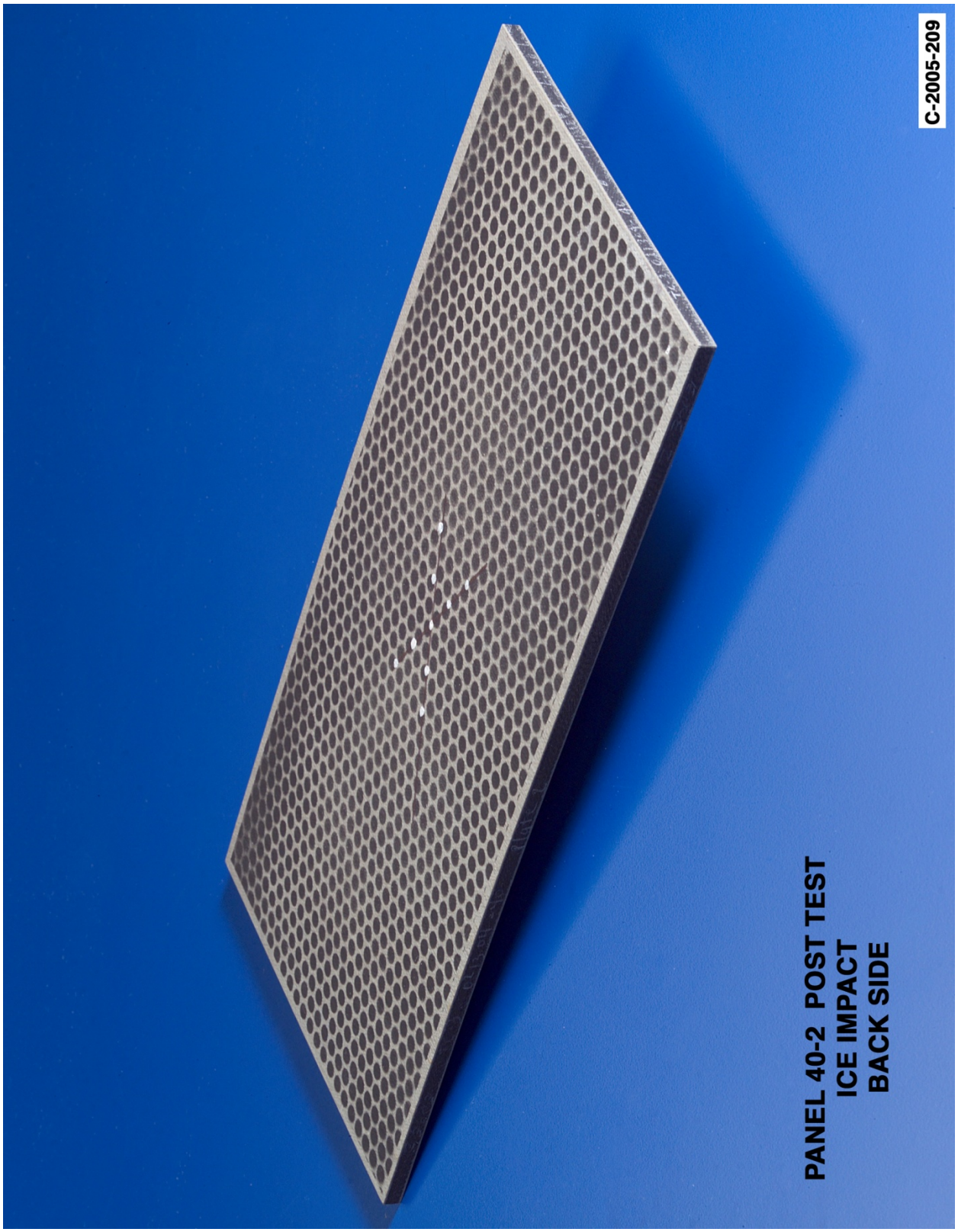

Figure C5–3.—Back face of panel 40-2 at 265 ft/s with a high-density, single-crystal ice cylinder (nominally 0.66 in. in diameter by 1.66 in.) at 90° impact angle. Test GRCC 159.

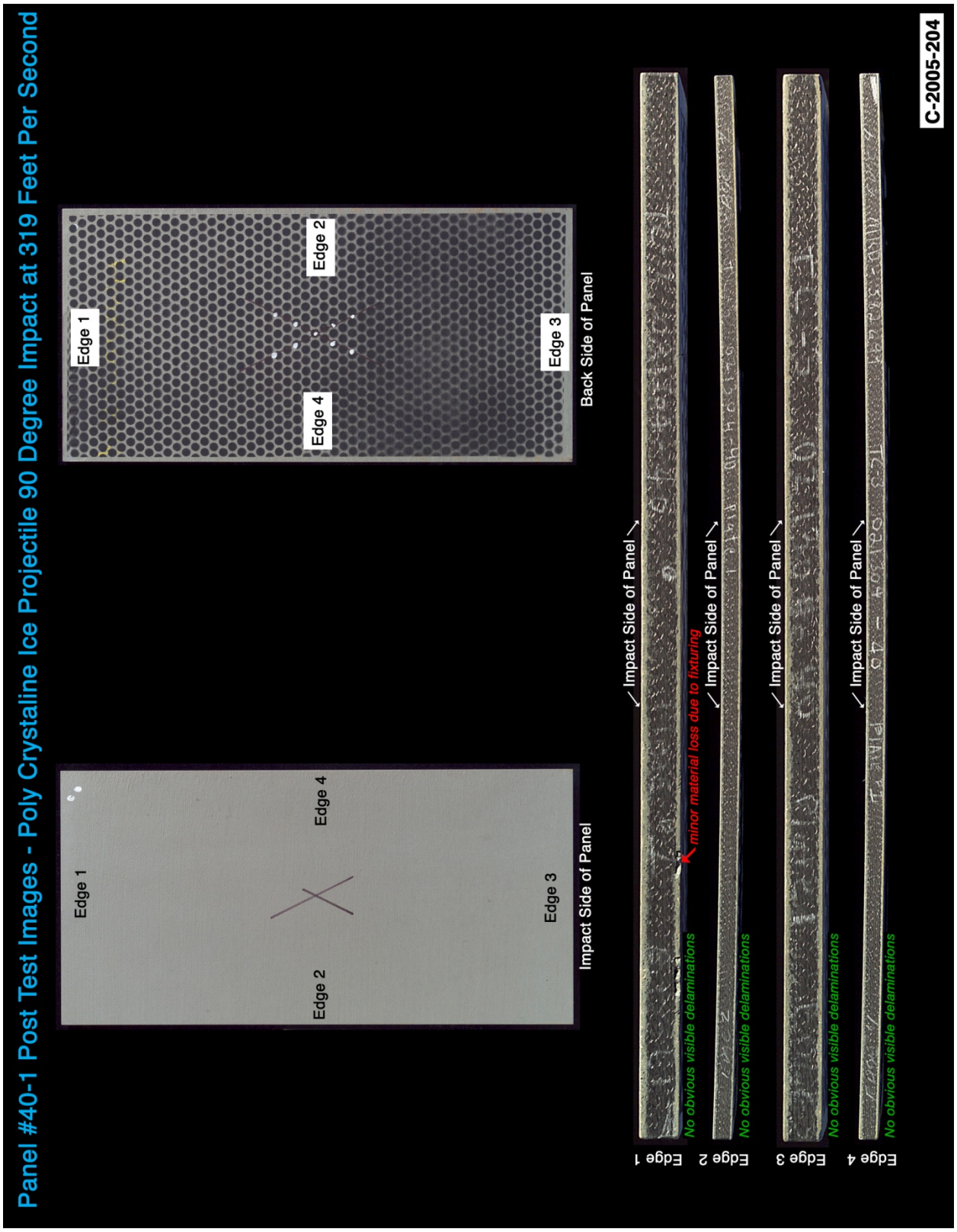

Figure C6–1.—Edges and faces of panel 40–1 at 319 ft/s with a high-density, poly-crystal ice cylinder (nominally 0.66 in. in diameter by 1.66 in.) at 90° impact. Test GRCC 157.

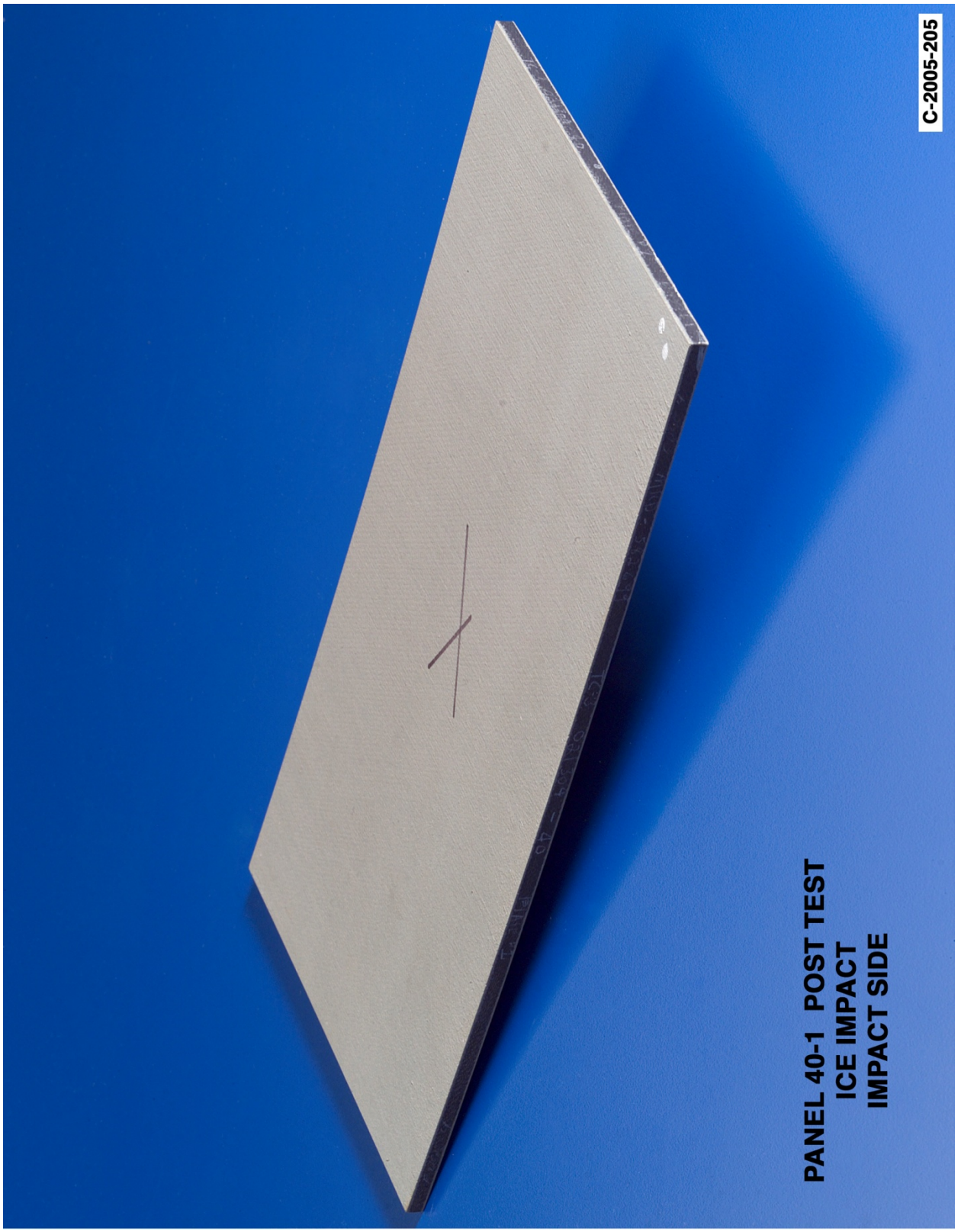

Figure C6–2.—Front (impact side) of panel 40-1 at 319 ft/s with a high-density, poly-crystal ice cylinder (nominally 0.66 in. in diameter by 1.66 in.) at 90° impact angle. Test GRCC 157.

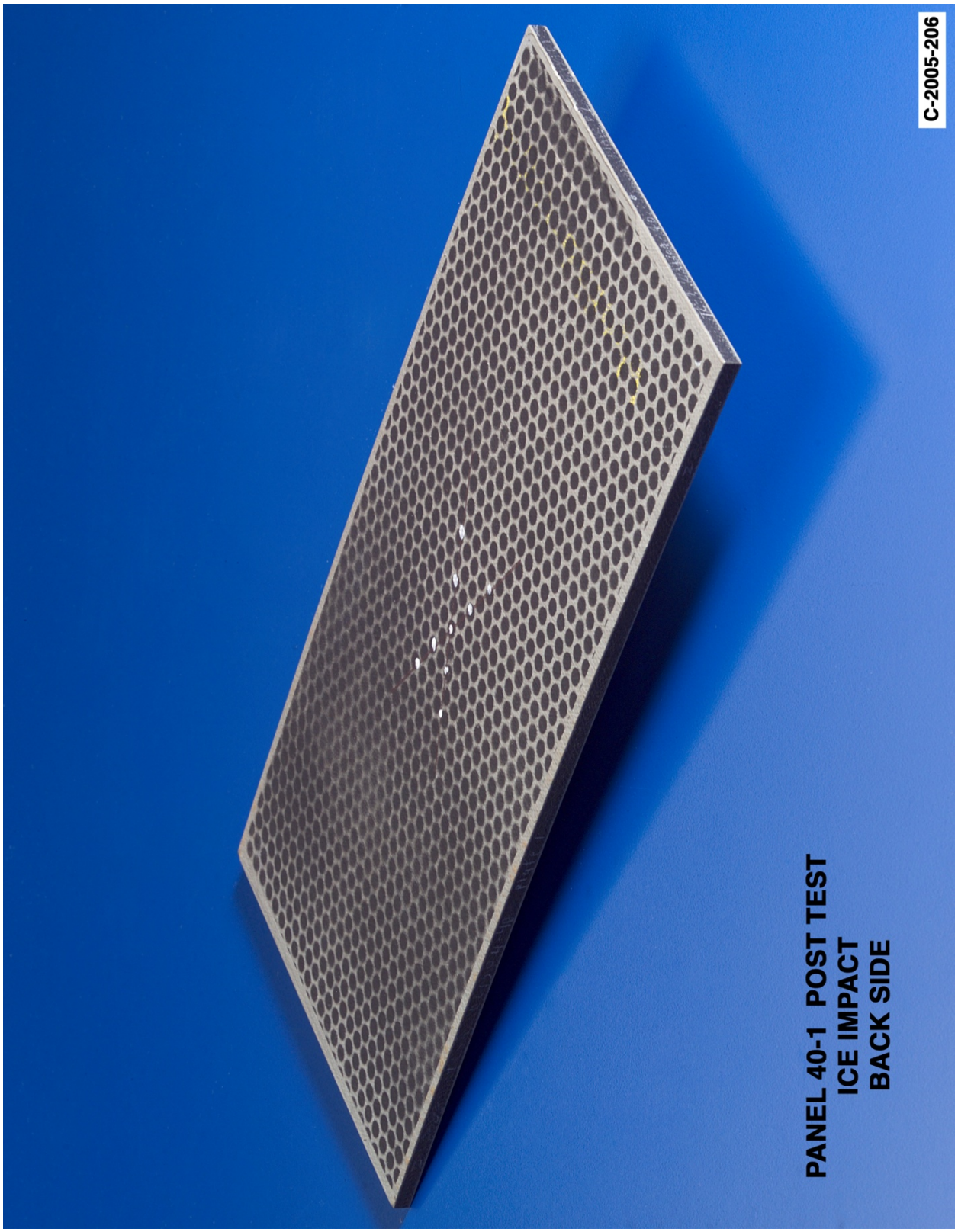

Figure C6–3.—Back face of panel 40-1 at 319 ft/s with a high-density, poly-crystal ice cylinder (nominally 0.66 in. in diameter by 1.66 in.) at 90° impact angle. Test GRCC 157.

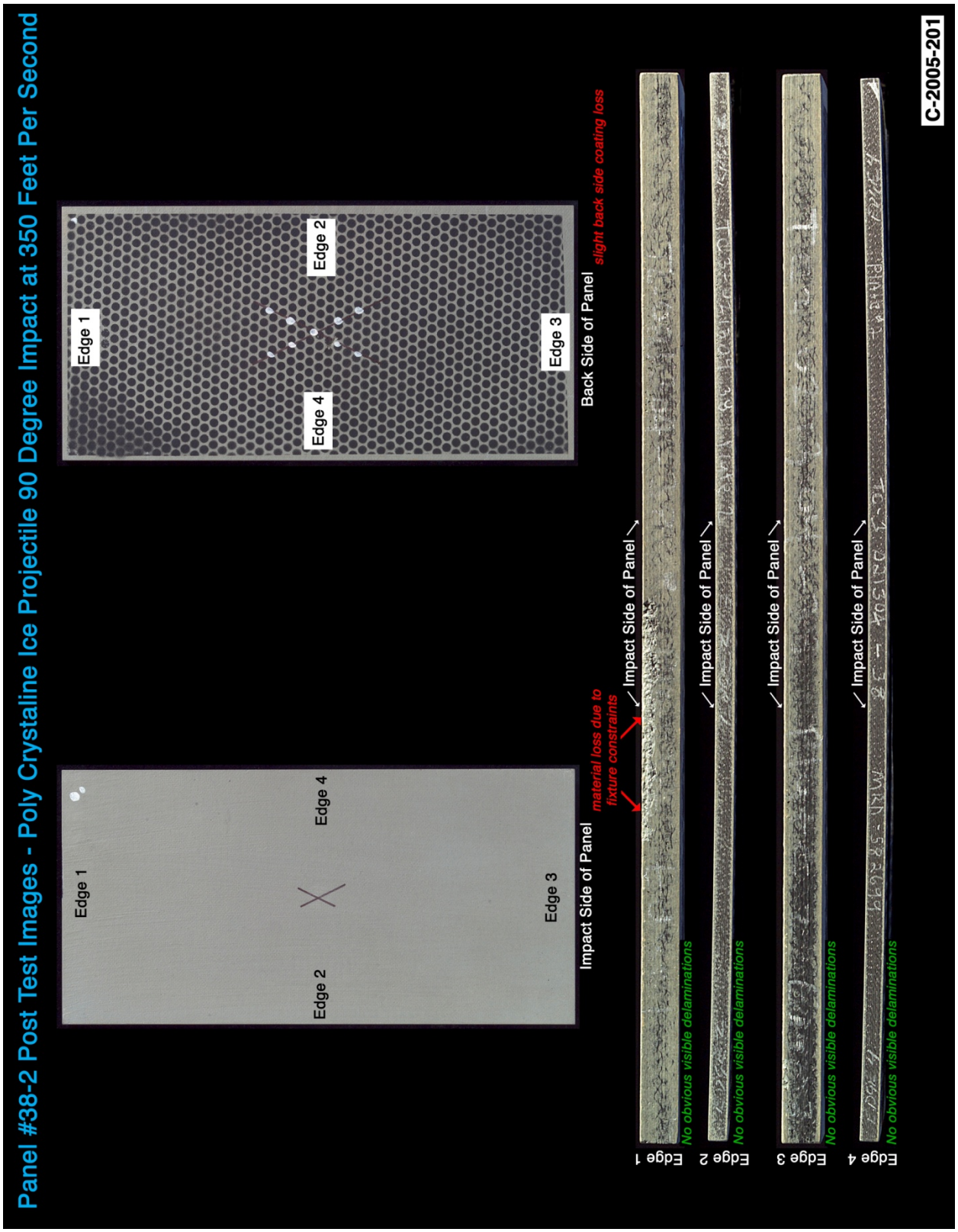

Figure C7–1.—Edges and faces of panel 38-2 at 350 ft/s with a high-density, poly-crystal ice cylinder (nominally 0.66 in. in diameter by 1.66 in.) at 90° impact. Test GRCC 156.

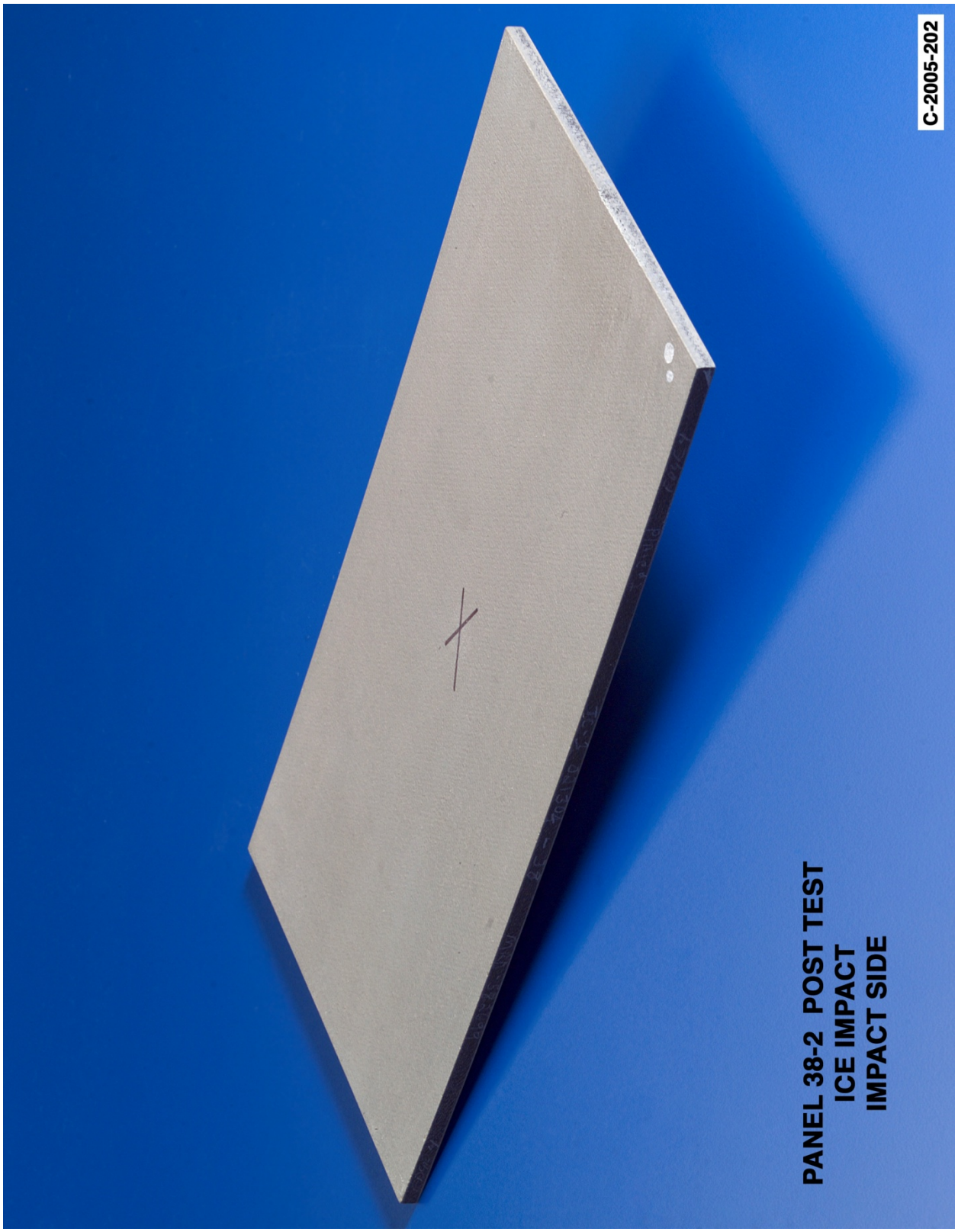

Figure C7–2.—Front (impact side) of panel 38-2 at 350 ft/s with a high-density, poly-crystal ice cylinder (nominally 0.66 in. in diameter by 1.66 in.) at 90° impact angle. Test GRCC 156.

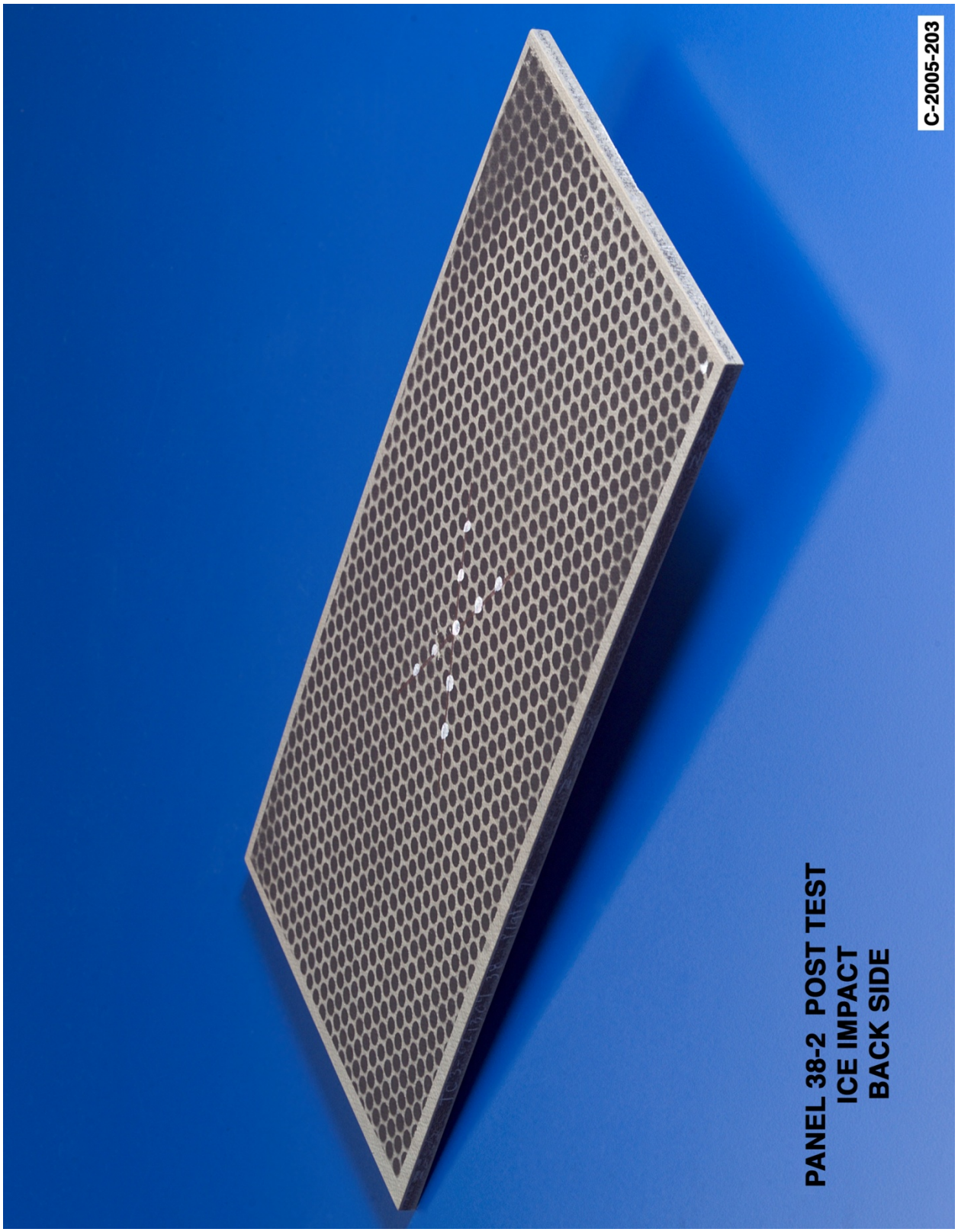

Figure C7–3.—Back face of panel 38-2 at 350 ft/s with a high-density, poly-crystal ice cylinder (nominally 0.66 in. in diameter by 1.66 in.) at 90° impact angle. Test GRCC 156.

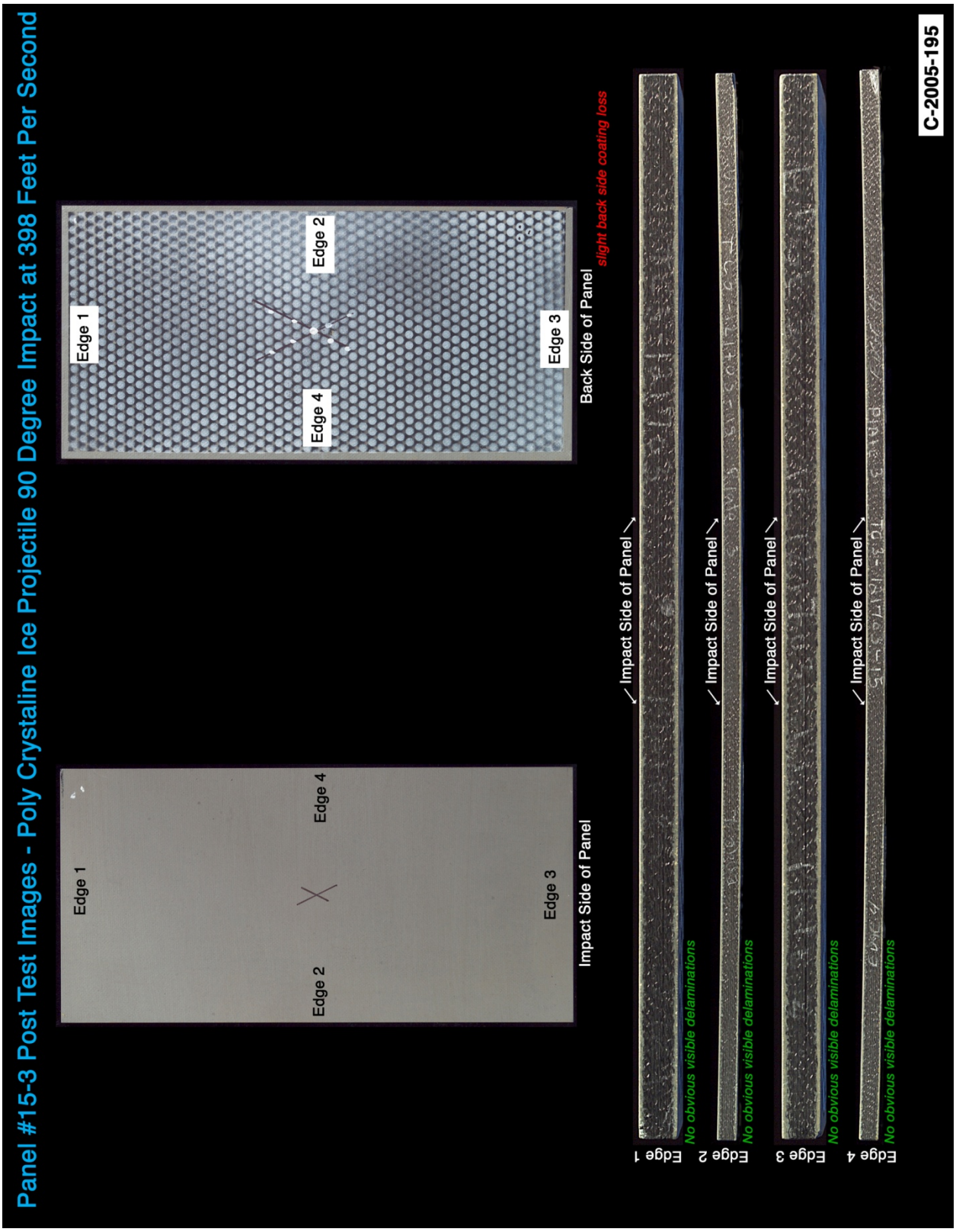

Figure C8–1.—Edges and faces of panel 15-3 at 398 ft/s with a high-density, poly-crystal ice cylinder (nominally 0.66 in. in diameter by 1.66 in.) at 90° impact. Test GRCC 154.

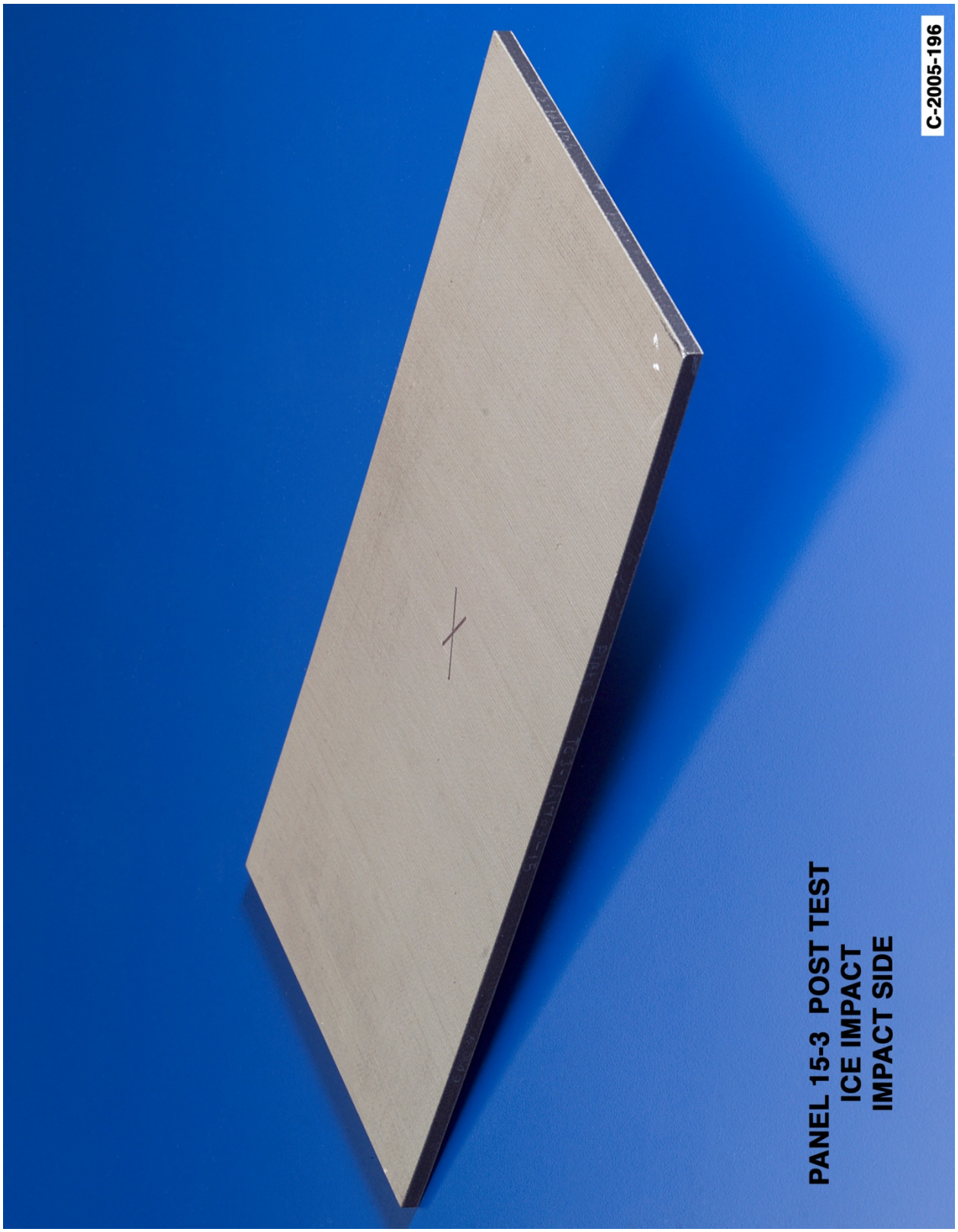

Figure C8–2.—Front (impact side) of panel 15-3 at 398 ft/s with a high-density, poly-crystal ice cylinder (nominally 0.66 in. in diameter by 1.66 in.) at 90° impact angle. Test GRCC 154.

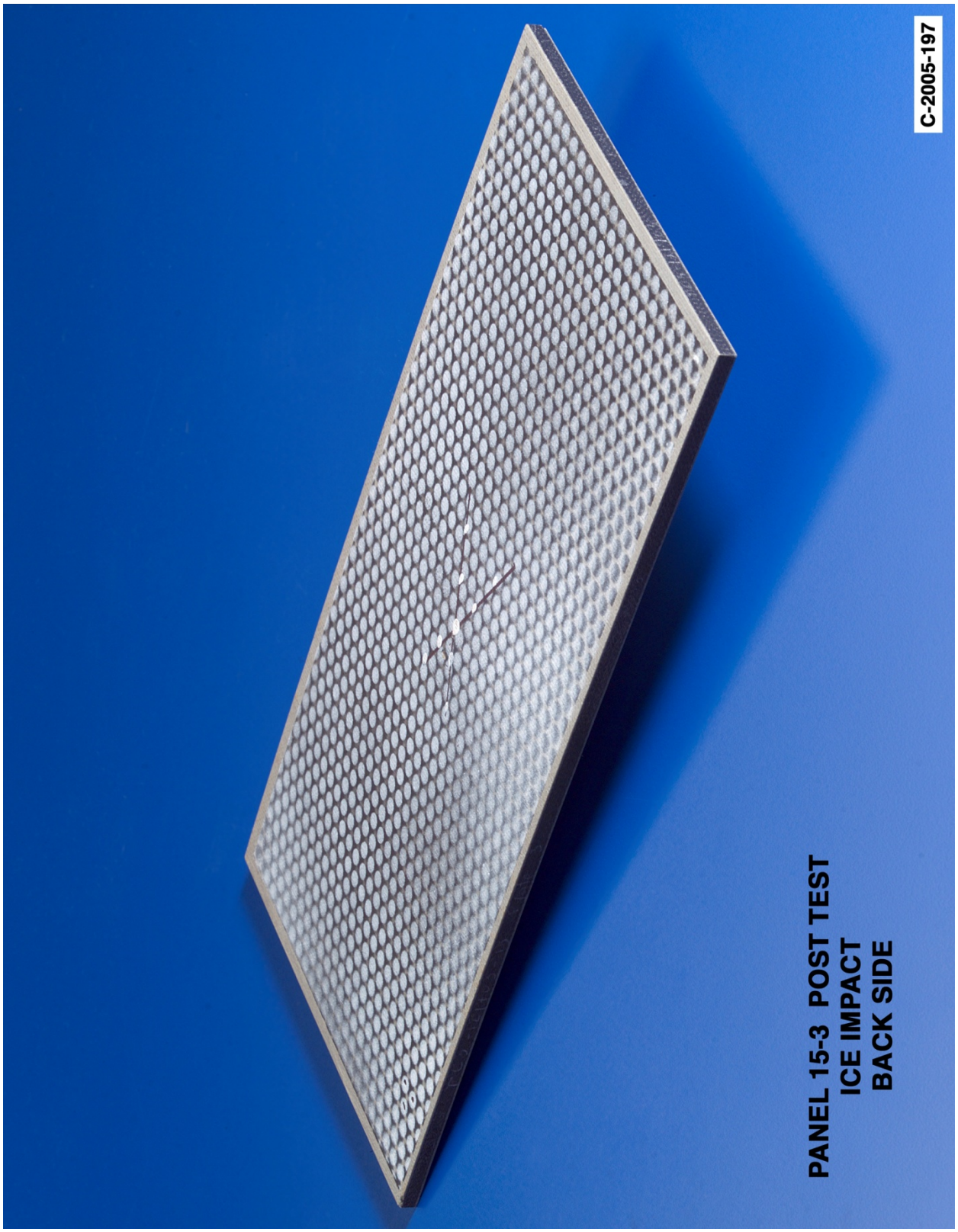

Figure C8–3.—Back face of panel 15-3 at 398 ft/s with a high-density, poly-crystal ice cylinder (nominally 0.66 in. in diameter by 1.66 in.) at 90° impact angle. Test GRCC 154.

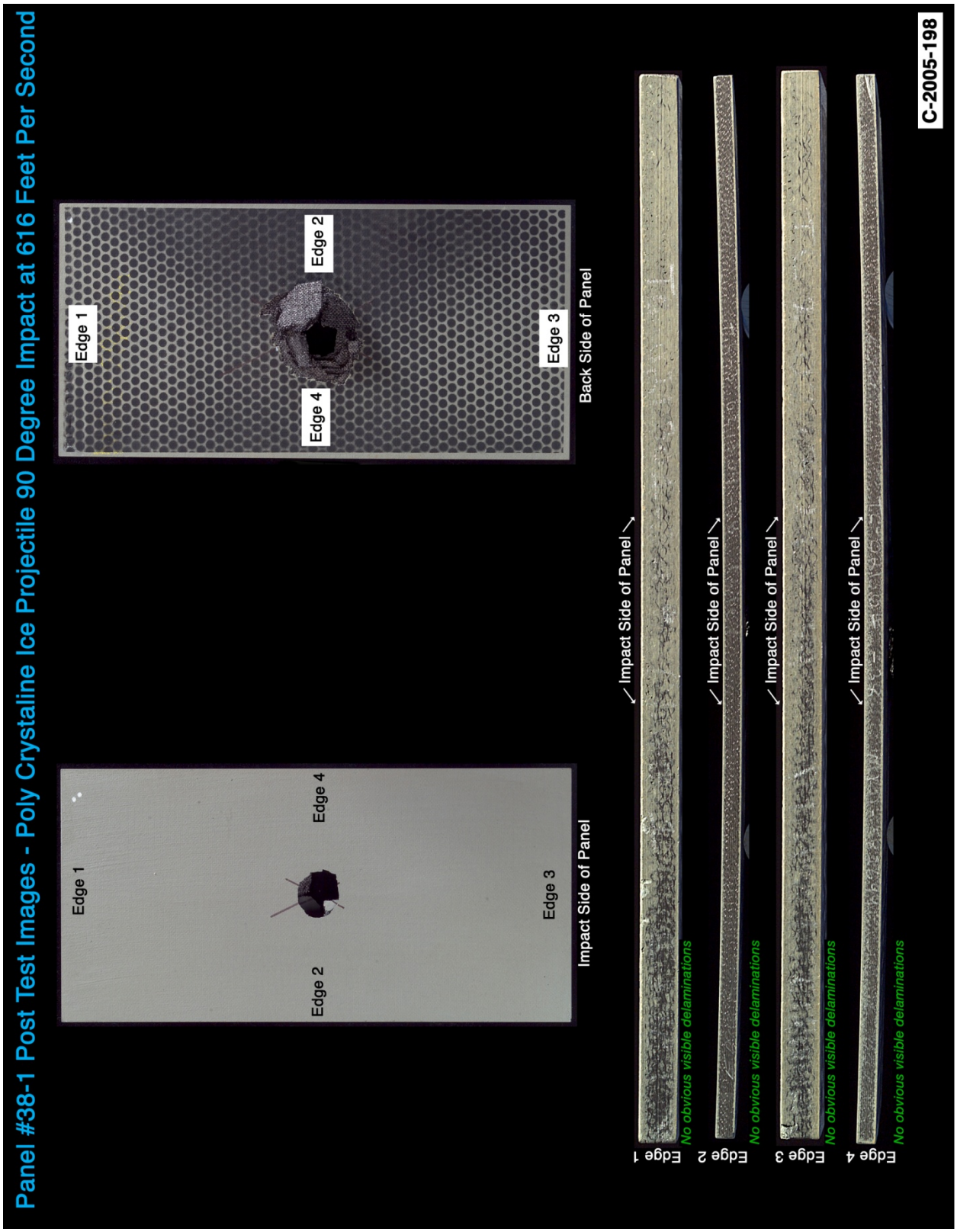

Figure C9–1.—Edges and faces of panel 38-1 at 616 ft/s with a high-density, poly-crystal ice cylinder (nominally 0.66 in. in diameter by 1.66 in.) at 90° impact. Test GRCC 155.

Figure C9–2.—Front (impact side) of panel 38-1 at 616 ft/s with a high-density, poly-crystal ice cylinder (nominally 0.66 in. in diameter by 1.66 in.) at 90° impact angle. Test GRCC 155.

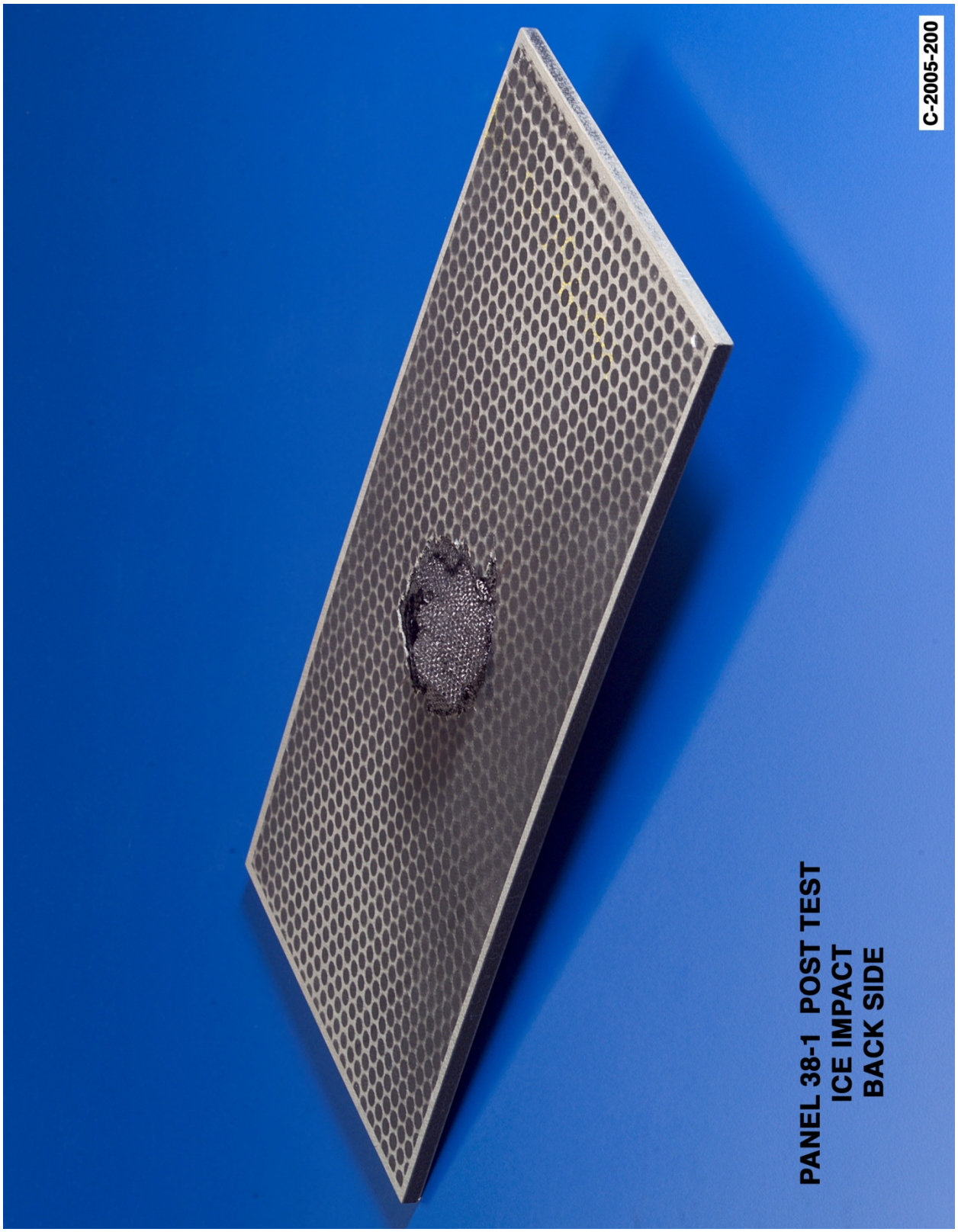

Figure C9–3.—Back face of panel 38-1 at 616 ft/s with a high-density, poly-crystal ice cylinder (nominally 0.66 in. in diameter by 1.66 in.) at 90° impact angle. Test GRCC 155.

Appendix D.—High-Density Ice Testing at 45° Angle on 6- by 12-in. Reinforced Carbon-Carbon (RCC) Flat Panels

Notable Observations From the Appendix D Test Series

1. ARAMIS data existed for nearly all ice impact tests but are not presented when considered to be uninterpretable.

Appendix D Test Series

High Density Ice 45 Degree Impact Test Parameters on 6" x 12" Reinforced Carbon-Carbon Panels

Test No.	Glenn Test Reference Number	Impact Velocity (ft/sec)	Panel ID Number	Average Panel Thickness (inches)	Visual Damage Observations	Mass of panel before test (grams)	Mass of panel after test (grams)	Projectile Mass (g)	Projectile Length (in)	Projectile Diameter (in)	Projectile Density lb_m/ft^3	Test Date	Projectile ID Number
2-45-251-01	GRCC182	493	25-1	0.220	No Visible Damage	410.26	410.58	8.73	1.658	0.667	47.341	3/14/05	Ice: 14-PX-6
2-45-252-02	GRCC183	621	25-2	0.221	No Visible Damage	415.14	415.45	8.54	1.656	0.66	47.355	3/15/05	Ice: 14-PX-3
2-45-322-06	GRCC189	664	32-2	0.218	No Visible damage	407.78	408.13	8.60	1.656	0.665	46.974	3/15/05	Ice: 14-PX-7
2-45-311-03	GRCC185	709	31-1	0.221	No Visible Damage	411.56	412.07	8.87	1.656	0.673	47.303	3/15/05	Ice: 14-PX-10
2-45-321-05	GRCC188	750	32-1	0.219	Back side damage	402.85	402.89	8.63	1.659	0.666	46.911	3/15/05	Ice: 14-PX-4
2-45-312-04	GRCC187	809	31-2	0.220	Back side damage;front small crack	413.19	413.27	8.58	1.656	0.662	47.290	3/15/05	Ice: 14-PX-8

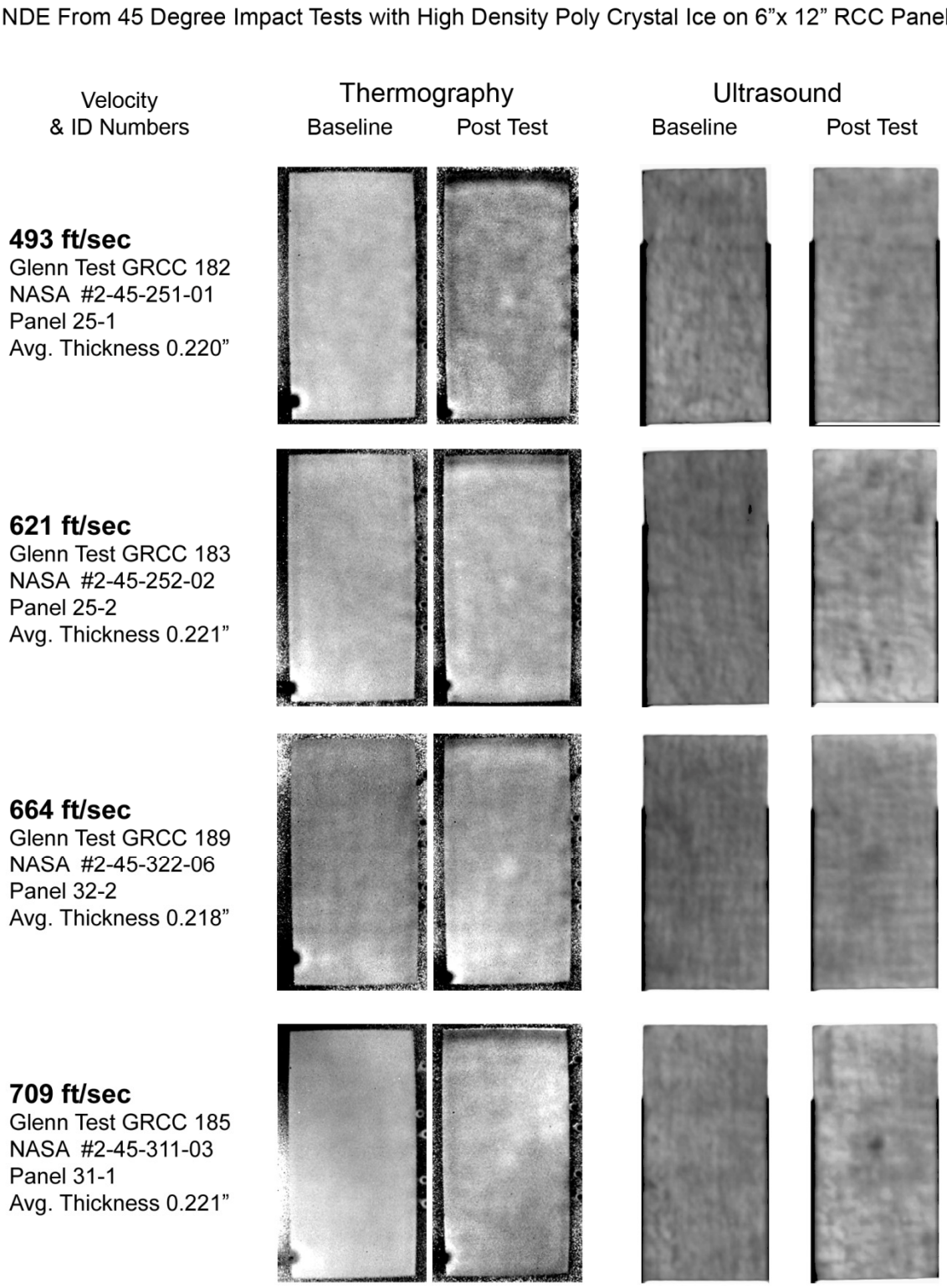

Figure D1–1.—Pulse thermography and ultrasound post impact pre- and posttest images of reinforced carbon-carbon 6- by 12-in. flat panels impacted with high-density ice cylinders (nominally 0.66 in. in diameter by 1.66 in.) at 45° angle.

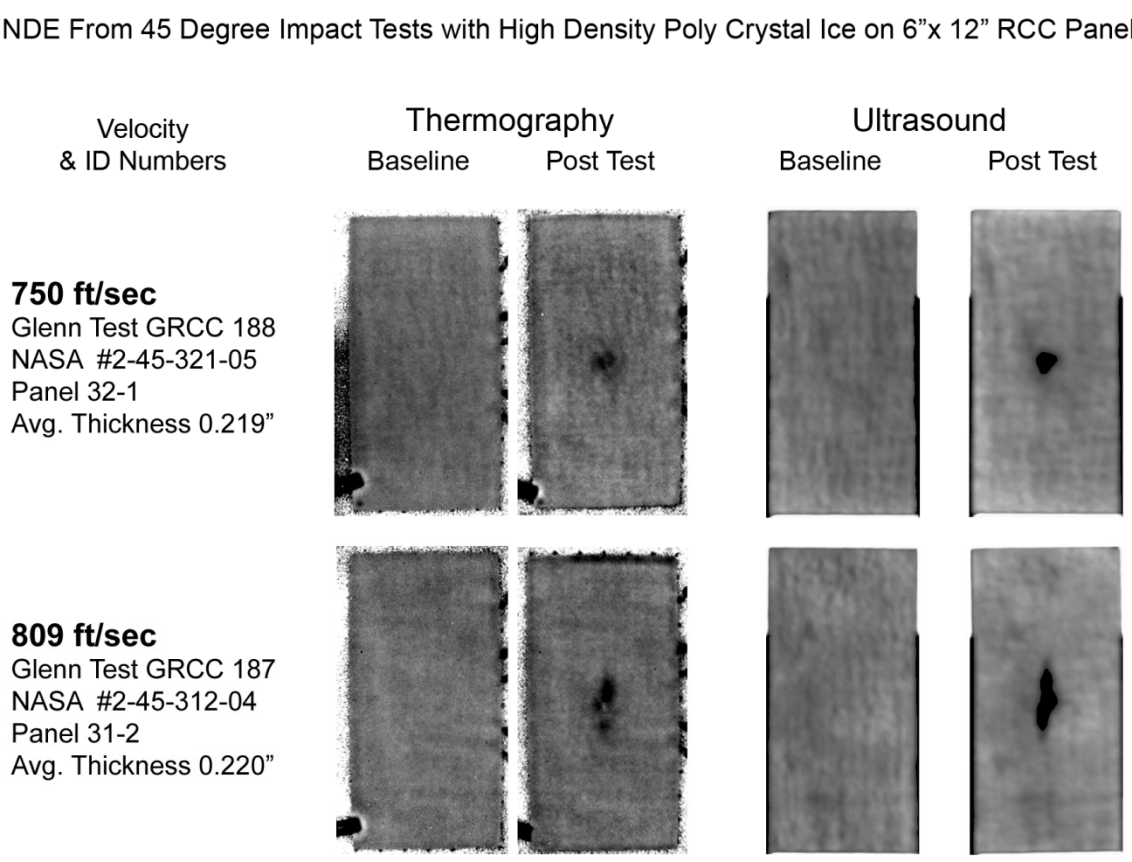

Figure D1–2.—Pulse thermography and ultrasound post impact pre- and posttest images of reinforced carbon-carbon 6- by 12-in. flat panels impacted with high-density ice cylinders (nominally 0.66 in. in diameter by 1.66 in.) at 45° angle.

Aramis Displacement Contours from 45 Degree Impact Tests with High Density Poly-Crystal Ice on 6”x 12” RCC Panels

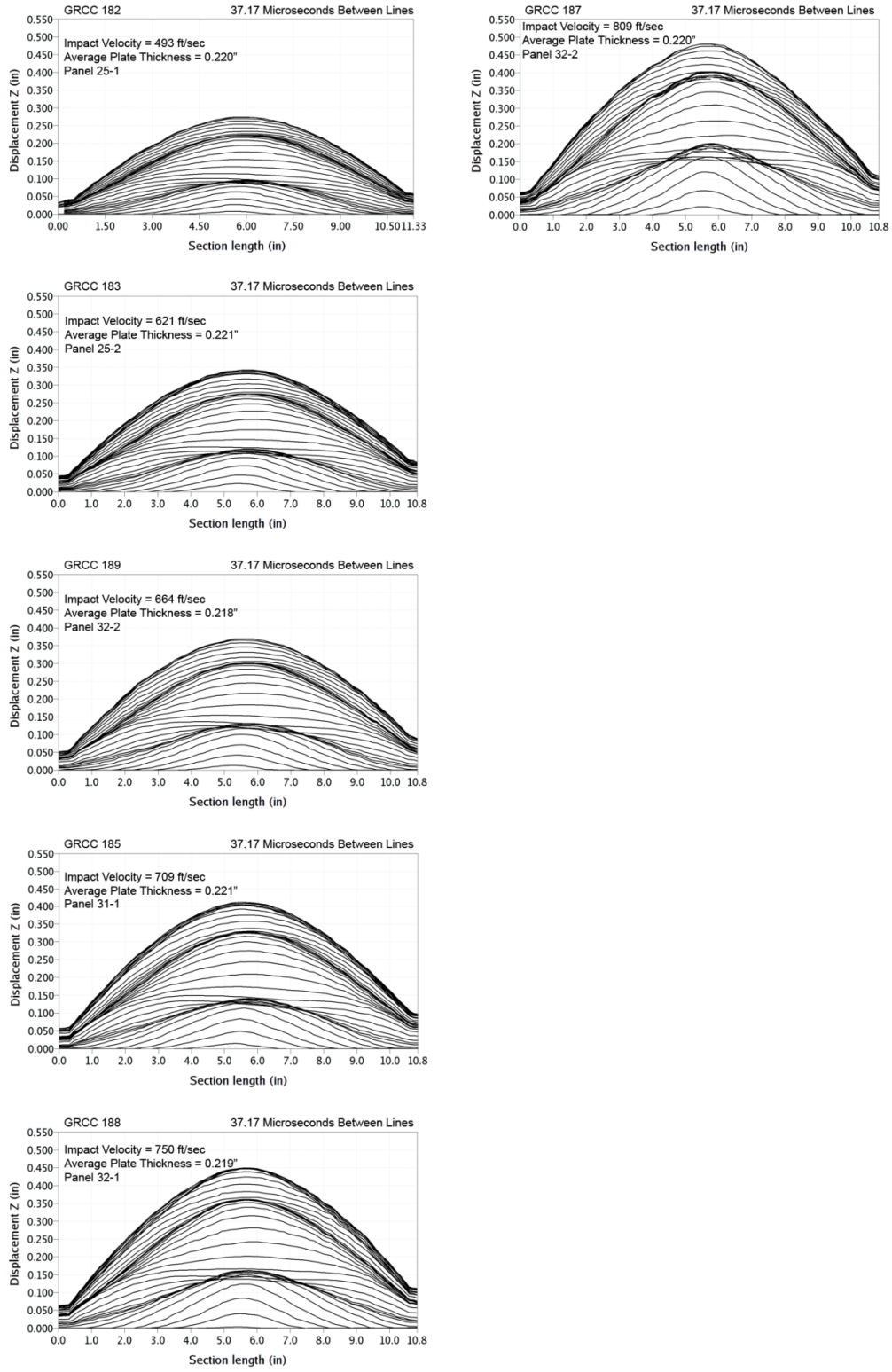

Figure D2–1.—ARAMIS out-of-plane deformation contours across centerline of 6- by 12-in. reinforced carbon-carbon flat panels measured at 37 μs increments undergoing impact with high-density ice cylinders (nominally 0.66 in. in diameter by 1.66 in.) at 45° angle.

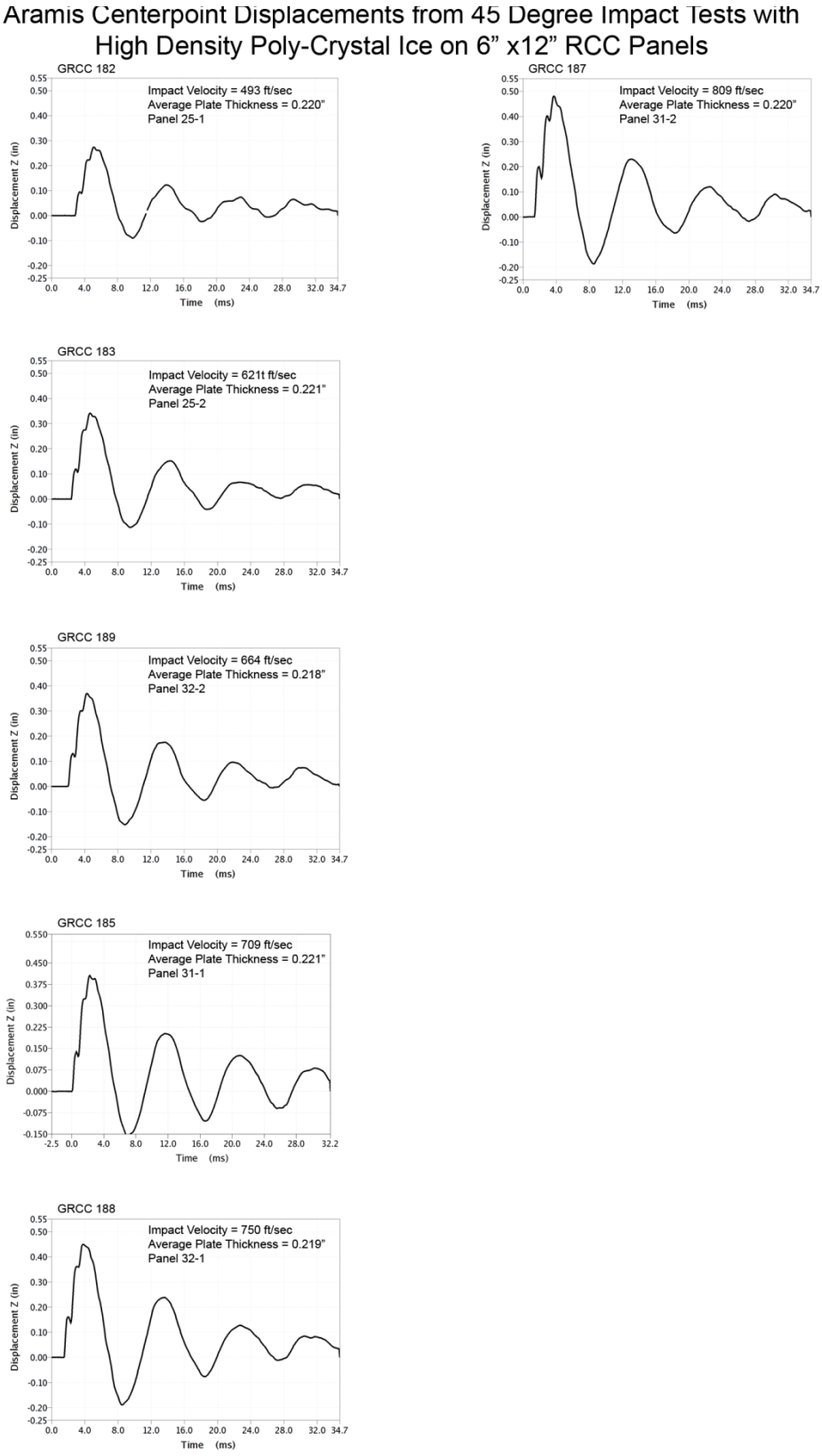

Figure D3–1.—ARAMIS centerpoint out-of-plane deformation vs. time of 6- by 12-in. reinforced carbon-carbon flat panels impacted with high-density ice cylinders (nominally 0.66 in. in diameter by 1.66 in.) at 45° angle.

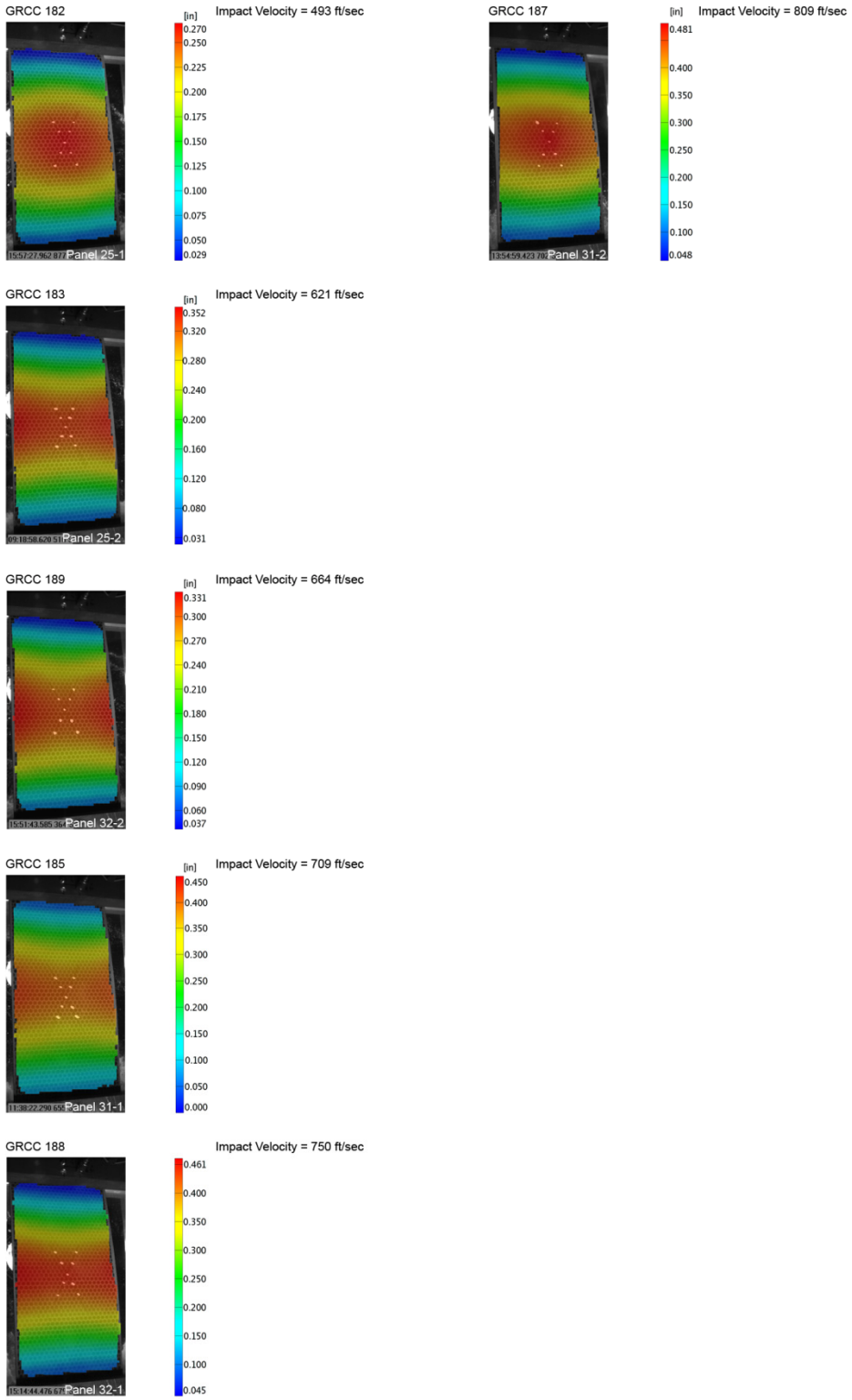

Figure D4–1.—ARAMIS color fringe plots depicting maximum deformation prior to material failure of 6- by 12-in. reinforced carbon-carbon flat panels as they undergo impact with high-density ice cylinders (nominally 0.66 in. in diameter by 1.66 in.) at 45° angle.

Figure D5–1.—Edges and faces of panel 25-1 at 493 ft/s with a high-density, poly-crystal ice cylinder (nominally 0.66 in. in diameter by 1.66 in.) at 45° impact angle. Test GRCC 182.

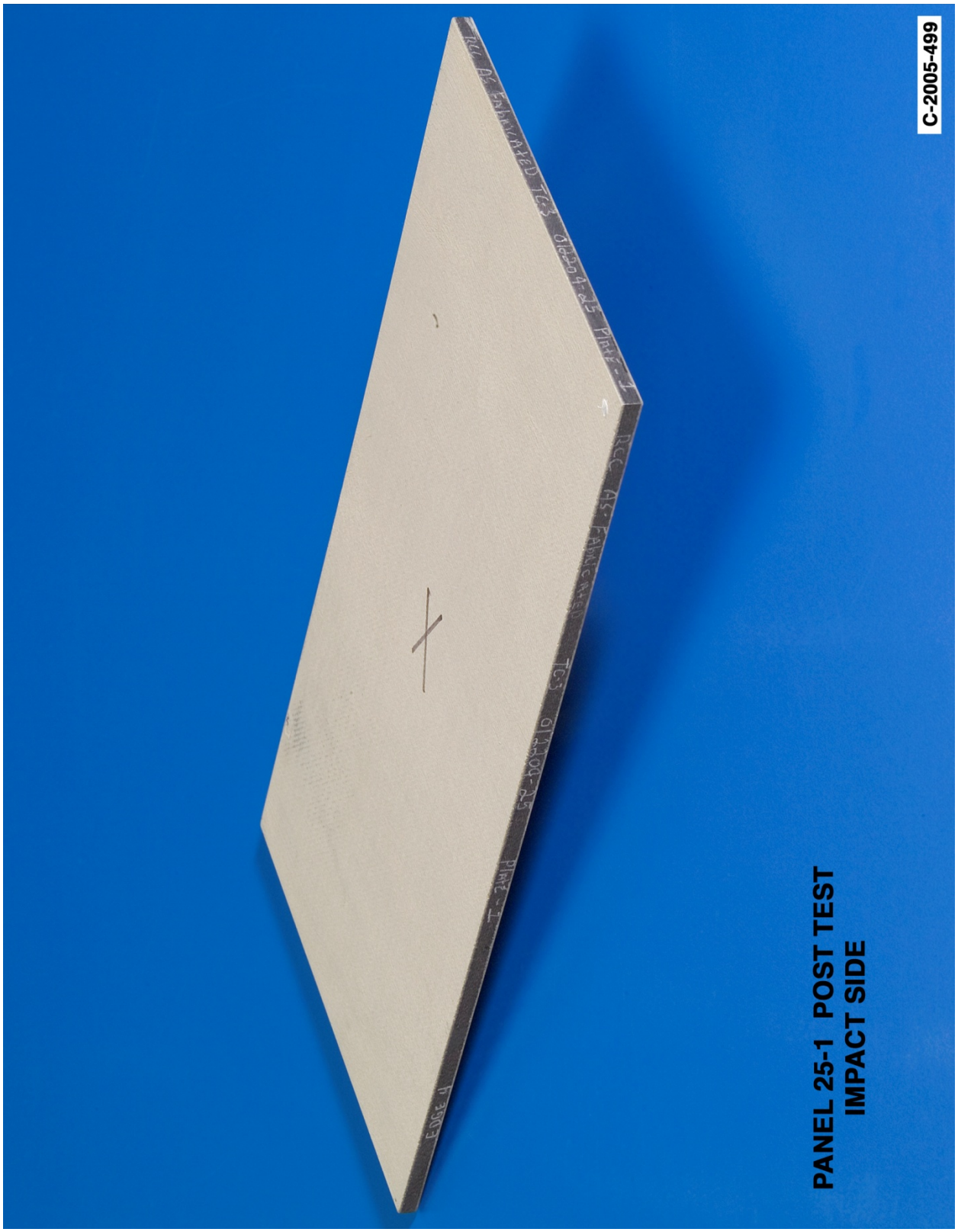

Figure D5–2.—Front (impact side) of panel 25-1 at 493 ft/s with a high-density, poly-crystal ice cylinder (nominally 0.66 in. in diameter by 1.66 in.) at 45° impact angle. Test GRCC 182.

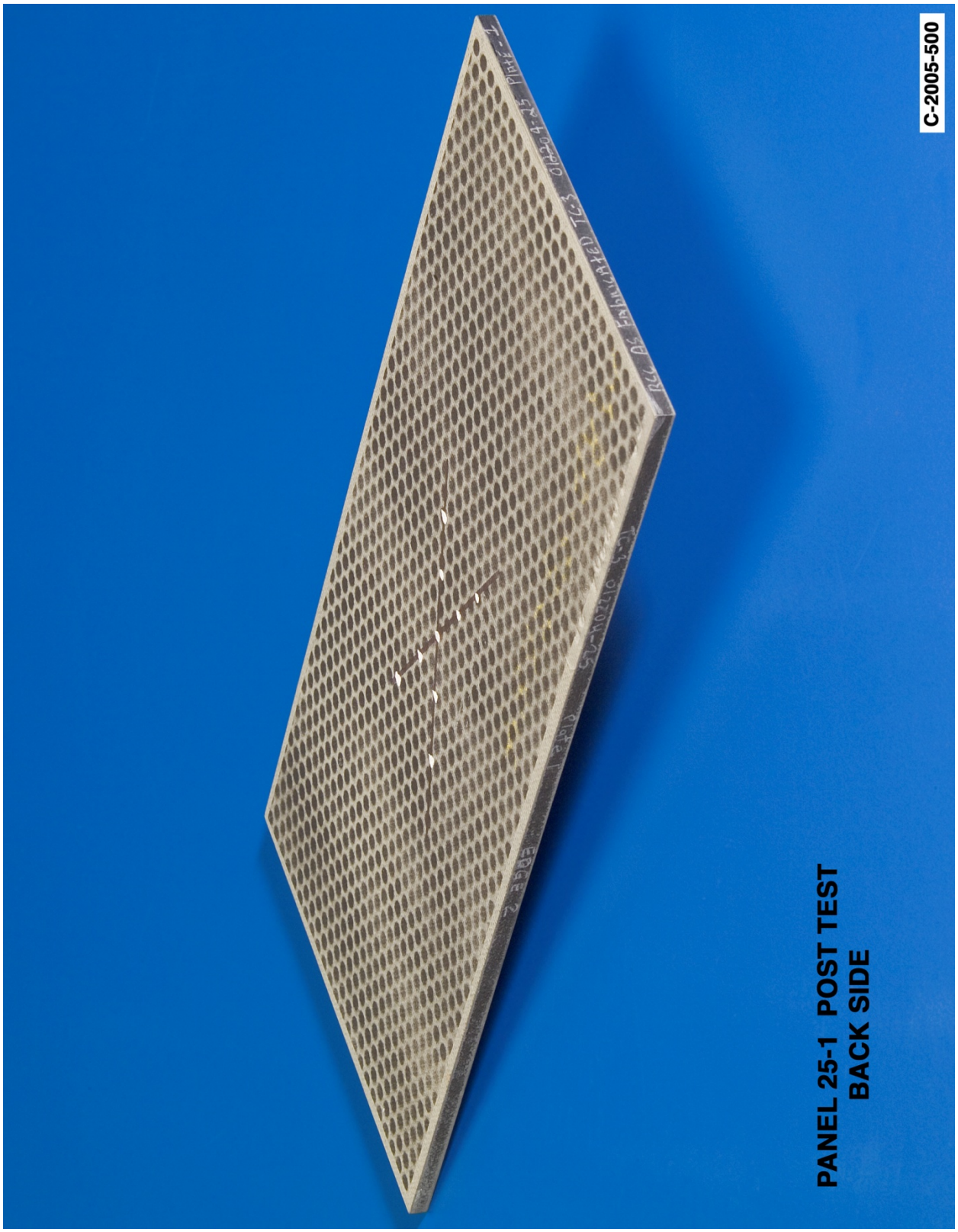

Figure D5–3.—Back face of panel 25-1 at 493 ft/s with a high-density, poly-crystal ice cylinder (nominally 0.66 in. in diameter by 1.66 in.) at 45° impact angle. Test GRCC 182.

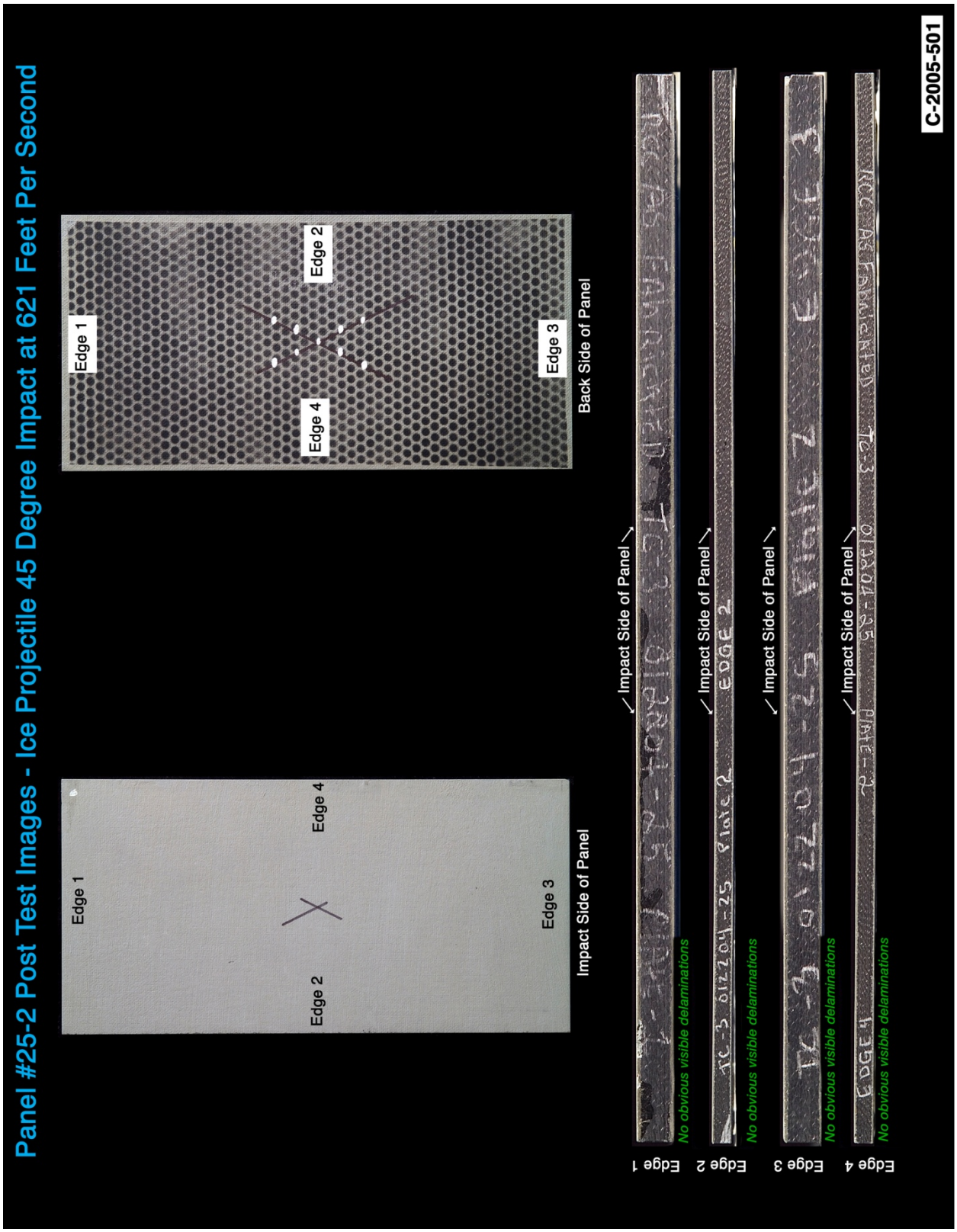

Figure D6–1.—Edges and faces of panel 25-2 at 621 ft/s with a high-density, poly-crystal ice cylinder (nominally 0.66 in. in diameter by 1.66 in.) at 45° impact. Test GRCC 183.

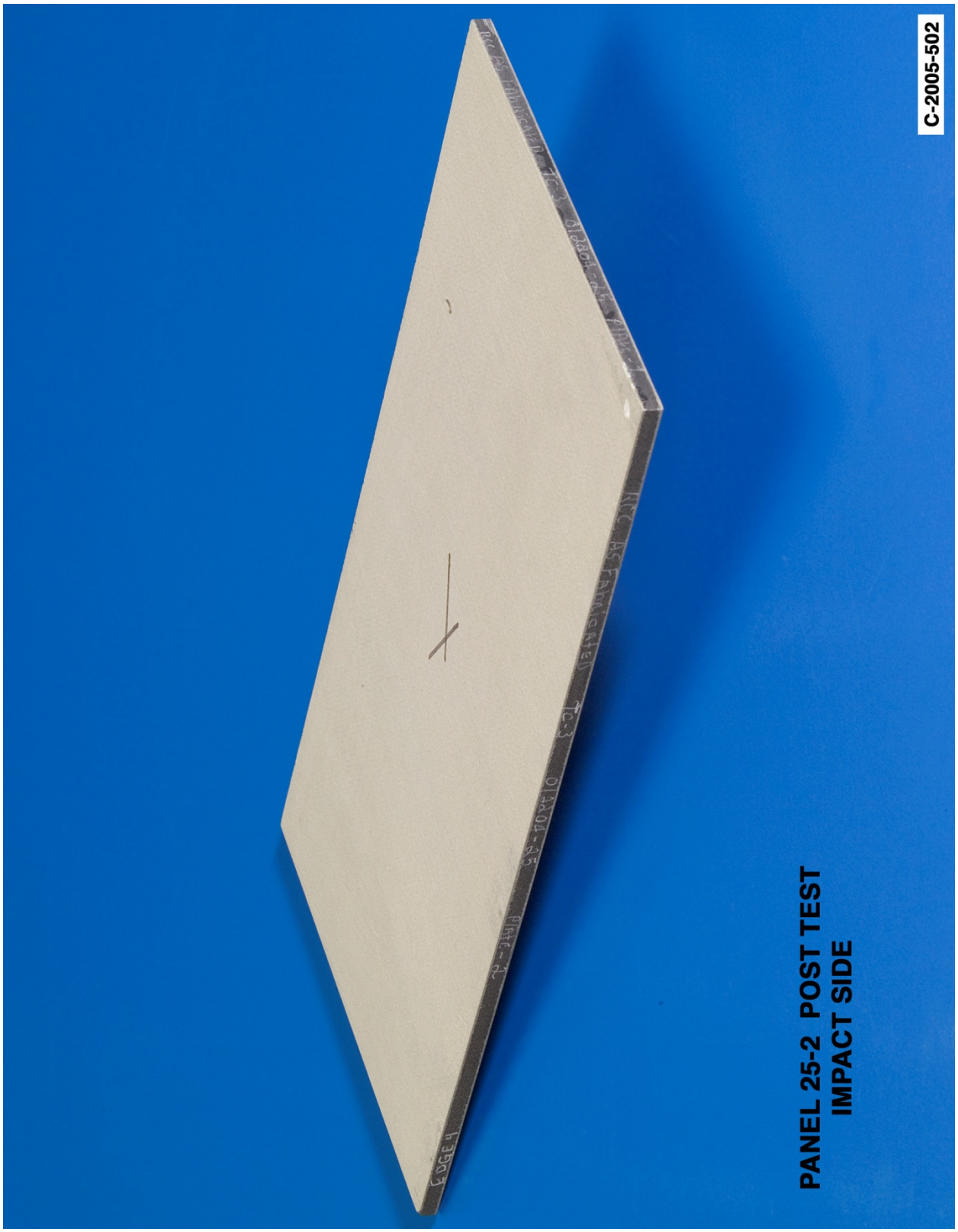

Figure D6–2.—Front (impact side) of panel 25-2 at 621 ft/s with a high-density, poly-crystal ice cylinder (nominally 0.66 in. in diameter by 1.66 in.) at 45° impact angle. Test GRCC 183.

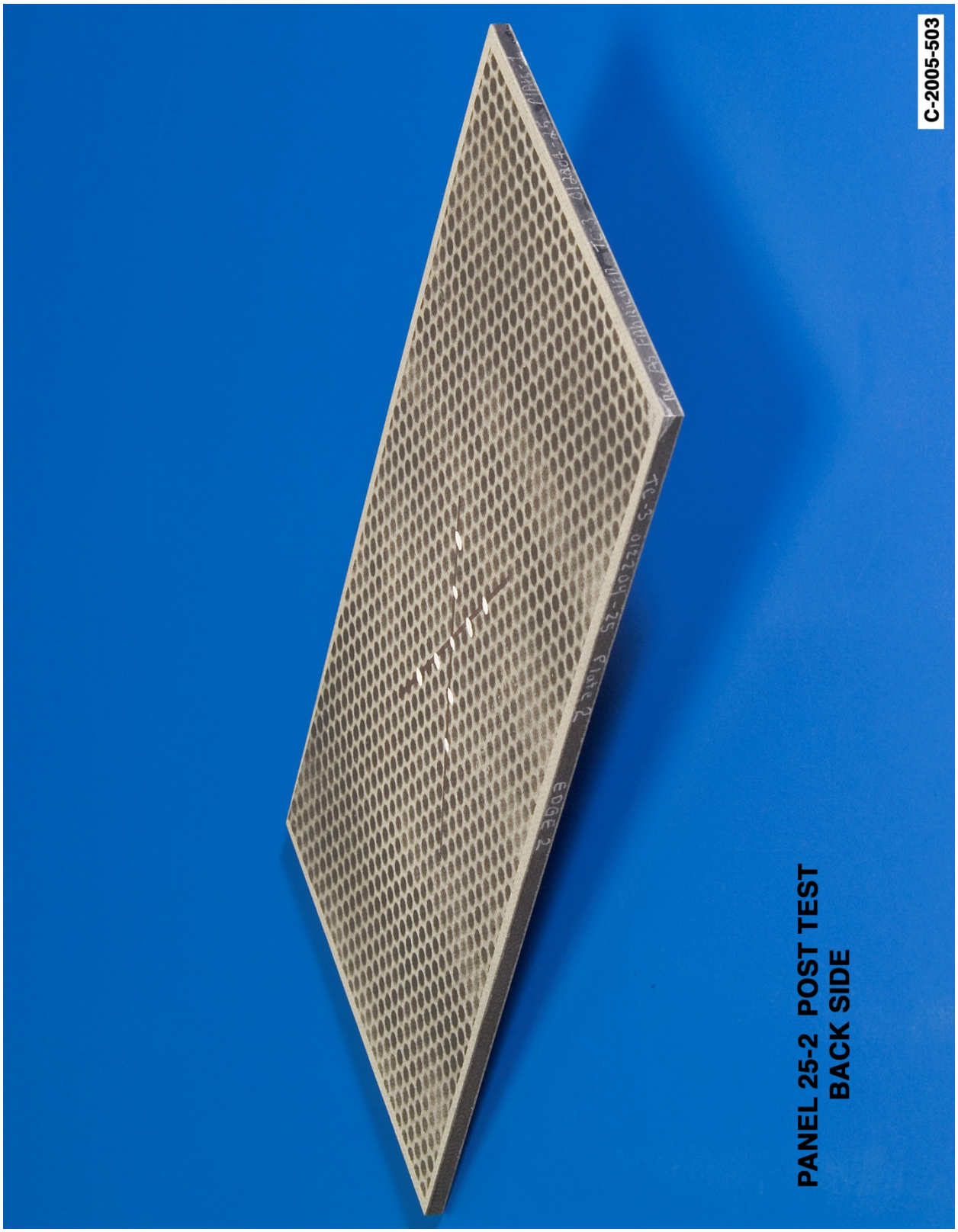

Figure D6–3.—Back face of panel 25-2 at 621 ft/s with a high-density, poly-crystal ice cylinder (nominally 0.66 in. in diameter by 1.66 in.) at 45° impact angle. Test GRCC 183.

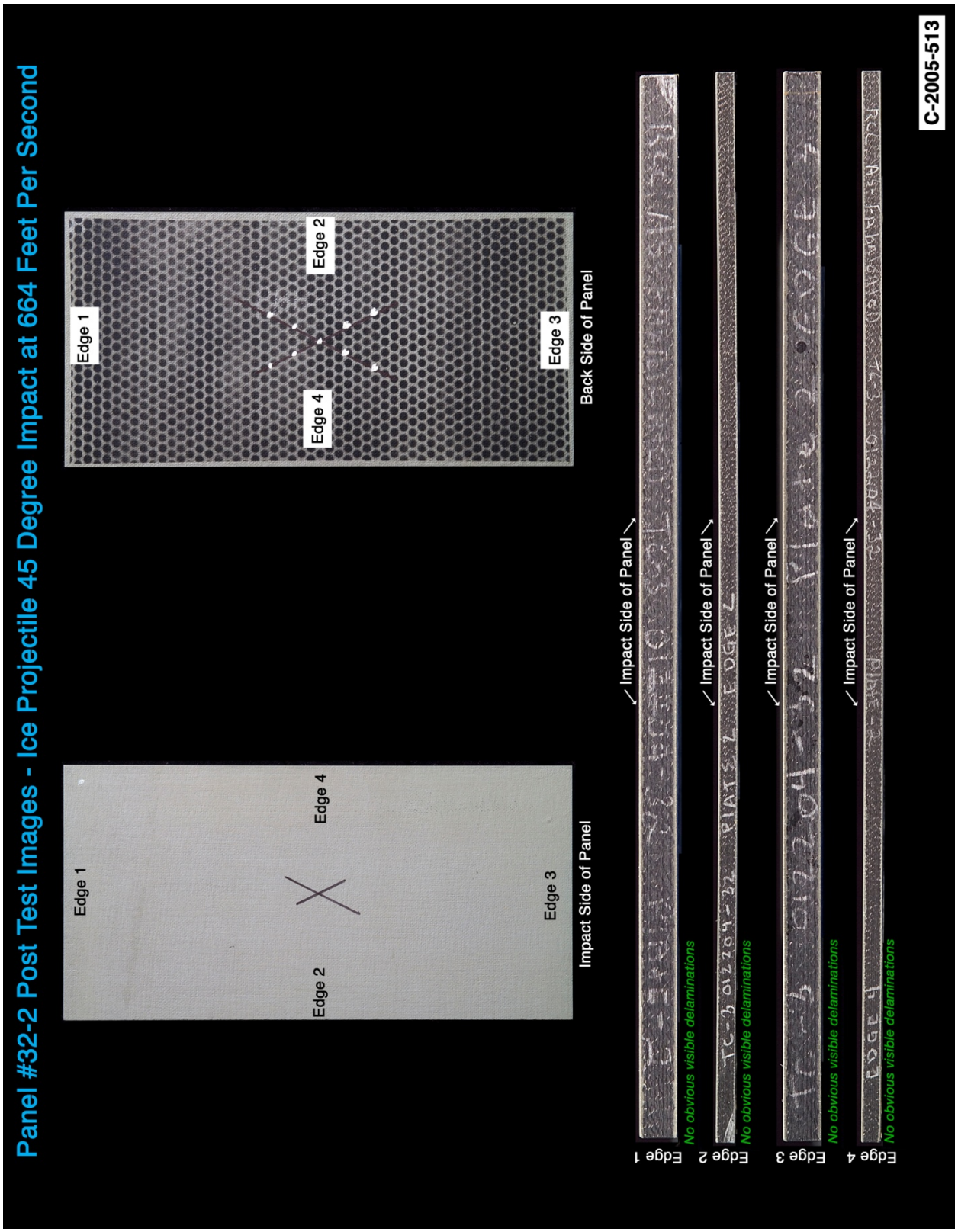

Figure D7–1.—Edges and faces of panel 32-2 at 664 ft/s with a high-density, poly-crystal ice cylinder (nominally 0.66 in. in diameter by 1.66 in.) at 45° impact. Test GRCC 189.

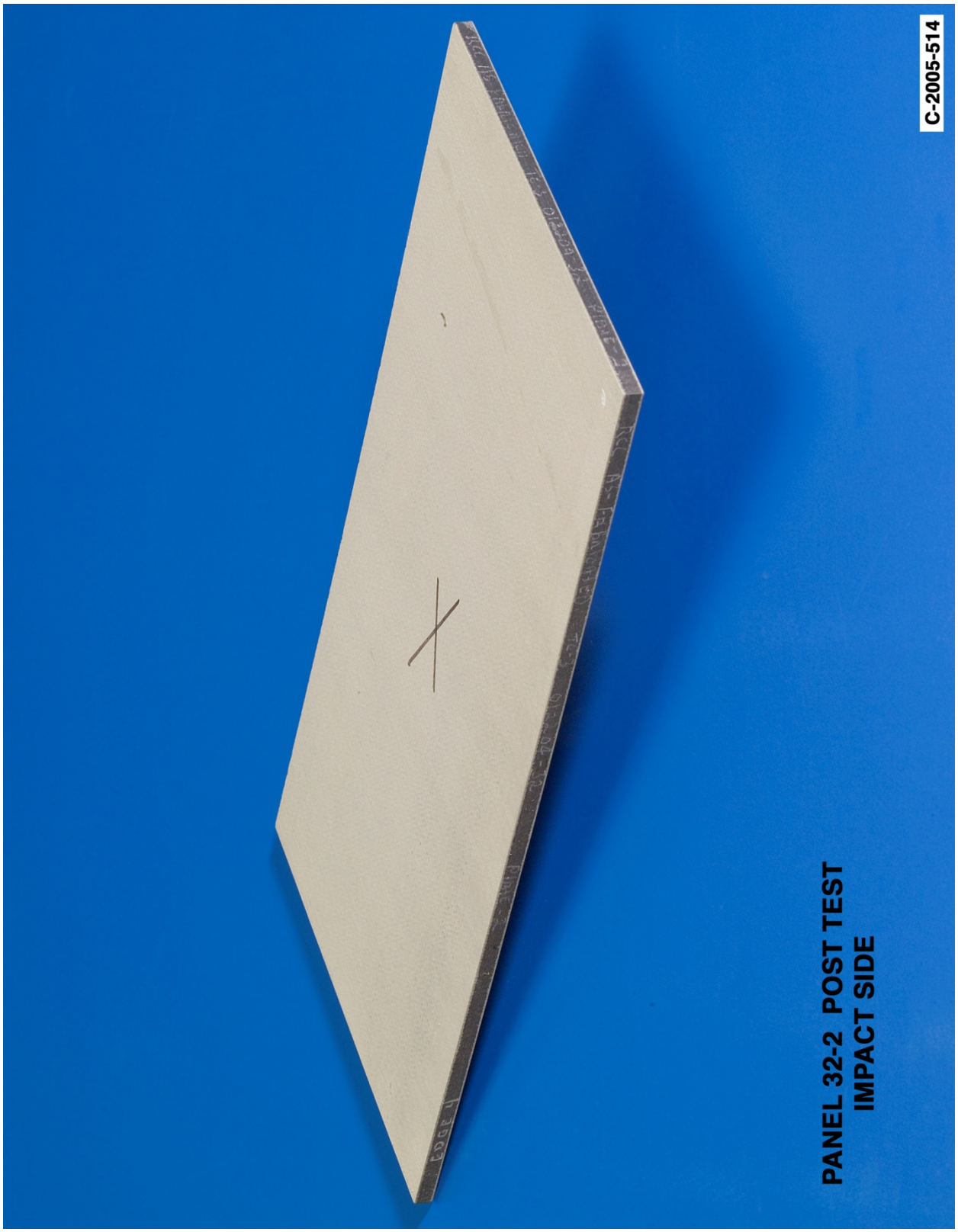

Figure D7–2.—Front (impact side) of panel 32-2 at 664 ft/s with a high-density, poly-crystal ice cylinder (nominally 0.66 in. in diameter by 1.66 in.) at 45° impact angle. Test GRCC 189.

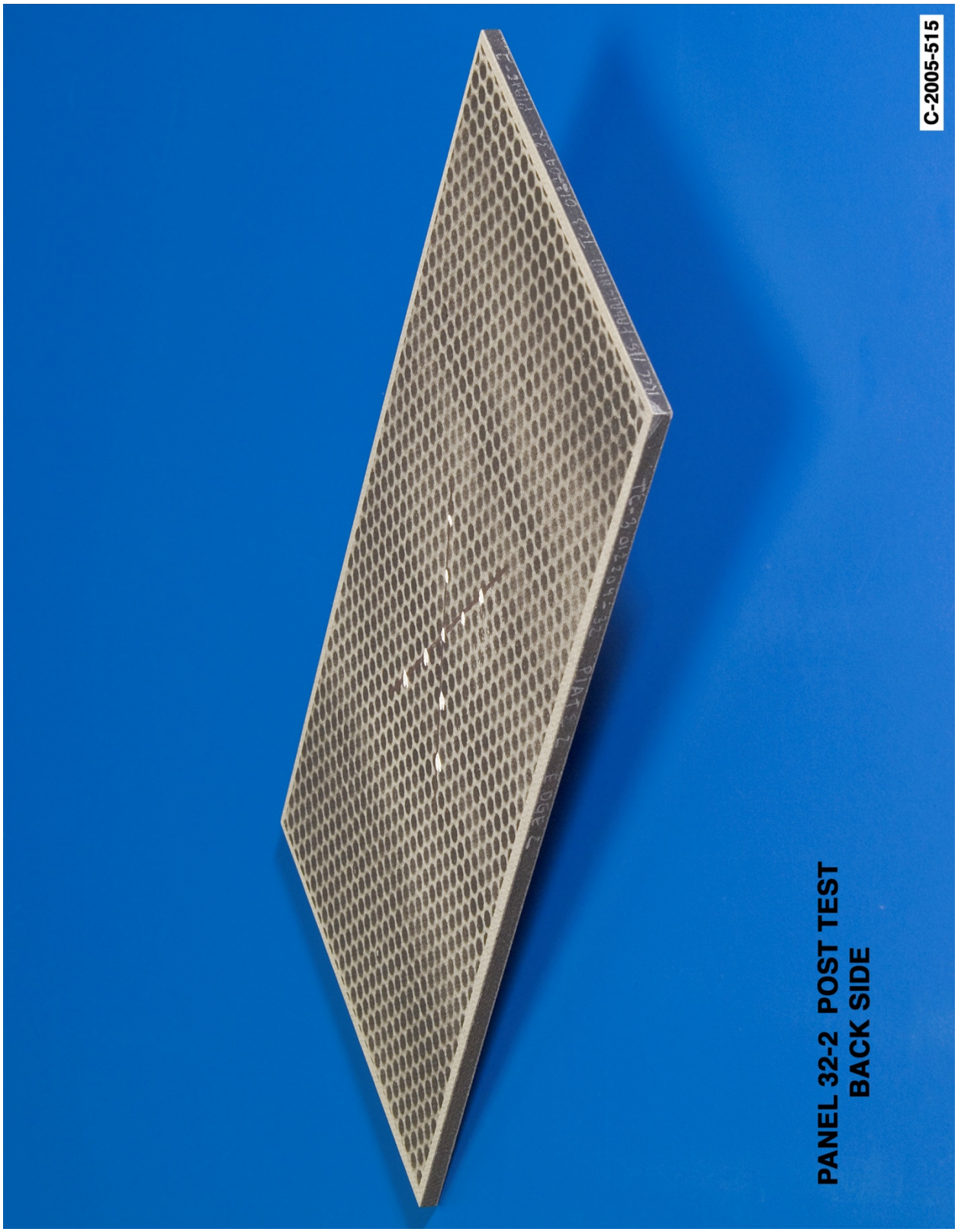

Figure D7–3.—Back face of panel 32-2 at 664 ft/s with a high-density, poly-crystal ice cylinder (nominally 0.66 in. in diameter by 1.66 in.) at 45° impact angle. Test GRCC 189.

Figure D8–1.—Edges and faces of panel 31-1 at 709 ft/s with a high-density, poly-crystal ice cylinder (nominally 0.66 in. in diameter by 1.66 in.) at 45° impact. Test GRCC 185.

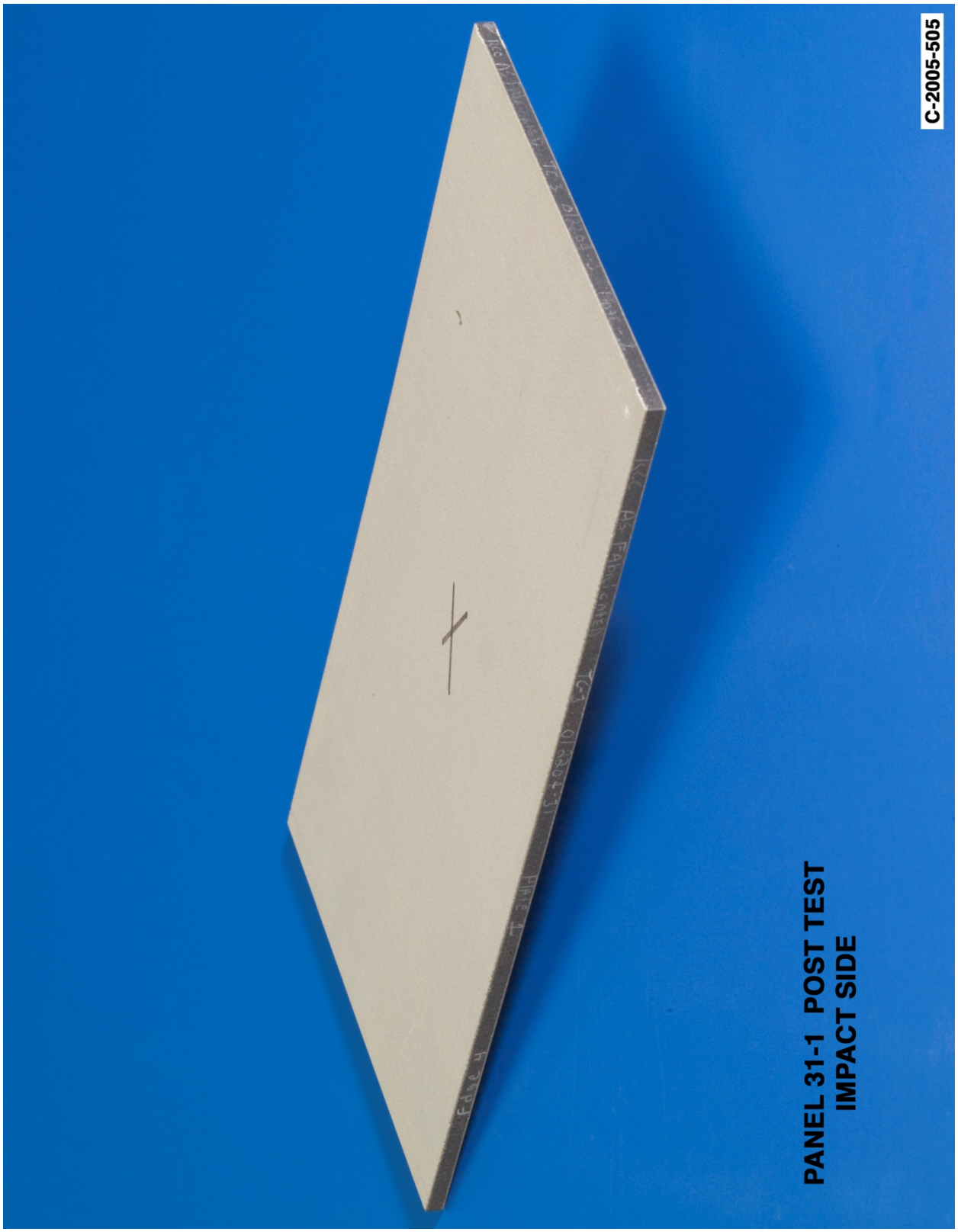

Figure D8–2.—Front (impact side) of panel 31-1 at 709 ft/s with a high-density, poly-crystal ice cylinder (nominally 0.66 in. in diameter by 1.66 in.) at 45° impact angle. Test GRCC 185.

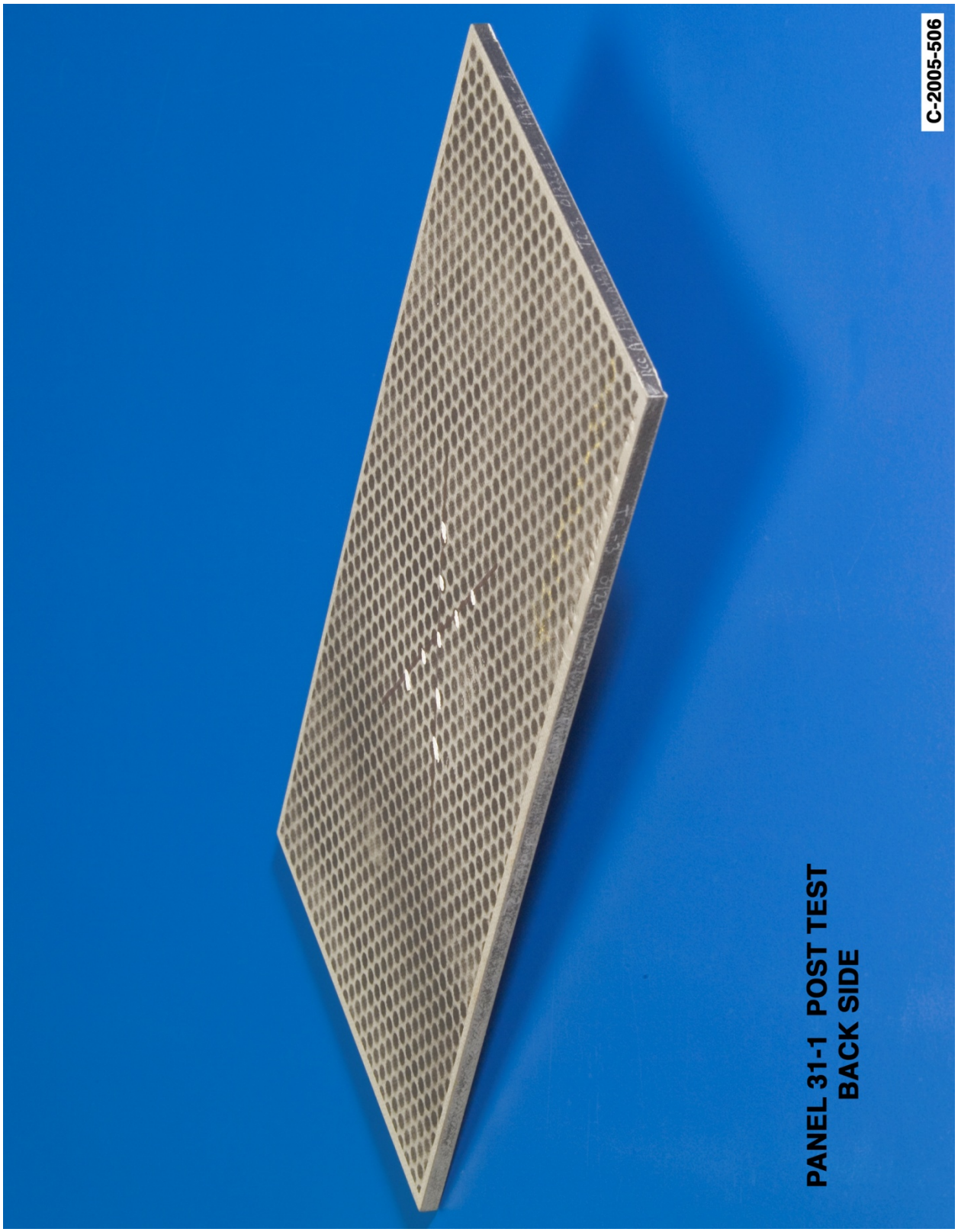

Figure D8–3.—Back face of panel 31-1 at 709 ft/s with a high-density, poly-crystal ice cylinder (nominally 0.66 in. in diameter by 1.66 in.) at 45° impact angle. Test GRCC 185.

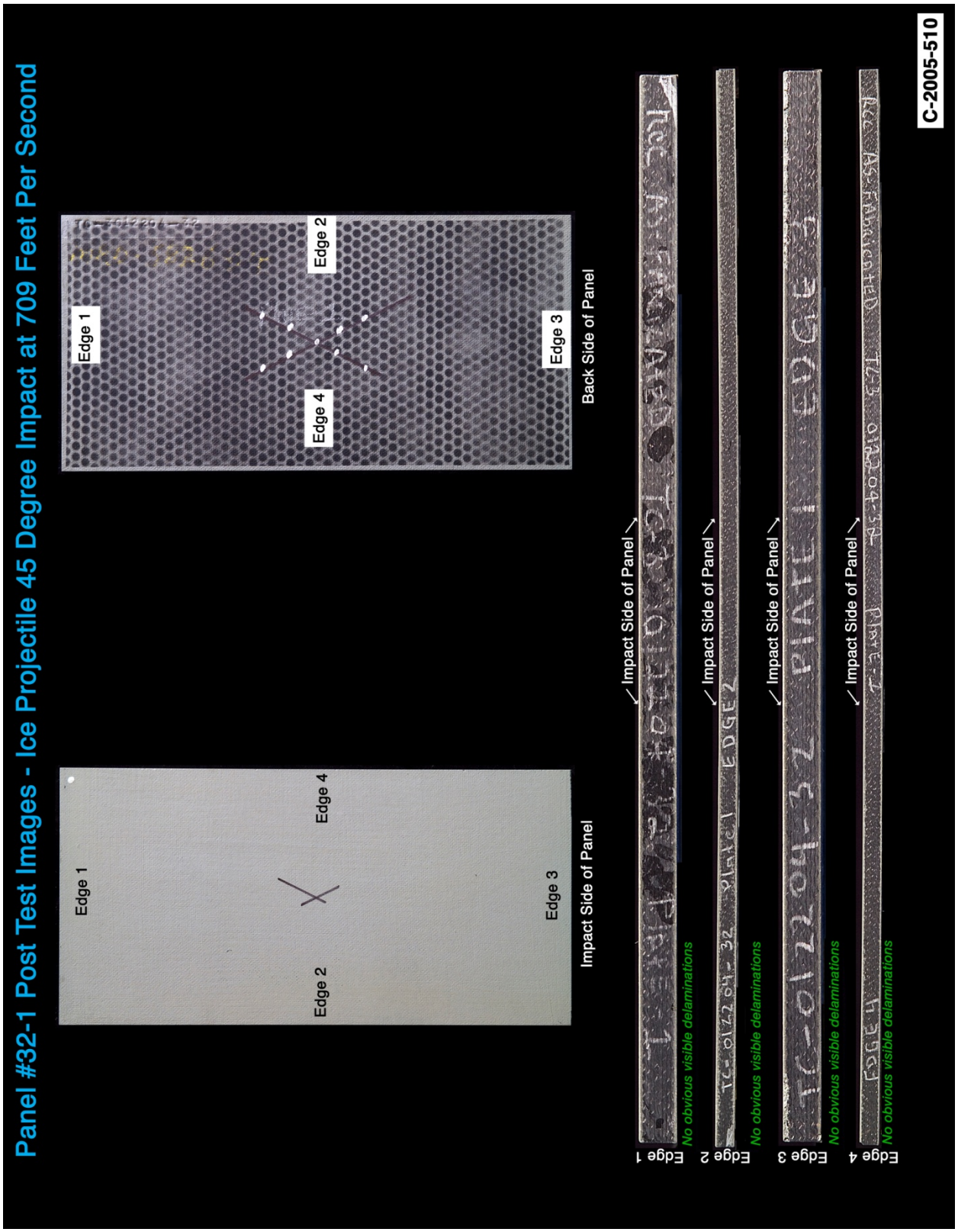

Figure D9–1.—Edges and faces of panel 32-1 at 750 ft/s with a high-density, poly-crystal ice cylinder (nominally 0.66 in. in diameter by 1.66 in.) at 45° impact. Test GRCC 188.

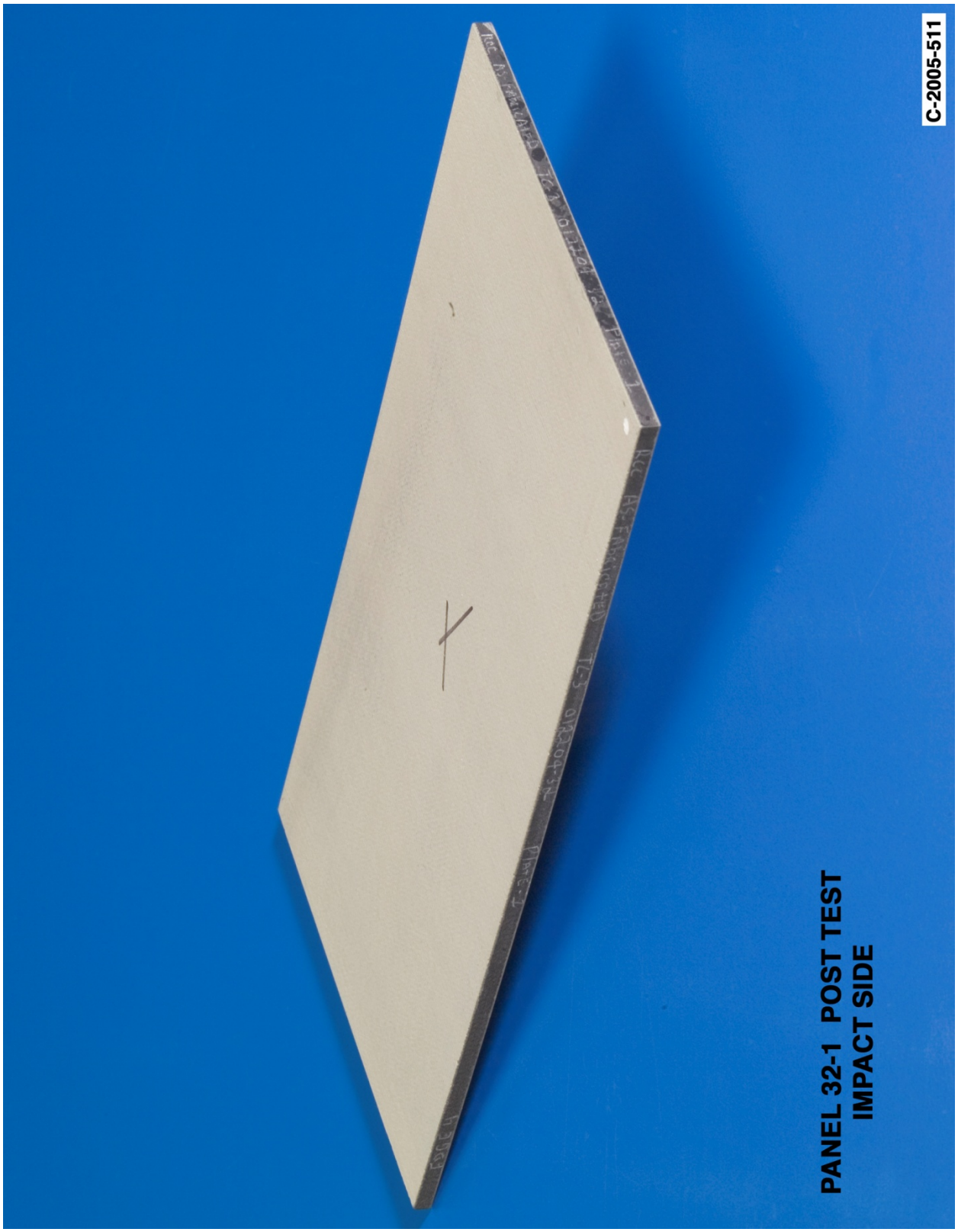

Figure D9–2.—Front (impact side) of panel 32-1 at 750 ft/s with a high-density, poly-crystal ice cylinder (nominally 0.66 in. in diameter by 1.66 in.) at 45° impact angle. Test GRCC 188.

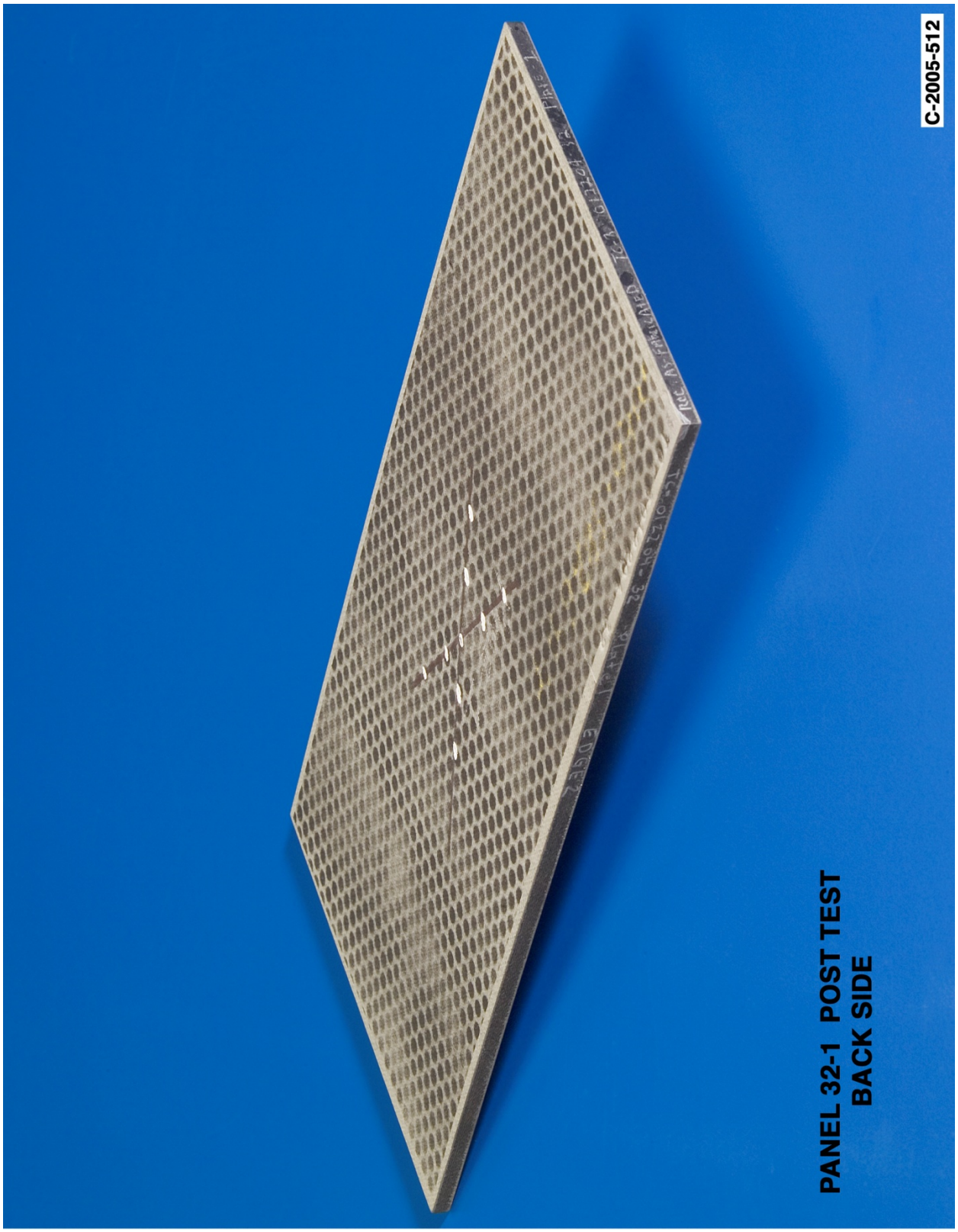

Figure D9–3.—Back face of panel 32-1 at 750 ft/s with a high-density, poly-crystal ice cylinder (nominally 0.66 in. in diameter by 1.66 in.) at 45° impact angle. Test GRCC 188.

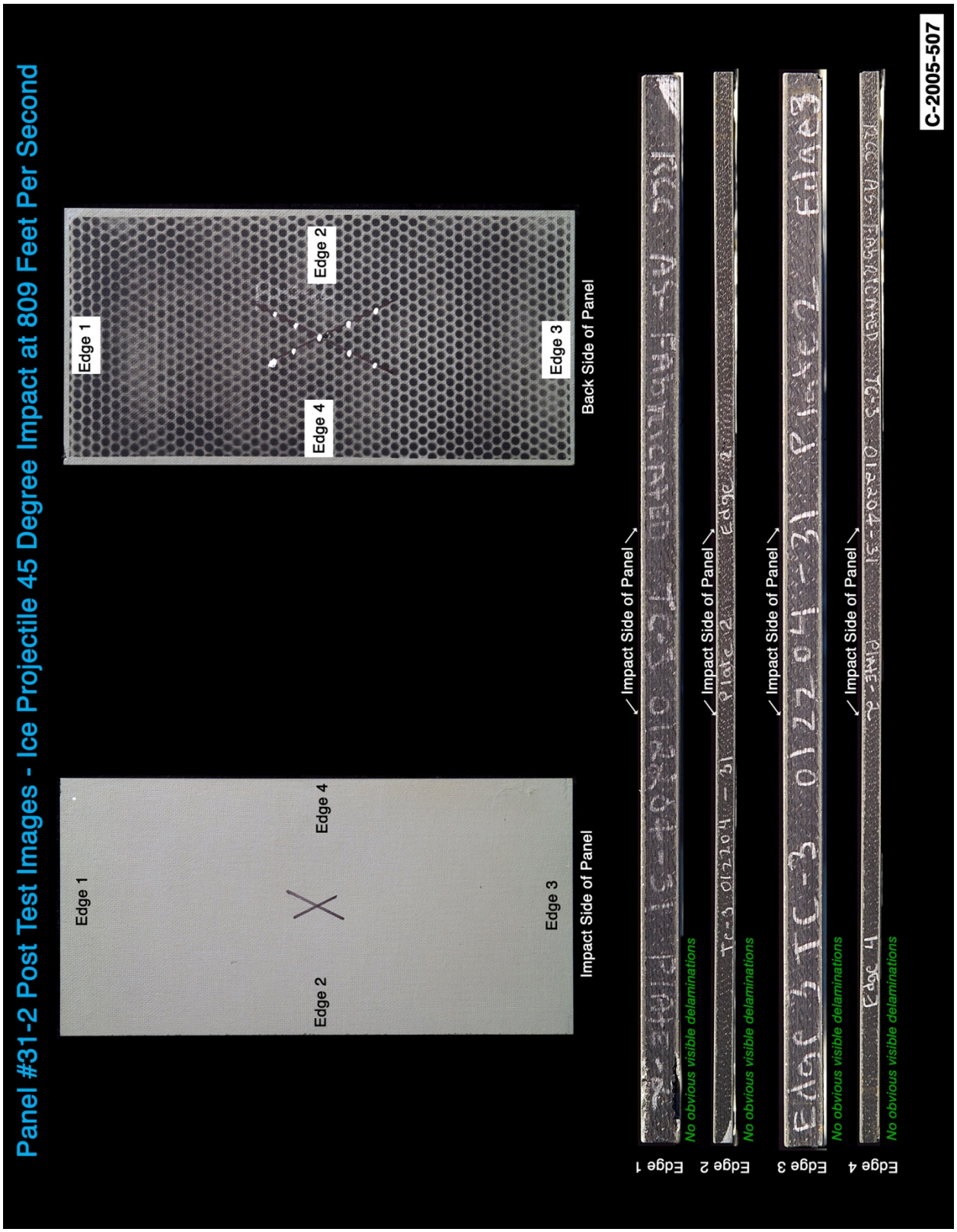

Figure D10–1.—Edges and faces of panel 31-2 at 809 ft/s with a high-density, poly-crystal ice cylinder (nominally 0.66 in. in diameter by 1.66 in.) at 45° impact. Test GRCC 187.

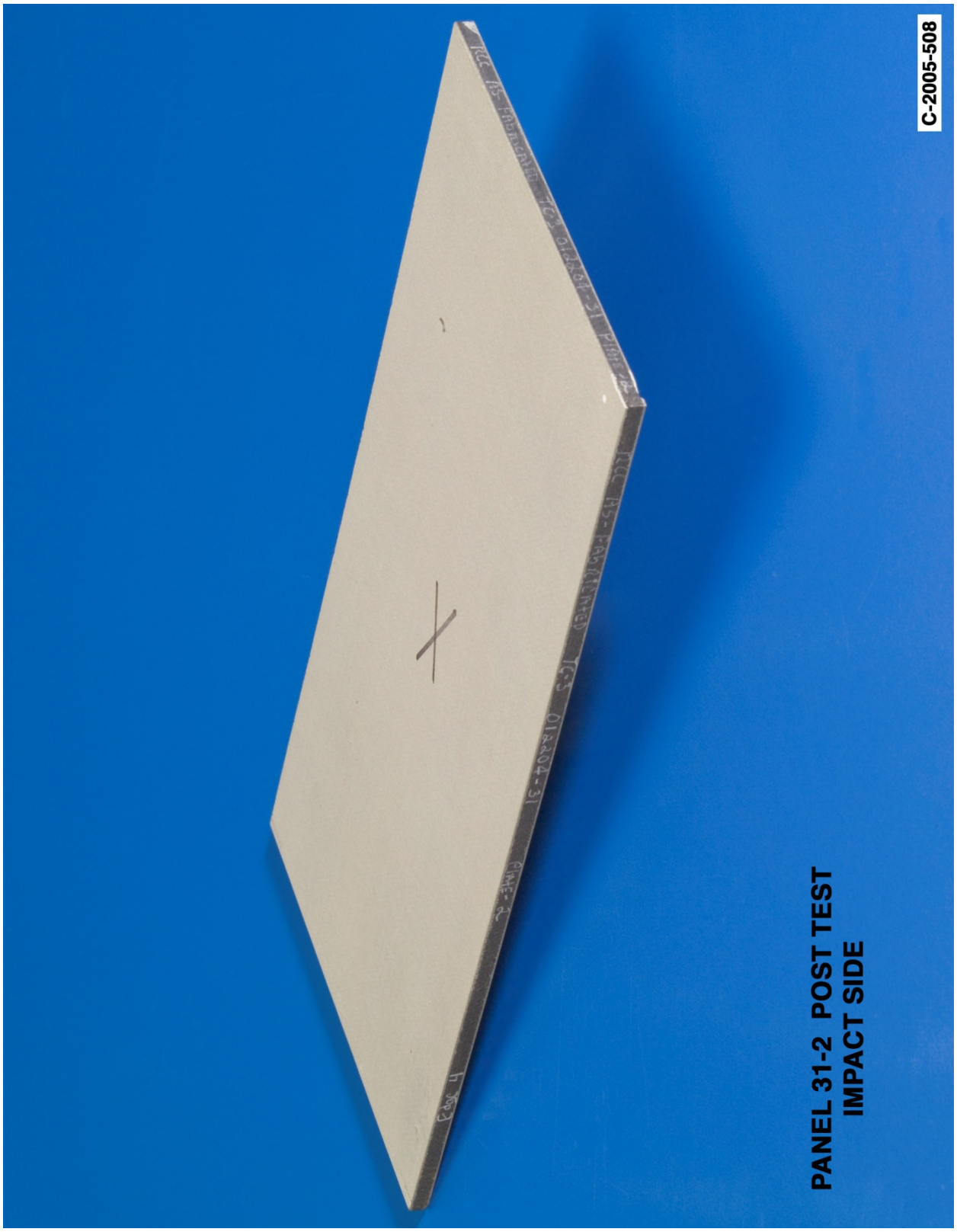

Figure D10–2.—Front (impact side) of panel 31-2 at 809 ft/s with a high-density, poly-crystal ice cylinder (nominally 0.66 in. in diameter by 1.66 in.) at 45° impact angle. Test GRCC 187.

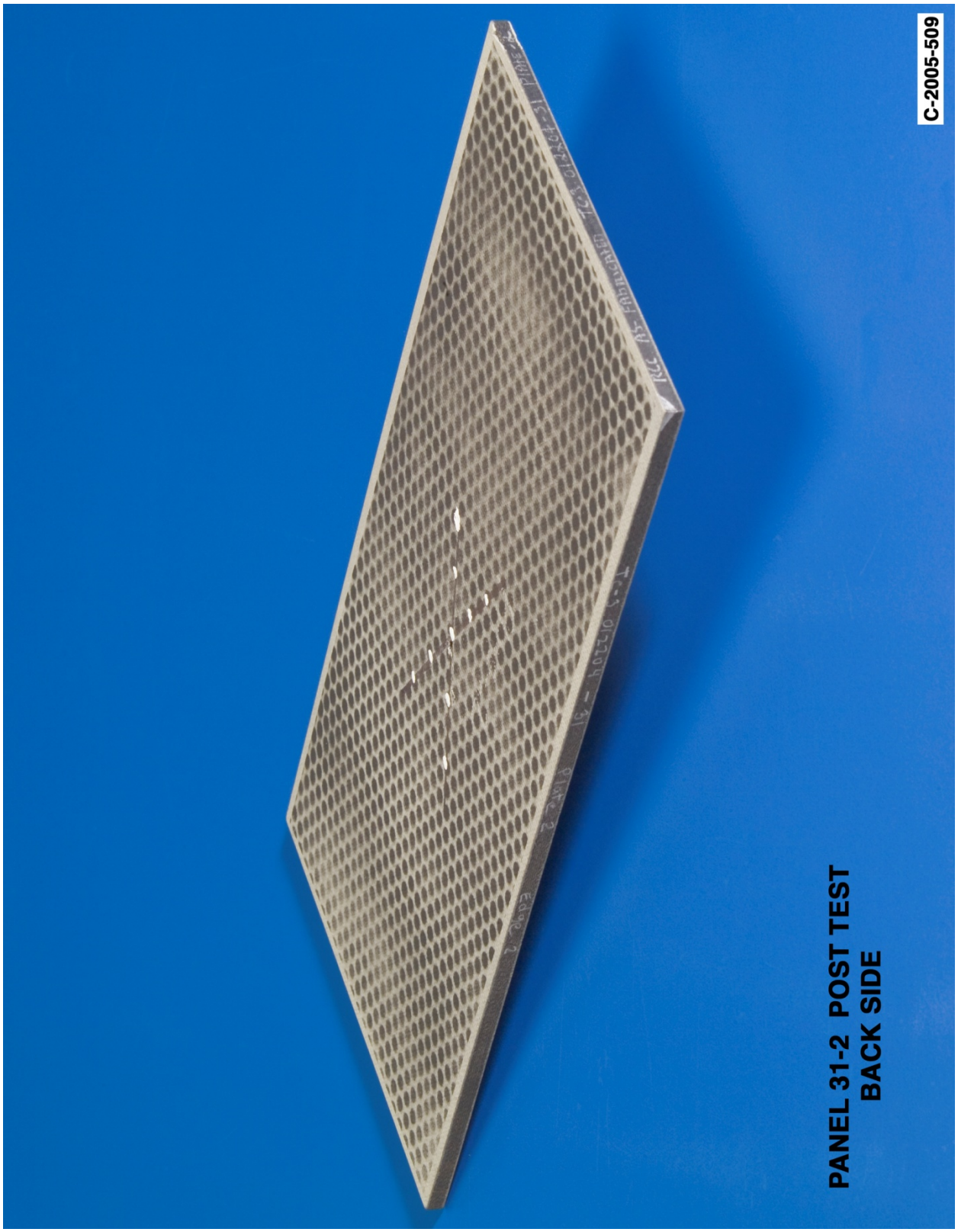

Figure D10–3.—Back face of panel 31-2 at 809 ft/s with a high-density, poly-crystal ice cylinder (nominally 0.66 in. in diameter by 1.66 in.) at 45° impact angle. Test GRCC 187.

Appendix E.—Low-Density Ice Impact Testing at 90° Angle on 6- by 6-in. Reinforced Carbon-Carbon (RCC) Flat Panels

Notable Observations From the Appendix E Test Series

1. ARAMIS data existed for nearly all ice impact tests but are not presented when considered to be uninterpretable.

Appendix E Test Series

Low Density Ice 90 Degree Impact Test Parameters on 6" x 6" Reinforced Carbon-Carbon Panels													
Test No.	Glenn Test Reference Number	Impact Velocity (ft/sec)	Panel ID Number	Average Panel Thickness (inches)	Visual Damage Observations	Mass of panel before test (grams)	Mass of panel after test (grams)	Projectile Mass (g)	Projectile Length (in)	Projectile Diameter (in)	Projectile Density lb_m/ft^3	Test Date	Projectile ID Number
2-90-643-05	GRCC144	431	64-3	0.230	No damage - shoot again	208.30	208.87	9.18	1.9	0.8	36.618	1/13/05	Ice: Soft 18-7
2-90-654-08	GRCC149	441	65-4	0.227	No visible damage	206.43	206.98	9.48	1.9	0.8	37.814	1/14/05	Ice: Soft 18-12
2-90-454-05	GRCC127	471	45-4	0.220		212.13	212.57					1/6/05	Ice: Soft 18-26
2-90-644-06	GRCC146	476	64-4	0.226	No apparent damage; just a kiss	208.39	209.19	9.55	1.9	0.8	38.094	1/13/05	Ice: Soft 18-11
2-90-491-01	GRCC123	494	49-1	0.227	Thru crack on back	205.59	206.01	9.55	1.9	0.8	38.094	1/5/05	Ice: Soft 18-18
2-90-653-07	GRCC148	502	65-3	0.230	No visible damage	207.69	208.33	9.11	1.9	0.8	36.338		Ice: Soft 18-3
2-90-492-02	GRCC124	526	49-2	0.223	Some damage on back	205.41	205.91	9.54	1.92	0.8	37.657	1/6/05	Ice: Soft 18-15
2-90-494-04	GRCC126	556	49-4	0.222	No apparent damage	207.68	208.22	9.14	1.9	0.8	36.458	1/5/05	Ice: Soft 18-16
2-90-493-03	GRCC125	607	49-3	0.222	Cracks on front and back	208.24	208.53	9.43	1.9	0.8	37.615	1/6/05	Ice: Soft 18-23
2-90-643-09	GRCC151	612	64-3 (retest)	0.228	Front side cracks, back coat loss	208.34	208.71	8.77				1/14/05	Ice: JSC no ID

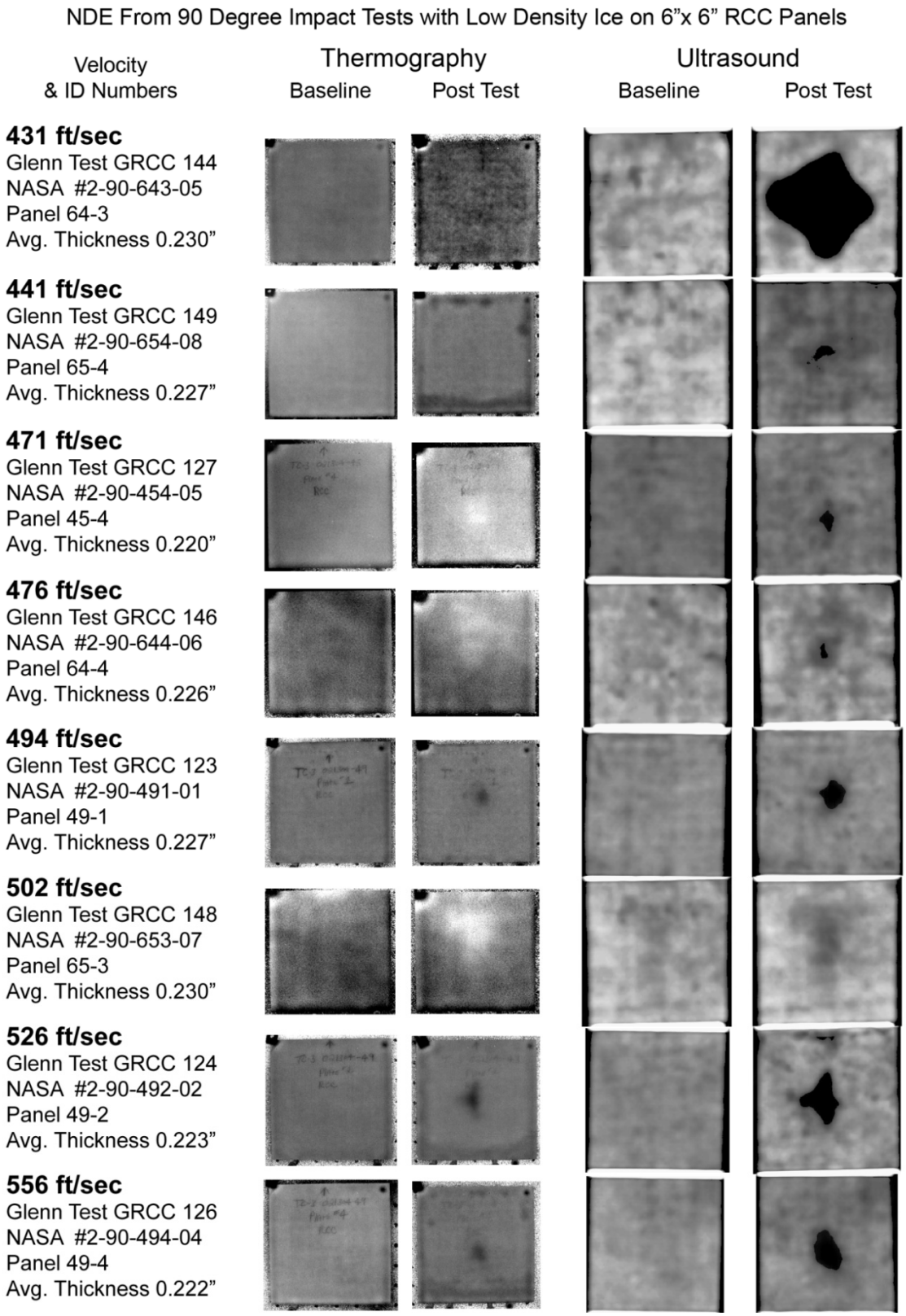

Figure E1–1.—Pulse thermography and ultrasound post impact pretest and posttest images of reinforced carbon-carbon 6- by 6-in. flat panels impacted with low-density ice cylinders (nominally 0.80 in. in diameter by 1.90 in.) at a 90° angle.

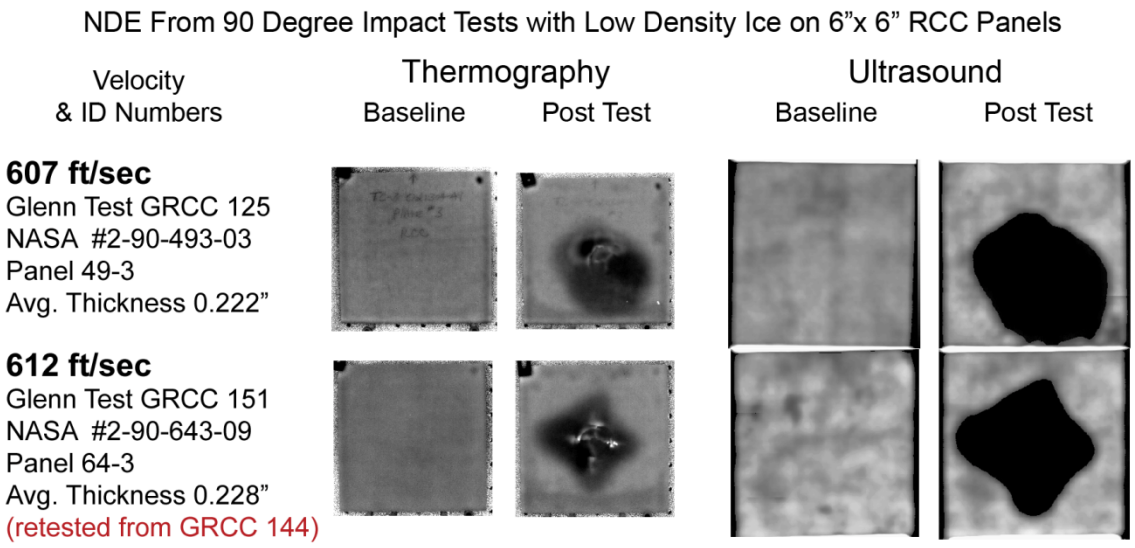

Figure E1–2.—Pulse thermography and ultrasound post impact pretest and posttest images of reinforced carbon-carbon 6- by 6-in. flat panels impacted with low-density ice cylinders (nominally 0.80 in. in diameter by 1.90 in.) at a 90° angle.

Aramis Displacement Contours from 90 Degree Impact Tests with Low Density Ice on 6”x 6” RCC Panels

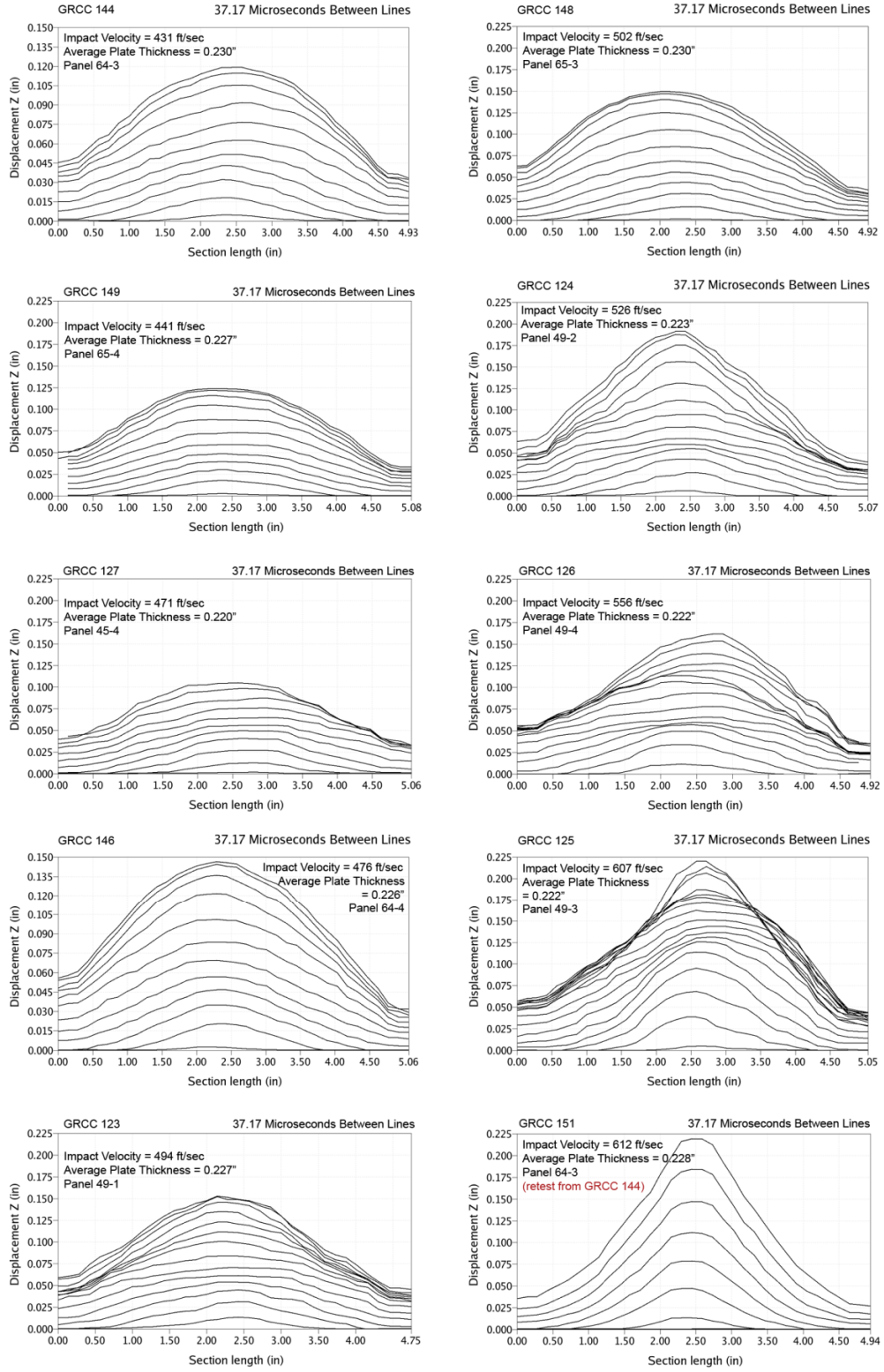

Figure E2–1.—ARAMIS out-of-plane deformation contours across centerline of 6- by 6-in. reinforced carbon-carbon flat panels measured at 37 μs increments undergoing impact with low-density ice cylinders (nominally 0.80 in. in diameter by 1.90 in.) at a 90° angle.

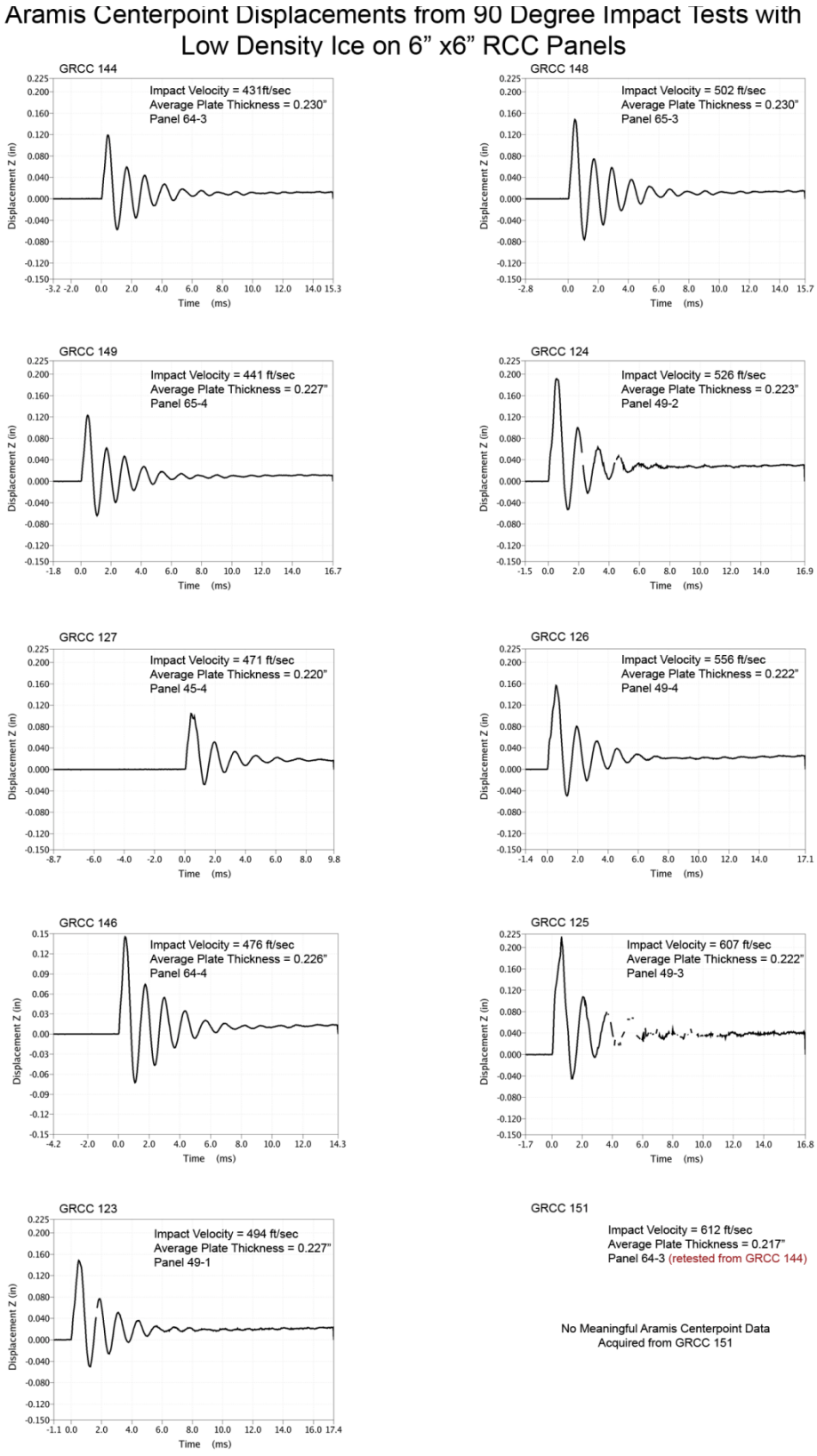

Figure E3–1.—ARAMIS centerpoint out-of-plane deformation vs. time of 6- by 6-in. reinforced carbon-carbon flat panels impacted with low-density ice cylinders (nominally 0.80 in. in diameter by 1.90 in.) at a 90° angle.

Aramis Maximum Displacement Fringe Plots from 90 Degree Impact Tests with Low Density Ice on 6” x 6” RCC Panels

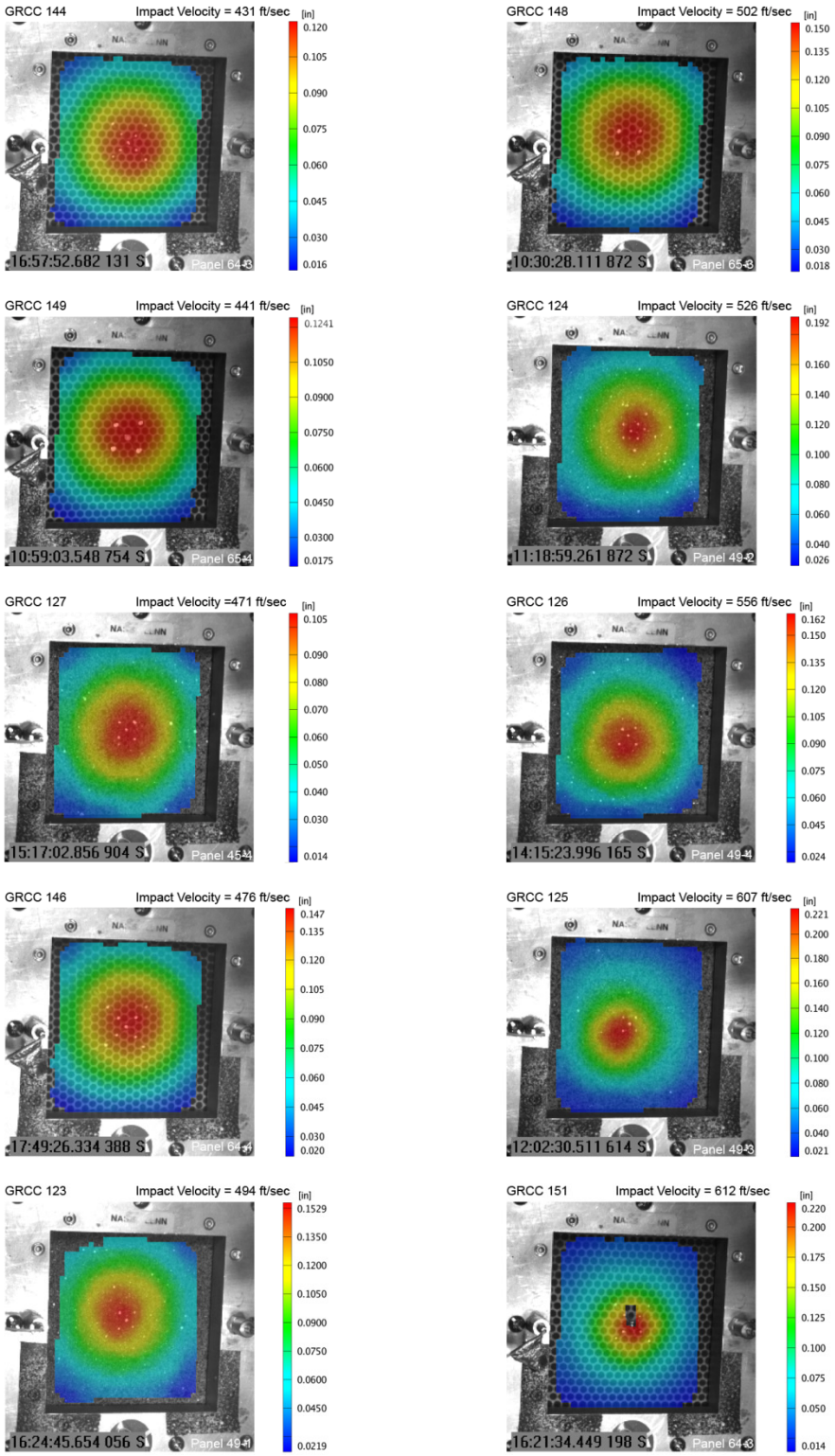

Figure E4–1.—ARAMIS color fringe plots depicting maximum deformation prior to material failure of 6- by 6-in. reinforced carbon-carbon flat panels as they undergo impact with low-density ice cylinders (nominally 0.80 in. in diameter by 1.90 in.) at a 90° angle.

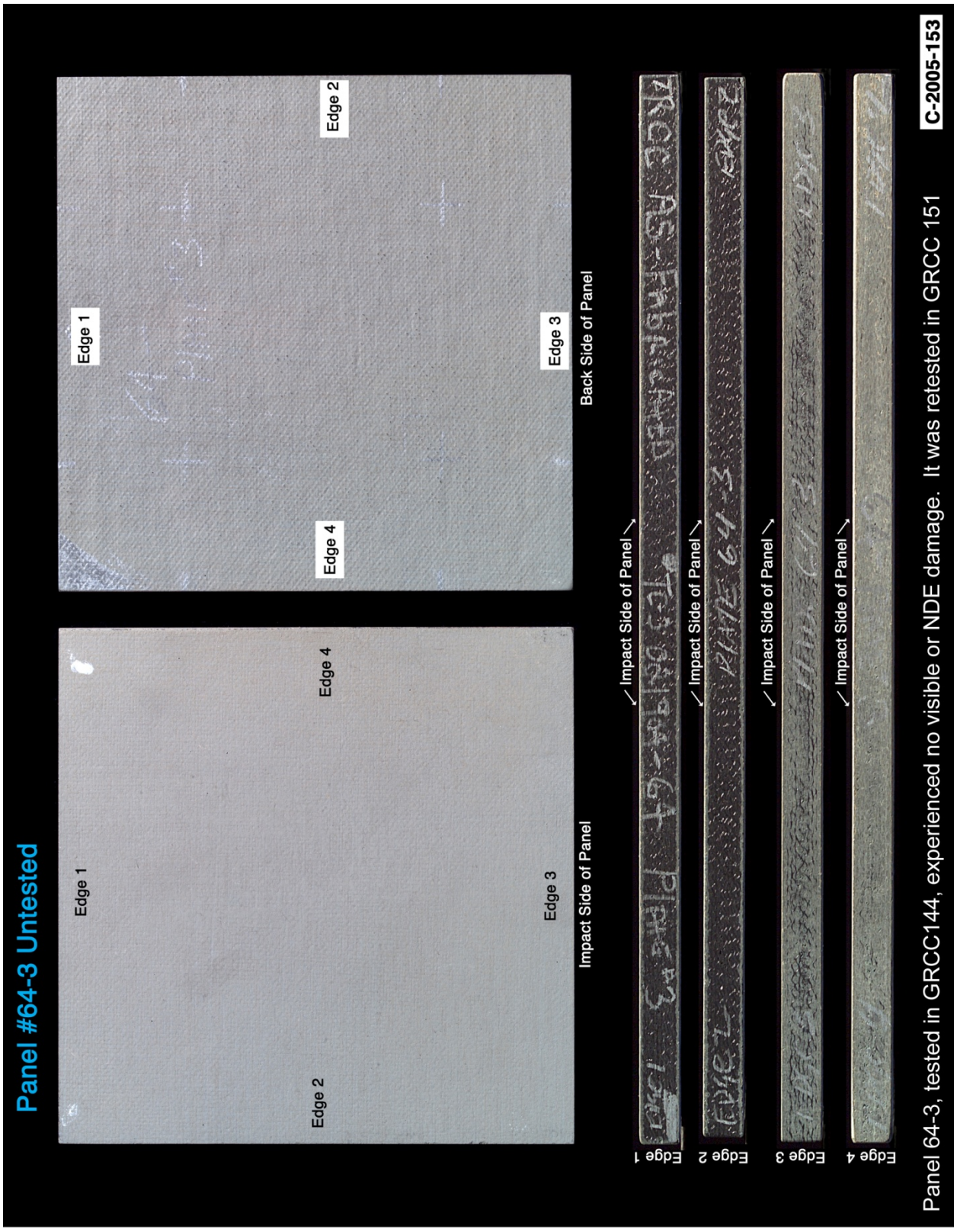

Figure E5–1.—Edges and faces of panel 64-3 at 431 ft/s with a low-density soft ice cylinder (nominally 0.80 in. in diameter by 1.90 in.) at 90° impact angle. Test GRCC 144.

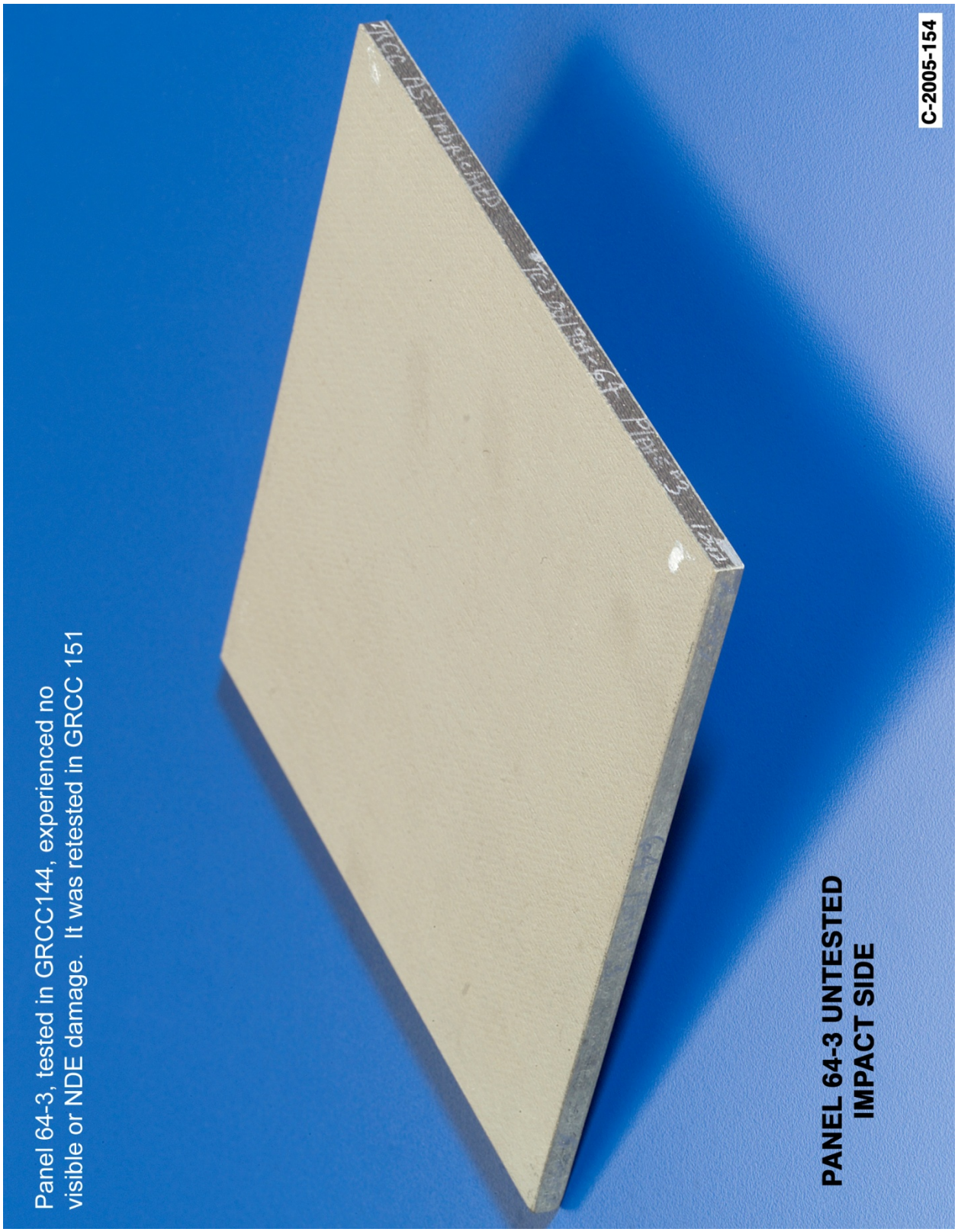

Figure E5–2.—Front (impact side) of panel 64-3 at 431 ft/s with a low-density soft ice cylinder (nominally 0.80 in. in diameter by 1.90 in.) at 90° impact angle. Test GRCC 144.

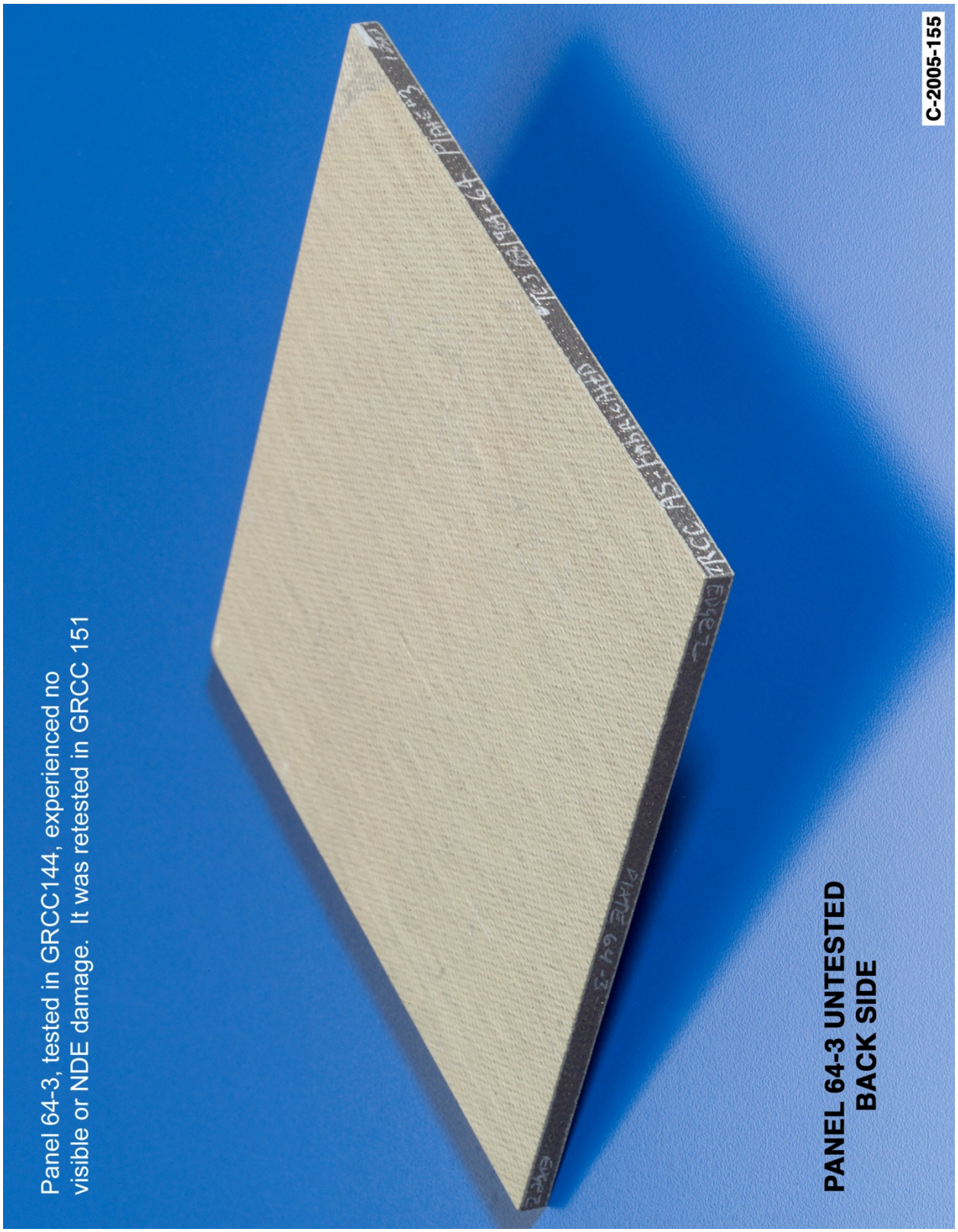

Figure E5–3.—Back face of panel 64-3 at 431 ft/s with a low-density soft ice cylinder (nominally 0.80 in. in diameter by 1.90 in.) at 90° impact angle. Test GRCC 144.

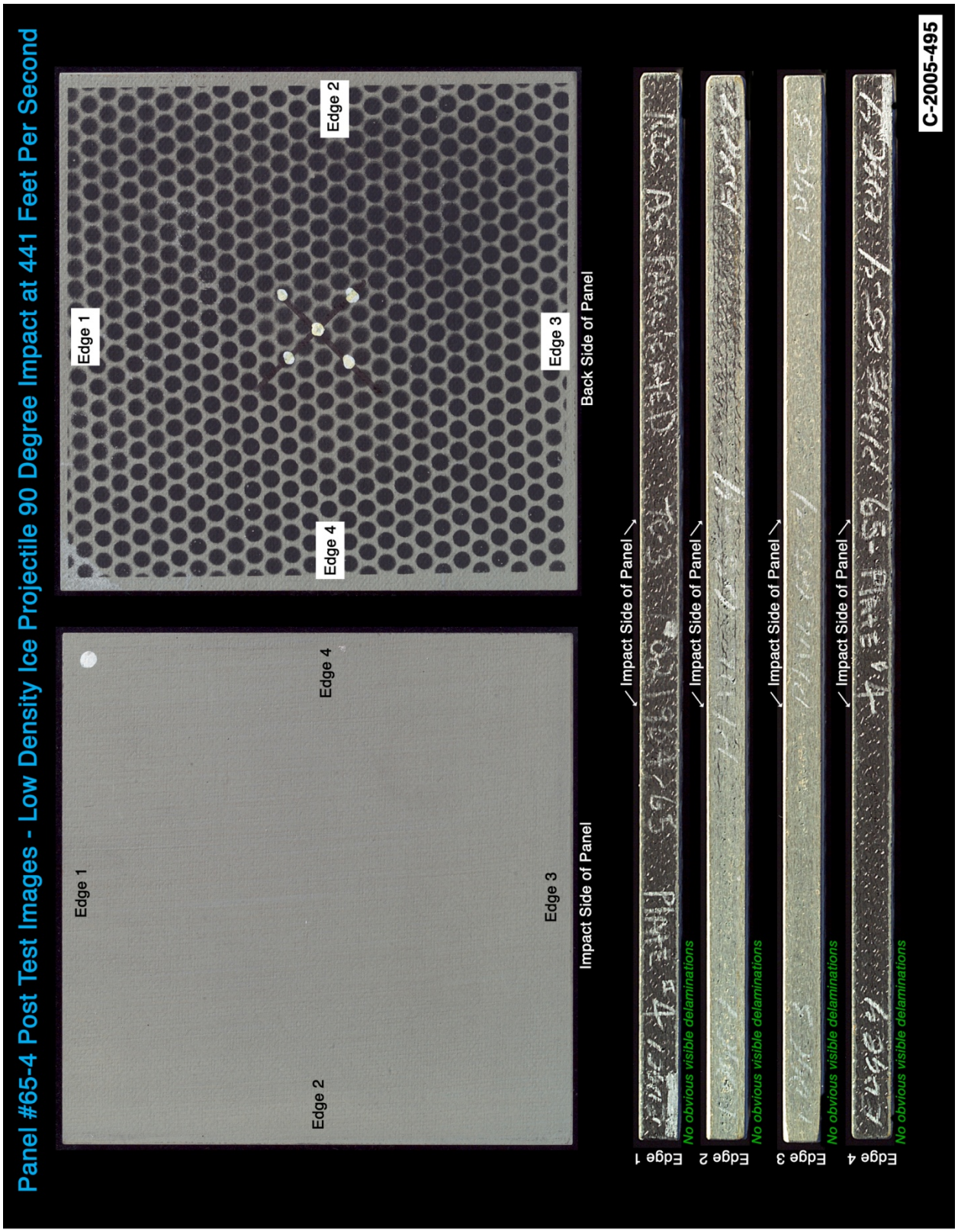

Figure E6–1.—Edges and faces of panel 65-4 at 441 ft/s with a low-density soft ice cylinder (nominally 0.8 in. in diameter by 1.90 in.) at 90° impact. Test GRCC 149.

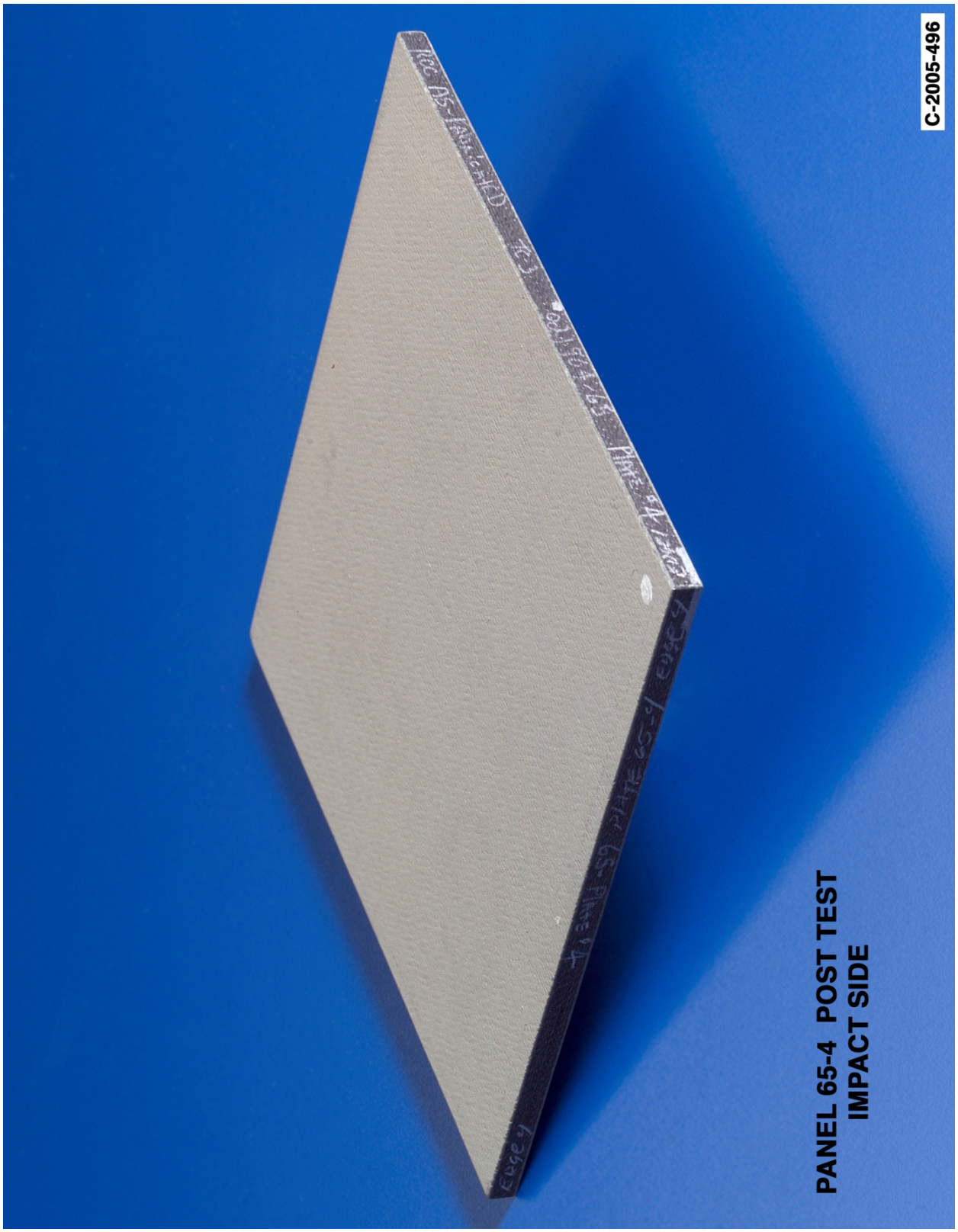

Figure E6–2.—Front (impact side) of panel 65-4 at 441 ft/s with a low-density soft ice cylinder (nominally 0.80 in. in diameter by 1.90 in.) at 90° impact angle. Test GRCC 149.

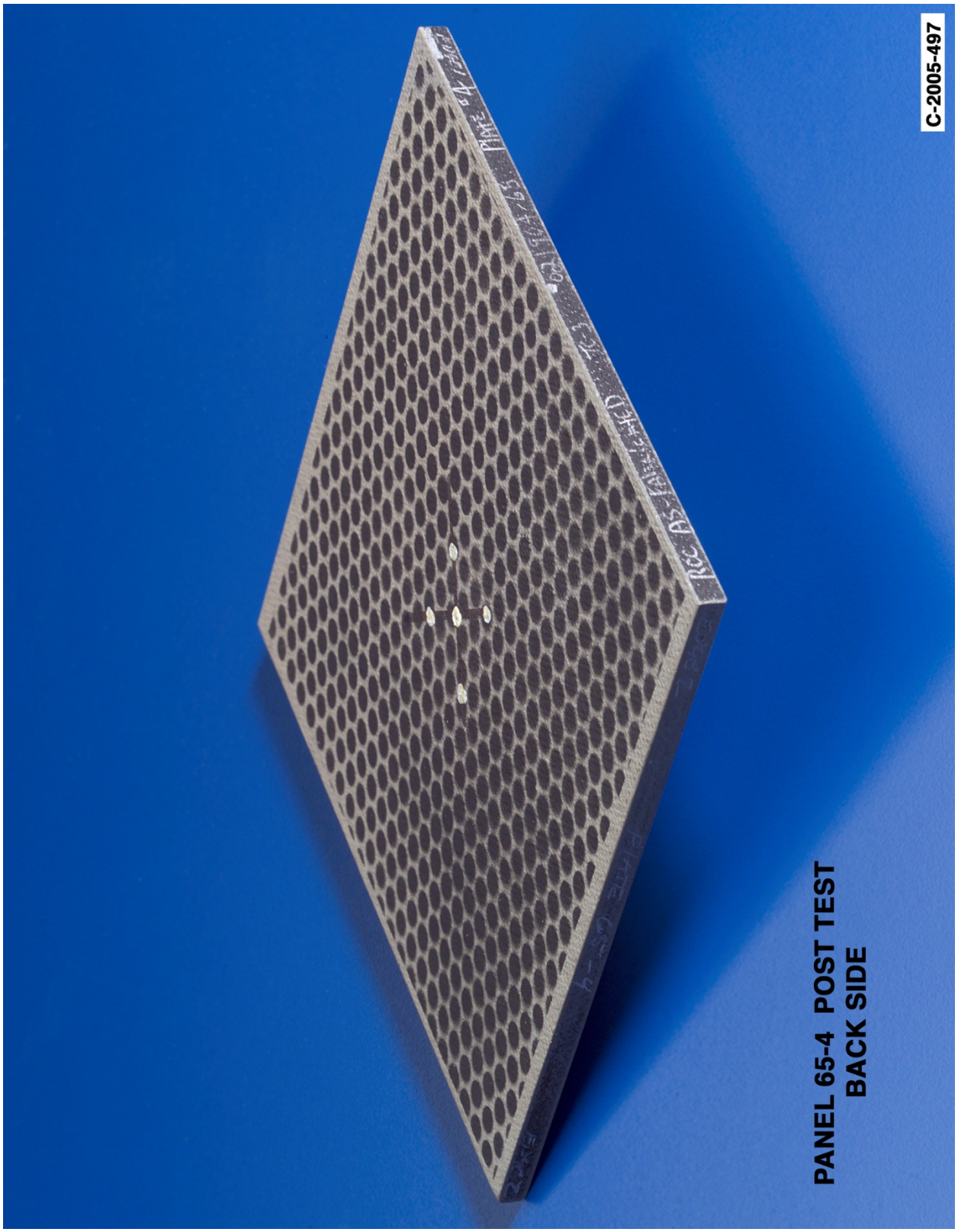

Figure E6–3.—Back face of panel 65-4 at 441 ft/s with a low-density soft ice cylinder (nominally 0.80 in. in diameter by 1.90 in.) at 90° impact angle. Test GRCC 149.

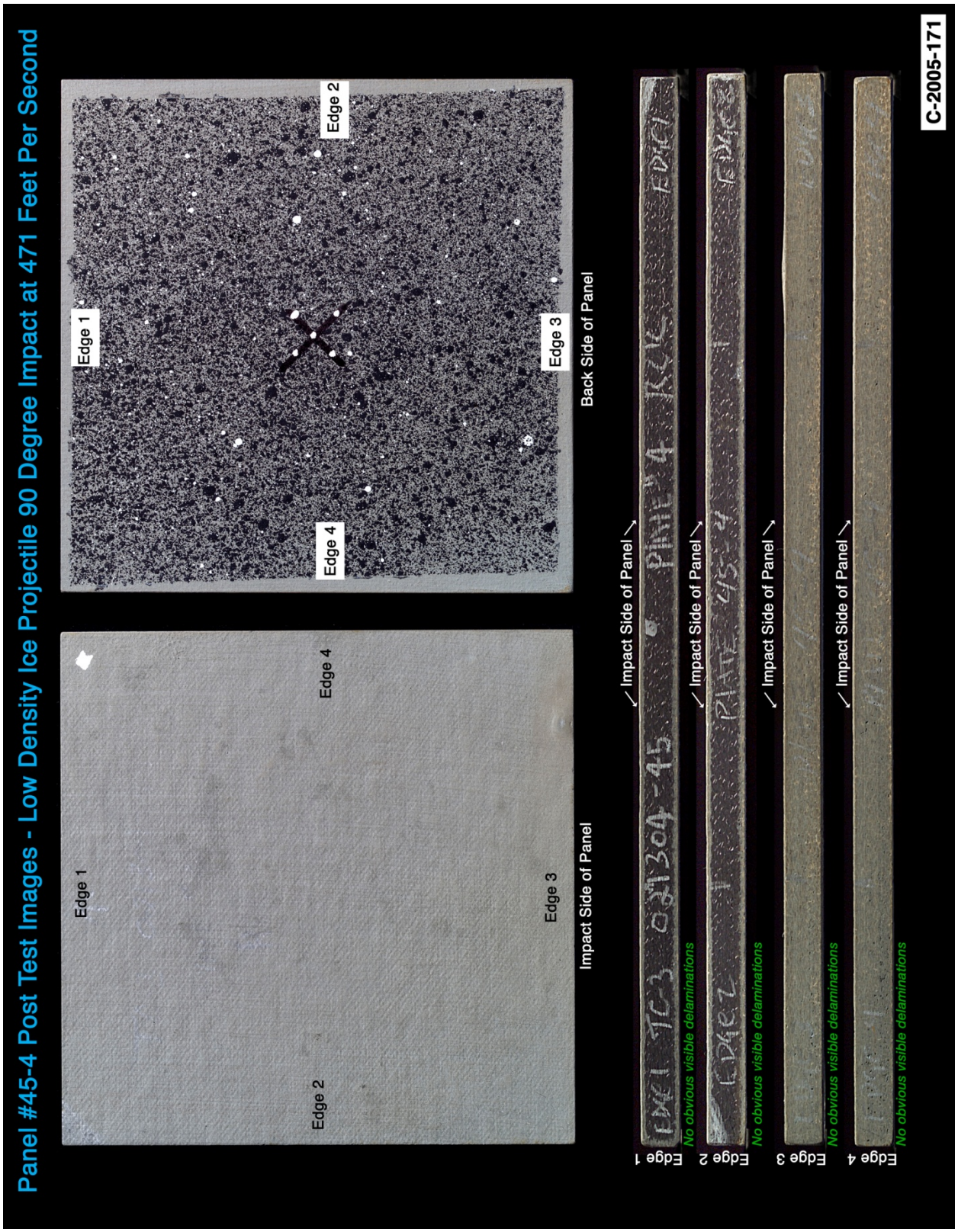

Figure E7–1.—Edges and faces of panel 45-4 at 471 ft/s with a low-density soft ice cylinder (nominally 0.8 in. in diameter by 1.90 in.) at 90° impact. Test GRCC 127.

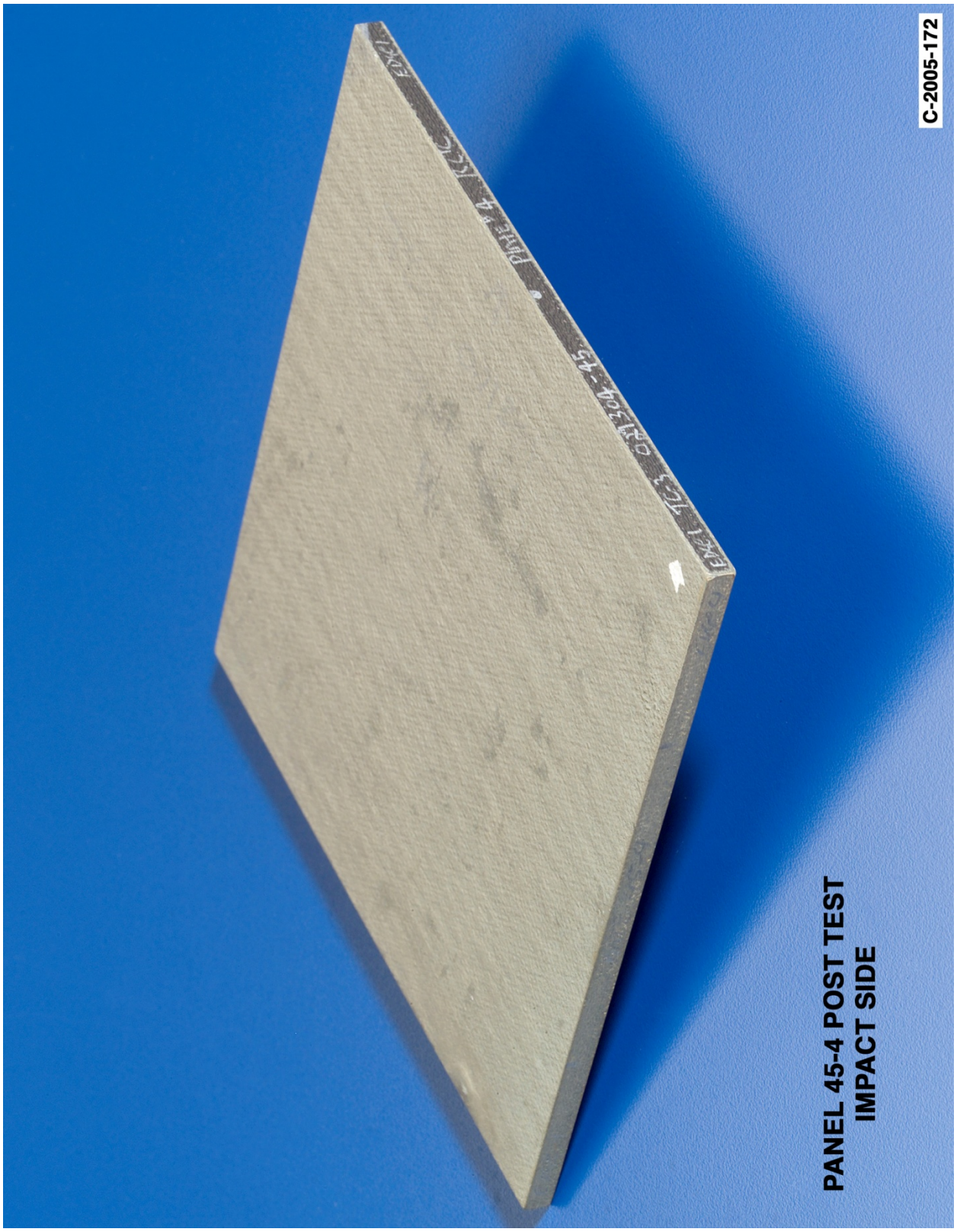

Figure E7–2.—Front (impact side) of panel 45-4 at 471 ft/s with a low-density soft ice cylinder (nominally 0.80 in. in diameter by 1.90 in.) at 90° impact angle. Test GRCC 127.

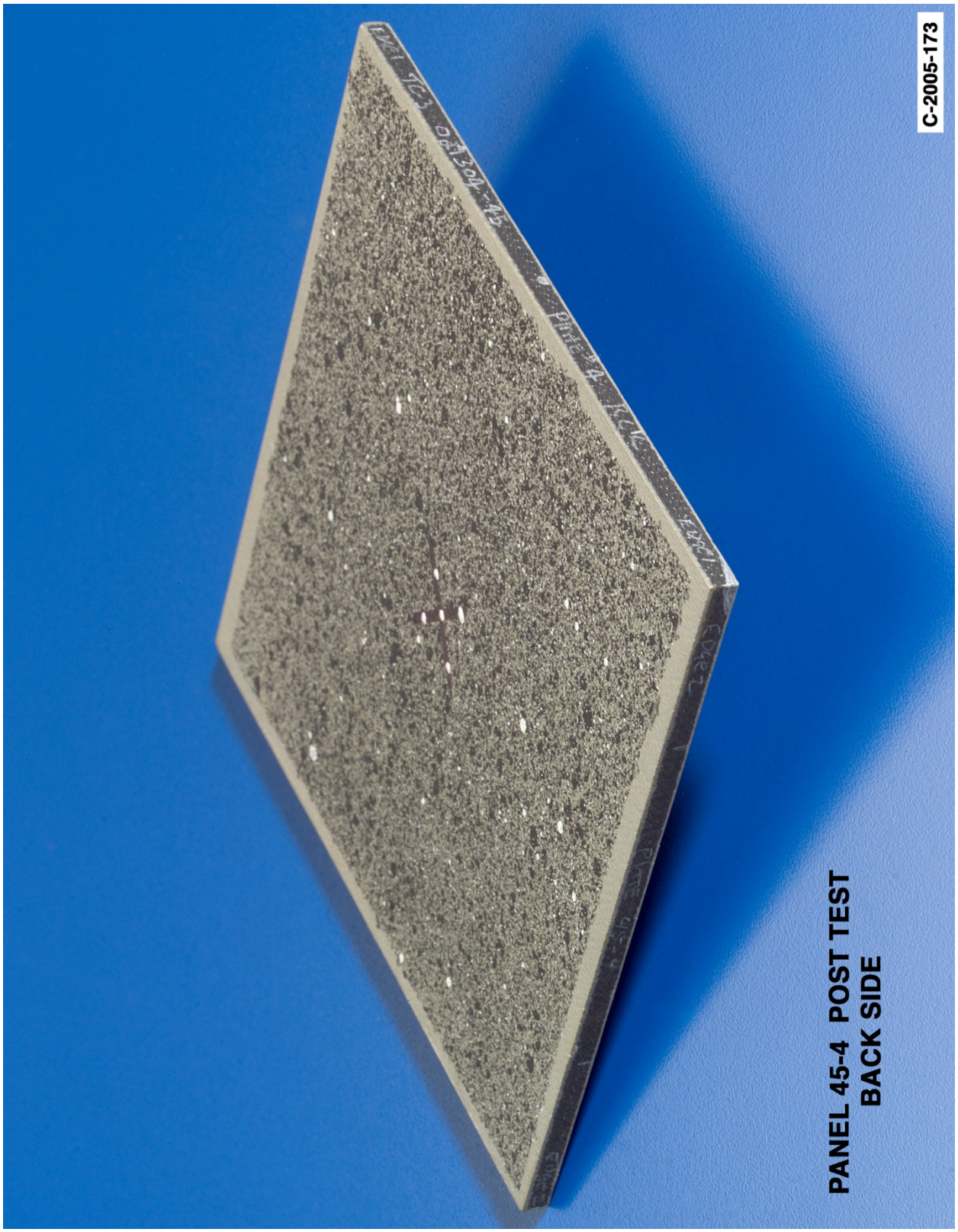

Figure E7–3.—Back face of panel 45-4 at 471 ft/s with a low-density soft ice cylinder (nominally 0.80 in. in diameter by 1.90 in.) at 90° impact angle. Test GRCC 127.

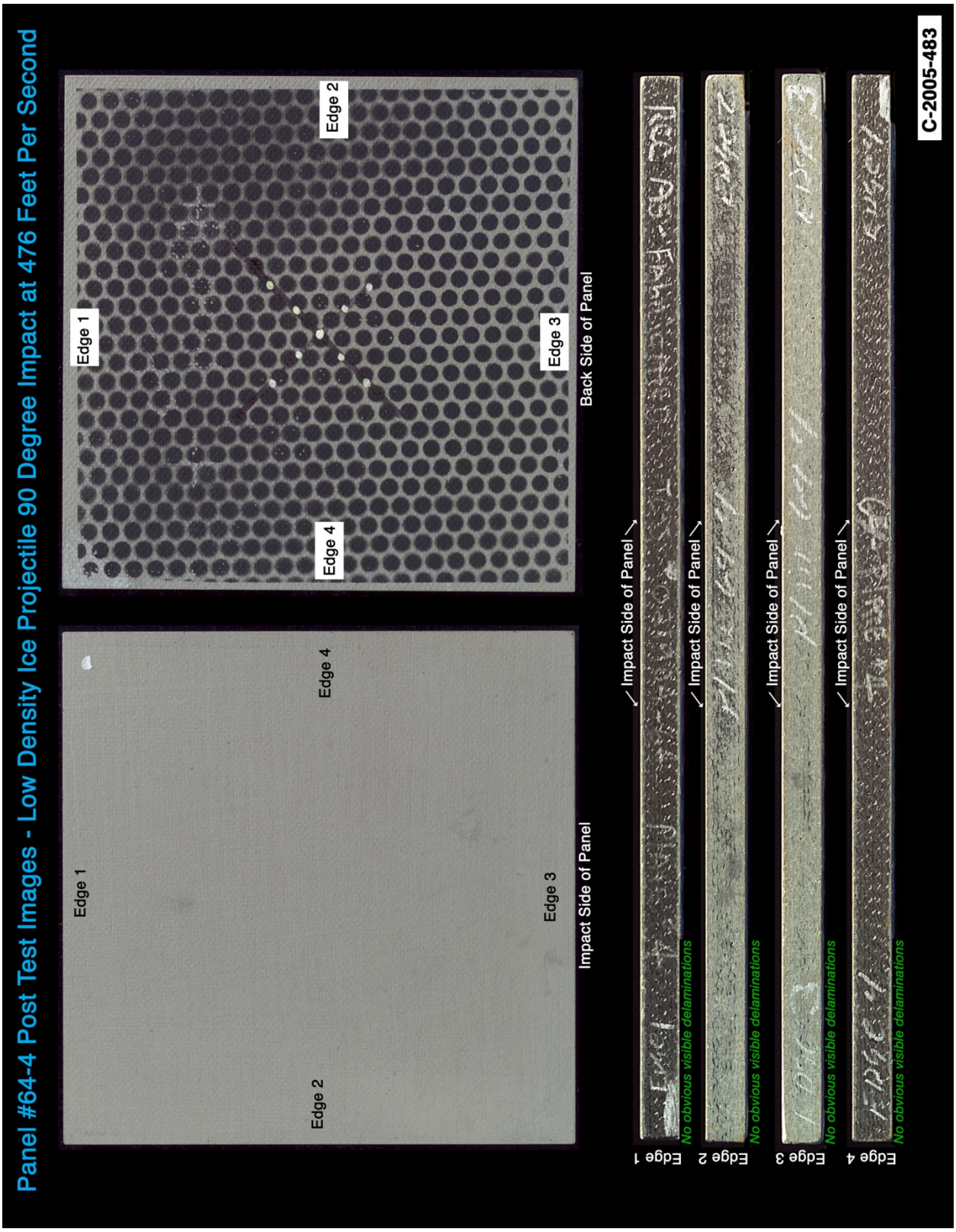

Figure E8–1.—Edges and faces of panel 64-4 at 476 ft/s with a low-density soft ice cylinder (nominally 0.8 in. in diameter by 1.90 in.) at 90° impact. Test GRCC 146.

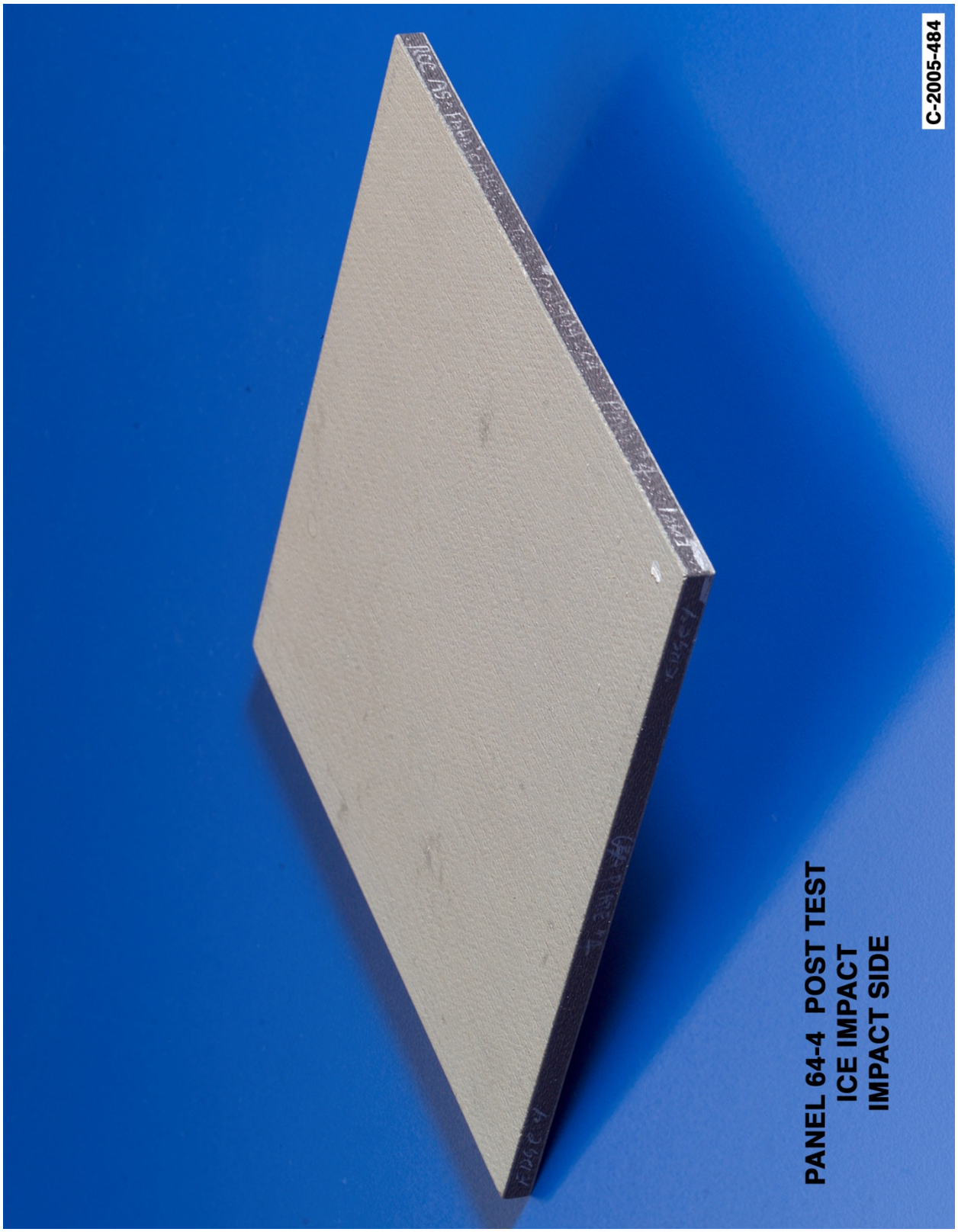

Figure E8–2.—Front (impact side) of panel 64-4 at 476 ft/s with a low-density soft ice cylinder (nominally 0.80 in. in diameter by 1.90 in.) at 90° impact angle. Test GRCC 146.

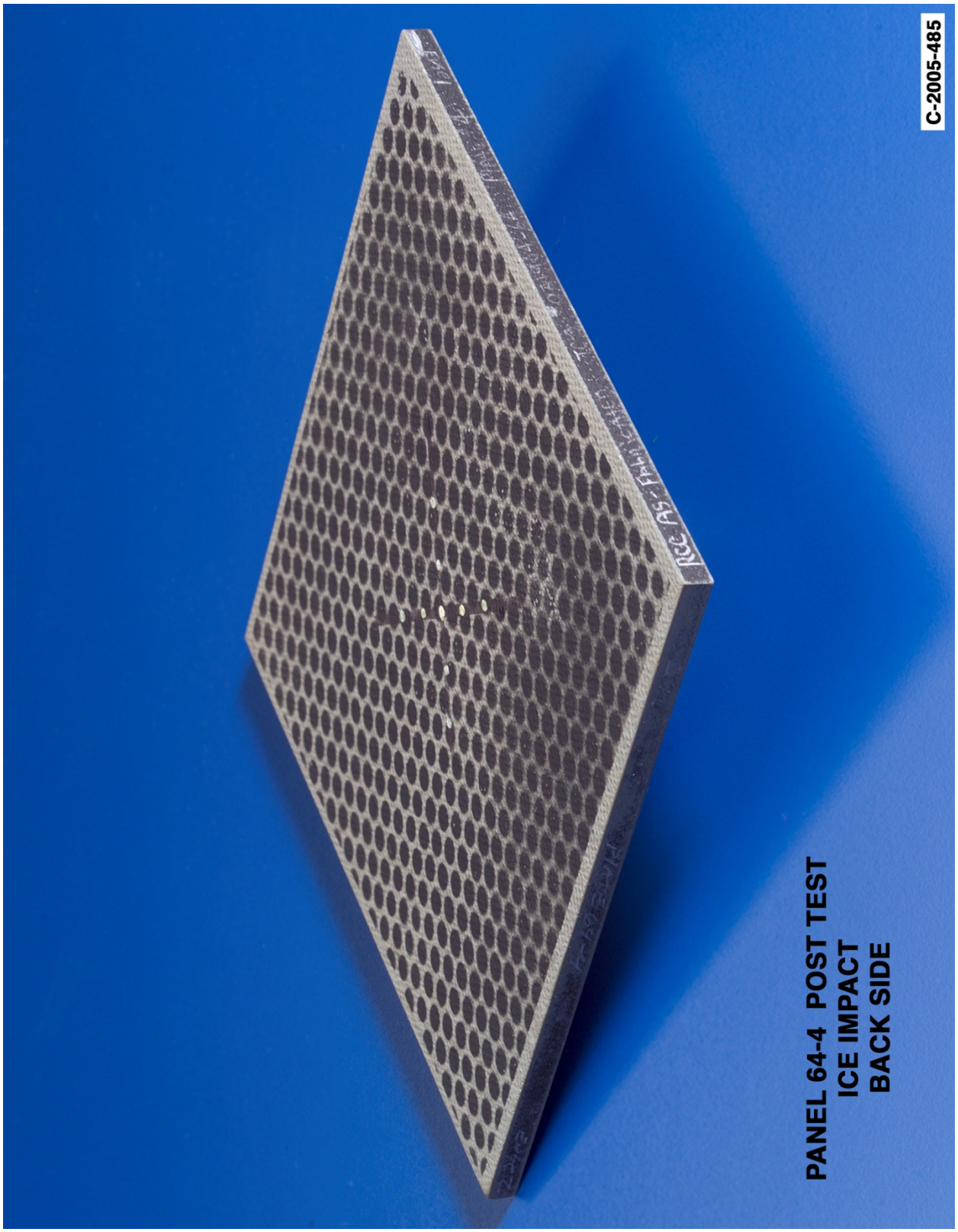

Figure E8–3.—Back face of panel 64-4 at 476 ft/s with a low-density soft ice cylinder (nominally 0.80 in. in diameter by 1.90 in.) at 90° impact angle. Test GRCC 146.

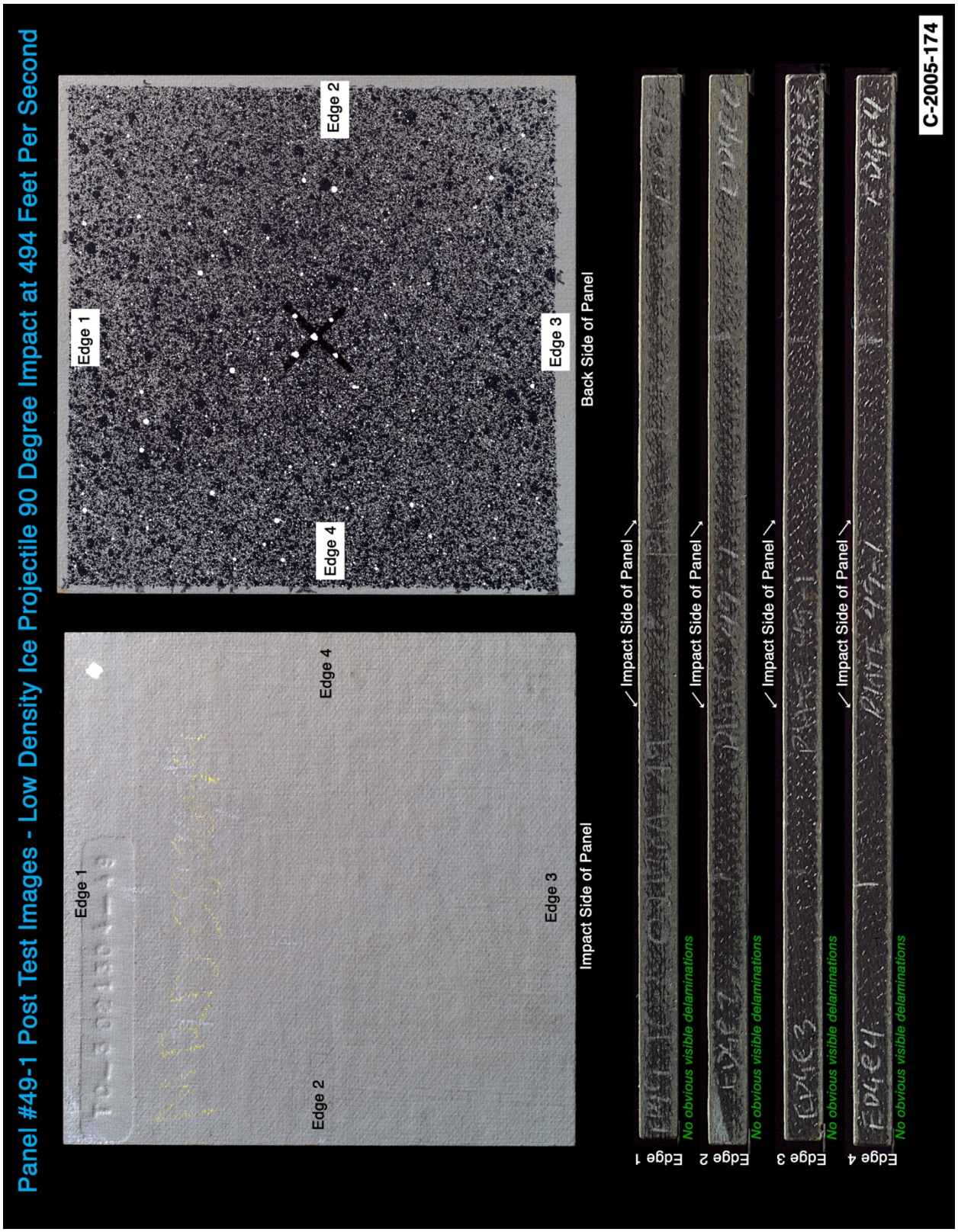

Figure E9–1.—Edges and faces of panel 49-1 at 494 ft/s with a low-density soft ice cylinder (nominally 0.8 in. in diameter by 1.90 in.) at 90° impact. Test GRCC 123.

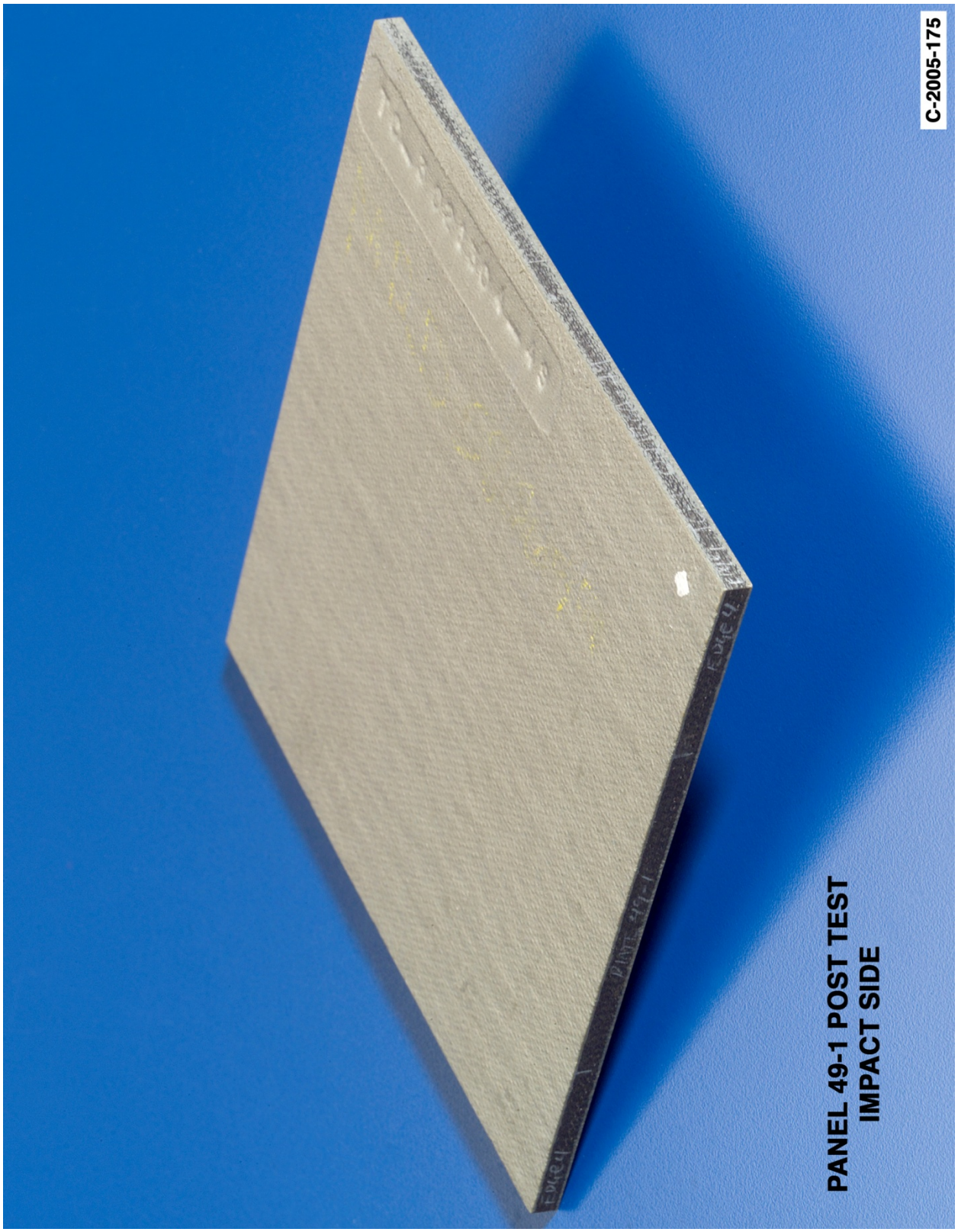

Figure E9–2.—Front (impact side) of panel 49-1 at 494 ft/s with a low-density soft ice cylinder (nominally 0.80 in. in diameter by 1.90 in.) at 90° impact angle. Test GRCC 123.

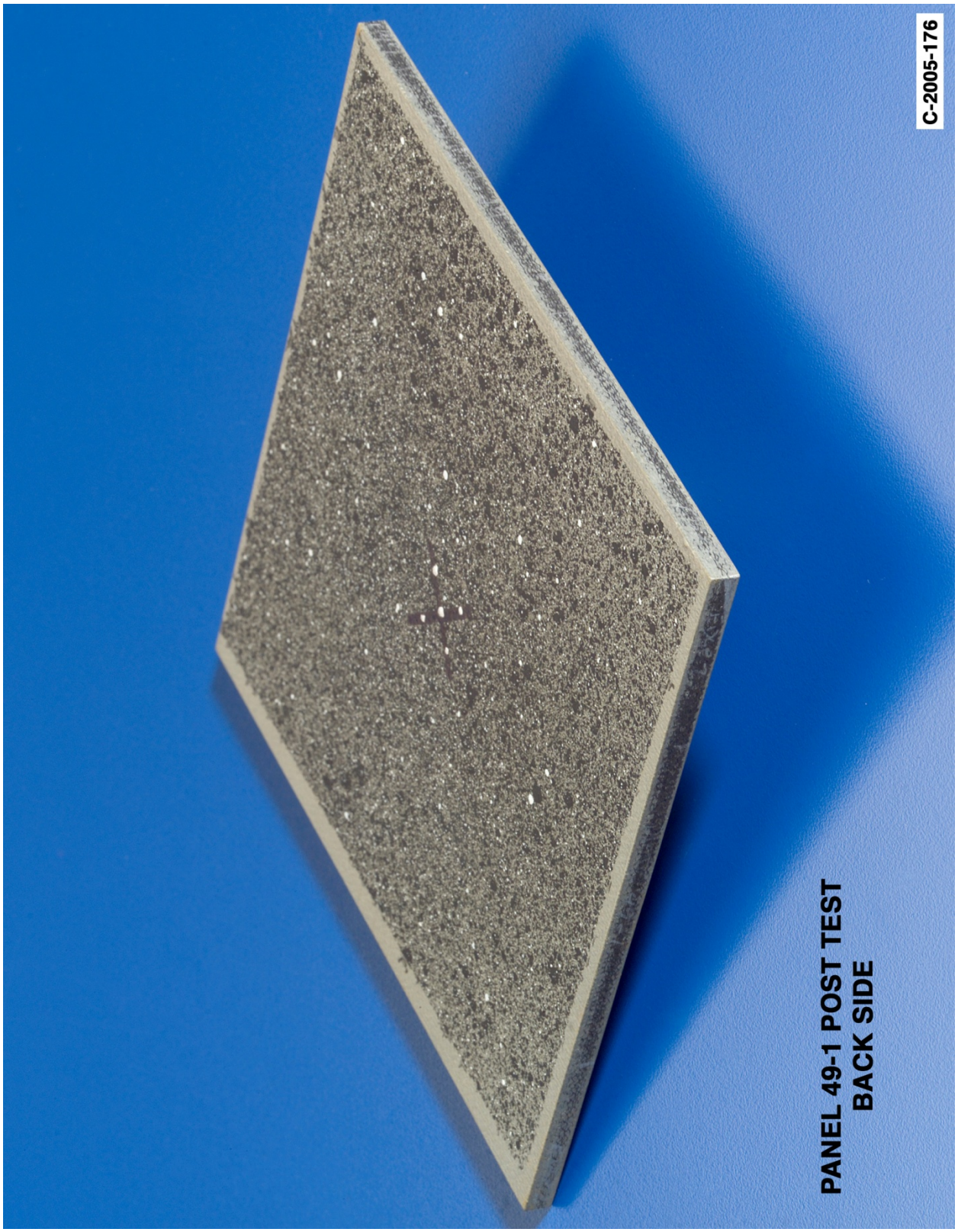

Figure E9–3.—Back face of panel 49-1 at 494 ft/s with a low-density soft ice cylinder (nominally 0.80 in. in diameter by 1.90 in.) at 90° impact angle. Test GRCC 123.

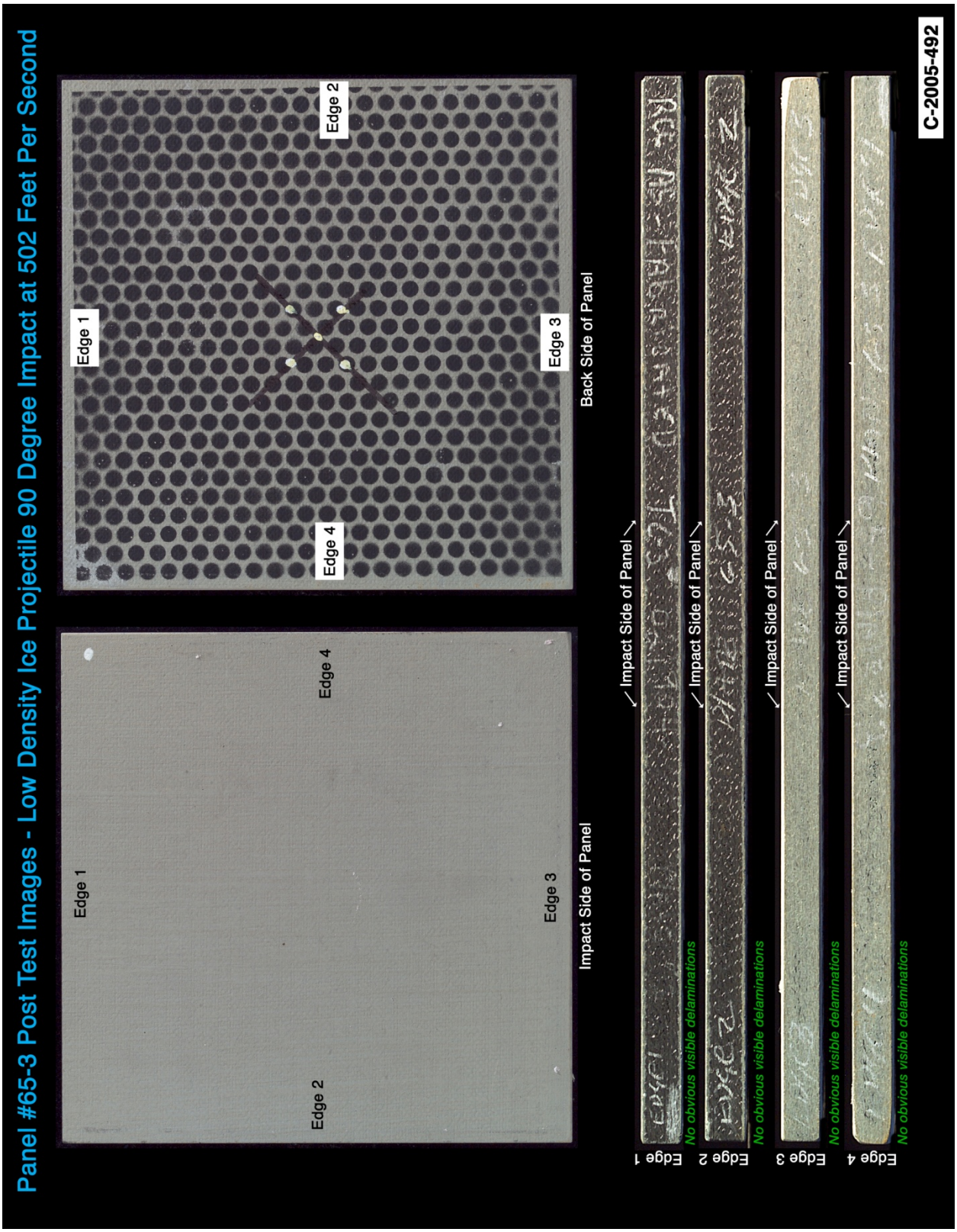

Figure E10–1.—Edges and faces of panel 65-3 at 502 ft/s with a low-density soft ice cylinder (nominally 0.8 in. in diameter by 1.90 in.) at 90° impact. Test GRCC 148.

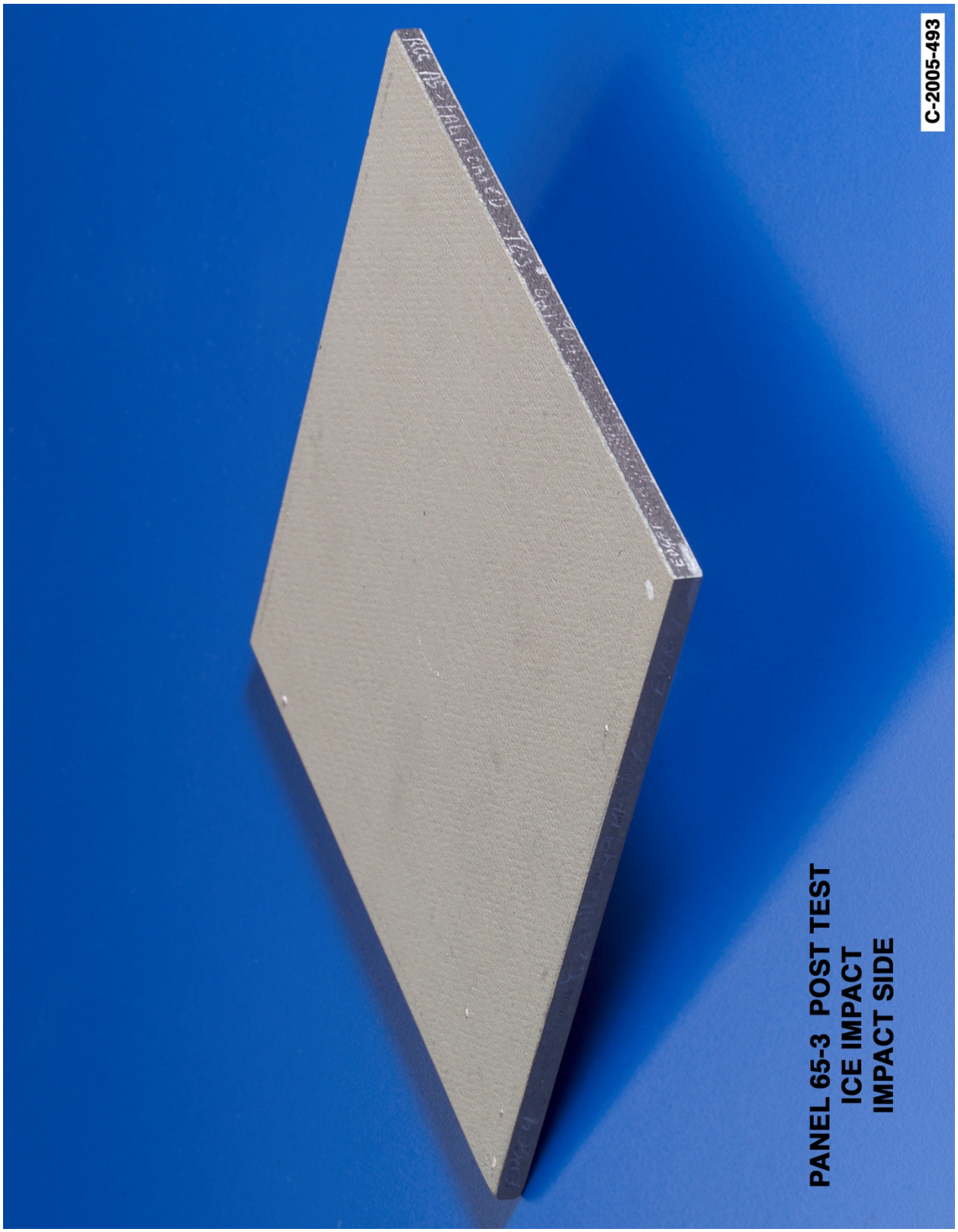

Figure E10–2.—Front (impact side) of panel 65-3 at 502 ft/s with a low-density soft ice cylinder (nominally 0.80 in. in diameter by 1.90 in.) at 90° impact angle. Test GRCC 148.

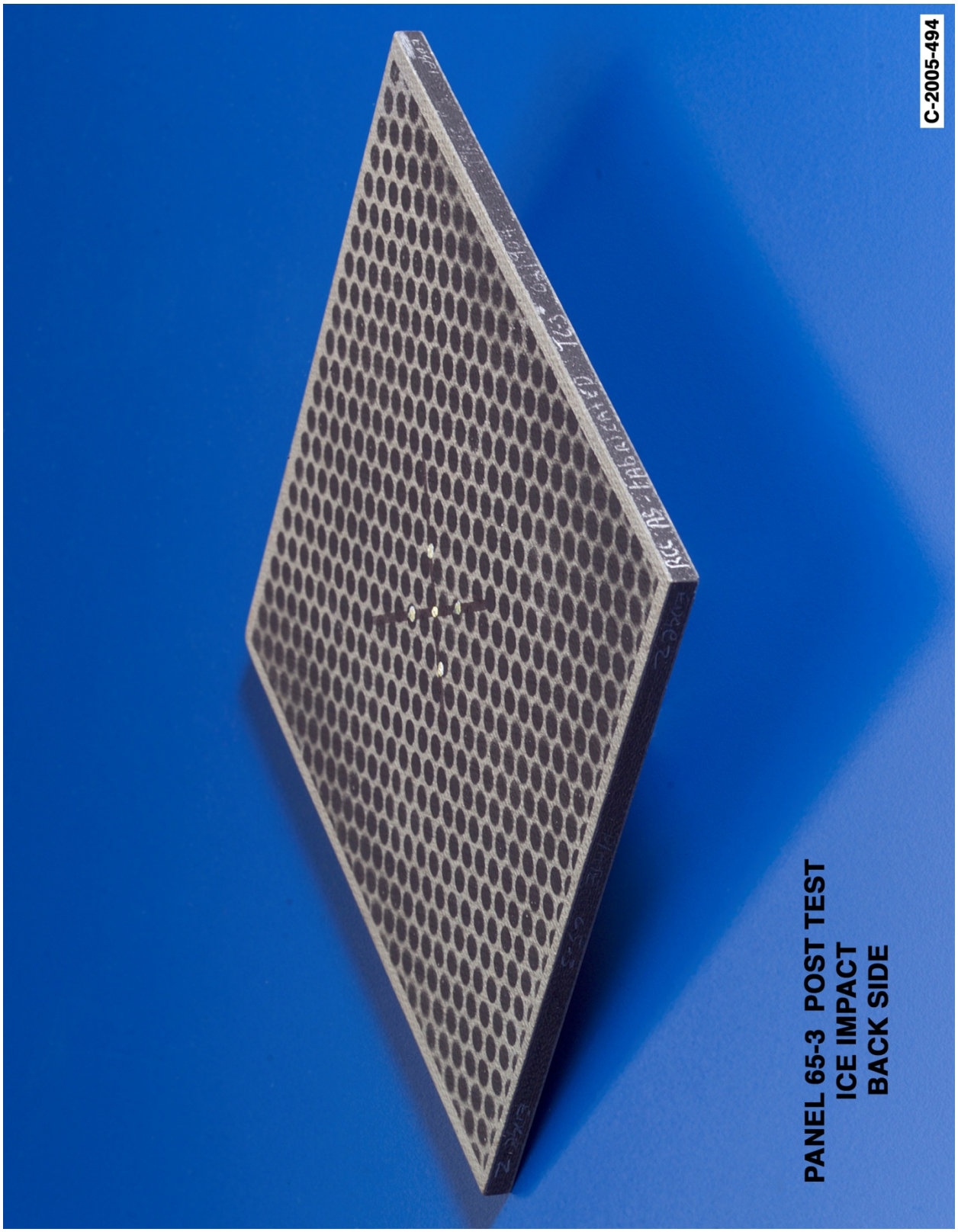

Figure E10–3.—Back face of panel 65-3 at 502 ft/s with a low-density soft ice cylinder (nominally 0.80 in. in diameter by 1.90 in.) at 90° impact angle. Test GRCC 148.

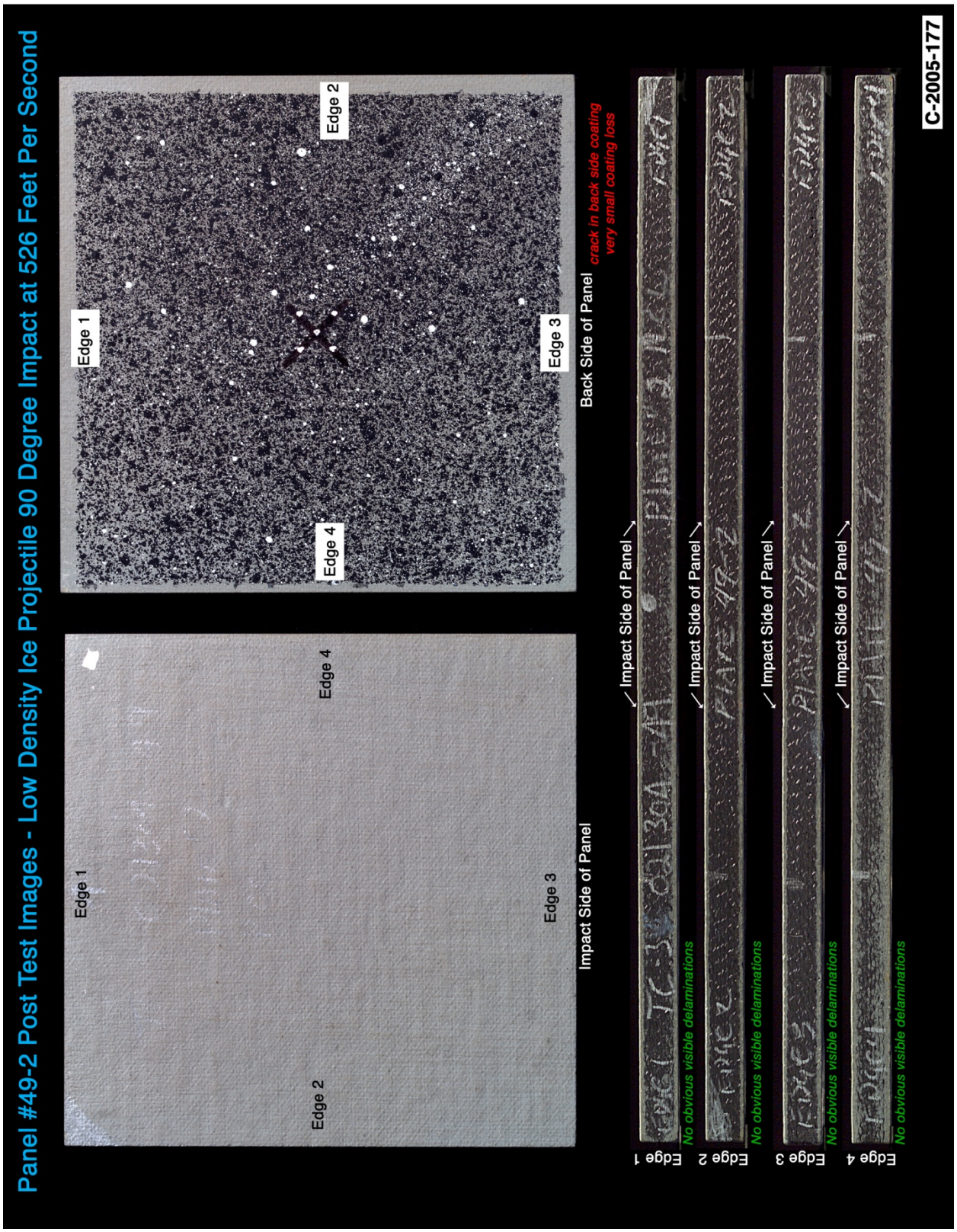

Figure E11–1.—Edges and faces of panel 49-2 at 526 ft/s with a low-density soft ice cylinder (nominally 0.8 in. in diameter by 1.90 in.) at 90° impact. Test GRCC 124.

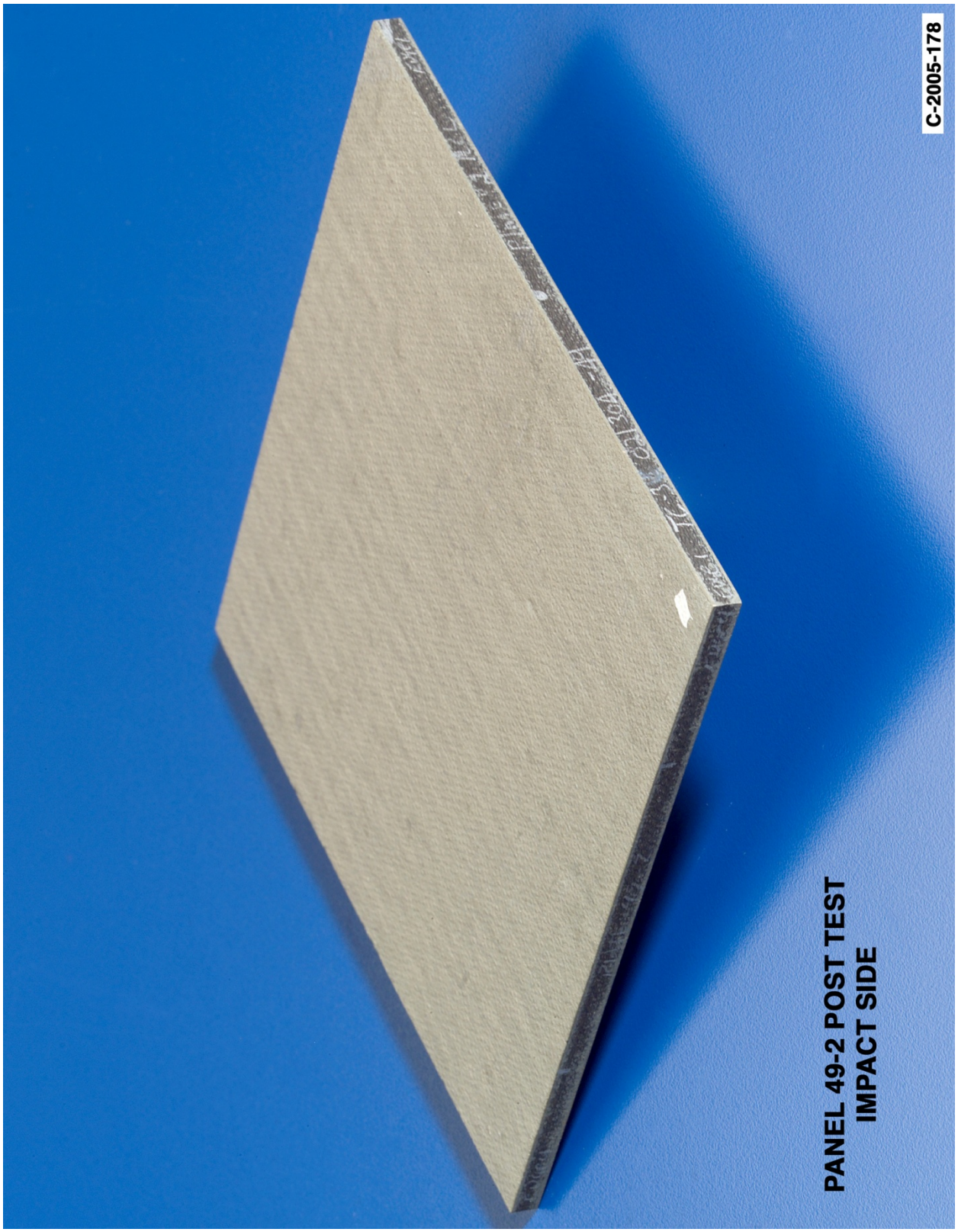

Figure E11–2.—Front (impact side) of panel 49-2 at 526 ft/s with a low-density soft ice cylinder (nominally 0.80 in. in diameter by 1.90 in.) at 90° impact angle. Test GRCC 124.

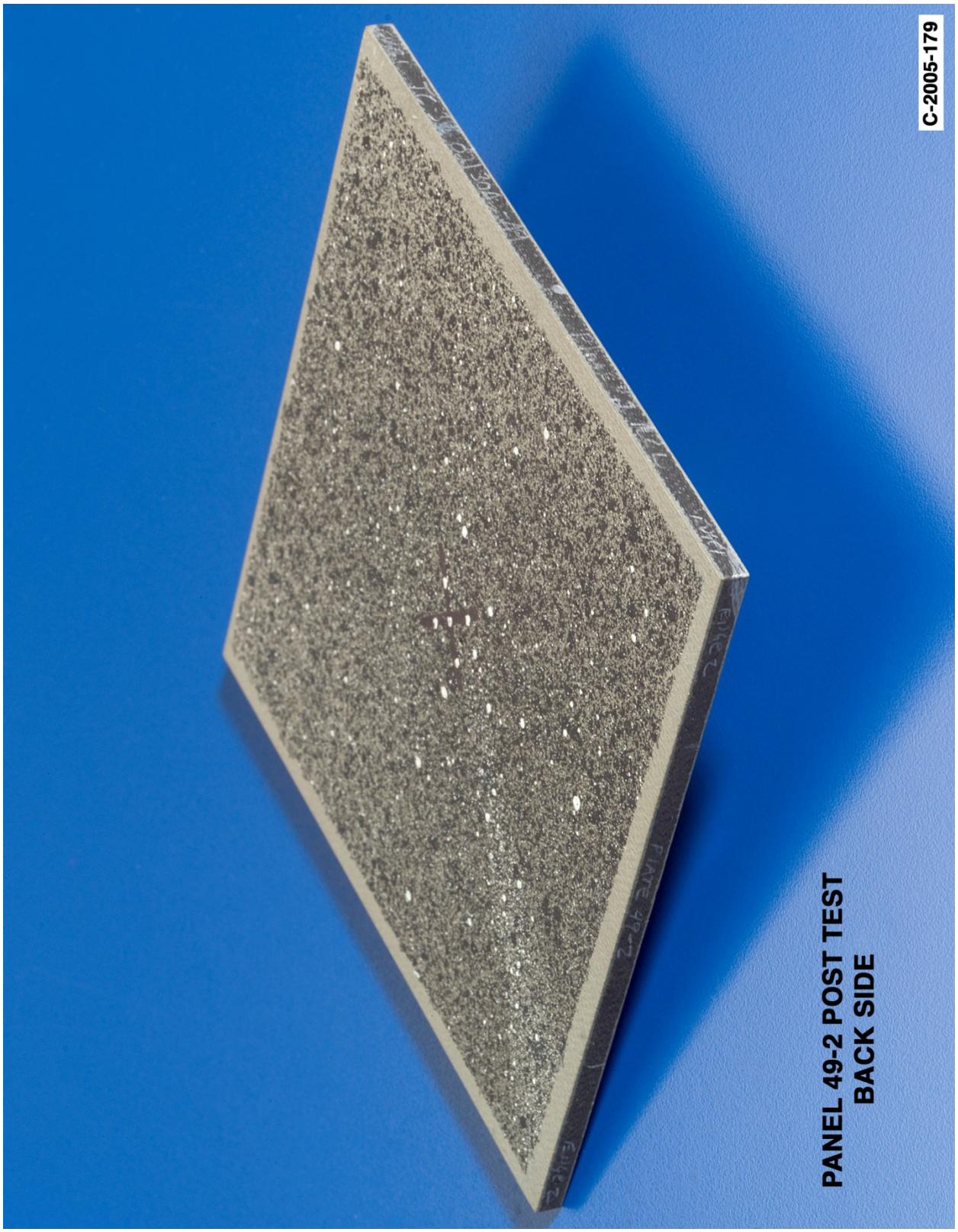

Figure E11–3.—Back face of panel 49-2 at 526 ft/s with a low-density soft ice cylinder (nominally 0.80 in. in diameter by 1.90 in.) at 90° impact angle. Test GRCC 124.

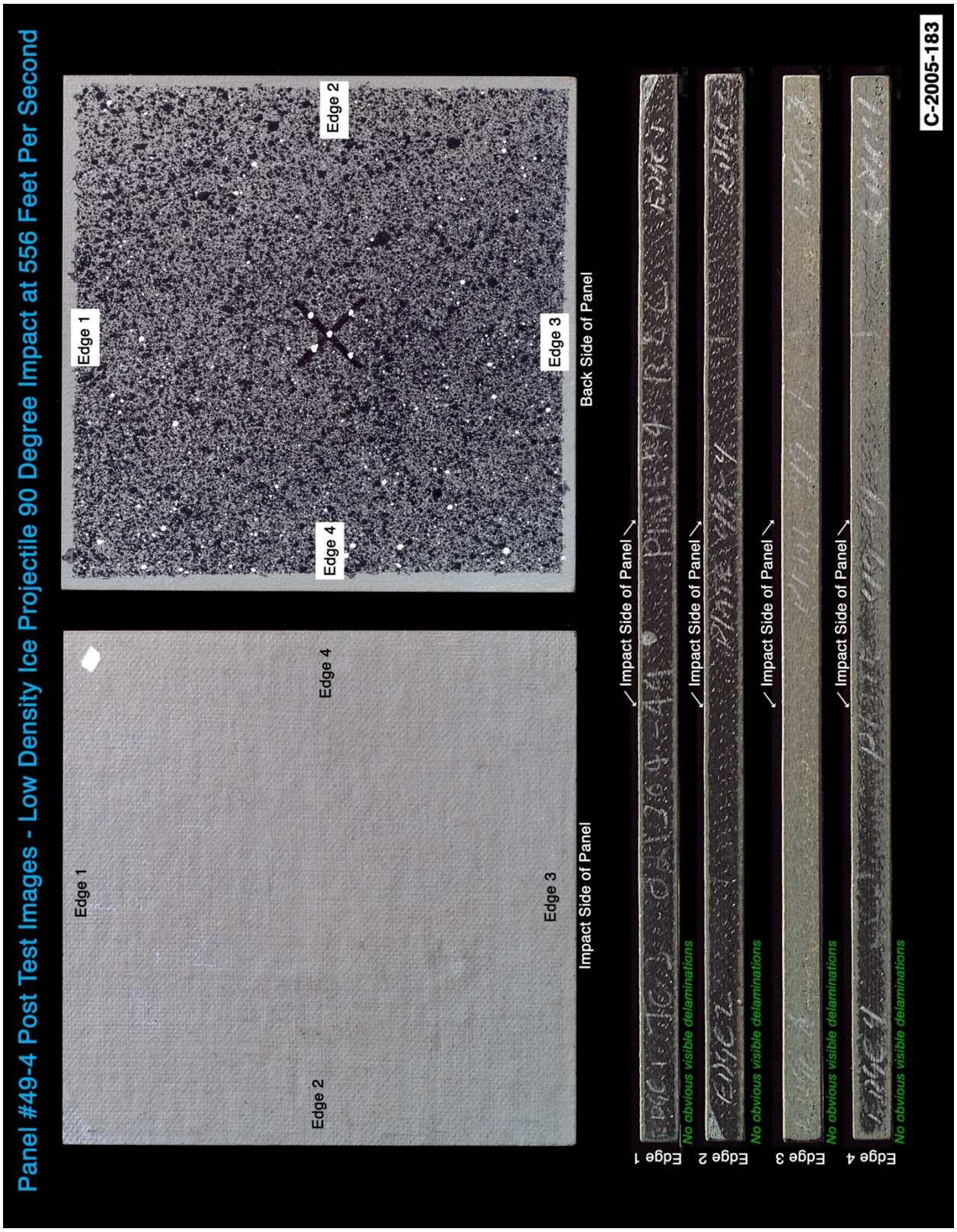

Figure E12–1.—Edges and faces of panel 49-4 at 556 ft/s with a low-density soft ice cylinder (nominally 0.8 in. in diameter by 1.90 in.) at 90° impact. Test GRCC 126.

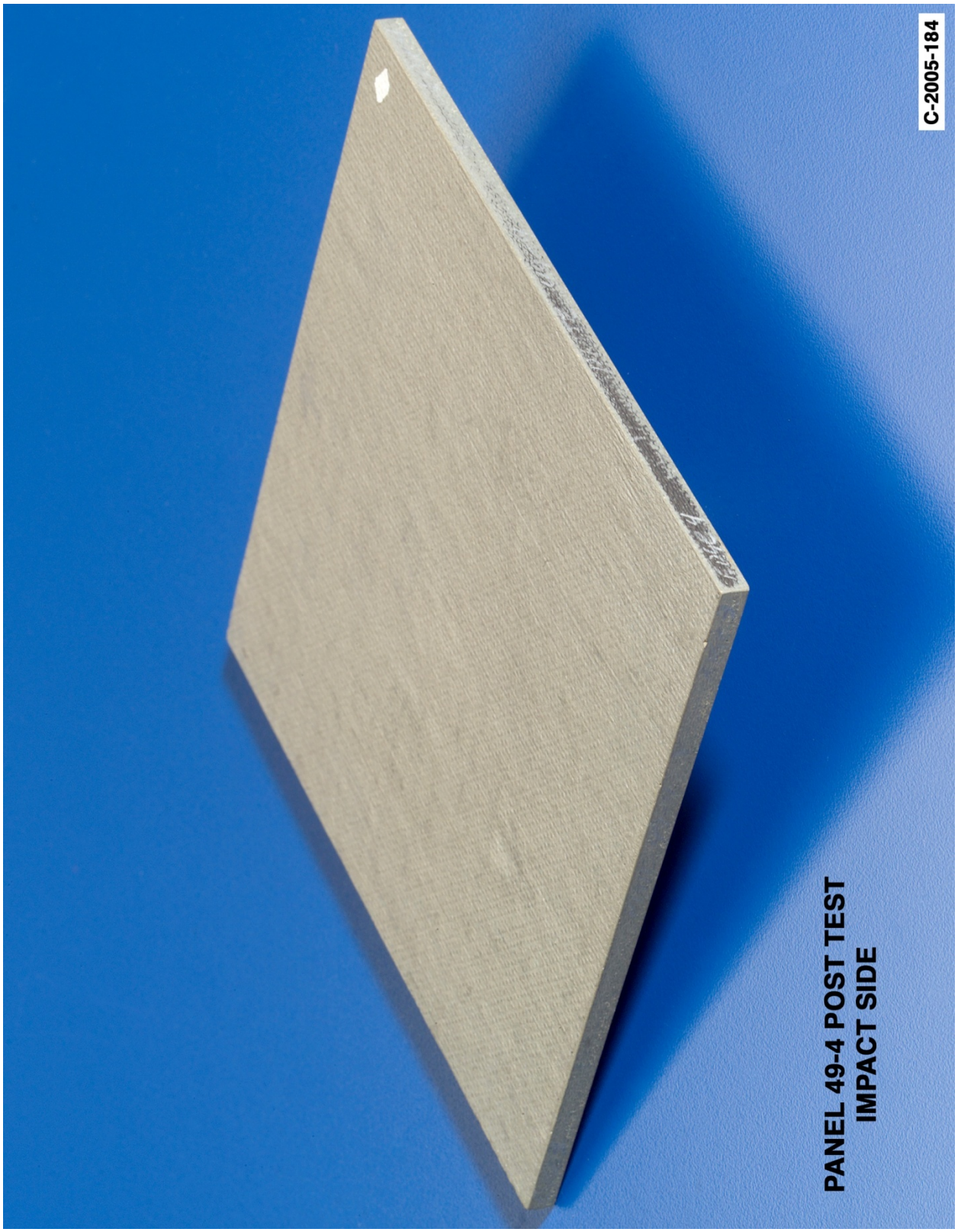

Figure E12–2.—Front (impact side) of panel 49-4 at 556 ft/s with a low-density soft ice cylinder (nominally 0.80 in. in diameter by 1.90 in.) at 90° impact angle. Test GRCC 126.

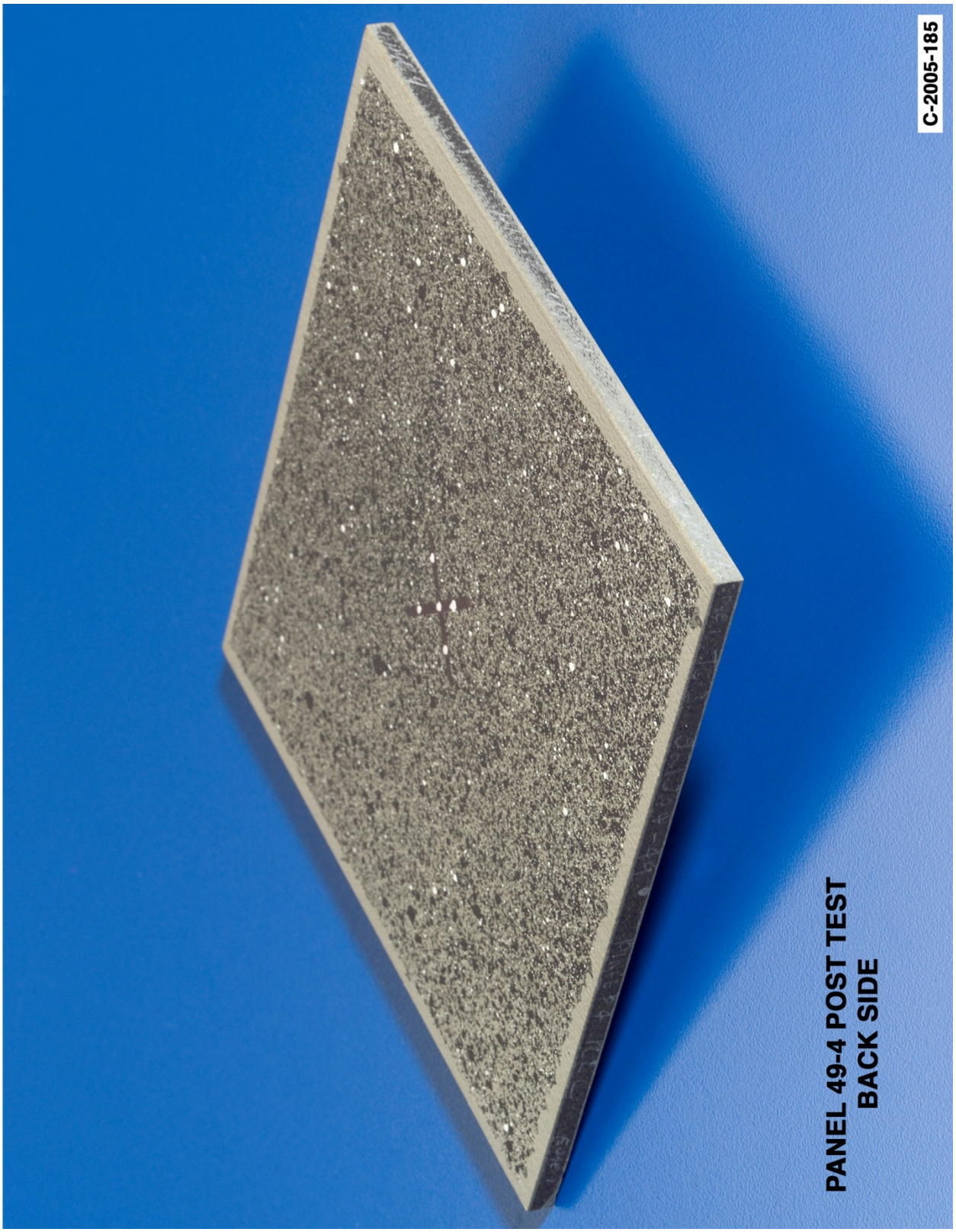

Figure E12–3.—Back face of panel 49-4 at 556 ft/s with a low-density soft ice cylinder (nominally 0.80 in. in diameter by 1.90 in.) at 90° impact angle. Test GRCC 126.

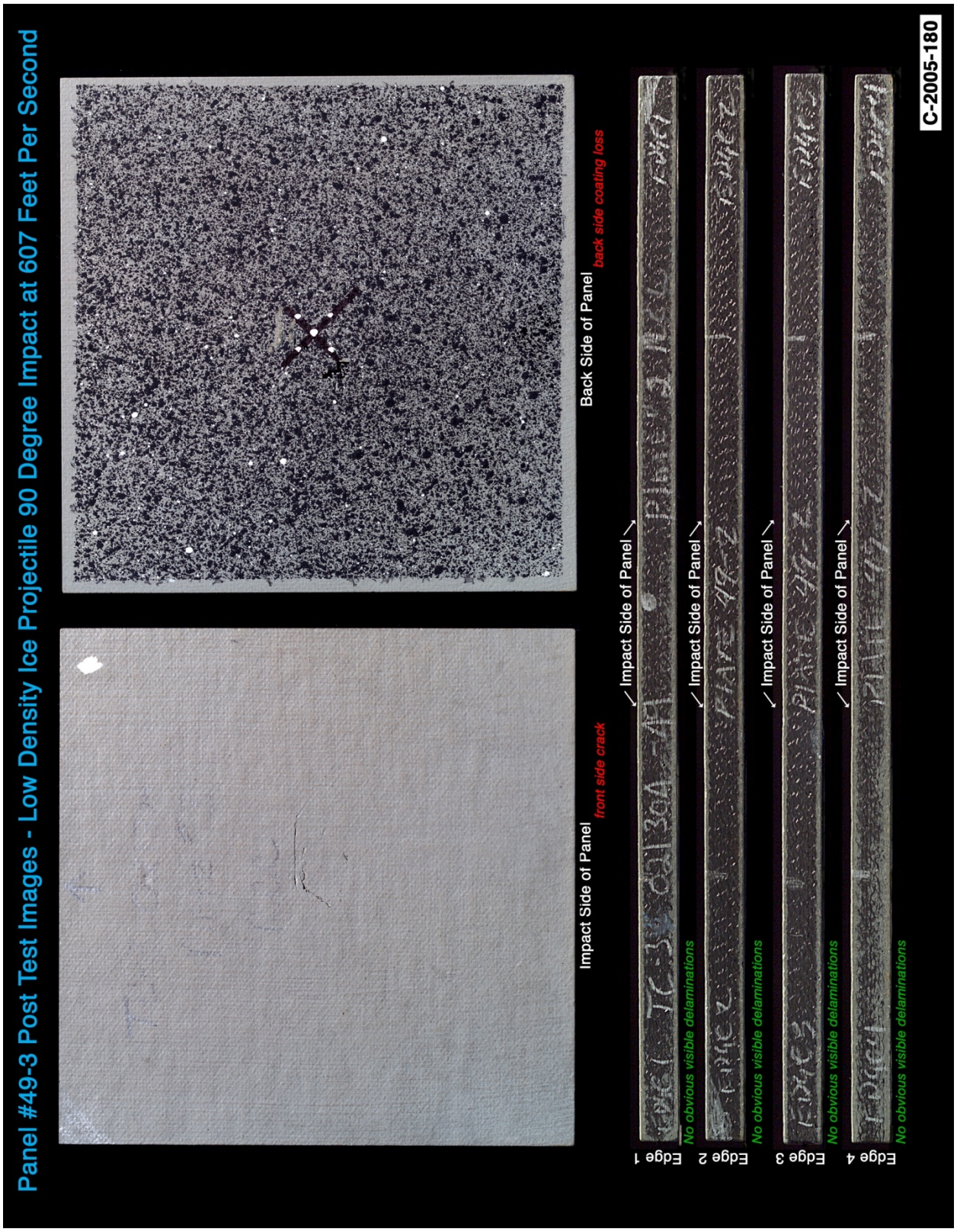

Figure E13–1.—Edges and faces of panel 49-3 at 607 ft/s with a low-density soft ice cylinder (nominally 0.8 in. in diameter by 1.90 in.) at 90° impact. Test GRCC 125.

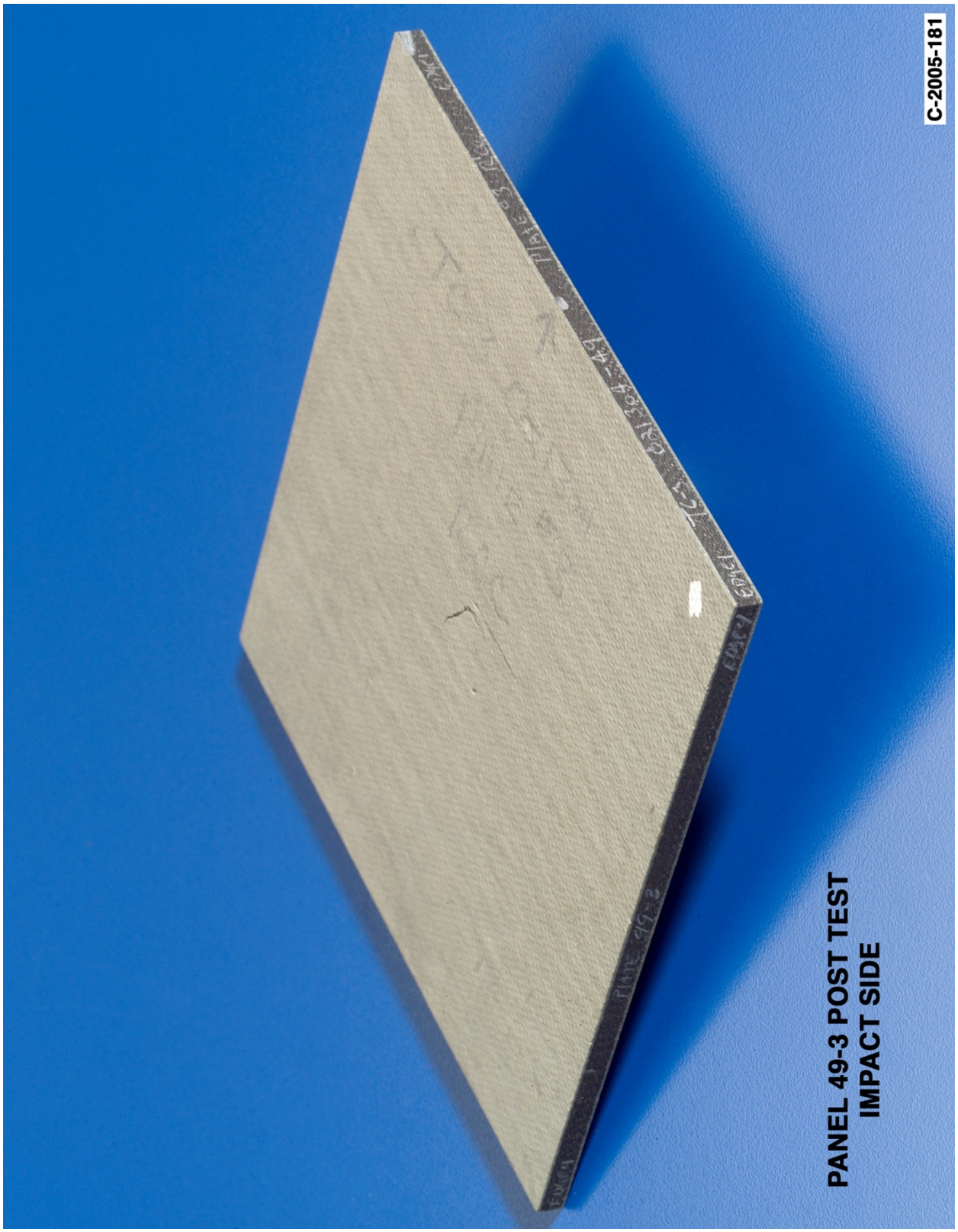

Figure E13–2.—Front (impact side) of panel 49-3 at 607 ft/s with a low-density soft ice cylinder (nominally 0.80 in. in diameter by 1.90 in.) at 90° impact angle. Test GRCC 125.

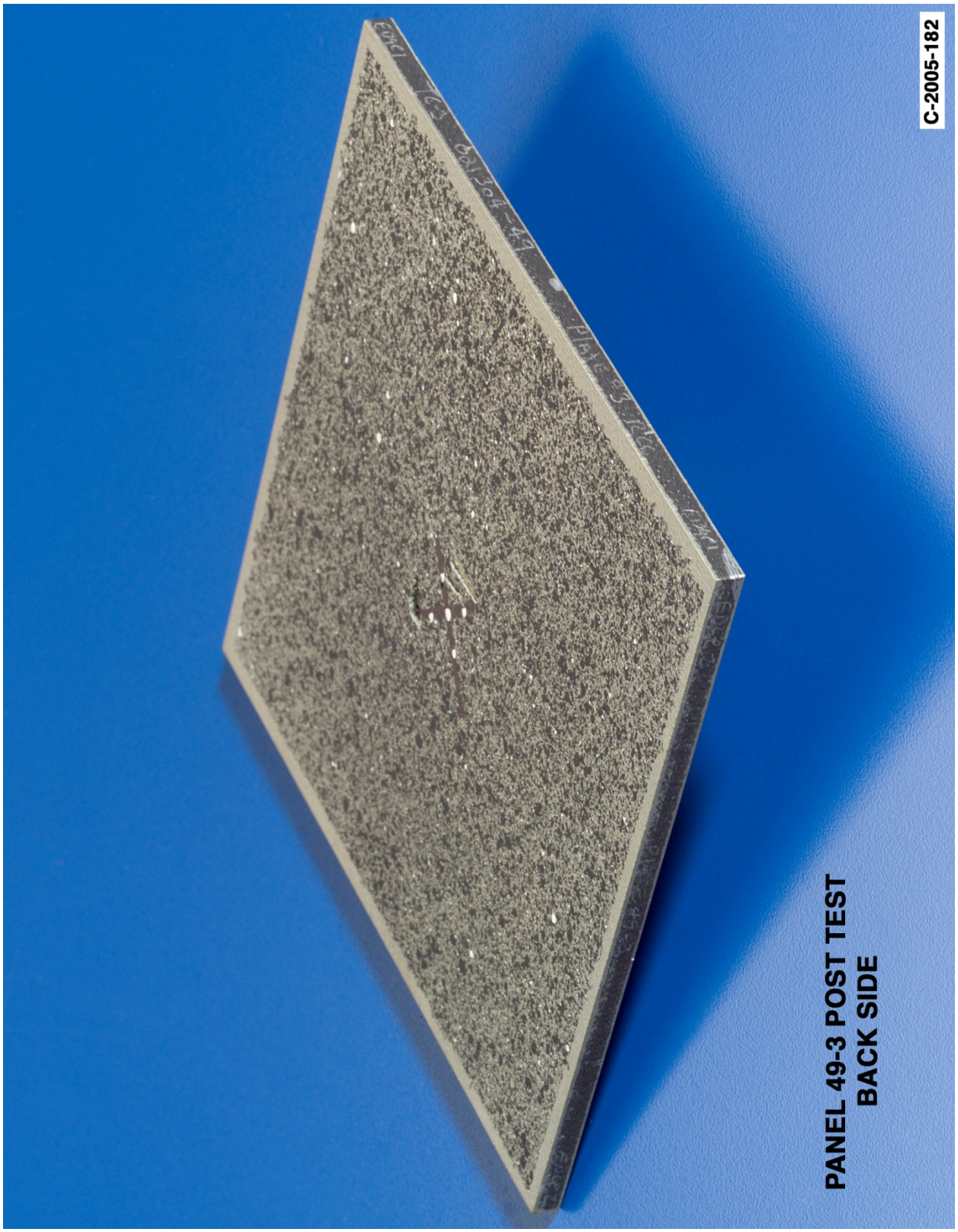

Figure E13–3.—Back face of panel 49-3 at 607 ft/s with a low-density soft ice cylinder (nominally 0.80 in. in diameter by 1.90 in.) at 90° impact angle. Test GRCC 125.

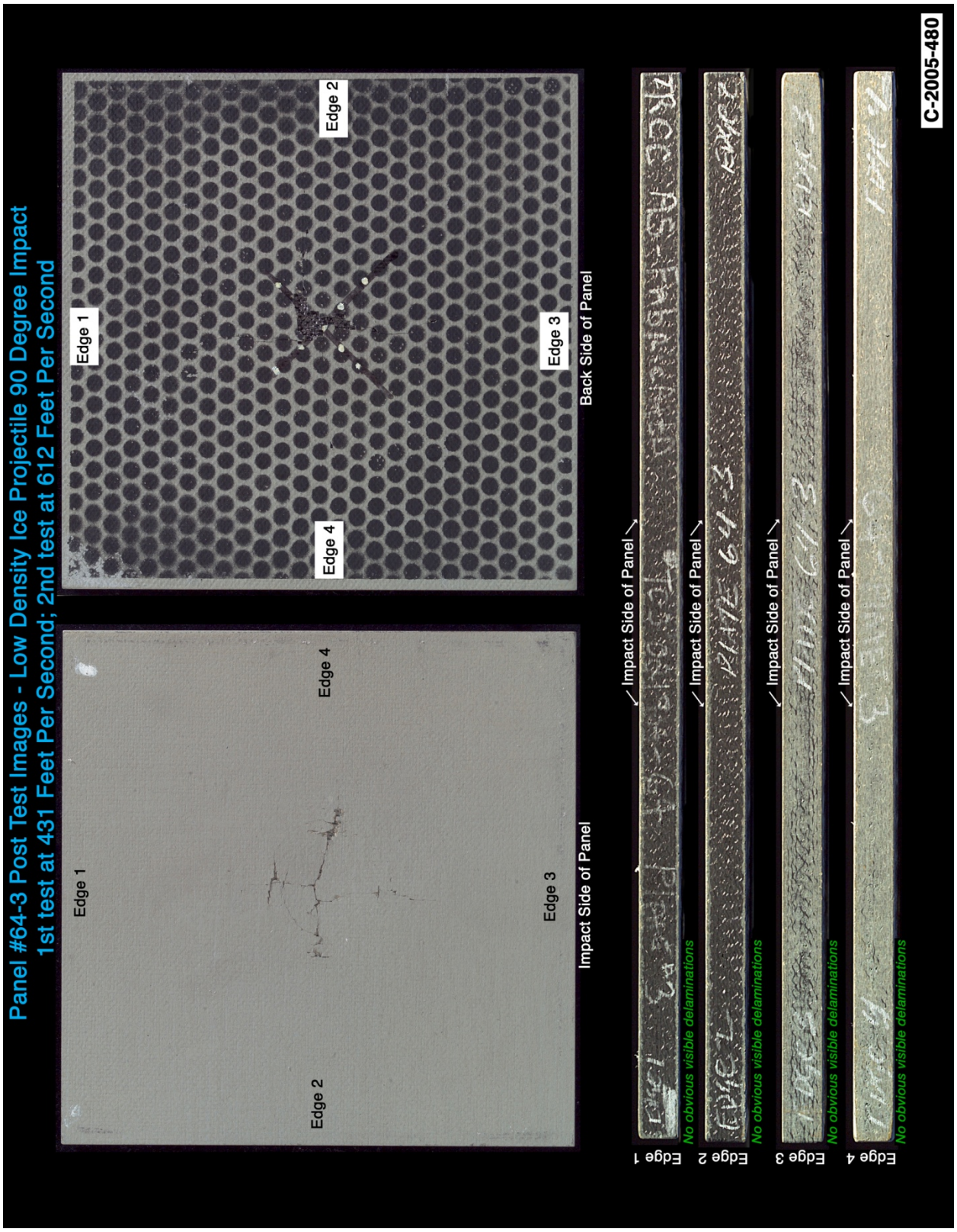

Figure E14–1.—Edges and faces of panel 64-3 at 612 ft/s with a low-density soft ice cylinder (nominally 0.8 in. in diameter by 1.90 in.) at 90° impact. Test GRCC 151.

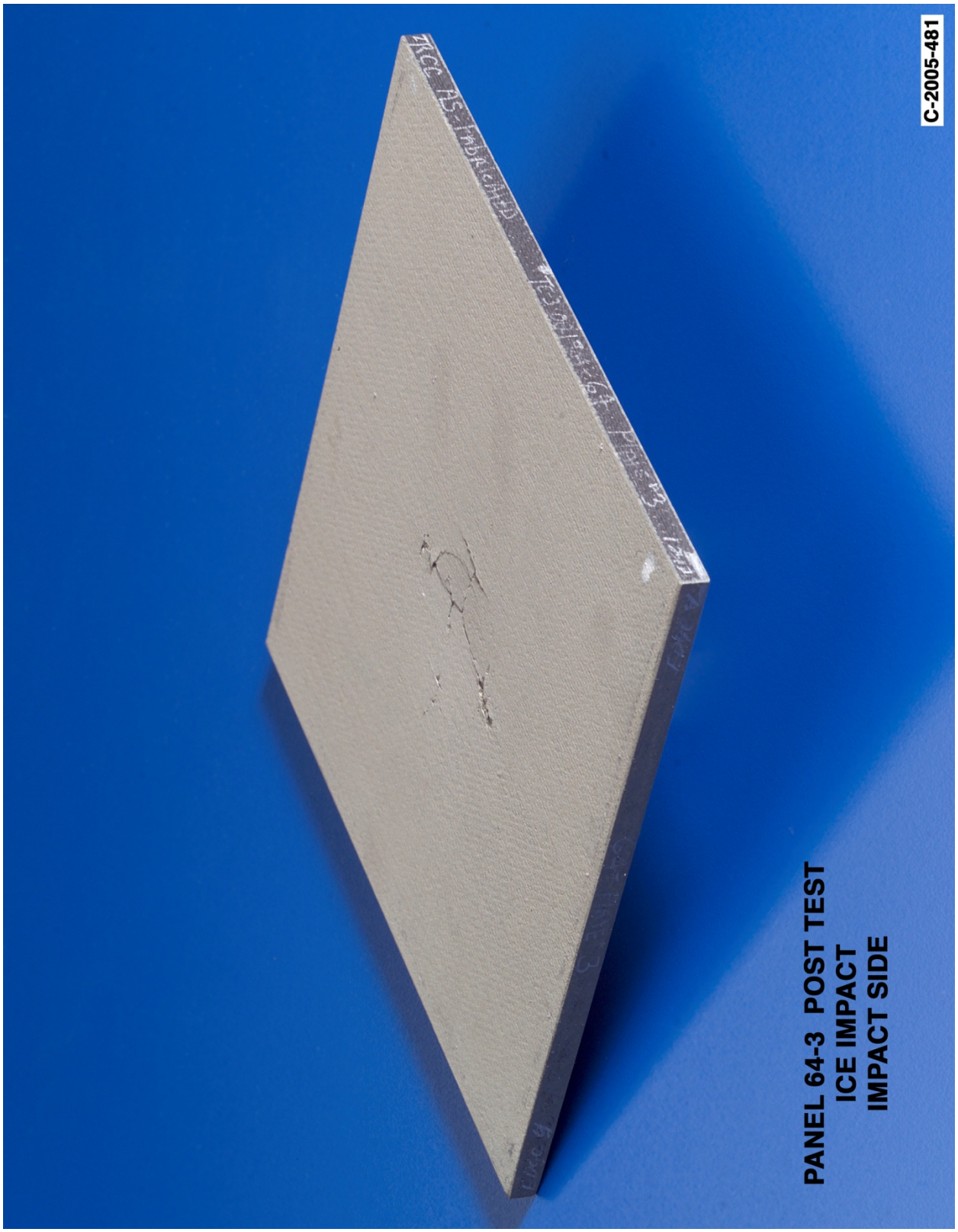

Figure E14–2.—Front (impact side) of panel 64-3 at 612 ft/s with a low-density soft ice cylinder (nominally 0.80 in. in diameter by 1.90 in.) at 90° impact angle. Test GRCC 151.

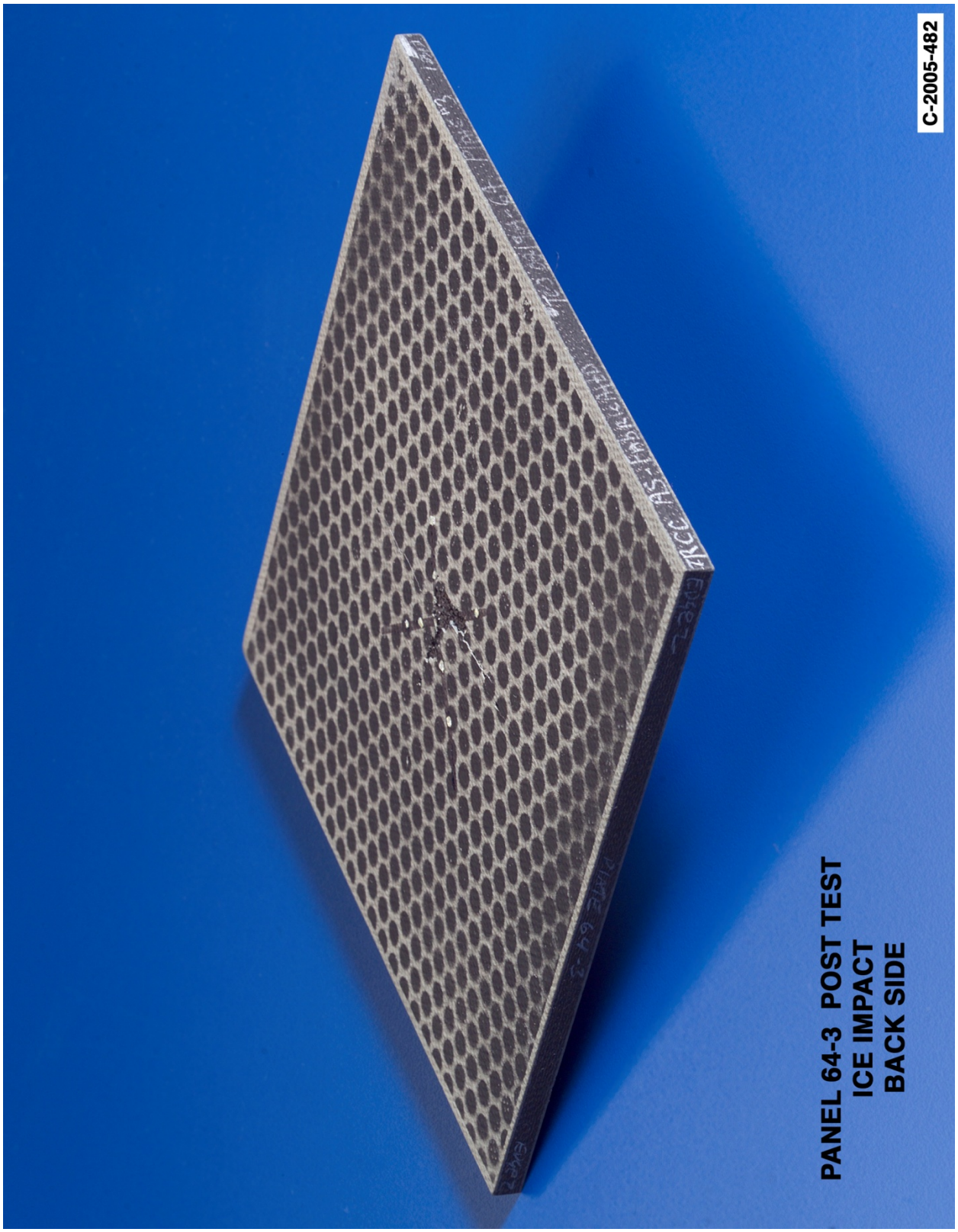

Figure E14–3.—Back face of panel 64-3 at 612 ft/s with a low-density soft ice cylinder (nominally 0.80 in. in diameter by 1.90 in.) at 90° impact angle. Test GRCC 151.

References

1. Gehman, Harold W., Jr., et al.: Columbia Accident Investigation Board Report. Vol. I, Government Printing Office, Washington, DC, 2003.
2. LS−DYNA Keyword User's Manual. Version 970, Livermore Software Technology Corporation, Livermore, CA, 2003.
3. Melis, Matthew E., et al.: Impact Testing on Reinforced Carbon-Carbon Flat Panels With BX−265 and PDL−1034 External Tank Foam for the Space Shuttle Return to Flight Program. NASA/TM—2007-213642, 2007. http://gltrs.grc.nasa.gov/
4. Orbiter RCC Panel 16R Damage Impact Testing Plan Threshold. NASA JSC No. 62702, 2004.
5. Vision Research. High Speed Digital Imaging Systems, Vision Research, Inc., Wayne, NJ, 2007. www.visionresearch.com Accessed July 11, 2007.
6. Photron. Precision High-Speed Imaging Systems, Photron USA, Inc., San Diego, CA, 2007. www.photron.com Accessed July 11, 2007.
7. GOM Optical Measuring Techniques, GOM mbH. Braunschweig, Germany, 2007. www.gom.com Accessed July 11, 2007.
8. Trilion. Optical Quality Systems. Trilion Quality Systems, West Conshohocken, PA, 2007. www.trilion.com. Accessed July 11, 2007.
9. Schmidt, T.; Tyson, J.; and Galanulis, K.: Full-Field Dynamic Displacement and Strain Measurement Using Advanced 3D Image Correlation Photogrammetry: Part I. Exp. Tech., vol. 27, issue 3, 2006, pp. 47−50.
10. Lee, Mikyoung, et al.: Application of 3D Measurement System With CCD Camera in Microelectronics. Advanced Packaging, 2003, pp. 33−34.
11. Koenig, J.: Silicon Carbide Coating Thickness Measurements of Various RCC Panels and Plates, Final Report to NASA MSFC. George C. Marshall Space Flight Center, Huntsville, AL, Contract No. NAS8−00159, SRI−ENG−05−23−10359.14, Dec. 2005.
12. Koenig, J.: Correlation of RCC Substrate Properties, Final Report to NASA MSFC, George C. Marshall Space Flight Center, Huntsville, AL, Contract No. NAS8−00159, SRI−ENG−06−22−10359.14, Apr. 2005.
13. Curry, Donald M.; Wong, Kenneth A.; and Baccus, Ronald K.: Mechanical Property Characterization of Reinforced Carbon-Carbon (RCC) for the Space Shuttle Return to Flight Effort. NASA JSC No. 63036, 2006.
14. Gilat Amos; and Goldberg Robert K.: Experimental Study of the High Strain Rate Tensile and Shear Response of Reinforced Carbon Carbon (RCC) Composites. NASA/TM—2008-213644, 2008.
15. Carney, Kelly, et al.: Material Modeling of Space Shuttle Leading Edge and External TankMaterials for Use in the Columbia Accident Investigation. Proceedings of the 8th International LS−DYNA Users Conference, Dearborn, MI, 2004, p. 3−35.
16. Goldberg, Robert K.; and Carney, Kelly S.: Modeling the Nonlinear, Strain Rate Dependent Deformation of Shuttle Leading Edge Materials With Hydrostatic Stress Effects Included. Proceedings of the 8th International LS−DYNA Users Conference, Dearborn, MI, 2004, p. 3−45.
17. Lyle, K., et al.: Application of Non-Deterministic Methods to Assess Modelling Uncertainties for Reinforced Carbon-Carbon Debris Impacts. Proceedings of the 8th International LS−DYNA Users Conference, Dearborn, MI, 2004, p. 1−1.
18. Fasanella, Edwin L., et al.: Test and Analysis Correlation of Foam Impact Onto Space Shuttle Wing Leading Edge RCC Panel 8. Proceedings of the 8th International LS−DYNA Users Conference, Dearborn, MI, 2004, p. 3−11.
19. Gabrys, Jonathan, et al.: The Use of LS−DYNA in the Columbia Accident Investigation and Return to Flight Activities. Proceedings of the 8th International LS−DYNA Users Conference, Dearborn, MI, 2004, p. 3−1.

20. Fasanella, Edwin L.; Boitnott, Richard L.; and Kellas, Sotiris: Dynamic Crush Characterization of Ice. NASA/TM—2006-214278 (ARL−TR−3753), 2006. http://gltrs.grc.nasa.gov/
21. Pereira, J. Michael, et al.: Forces Generated by High Velocity Impact of Ice on a Rigid Structure. NASA/TM—2006-214263, 2006. http://gltrs.grc.nasa.gov/
22. Pereira, J. Michael; Melis, Matthew E.; and Revilock, Duane M.: A Summary of the Space Shuttle Columbia Tragedy and the Use of Digital High Speed Photography in the Accident Investigation and NASA's Return-to-Flight Effort. Proceedings of the SPIE 26th International Congress on High-Speed Photography and Photonics, vol. 5580, no. 1, 2005.
23. Goldberg, Robert K.; Baccus, Ronald K.; and Carney, Kelly S.: Analysis of the Nonlinear Deformation Response of Shuttle Leading Edge Materials Including Coating Effects. NASA/TM—2005-213842, 2005. Available from the NASA Center for AeroSpace Information.
24. Fasanella, Edwin L., et al.: Dynamic Impact Tolerance of Shuttle RCC Leading Edge Panels Using LS−DYNA. AIAA 2005−3631, 2005.
25. Schulson, Erland M.; Iliescu, Daniel; and Fortt, Andrew: Characterization of Ice for Return-to-Flight of the Space Shuttle. Part 1—Hard Ice. NASA/CR—2005-213643/PART1, 2005. http://gltrs.grc.nasa.gov/
26. Schulson, Erland M.; and Iliescu, Daniel: Characterization of Ice for Return-to-Flight of the Space Shuttle. Part 2—Soft Ice. NASA/CR—2005-213643/PART2, 2005. http://gltrs.grc.nasa.gov/
27. Shazly, Mostafa; Prakash, Vikas; and Lerch, Bradley A.: High-Strain-Rate Compression Testing of Ice. NASA/TM—2006-213966, 2006. http://gltrs.grc.nasa.gov/
28. Carney, Kelly S., et al.: A Phenomenological High Strain Rate Model With Failure for Ice. Int. J. Solids Struct., vol. 43, 2006, pp. 7820−7839.

REPORT DOCUMENTATION PAGE	Form Approved OMB No. 0704-0188

1. REPORT DATE *(DD-MM-YYYY)*	2. REPORT TYPE	3. DATES COVERED *(From - To)*
01-11-2009	Technical Memorandum	

4. TITLE AND SUBTITLE
Impact Testing on Reinforced Carbon-Carbon Flat Panels With Ice Projectiles for the Space Shuttle Return to Flight Program

5a. CONTRACT NUMBER

5b. GRANT NUMBER

5c. PROGRAM ELEMENT NUMBER

6. AUTHOR(S)
Melis, Matthew, E.; Revilock, Duane, M.; Pereira, Michael, J.; Lyle, Karen, H.

5d. PROJECT NUMBER

5e. TASK NUMBER

5f. WORK UNIT NUMBER
WBS 377816.06.03.02.04

7. PERFORMING ORGANIZATION NAME(S) AND ADDRESS(ES)
National Aeronautics and Space Administration
John H. Glenn Research Center at Lewis Field
Cleveland, Ohio 44135-3191

8. PERFORMING ORGANIZATION REPORT NUMBER
E-15129

9. SPONSORING/MONITORING AGENCY NAME(S) AND ADDRESS(ES)
National Aeronautics and Space Administration
Washington, DC 20546-0001

10. SPONSORING/MONITOR'S ACRONYM(S)
NASA

11. SPONSORING/MONITORING REPORT NUMBER
NASA/TM-2009-213641

12. DISTRIBUTION/AVAILABILITY STATEMENT
Unclassified-Unlimited
Subject Categories: 15, 24, and 27
Available electronically at http://gltrs.grc.nasa.gov
This publication is available from the NASA Center for AeroSpace Information, 443-757-5802

13. SUPPLEMENTARY NOTES

14. ABSTRACT

Following the tragedy of the Orbiter *Columbia* (STS-107) on February 1, 2003, a major effort commenced to develop a better understanding of debris impacts and their effect on the space shuttle subsystems. An initiative to develop and validate physics-based computer models to predict damage from such impacts was a fundamental component of this effort. To develop the models it was necessary to physically characterize reinforced carbon-carbon (RCC) along with ice and foam debris materials, which could shed on ascent and impact the orbiter RCC leading edges. The validated models enabled the launch system community to use the impact analysis software LS-DYNA (Livermore Software Technology Corp.) to predict damage by potential and actual impact events on the orbiter leading edge and nose cap thermal protection systems. Validation of the material models was done through a three-level approach: Level 1--fundamental tests to obtain independent static and dynamic constitutive model properties of materials of interest, Level 2--subcomponent impact tests to provide highly controlled impact test data for the correlation and validation of the models, and Level 3--full-scale orbiter leading-edge impact tests to establish the final level of confidence for the analysis methodology. This report discusses the Level 2 test program conducted in the NASA Glenn Research Center (GRC) Ballistic Impact Laboratory with ice projectile impact tests on flat RCC panels, and presents the data observed. The Level 2 testing consisted of 54 impact tests in the NASA GRC Ballistic Impact Laboratory on 6- by 6-in. and 6- by 12-in. flat plates of RCC and evaluated three types of debris projectiles: Single-crystal, polycrystal, and "soft" ice. These impact tests helped determine the level of damage generated in the RCC flat plates by each projectile and validated the use of the ice and RCC models for use in LS-DYNA.

15. SUBJECT TERMS
Space shuttle; Debris; Impact; Reinforced carbon-carbon; Ice; External tank

16. SECURITY CLASSIFICATION OF:			17. LIMITATION OF ABSTRACT	18. NUMBER OF PAGES	19a. NAME OF RESPONSIBLE PERSON
a. REPORT	b. ABSTRACT	c. THIS PAGE			STI Help Desk (email:help@sti.nasa.gov)
U	U	U	UU	229	19b. TELEPHONE NUMBER *(include area code)* 443-757-5802